Influence of Gas Additives on the Performance of Barium Vapour Lasers

Simon N Halliwell

Thesis submitted in the application for the degree of

Doctor of Philosophy

in the

School of Physics and Astronomy

University of St. Andrews

February 1995

To my Mother and Father

Declaration

I Simon Neil Halliwell certify that this thesis has been composed by myself, that it is a record of my own work and that it has not been accepted in partial or complete fulfilment for any other degree or professional qualification.

I was admitted to the Faculty of the University of St. Andrews under Ordinance General No. 12 on the 1st October 1991.

Signed Date

I hereby certify that the candidate has fulfilled the conditions of the Resolution and Regulations appropriate to the degree of PhD.

Signature of Supervisor Date

Copyright

Abstract

A Study of Buffer Gas Additives to Barium Vapour Lasers

S. N. Halliwell

School of Physics and Astronomy, St. Andrews University

Submitted for the degree of Doctor of Philosophy

February 1995

The effects of H_2, D_2 and He addition to the buffer-gas of a barium vapour laser on its laser output power and efficiency have been investigated. A barium vapour laser was designed and constructed to operate in the self heating regime using a longitudinal pulsed electrical discharge. The barium metal was contained within a molybdenum boat at the anode end of the laser tube in a region which contained reduced insulation. This prevented contact of the molten barium with the tube wall. Using this tube design, laser tube lifetimes of greater than 500 hours of laser oscillation were obtained.

The laser output power and efficiency increased by over 40% when 3% H_2 was added to a Ne buffer gas under discharge conditions which were otherwise optimum using only Ne as the buffer gas. The laser output power and efficiency increased to 14.3 W and 1.0% which represents the highest recorded laser output power and efficiency to date. Similar increases in laser output power were obtained when D_2 was added to the buffer-gas with smaller increases being obtained when He was added to a Ne buffer-gas. Although no increase to the laser output power was observed when H_2 and D_2 was added to a He buffer-gas, the contributions from the 1.13 μm and 1.50 μm transitions to the total laser output power were found to change.

H_2, D_2 and He addition to a Ne buffer-gas reduced the prepulse free electron density thereby raising the tube impedance leading to enhanced upper laser level excitation. The degree to which each of the additives reduced the prepulse free electron density reflected the relative ability of each of the additives to cool the electrons in the interpulse period. Electron cooling is important since electron/ion recombination is dependent on the electron temperature. The power delivery to the laser tube was experimentally determined by the analysis of the tube current and tube voltage waveforms. H_2, D_2 or He addition to a Ne buffer-gas was found to increase the total power delivery to the laser tube and also modify the temporal power delivery to the tube. The addition of H_2 to a Ne buffer-gas enhanced laser oscillation on the tube axis resulting in a change from a flat top intensity profile across the bore of the tube to a near Gaussian profile. The upper limit to the PRF was extended when H_2 was added to a Ne buffer-gas which was attributed to faster electron cooling in the interpulse period when H_2 was present.

Acknowledgements

I would like to thank my supervisor Dr. Chris Little for his advice and guidance throughout my PhD and for giving me the opportunity to present my work at a number of international conferences. Also Dave Jones for numerous academic and non-academic discussions in the lab, and the seemingly endless supply of coffee and chocolate biscuits! Colin Whyte and Dee Jones for providing me with somewhere to stay towards the end of my time at St Andrews, and to Helen Milligan for having the tedious task of correcting numerous mistakes throughout this thesis. Fritz Akerboom for being tremendously patient with me every time I broke a laser tube. I would also like to thank all my friends and colleagues at St Andrews (including Jason, Smelly Trev and Steve 'trains') for the support that they gave me whilst I was in St Andrews.

I would particularly like to thank Fritz and Kath Akerboom for being the hosts for some very entertaining lunches and evening meals, to thank Pete Hirst and Natalie Ridge for their organisational skills which made 'Laser 1' such a unique group, and to Arthur Maitland for whose boundless enthusiasm and dedication to his subject was such an inspiration for me.

I am grateful for the financial support from the SERC for the funding of my Research Studentship and to my parents for occasional loans when this proved to be insufficient.

I am indebted to Clare Parnell for helping me to remain sane by whisking me away from St Andrews to climb the Munros in the highlands of Scotland, without whom I almost certainly would have not have completed them all. I also wish to thank Clare for showing me the fundamentals to Fortran 77 programming and in my absence, arranging for printing and binding of this work.

Contents

Chapter 1: Introduction

Chapter 2: Experimental Design

Chapter 3: Experimental Techniques, Measurements and Analysis

Chapter 4: Influence of H_2, D_2 and He Additives on BVL Operation with a Ne Buffer Gas

Chapter 5: Hydrogen Addition to a BVL with a Neon Buffer Gas

Chapter 6: Helium Buffer Gas

Chapter 7: Summary and Discussion for Future Work

Appendices

Chapter 1

Introduction

1.1 Introduction

Pulsed cyclic metal vapour lasers were first demonstrated in the mid 1960s and have been developed since then to more reliable devices giving large average laser output powers at relatively high wall plug efficiencies. A number of metal vapour lasers has been developed into commercial systems, namely the well established copper vapour laser (CVL), as well as gold, barium and strontium vapour lasers (GVLs, BVLs and SVLs respectively). With these lasers, high average output powers may be obtained in the violet/ultraviolet (UV) spectral region using strontium; in the yellow and green using CVLs; in the red using GVLs, and finally in the near to mid infrared using BVLs.

There are numerous applications for high average power metal vapour lasers. In the case of CVLs, the main use is either for the pumping of dye lasers for atomic vapour laser isotope separation (AVLIS) [1], for precision machining of metals and ceramics [2] and for dermatology. Gold vapour lasers are used almost exclusively for the treatment of cancer [1] (photodynamic therapy). Barium vapour lasers have been used in the telecommunications industry for diagnostics of silica based optical fibres [3] and strontium lasers have potential uses in projection television [4]. The rapid development of metal vapour lasers over the years has been brought about both by advances in technology and also by a fuller understanding of the principles and limitations of these lasers.

Within the last 10 years it was found that the addition of hydrogen to a neon buffer gas could significantly increase the average laser output power of both CVLs and GVLs. Because the limitations to laser power of BVLs is similar to CVLs and GVLs, it was the purpose of this present study to investigate for the first time, the effect of hydrogen additives to the laser output power and the operating conditions of a BVL.

This chapter begins with a brief historical review and then an overview of the excitation mechanisms that are most important in pulsed metal vapour lasers, and then continues with a more detailed discussion concerning the chief mechanisms which govern both the upper level excitation and the metastable deactivation in BVLs. The development and experimental studies of BVLs are then presented. Also discussed in this chapter are results and conclusions drawn from previous studies of the effects of hydrogen additives in the discharges of CVLs. These results are compared with those obtained with hydrogen addition to BVLs (discussed in Chapters 4 to 6), and possible kinetic mechanisms are discussed to account for the observed increase.

1.1.1 Metal Vapour Lasers - Historical Background

The barium vapour laser (BVL) belongs to the family of pulsed cyclic lasers which also includes some other metal vapour lasers such as CVLs, GVLs, manganese and lead vapour lasers. They are all kinetically similar in so far as they are all nominally 3-level lasers with a ground state, an upper laser level which is an optically allowed transition to the ground-state (ie a resonance level) and a lower laser level which must be a metastable level, i.e. unconnected to the ground state [5]. The principal kinetic mechanisms involved in CVLs, GVLs and BVLs are all very similar.

The first cyclic metal vapour laser was a lead vapour laser which was developed by Fowles and Silfvast in 1965 [5]. Following this pioneering work, in 1966 Walter *et. al.* successfully demonstrated the first CVL [6]. The latter was an externally heated device which used an oven arrangement to heat a central alumina tube to temperatures approaching 1500°C. At these temperatures, copper pieces which were evenly distributed along the inside of the alumina tube were liquid, and a vapour pressure of copper was established

within the tube which was governed by the tube wall temperature. A pulsed electrical discharge was operated longitudinally along the length of the alumina tube through a low pressure inert gas such as neon or helium at a pressure of between 20 and 100 torr in which the metal vapour was present. This buffer gas served to sustain a uniform discharge and prevented metal from diffusing to the laser windows. Laser oscillation was observed at 510.5 and 578.2 nm with gain coefficients of 58 dB/m and 42 dB/m respectively. The repetition rate of the device was only about 60 Hz and the average laser output power was 20 mW.

The development of self-heated CVLs by Isaev *et al.* early in the 1970s [7] resulted in a significant increase in both the total average laser output power and laser efficiency. The idea behind self-heated CVLs is that they only use the heat produced by the electrical discharge to heat the tube walls to the required temperature. The large increase in average laser power was chiefly a result of the increased pulse recurrence frequencies (PRFs) at which the laser was operated. These were increased by several orders of magnitude from those of early devices (typically 1-10 Hz) to 1-10 kHz.

Since the advent of CVLs, a number of other self-heated neutral atom metal vapour lasers have been developed, such as barium, gold and manganese lasers. In each case, the average laser output power was significantly higher than the equivalent systems which used an externally heated oven. It should be pointed out that, although the average laser power is significantly lower in externally heated devices than in self heated ones, the specific output pulse energy is often much higher due mainly to the complications of gas temperature gradients at high PRFs.

1.2 Excitation Mechanisms of Metal Vapour Lasers

1.2.1 Excitation of Upper Laser Levels

A pulsed electrical discharge through an inert gas mixture is used to generate an electric field longitudinally along the laser tube which accelerates electrons from the cathode region to the anode region. The average electron energy in the excitation pulse increases as the electric field across the tube increases. It is electron collision with the ground-state metal

atoms which is the mechanism by which the upper laser level of the neutral lasant atoms is populated. Since these lasers are essentially three level ones, involving ground, resonance and metastable levels, it is essential for the pulsed electrical discharge to create large electric fields to generate electrons of high enough energy to excite metal from the ground state to the resonance upper level in preference to excitation to the metastable lower laser level [8]. In addition, because the population is transient (ie has a fast decay rate), fast excitation to the resonance upper laser level is important in order to establish a population inversion (and hence a sufficiently fast tube current rise-time must be obtained). Laser oscillation begins on the leading edge of the current pulse when the excitation to the upper resonance laser level is fastest (the applied electric field is still high). In the case of the 1.13 μm and 1.50 μm laser transitions of barium, excitation occurs to a resonance upper laser level which lies 2.2 eV above the ground state.

Under optimum or near-optimum discharge conditions for laser oscillation, fast radiative transitions from the resonance level to the ground-state are inhibited because of radiation trapping (see Section 1.2.4), whereas transitions from the resonance to metastable state are not trapped. As for all pulsed cyclic metal vapour lasers, the lifetime of the lower level is very long compared to that of the upper level [5] and thus laser oscillation ceases when the metastable population becomes sufficiently large during the pulse. This is why these cyclic lasers are often referred to as 'self-terminating'. Because of the requirement to depopulate the lower metastable laser level before the next excitation pulse, they are inherently pulsed lasers. The metastable lower laser level is depopulated back to the ground state either by electron collisions or by tube wall collisions in the interpulse period [9]. The mechanism which determines how the metastable level is depopulated depends upon both the dimensions of the laser tube and the discharge conditions [10]. One of the chief mechanisms believed to limit the pulse recurrence frequency of pulsed cyclic metal vapour lasers is the requirement to depopulate the metastable lower laser level sufficiently in the interpulse period [11].

It is usually the metal atoms which become collisionally ionised in the pulsed gas discharge, and not the buffer gas atoms, because the metal atoms have significantly lower

ionisation potentials than either neon or helium, which are the most often used buffer gases in MVLs. The ionisation potential of barium is 5.21 eV compared to 21.6 and 24.5 eV for neon and helium respectively [12]. A short current rise-time implies a high electron production rate in the excitation pulse and hence a high rate of upper level excitation and a high degree of ionisation. In CVLs, the degree of ionisation of metal atoms can be as high as 40-50% during the current pulse [13].

This high degree of ionisation is clearly not desirable since it reduces the number of ground-state metal atoms available for excitation to the upper laser levels. However, there is also a need to have a fast excitation pulse to generate a large electron density while there is still a high field across the laser for efficient upper laser level excitation. Using conventional excitation circuits in practice, the faster the discharge pulse the better, despite the excessive ionisation of metal which accompanies it. Slowly rising current pulses can also lead to low electron energies during the excitation period, which can deleteriously cause excessive pumping of the metastable lower levels.

There is an additional constraint on the excitation pulse, which is that it should be of a sufficiently short duration. This is because once laser oscillation has terminated it cannot then begin again until there has been sufficient depopulation of the metastable level. This is only effected by slow processes such as superelastic electron collisions or the diffusion to the tube wall in the discharge afterglow. If the excitation pulse is too long then the energy which is deposited into the plasma after the laser oscillation has ceased is wasted and reduces the operating efficiency of the laser as well as leading to unnecessary heating which may hinder the deactivation of metastable levels [14] and hence lower the maximum PRF (i.e. average laser output power) of the device.

A high prepulse electron density is another factor which can inhibit excitation to the upper laser level and consequently the total laser power [10]. This is because a high prepulse electron density reduces the overall tube impedance and consequently reduces the tube voltage which may be generated across the tube during the excitation pulse. This reduced voltage (and hence E/N ratio) has the effect of reducing the average electron energy in the excitation pulse which can lead to reduced upper level excitation (see Section 1.3.5).

1.2.2 Metastable Level Deactivation

The build up in the population of the metastable lower laser level is believed to be one of the major reasons for termination of laser oscillation, and a principal factor which limits the laser output pulse duration [15]. As mentioned above, the mechanism responsible for the depopulation of the metastable level depends upon the laser tube dimensions and the discharge operating conditions [10]. With narrow bore tubes [16] (<2-3 mm) it is predominantly collisions of the excited metal with the tube walls which is held to be responsible for the metastable depopulation, and not collisions with buffer gas atoms or electrons. This is one of the reasons that very high repetition rate lasers (>50 kHz) generally have very narrow bore tubes. With low pressure discharges, when the mean free path becomes sufficiently long, metastable depopulation can also be effected by wall collisions in tubes of bore >2-3 mm [16], but the optimum pressure for larger bore tubes is normally high enough such that the mean free path is significantly shorter than the diameter of the tube. As the tube bore increases, however, collisions with the tube walls become less significant. With wide bore tubes (≥1 cm), the mechanism for metastable depopulation is thought to be only volumetric electron collision in the discharge afterglow [17]. With this mechanism, CVLs can be scaled to 8 cm bore and more [17].

The electric field across the tube is fully collapsed in the interpulse period, during which time the average electron temperature rapidly falls because of elastic collisions with either the buffer gas or metal atoms and ions. The rate of electron cooling decreases as the local electron temperature approaches the local gas temperature within the tube and would eventually reach the gas temperature (which is itself reducing), provided that a sufficient amount of time is allowed before the next excitation pulse. The electron cooling rate is primarily dependent upon the buffer gas type and the buffer gas pressure. In general a buffer gas with a lighter mass will remove a larger fraction of energy from the electron [18]. Also, raising the buffer-gas pressure will increase the rate of electron cooling in the interpulse period because of the increased electron/buffer gas collision frequency.

Unfortunately, some of the discharge conditions which favour increased metastable depopulation can have a detrimental effect upon upper laser level excitation. For example, if

the buffer gas pressure is increased then the metastable population should decrease for reasons cited above. However, increasing the pressure also tends to cause the E/N (electric field to number density) ratio to decrease which decreases the average electron energy in the excitation pulse because of the increased collision frequency [19]. This is detrimental to efficient excitation of the upper laser level.

1.2.3 Plasma Recombination

Another process which occurs in the discharge afterglow is the recombination of electrons with ions. This is an important process since it determines the number density of free electrons prior to each excitation pulse and hence determines the discharge tube impedance at the onset of excitation. Greater recombination results in higher tube impedances and hence larger voltage hold-off which results in higher average electron energies in the excitation pulse and hence faster upper level excitation. Some reports suggest that one of the principal mechanisms limiting the maximum PRF of CVLs and BVLs is a high preionisation density [10,20]. If the recombination is primarily by three-body collision involving a buffer gas atom/molecule as the third body, as it is believed to be [10,20], then the plasma recombination rate between electrons and ions is proportional to $T_e^{-9/2}$, where T_e is the electron temperature. For this reason, the degree of recombination is strongly dependent upon electron cooling, and hence on both the buffer gas pressure and, in particular, the buffer gas type.

1.2.4 Radiation Trapping

The lifetime of the upper resonance levels of metal atoms is generally very short and in the case of barium is only around 8.6 ns for transitions from the $6p^1P_1$ resonance upper laser level to the ground-state [19]. A comparison of the probabilities for the resonance-to-ground transition for the 1.13 μm and 1.50 μm laser transitions show that under conditions of 'low' metal vapour pressure, the $6p^1P_1$ resonance level lifetime is governed by spontaneous emission at the resonance wavelength. The decay rates [19] for the resonance wavelength, 1.13 μm and 1.50 μm transitions are 1.19×10^8 s^{-1},

$1.2x10^5$ s^{-1} and $2.5x10^5$ s^{-1} respectively. Laser oscillation is impossible when the decay rate for the resonance transition is faster than for the laser transitions.

However, at the operating temperature of metal vapour lasers, a phenomenon known as radiation trapping occurs [14]. At high (≥700°C) tube wall temperatures, the barium density is sufficient to reduce the loss of resonance level atoms to the ground-state. Although the individual level lifetimes are not extended, reabsorption of 553 nm resonance radiation by other barium atoms in their ground-states prevents the loss of the resonance photons from the gain medium. At high enough barium vapour densities, the lifetime of the $6p^1P_1$ level becomes dominated by the untrapped 1.13 μm and 1.50 μm transitions to the metastable states. Thus the lifetime of the resonance level is effectively 22 μs at 700°C and 692 μs at 900°C [19]. The barium vapour density which corresponds to the onset of radiation trapping is around 0.7 Pa (at a wall temperature of 700°C) [19].

1.3 The Barium Vapour Laser

1.3.1 Introduction

Laser oscillation in barium vapour was first observed by Cahuzac [21] in 1970 using an externally heated device similar in design to the first CVLs. He observed approximately 20 infrared laser transitions ranging from 1.13 μm to 6.45 μm. It was not until the advent of self-heated metal vapour lasers that further research was undertaken on BVLs. Due to its potential for high average powers, there arose a great interest in the development of this type of laser.

Figures 1.1a and 1.1b show energy level diagrams with all the laser transitions observed to date indicated. Prior to the present investigation, the highest reported total laser output power from a BVL was 12.5 W [22], corresponding to an overall laser efficiency of 0.54%. Higher laser efficiencies of 0.72% were obtained in [22] when the conditions were altered away from those for maximum laser power. The 1.13 μm and 1.50 μm transitions contributed to the majority of the laser output power with smaller yet significant contributions at 2.55, 2.92 and 4.72 μm. In all cases, excitation is from the ground state to an upper resonance level. The BVL is particularly interesting from a kinetics point of view

because a number of the laser transitions share either a common upper resonance level or a common lower metastable level. This has been found to lead to competition effects between certain transitions with some interesting results [23]. For example, the 1.13 μm and 1.50 μm transitions share a common lower laser level which can lead to enhancement of the laser power at 1.50 μm at the expense of laser power at 1.13 μm under some discharge conditions. Another example is the 2.55 μm transition which shares a common upper laser level with the 4.72 μm transition. As a result of this, strong laser oscillation at 2.55 μm is not accompanied by strong emission on the 4.72 μm transition.

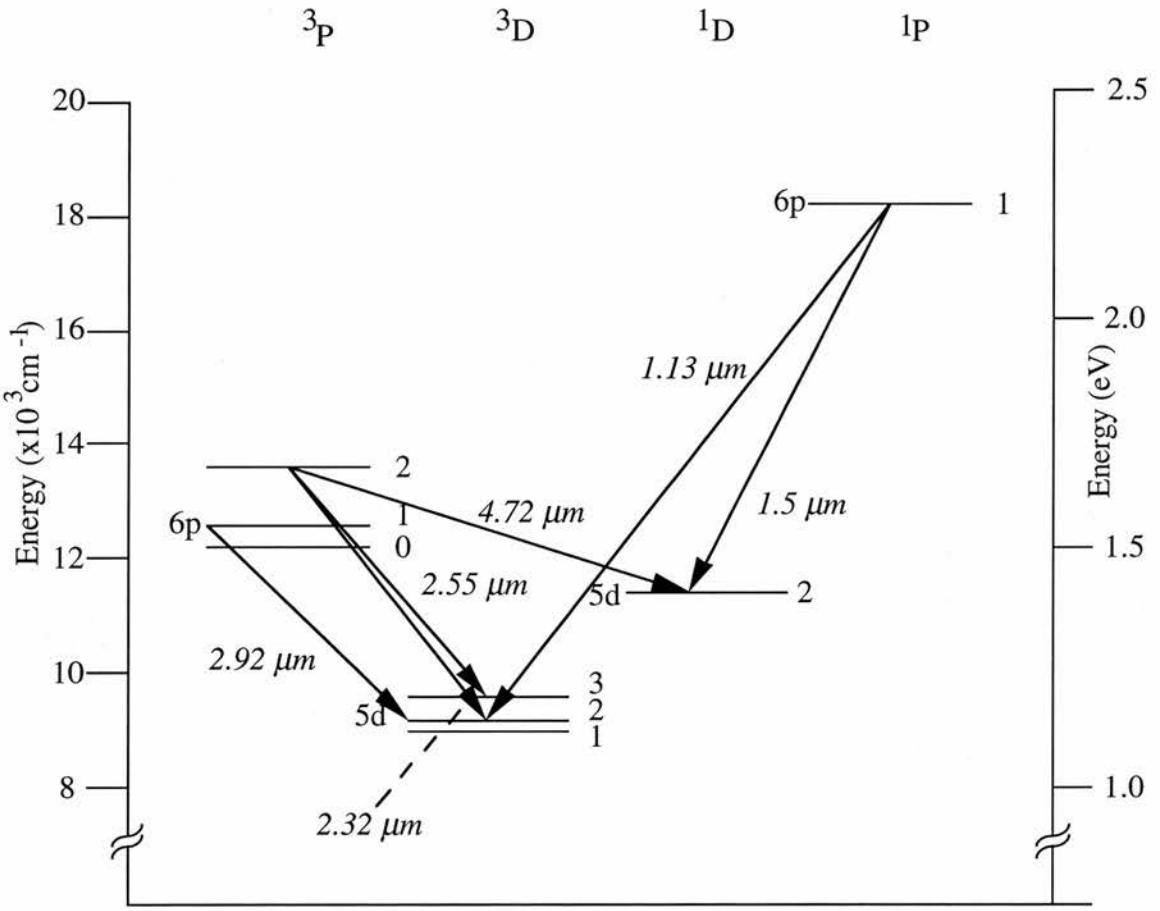

Fig 1.1a: Energy level diagram showing laser transitions from the lower energy resonance levels [18].

The main applications of BVLs are in the telecommunications industry. Here the main interest lies in the use of the 1.5000 and 2.55 μm laser transitions for efficient propagation of high peak powers through silica and fluoride-based fibres respectively. This is because the 1.50 μm and 2.55 μm laser transitions correspond to the wavelength for maximum transmission through silica and fluoride based fibres respectively.

Unfortunately, as for CVLs, the high gain of BVLs leads to a relatively poor beam quality, making it unsuitable for communications. However, the relatively high peak powers (10s of kW) make it very useful for diagnostics of optical fibres by measuring the SRS (Stimulated Raman Scattering) caused by impurities [3]. The BVL also has potential uses for applications involving atmospheric propagation, since a number of the principal laser transitions (e.g. 2.16, 2.32 and 4.72 μm) fall within transmission windows for water vapour and thus there is only minimal attenuation. Other uses include infrared projection microscopy [24] which utilises the high gain of the barium vapour to amplify the light scattered off the specimen.

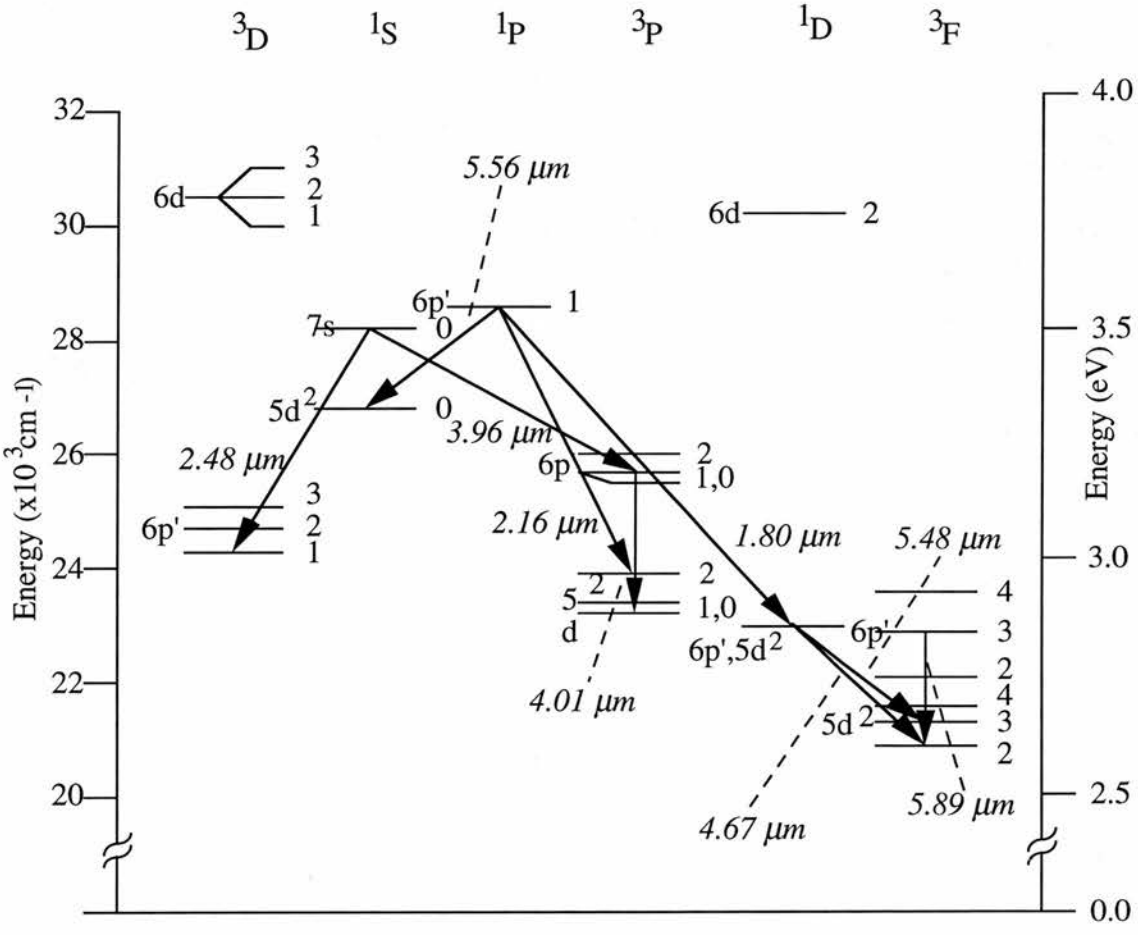

Fig 1.1b: Energy level diagram showing laser transitions between the higher energy levels [18].

1.3.2 Laser Operating Conditions

Most of the studies of the BVL to date include in their reports problems associated with the chemical activity of barium, which limits the laser tube lifetime severely. In some

cases the laser tubes were found to crack after only a few hours of laser operation. One report suggested that if the barium metal were contained inside tantalum boats [22] then the laser tube lifetime could be significantly extended. Initially problems were found in the present study of BVLs, but these were eventually overcome with tube lifetimes being extended to 500 hours of laser operating time by controlling the placement of the barium metal in the laser tube. The method of metal placement adopted is discussed in Section 2.5.

The operating temperature of the BVL is between 800-1000°C, which is somewhat lower than the tube-wall temperature of CVLs (1400-1600°C). Nevertheless, a considerable amount of time (~1 hour) was required to reach thermal stability of laser operation after initially turning on the laser. A similar time was required to run the laser down to switch-off in order to prevent excessive thermal stress on the alumina.

There have been several reports concerning characterisation of BVLs with respect to discharge operating conditions, such as the dependence of output power on input power, charging voltage and buffer gas pressure amongst other factors. It should be pointed out that there are various reports which are not consistent in their description of the optimum operating parameters for laser operation. For example, a number of reports [25,26] suggests that laser power is weaker when a helium buffer gas is used instead of neon, whilst another report [19] suggests that the laser output power is greater with a helium buffer gas than with neon. Neon was used at first in the present study because a greater number of reports suggested that neon gave higher powers than helium. However, this was found not to be the case (see Section 6.1.1).

1.3.3 Saturation Absorption Experiments

One of the principal reasons for the dramatic increase in the total average laser power of pulsed metal vapour lasers over recent years has been the ability to increase the PRF of the laser. This has been partly as a result of advances in technology, for example, improved thyratrons and a better design of pulsed power circuitry to drive the laser, but it has also been a result of the better understanding of the physical processes which occur within the laser discharge. One method to gain a better understanding is to undertake beam

probing experiments such as saturation absorption studies to measure directly the metastable population during the interpulse period, or perturbation techniques on upper and lower laser levels to monitor particular excitation/deactivation pathways.

The saturation absorption experiment undertaken by Kazakov *et al.* [15] used two BVLs with the 1.50 μm transition of one BVL to probe the discharge of the second BVL. The degree of absorption of the probe beam in the second BVL was measured as a function of time from the end of the excitation pulse. As the population of the metastable level increased in the second BVL, the degree of amplification of the 1.50 μm probe beam decreased, because of reduced stimulated emission from the upper laser level. After the gain period, the probe beam was strongly absorbed, with absorption reducing with time as the metastable population decayed away. This saturation absorption experiment was used to give an indication of the temporal evolution of the metastable population in the interpulse period.

Kazakov *et al.* found that immediately after the excitation pulse, the 1.50 μm metastable level ($5d^1D_2$) decayed exponentially with a time constant τ_1 and that at later times the decay rate was slower with a time constant τ_2. The metastable population decayed with the rate constant τ_1 until quasi-equilibrium was established between the metastable lower laser level and the electron temperature. Once quasi-equilibrium was reached, the metastable population then decayed with the rate constant τ_2 which was governed by the electron cooling rate. The values of τ_1 and τ_2 were found to be very dependent upon both the buffer gas pressure and the buffer gas type. Increasing the pressure tended to result in a decrease in the time constant and hence an increase in the metastable depopulation rate. The decay was also found to be fastest when helium was used as the buffer gas, followed by neon and finally xenon. This trend reflected the ability of the buffer gas to cool the electrons in the discharge afterglow. They also found that, over the tube wall temperature ranges selected, the 1.50 μm metastable decay rate was independent of temperature.

An analysis of the laser power at 1.50 μm and also of the metastable population in the interpulse period of a double pulse excitation circuit (with varying time intervals between pulses) suggested that "under the condition of these experiments, the main factor

limiting the maximum frequency of the excitation pulses was the high residual population of the $5d^1D_2$ metastable level by the time of arrival of the next excitation pulse". In addition, their results also suggested that the mechanism by which the 1.50 μm metastable level was deactivated could be electron collision, and conclusively that the deactivation was not by diffusion to the tube wall.

Similar studies were carried out by Bokhan [10] who was somewhat critical of the above-mentioned study [15]. In the conclusion to this work [10], he stated that the metastable level played no appreciable role in the mechanism limiting the average laser output power and that the limitation came from a high prepulse free electron density, which he had previously found to be the case for manganese and lead vapour lasers.

Clearly, the dominant mechanisms limiting the laser power and the PRF of the BVL still have to be clarified.

1.3.4 Laser Level Perturbation Experiments

As shown in Figures 1.1a and 1.1b, a number of the transitions share either a common upper or lower laser level. This can lead to strong competition between a number of the transitions, with the effect of enhancing the laser power at some wavelengths at the expense of others. It is possible to gain a qualitative understanding of the kinetics of the excitation pathways and hence an explanation for the suppression of particular laser transitions by a method of laser-induced perturbation of particular laser transitions.

Such an investigation was undertaken by Pask *et al.* [23]. In that study a pulsed dye laser was used to perturb selectively either upper or lower laser levels. The transitions of particular interest were at 1.13 μm and 1.50 μm because most of the laser power occurred at these wavelengths and they share a common upper level; the 2.55 μm transition was also chosen because this had previously been found to optimise under very different conditions to any of the other laser transitions; and the 4.72 μm transition was examined, because it shares a common lower metastable level with the 1.50 μm transition.

Laser action at 1.13 μm and 1.50 μm was perturbed in one of 3 ways. The first was by causing depletion of the upper laser level by pumping to a higher lying level. The

second was by increasing the population of the upper laser level by pumping at the resonance wavelength. The third was by depleting the 1.50 μm metastable lower level by pumping to a higher level. In each case, the delay of the probe pulse was timed to occur just before the onset of laser oscillation at 1.13 μm.

When the 1.13 μm and 1.50 μm upper ($6p^1P_1$) laser level was selectively depopulated, the laser power at 1.50 μm momentarily decreased before increasing in power until laser oscillation at 1.13 μm began. The probe beam tended to cause a delay for the onset of laser oscillation which was attributed to an extended period of time taken to reach the threshold inversion. However, the most striking effect on the 1.13 μm and the 1.50 μm transitions was demonstrated when the 1.50 μm lower laser level ($5d^1D_2$) was selectively depopulated. In this instance the laser power increased at 1.50 μm and correspondingly decreased at 1.13 μm.

The perturbation studies on the $6p^1P_1$ level also had a significant effect upon the laser power at 2.55 μm. An increase in the $6p^1P_1$ upper laser level excitation was found to increase the laser power at 2.55 μm. This suggested that the excitation mechanism to the $6p^3P_2$ upper laser level of the 2.55 μm transition was a result of the transfer of population from the $6p^1P_1$ level which was probably a result of rapid superelastic electron collisions, rather than slower spin-changing collisions between excited barium in the $6p^1P_1$ level with buffer gas atoms.

Strong competition was also found to occur between a number of other transitions, for example the 2.55 μm and the 4.72 μm transitions. This was believed to be primarily by competition for the upper level population. The kinetics of BVLs for the majority of their laser transitions are highly complex and far more complicated than for other pulsed metal vapour lasers. There is still a great deal of investigation required to unravel the excitation pathways of even the principal laser transitions.

1.3.5 Upper and Lower Laser Level Kinetic Mechanisms

In later chapters various kinetic mechanisms which are responsible for excitation to the upper laser level and the depopulation of the metastable lower laser level are discussed.

It is the purpose of this section to provide a overview of the known kinetic mechanisms which govern upper and lower laser level populations of BVLs. This section will often be referred to, particularly in Chapters 4 to 6 where the results are used to discuss the influence of buffer gas additives on the laser output power, the temporal evolution of selected laser transitions and various discharge parameters.

This section begins with a discussion of the chief mechanisms which are responsible for excitation to the upper laser levels and then leads onto a discussion of the mechanisms which influence the depopulation of the metastable lower laser levels.

As discussed in Section 1.2.1, excitation to the upper laser levels usually occurs from the ground-state level by direct electron collision in the excitation pulse [16]. Electrons of sufficiently high energy are generated by means of a longitudinal pulsed electrical discharge. The electric field must be of sufficient strength to generate electron energies greater than the minimum required for efficient upper level excitation [19]. This has been found to be around 1.0 eV for excitation to the $6P^1P_1$ energy level [16]. If the electron energy is too low then electron collision with ground-state barium may result in significant population of the lower lying levels (including the metastable levels). Increasing the average electron energy by between 0.5 eV and 1.0 eV above this minimum electron energy has been found to increase the laser output power by a factor of between 10 and 100 [16]. The average electron energy in the excitation pulse is dependent upon the electric field across the tube, E, and the buffer-gas number density, N [19]. Increasing E whilst maintaining N fixed will generate higher electron energies, whereas increasing N whilst maintaining E fixed will reduce the electron energy. It is for this reason that reference is often made to the E/N ratio when discussing the electron energy in the excitation pulse.

The buffer-gas number density is proportional to the buffer-gas pressure. The electric field which may be generated across the discharge tube is strongly dependent upon the discharge tube impedance and consequently on the electron density at the beginning of the excitation pulse. A high discharge tube impedance (corresponding to a low electron density) at the beginning of the excitation pulse aids in the generation of a high electric field

across the discharge tube [27]. The discharge conditions which lead to a high tube impedance are dependent upon a number of factors and are discussed as follows.

Immediately after the excitation pulse, when the electric field across the tube has fully collapsed, elastic collisions between electrons and the buffer-gas atoms reduce the average electron energy (often referred to as electron temperature). It is at these times ($\leq$0.5 μs) that the rate of electron cooling is at its fastest [28]. At later times ($\geq$0.5 μs) in the interpulse period, the rate of electron cooling decreases until the average gas temperature of the buffer gas is reached [28]. Electron-ion recombination takes place during the interpulse period. However, because electron ion recombination is a three-body recombination process whose rate is inversely proportional to a power of the electron temperature ($T_e^{-9/2}$, where T_e is the electron temperature), initially the rate of recombination is slow and becomes faster as the electron temperature reduces (ie at later times) [29].

There are two main factors which influence the electron cooling rate. The first is the buffer gas pressure [30]. Increasing the buffer gas pressure will increase the electron buffer-gas collision frequency. The second factor is the type of buffer gas used [30]. The efficiency of energy transfer for an elastic collision is inversely proportional to the mass of the buffer gas [27]. In addition, a buffer gas with a low atomic mass is likely to have a larger electron collision cross-section for momentum transfer than a buffer gas with a high atomic mass [31] and consequently will have a larger electron collision frequency.

The metastable lower laser levels are depopulated primarily by elastic collisions with electrons in the discharge afterglow. It is therefore important to cool the electrons as efficiently as possible for rapid metastable depopulation as well as for fast recombination. As discussed in Section 1.3.3, in the interpulse period the metastable population is depopulated at a rate which is comparable to the electron cooling rate and consequently a buffer gas which efficiently cools electrons will also efficiently depopulate the metastable lower laser level. Mildren *et.al.* [32] investigated the role of the buffer gas on the metastable population in the interpulse period, and in particular the influence on metastable population of H_2 additives in a neon buffer gas. In this particular study it was found that

one of the main effects of H_2 addition to a neon buffer gas was to significantly decrease the metastable population to values which were more comparable to those when only a helium buffer gas was used. In addition, when only neon was used as the buffer gas, the metastable population was higher than that expected from the average gas temperature, a phenomenon not observed when either a helium buffer gas was used or indeed when a neon buffer gas was used with H_2 additives.

Because the metastable lower laser level for the 1.50 μm transition is significantly higher than that of the 1.13 μm transition, depopulation of the 1.50 μm metastable lower laser level begins before that of the 1.13 μm transition. Indeed, the metastable lower laser level for the 1.13 μm transition is of low enough energy that it may easily become thermally over populated (assuming a Boltzmann population distribution). The metastable lower laser level population is greatest on-axis [33]. This is caused by higher excitation there during the pulse, and in the interpulse period the thermal gradient across the bore of the tube (which is greatest in the centre of the tube) results in a greater thermal population of the metastable levels on the tube axis. In addition, the high on-axis gas temperature reduces the on-axis neutral number density, thereby raising the on-axis E/N ratio which will affect the degree of ionization and upper level excitation there [33].

A number of the laser transitions share either common upper or lower laser levels which can lead to competition between the transitions [23]. For example, the 1.13 μm and 1.50 μm laser transitions share a common upper level but have different lower laser levels. Laser oscillation at 1.50 μm occurs first because this has the higher stimulated emission cross-section which thereby depletes the upper laser level and inhibits laser oscillation at 1.13 μm [23]. Only when the 1.50 μm lower laser level becomes sufficiently populated can a threshold inversion for the 1.13 μm transition be established and laser oscillation at 1.13 μm then commence. The effects of adding H_2, D_2 and He to the Ne buffer gas are described in Chapters 4 and 5, and provide some interesting results since the effects of the additives are believed to change the metastable lower laser level population by increasing the electron cooling rate in the interpulse period and hence change the competition between these two laser transitions.

1.4 Inclusion of Hydrogen in the Buffer Gases of MVLs

1.4.1 Introduction

The increase in the total laser output power and efficiency with the addition of hydrogen to the buffer gas of copper, copper halide and gold vapour lasers has been the subject of a number of reports over recent years [18,37-40]. Increases in laser power and efficiency of over 40% have been obtained when hydrogen was added to otherwise optimum laser discharges with a neon buffer gas. The following section is a review of the effects of hydrogen addition to CVLs, GVLs and copper halide lasers (CHLs) along with recently proposed mechanisms for the observed beneficial effects of adding hydrogen. Because the excitation mechanisms for BVLs are very similar to those of CVLs and GVLs, similar trends should be observed when hydrogen is added to BVLs as has previously been reported for CVLs and GVLs. This study discusses in detail, for the first time, the effects of hydrogen additives to the discharge of BVLs on the laser power, laser pulse waveforms and the tube impedance, and compares the results with the trends observed when hydrogen was added to CVLs and GVLs. Mechanisms are then proposed to explain the effect of hydrogen on the kinetic mechanisms of the BVL.

1.4.2 Preliminary Comments on Copper Vapour Lasers Relavent to a Discussion of the Effects of Hydrogen Addition on Their Performances

As outlined in Section 1.1.1, the laser output power of the first CVLs was limited by the low PRFs (<1 kHz) because of the externally heated oven arrangement adopted. The advent of self-heated lasers significantly raised the operating PRF (to 5-10 kHz) and consequently the laser output power. In the 1970s and 80s laser power and efficiency were further increased by raising the PRF to ~20 kHz by using a vapour of copper halide [38] instead of pure elemental copper vapour as the source of copper inside the laser discharge. The copper halide lasers usually used bromine or chlorine as the halogen, although iodine could also be used.

The working temperature for CHLs was significantly lower than more conventional CVLs, operating over temperature ranges between 500°C and 800°C instead of ~1600°C. The copper halide vapour quickly dissociates by electron bombardment in the pulsed electrical discharge to form copper and halogen atoms [39]. The copper atoms are then excited to the upper resonance levels and undergo the laser transitions in an identical manner to conventional CVLs.

The halogen atoms which form when the copper halide dissociates are strongly electronegative [40] and are able to form negative ions by attaching with electrons in the interpulse period. This can significantly reduce the prepulse free electron density and consequently can increase the discharge impedance, and allow better voltage hold-off and a higher E/N ratio for improved excitation to the upper laser levels. Furthermore, with conventional wide-bore CVLs, laser oscillation begins first at the tube wall and later on the tube axis [41], due to a phenomenon known as 'skin depth' [17]. The presence of electronegative species in the discharge of CHLs greatly reduces the conductivity of the plasma prior to each pulse by the formation of negative ions and accelerated electron-ion recombination processes. This may be particularly pronounced at or near the tube axis and can reduce or eliminate the 'skin depth' phenomenon because of the increase in the bulk tube impedance.

1.4.3 Hydrogen Additives; A Historical Development

It was only in 1985 that Astadjov *et al.* [34] first reported the influence of hydrogen addition to the neon buffer gas of a CHL. The discovery was made whilst they were investigating sealed-off CHLs with the aim of increasing the laser tube and laser load lifetimes. Their first sealed-off laser had a number of impurities present within the discharge, including H_2, CO and CO_2. When the laser was modified by improving the purity of both the electrodes and the laser tube, the total laser power was found to be significantly reduced. The laser was operated utilising a flowing neon buffer gas to decontaminate the laser tube further, during which it was found that both the laser power and laser efficiency decreased with time until a steady state value was reached. This

indicated that an impurity within the laser tube was enhancing the laser power and efficiency. Using a clean laser tube, hydrogen was slowly added to the neon buffer gas, whereupon laser power rapidly increased, by around 100% with the addition of 0.2 torr hydrogen to a neon buffer gas at a pressure of 16 torr.

Following these preliminary findings, similarly large increases in both total laser output power and laser efficiency were observed in both conventional CVLs [35] and also GVLs [18]. In the case of GVLs, the laser power increased by as much as 60% when between 0.5 and 1.0 torr hydrogen was added to a neon buffer gas. Sections 1.4.4 - 1.4.9, which follow, are concerned with a more detailed discussion of the effects of hydrogen on the operating conditions of CVLs and GVLs, and proposed kinetic mechanisms.

1.4.4 Effects of H_2 Addition on Discharge Tube Impedance

The addition of small amounts of hydrogen to the neon buffer gas of CVLs and GVLs has a pronounced effect upon the discharge tube impedance. This is reflected by a marked decrease in the tube current and an increase in the tube voltage with hydrogen addition. For example, the effect of the addition of 0.3 torr hydrogen to 15 torr neon on a copper bromide laser [37] was to increase the peak tube voltage from ~8 kV to ~11.3 kV and to decrease the peak tube current from ~215 A to ~170 A. In this example the laser power increased from ~3.4 W at 0.3% efficiency to ~9.3 W at 1.1% efficiency. There was also an observed increase in the delay between the beginning of the voltage and the beginning of the current pulse (from 25-40 ns) with hydrogen addition. This was believed [37] to lead to higher average electron energies in the excitation pulse and hence an increase in the excitation rate to the upper laser level. Both the resistive component to the tube voltage and the laser tube resistance generally increased with increasing hydrogen partial pressure (see Section 3.8).

In order to investigate whether the increased laser power with hydrogen addition was solely a result of the increased tube impedance, helium was used to replace the hydrogen. Helium was selected because the mass and hence electron collision cross-section

for momentum transfer is much closer to hydrogen than many other gases. It is also a very inert gas and does not react with either copper or bromine. Helium partial pressures ranged from 0.5 to 5 torr helium in 15 torr neon. In all cases, the laser power decreased with increasing helium pressure. Helium addition did, however, increase both the tube voltage and the discharge tube impedance. It therefore seemed unlikely that the sole reason for the increase in laser power with hydrogen addition was increased plasma impedance. The increase was more likely to be due to the atomic and/or molecular properties of the hydrogen.

1.4.5 Effects of H_2 on Laser Tube Wall Temperature

A further effect of hydrogen addition to the neon buffer gas of CHLs and CVLs is to increase the tube wall temperature [37]. This indicated that there was improved matching between the charging circuit and the laser tube resulting in more efficient energy transfer.

1.4.6 Metastable Depopulation and Plasma Recombination

As discussed in Section 1.2.2, it is essential to depopulate the metastable lower laser level prior to the next excitation pulse. With the exception of narrow (≤2-3 mm) bore tubes, metastable depopulation in CVLs and CHLs is predominantly by collisions with low energy electrons. In the discharge afterglow, electrons lose their energy either by wall collisions (dominant for narrow bore tubes) or elastic collisions with buffer gas atoms [17]. The ability of the buffer gas to cool electrons is dependent upon the mass of the buffer gas atoms/molecules with the energy transfer efficiency being inversely proportional to the relative atomic mass of the buffer gas [27]. It is also dependent upon the collision cross-section for momentum transfer, σ_m, which is dependent upon the electron energy (see Equations 3.12-3.14 in Chapter 3). Atoms and molecules such as hydrogen and helium generally have much larger cross sections than heavier atoms and allow the highest fractional removal of energy from electrons, and hence are more efficient at cooling electrons than others.

The addition of small quantities of hydrogen to a neon buffer gas can significantly increase the total collision frequency υ_c, because of the vast differences in the relative sizes of σ_m for atomic and molecular hydrogen to that of neon. For example, by substituting the values of σ_m for atomic hydrogen and neon (described by Equations 3.12 and 3.13) into Equation 3.15 to evaluate υ_c, the addition of 1.5 torr hydrogen to 50 torr of neon was found to increase υ_c by ~100% (assuming an electron energy of 0.2 eV in the discharge afterglow).

One of the possible mechanisms limiting the maximum PRF in CVLs and BVLs is too high a population of the metastable lower laser levels at the beginning of each excitation pulse [15]. Under these circumstances, the addition of small amounts of hydrogen may increase the maximum permissible PRF by cooling the electrons more rapidly in the interpulse period and hence decrease the time required to reduce the metastable level population by collisions with low energy electrons.

Another possible mechanism which may limit high PRFs is the prepulse free electron density [10]. Electron-ion recombination in the discharge afterglow is strongly dependent on the electron temperature [29] (rate $\propto T_e^{-9/2}$ for three body recombination), and hence the increased collision frequency with hydrogen addition (which leads to more efficient electron cooling) will also result in a reduction of the prepulse free-electron density.

When a high temperature CVL operates under conditions for maximum laser power the laser beam profile usually has a characteristic 'flat top' intensity profile. Increasing the input power further generally results in an increase in the laser power at the walls of the laser tube but a large decrease in the laser power on the tube axis [41]. This is believed to be due to a high metastable lower laser level on the tube axis which reduces the population inversion there. The introduction of hydrogen under such conditions can restore the laser power on the beam axis and also increase the overall laser power [35]. This may be due to one or more of the following (a) enhanced metastable deactivation by collisions of excited copper in the ^2D levels with hydrogen, (b) a reduction in the gas temperature on the tube axis due to the increase in the thermal conductivity of the buffer gas, (c) enhanced

metastable deactivation by collisions with cooler electrons, (d) reduced prepulse electron density by faster recombination involving cooler electrons. Some reports [37] suggest that (b) is not a plausible mechanism.

1.4.7 Formation of H^- Ions in the Discharge Afterglow

The formation of H^- ions was first reported by Lozier [42] in 1930 and later confirmed by Khvostenko [43] and also Schulz [44] in studies using a mass spectrometer. It was found that impurities of either molecular hydrogen or water vapour could result in the formation of H^- ions by electron impact.

The formation of H^- ions in the interpulse period is another possible mechanism for the observed increase in the laser power with the introduction of hydrogen to CHLs for two main reasons. First, the formation of H^- ions reduces the pre-pulse free electron density and hence increases the discharge impedance. This can enhance the upper level excitation by increasing the E/N ratio in the excitation pulse. Second, the electron detachment rate from H^- ions is higher than that from copper [37] and thus in the excitation pulse electron multiplication can occur, partly from the dissociation of H^- ions in preference to ionisation of the copper. This could lead to an increased prepulse neutral copper density and hence higher output powers.

The temporal evolution of the electron density has been analysed [37] by considering the conductivity of the discharge tube during the excitation pulse. The results for this suggest that at the beginning of the excitation pulse the electron density decreases by around one third with the addition of approximately 2% hydrogen. At the peak of the current pulse (occurring ~50 ns after the onset of the current), the electron density is similar with and without added hydrogen, whilst at later times, the electron density is considerably lower with hydrogen present in the discharge. This was all attributed to the formation of H^- ions during the interpulse period.

1.4.8 Rotational and Vibrational Excitation of the H_2 Molecule

Despite a number of reports concerning dissociation rate constants by both electron impact [45] and buffer gas collisions [46], it still remains unclear exactly what proportion of the hydrogen dissociates in the excitation pulse and then reforms in the interpulse period. This is because of the large number of possible mechanisms which could be responsible for hydrogen dissociation and recombination. Some of the data used to evaluate the time evolution of the electron density quoted by Astadjov *et al.* [37], for example the equilibrium constant for the dissociation of hydrogen molecules, were not referenced and therefore could not be used. The presence of molecular hydrogen within the laser tube in the interpulse period would probably lead to electron heating as the hydrogen states relaxed to the gas temperature. This could not explain the beneficial effects of hydrogen addition.

1.5 Summary of Mechanisms

This section is a summary of the excitation and metastable deactivation mechanisms which occur with pulsed cyclic MVLs.

A pulsed electrical discharge through an inert buffer gas is used to accelerate electrons to high enough energies to collisionally excite metal vapour atoms to resonance upper laser levels. Fast excitation to this upper level is required in order to reach the threshold inversion because the resonant upper laser level is relatively short lived. Stimulated emission occurs from this upper resonance level to a metastable lower laser level. Laser oscillation ceases when there is a significant build-up in the population of this lower level.

In the interpulse period, the electrons lose energy by collisions with the buffer gas atoms, metal atoms and ions within the active region. This is important for two main reasons. First, it is primarily electron collision with barium atoms which results in the depopulation of the metastable population. This is essential if a threshold inversion is to be established during the next excitation pulse. Second, the three-body electron-ion recombination rate is dependent upon the electron temperature. Electron-ion recombination is essential in order to raise the tube impedance and thus increase the average electron

energy attained during the next excitation pulse. It is primarily these two factors which limit the upper PRF in MVLs.

The addition of hydrogen to CVLs and GVLs has been found to significantly increase the laser output power and laser efficiency. Proposed mechanisms to account for these increases include (a) enhanced metastable deactivation caused by increased electron cooling, (b) reduced prepulse electron density by faster recombination, (c) reduced prepulse free electron density caused by the formation of negative ions.

1.6 Overview of Thesis

This thesis is divided into seven chapters and six appendices. A brief outline of the contents of each chapter is as follows:

Chapter 2 discusses in detail the excitation circuit developed for the BVL used in this investigation. Also discussed in Chapter 2 are the design considerations for the construction of a reliable BVL. A full description of the final design used in the current investigations is given.

Chapter 3 is concerned with the methods adopted to measure discharge conditions, operating parameters and laser power of the BVL. The chapter also includes calibration curves of the equipment used, and a consideration of the reliabilities of the measurements. A discussion is also made of the method used to evaluate the laser head inductance, temporal energy deposition into the laser tube, and the temporal evolution of the electron density.

In Chapter 4, the results are presented of the effects of varying the percentage of hydrogen, deuterium and helium additives in a neon buffer gas of a BVL. The effects of additives on the total laser power, laser powers at 1.13 μm and 1.50 μm, temporal and spatial evolutions of the 1.13 μm and 1.50 μm laser pulse intensities, discharge tube impedance, temporal energy deposition, and electron density are all discussed.

In Chapter 5, the dependence of total laser power, laser powers at 1.13 μm and 1.50 μm, discharge tube impedance and the temporal evolutions of the 1.13 μm and 1.50 μm laser pulse intensities are examined on the discharge parameters such as charging

voltage, PRF, buffer gas pressure and storage capacitance. The results and trends are compared for only neon as the buffer gas, and a premix of neon and 3% added hydrogen (found in Chapter 4 to be the optimum percentage of hydrogen to give maximum total laser power).

In Chapter 6, the results are presented when helium is the basic buffer gas. The dependences of total laser power, laser powers at 1.13 μm and 1.50 μm, discharge tube impedance and the temporal evolution of the 1.13 μm and 1.50 μm laser pulse intensities are examined on the discharge parameters such as charging voltage, PRF, buffer gas pressure and storage capacitance. Also discussed in Chapter 6 are the influences of hydrogen and deuterium additives on the output characteristics of the laser.

Appendices 2 to 6 are Fortran 77 program listings which were used in Chapters 4 to 6 to analyse the laser pulse data, evaluate the laser head inductance, the temporal energy deposition in to the tube and the temporal evolution of the electron density.

Throughout the text, the term laser power refers to the average laser power of the laser, the peak laser powers are referred to specifically.

1.7 References

[1] 'The Laser Guidebook' J. Hecht, McGraw Hill, New York, pp 162-173 (1988).

[2] Proc. Conference on Lasers and Electro-Optics Europe Technical Digest pp 254 (1994).

[3] H. M. Pask, J. A. Piper, Optical and Quantum Electron. **23** S563-S568 (1991).

[4] J. W. Bethel, PhD Thesis, St Andrews University, UK (1994).

[5] G. R. Fowles, W. T. Silfvast, Appl. Phys. Lett. **6** pp 23-237 (1965).

[6] W. T. Walter, N. Solimene, M. Piltch, G. Gould, IEEE J. Quantum. Electron. **QE-2** (9) pp 474-479 (1966).

[7] A. A. Isaev, M. A. Kazaryan, G. G. Petrash, JETP Lett. **16** pp 27 (1972).

[8] G. L. Clarke, PhD Thesis, University of St Andrews (1988).

[9] P. A. Bokan, Sov. J. Quantum Electron. **16** (9) pp 1207-1214 (1986).

[10] P. A. Bokan, Sov. J. Quantum Electron. **16** (8), pp 1041-1046 (1986).

[11] A. A. Isaev, V. V. Kazakov, M. A. Lesoni, S. V. Markova, G. G. Petrash, Sov. J. Quantum Electron. **16** (11) pp 1517-1521 (1986).

[12] 'American Institute of Physics Handbook', 3rd edition, New York (1972).

[13] G. G. Petrash, SPIE **1225** pp 216-227 (1990).

[14] T Holstein, Phys. Rev. **72** (12) pp 1212-1233 (1947).

[15] V. V. Kazakov, S. V. Markova, G. G. Petrash, Sov. J. Quantum Electron. **14** (5) pp 642-647 (1984).

[16] V. M. Batenin, S. V. Kalinin, I. I. Kilmovskii, Sov. J. Quantum Electron. **16** (11) pp 1475-1479 (1986).

[17] M. J. Kushner, B. E. Warner, J. Appl. Phys. **54** (6) pp 2970-2982 (1983).

[18] Z. G. Huang, H. Y. Shan, Y. Huo, H. Wang, Appl. Phys. B **44** pp 57-59 (1987).

[19] H. M. Pask, J. A. Piper, J. Appl. Phys **72** (12) pp 5545-5554 (1992).

[20] P. A. Bokhan, Sov. J. Quantum Electron. **15** (5) pp 622-626 (1985).

[21] Ph. Cahuzac, Phys. Lett. **32A** (3) (1970) pp 150-151.

[22] A. A. Isaev, G. Yu. Lemmerman, S. V. Markova, G. G. Petrash, Sov. J. Quantum Electron. **9** (9) pp 1144-1147 (1979).

[23] H. M. Pask, J. A. Piper, IEEE J. Quantum Electron. **29** (9) pp 2540-2546 (1993).

[24] K. I. Zemskov, M. A. Kazaryan, G. G. Petrash, V. N. Smorchkov, V. P. Timofeev, S. A. Fridman, Sov. J. Quantum Electron. **10** (11) pp 1428-1431 (1980).

[25] 'Metal Vapour and Metal Halide Vapour Lasers' ed by G. G. Petrash, Proc. Lebedeb Physics Institutc, Nova Science, Commack, pp 4 (1987).

[26] A. A. Isaev, M. A. Kazaryan, S. V. Markova, G. G. Petrash, Sov. J. Quantum Electron. **5** (3) pp 285-287 (1975).

[27] M. J. Withford, D. J. W. Brown, J. A. Piper, Opt. Comm. **110** pp 699-707 (1994).

[28] G. H. Hogan, PhD Thesis, Oxford University (1993).

[29] M. S. Butler, PhD Thesis, Macquarie University, Australia (1986).

[30] M. Madigan, L. O. Hocker, J. H. Flint, C. F. Dewey Jr, IEEE J. Quantum Electron. **QE-16** (12) pp 1294-1296.

[31] 'Plasma Physics', J. L. Delcrouix, **2**, Wiley, New York, pp 163-167 (1968).

[32] R. Mildren, Conference on Lasers and Electro-Optics Europe, RAI Conference Centre, Amsterdam (1994).

[33] H. M. Pask, J. A. Piper, IEEE J. Quantum Electron. **30** (10) pp 2376-2384 (1994).

[34] D. N. Astadjov, N. V. Sabotinov, N. K. Vuchkov, Optics Comm. **56** (4) pp 279-282 (1985).

[35] Z. G. Huang, K. Namba, F. Shimizi, Jpn. J. Appl. Phys. **25** (11) pp 1677-1679 (1986).

[36] D. N. Astajov, A. A Isaev, G. G. Petrash, I. V. Ponomarev, N. V. Sabotinov, N. K. Vuchkov, IEEE J Quantum Electron. **28** (10) pp 1966-1969 (1992).

[37] D. N. Astajov, N. K. Vuchkov,N. V. Sabotinov, IEEE J Quantum Electron. **24** (9) pp 1927-1935 (1988).

[38] O. S. Akirtava, V. L. Dzhikiya, Y. M. Oleinik, Sov. J. Quantum Electron. **5** pp 1001-1002 (1975).

[39] A. A. Vetter, N. M. Nerheim, Appl. Phys. Lett. **30** (8) pp 405-407 (1977).

[40] Yu. G. Chernov, IIigh Temp. **8** (5) pp 881-885 (1970).

[41] K. Hayashi, Y. Iseki, S. Suzuki, I. Watanabe, E. Noda, O. Morimiya, Jpn. J. Appl. Phys. **31** pp L1689-1691 (1992).

[42] W. W. Lozier, Phys. Rev. **36**, pp 1417 (1930).

[43] V. I. Khvostenko, V. M. Dukel'skii, Sov. Phys. JETP **6** (33), pp 657-660 (1958).

[44] G. J. Schulz, Phys. Rev. **113** (3), pp 816-819 (1959).

[45] F. G. Baksht, Sov. J. Tech. Phys. **27** (1) pp 1-4.

[46] D. W. Schwenke, J. Chem. Phys. **92** (12) pp 7267-7282.

Chapter 2

Experimental Design

2.1 Introduction

The design of the charging and discharge circuits of CVLs and BVLs is an important consideration because of the requirement for rapid excitation of the barium from the ground state to the upper laser levels. In the case of CVLs, the excitation process to the $^2P_{3/2}$ and $^2D_{5/2}$ upper resonance levels of copper is by high energy (~5 eV) electron collisions with ground state copper. If the excitation rate is too low then a population inversion will not be established because of the generation of low energy electrons which favours excitation to the lower metastable level. If the excitation pulse is too long then energy will be deposited into the plasma after the laser pulse has terminated [1]. This can lead to a reduction in the laser efficiency.

The driving circuit for pulsed cyclic lasers has been the subject of a number of studies over the years [2,3]. This has led to advanced excitation circuits and consequently has been one of the principal factors for the steady increase in laser output powers of such systems. The first half of this chapter is concerned with the charging circuit used for the BVL.

Many of the reports about BVLs outline problems associated with the short lifetime of the laser tubes. This was believed to be caused by the strong corrosive nature and high chemical reactivity of baruim vapour. In the present study, the first BVLs designed and constructed also had relatively short laser tube lifetimes, of between hours to tens of hours

of laser oscillation. Modifications to these preliminary designs extended the laser tube lifetime to several hundred hours of laser oscillation. The second half of this chapter is concerned with the overall design of the BVL.

2.2 Driving Circuits

2.2.1 Resonant Charging

The circuit most often used to drive CVLs and BVLs is the resonant charging capacitor transfer circuit and this was the circuit used throughout this work. This is shown fully in Figure 2.1. This allows a storage capacitor C_s to be charged to twice the supply voltage by resonantly charging through a charging choke, L_c, as shown in Figure 2.1. The time constant, τ, for such a process may be calculated by LCR circuit theory [4] and is described by Equation (2.1), where L is the total charging inductance and C takes the value of the storage capacitance:

$$\tau = \frac{2\pi}{\omega} = \pi\sqrt{(LC)} \qquad (2.1)$$

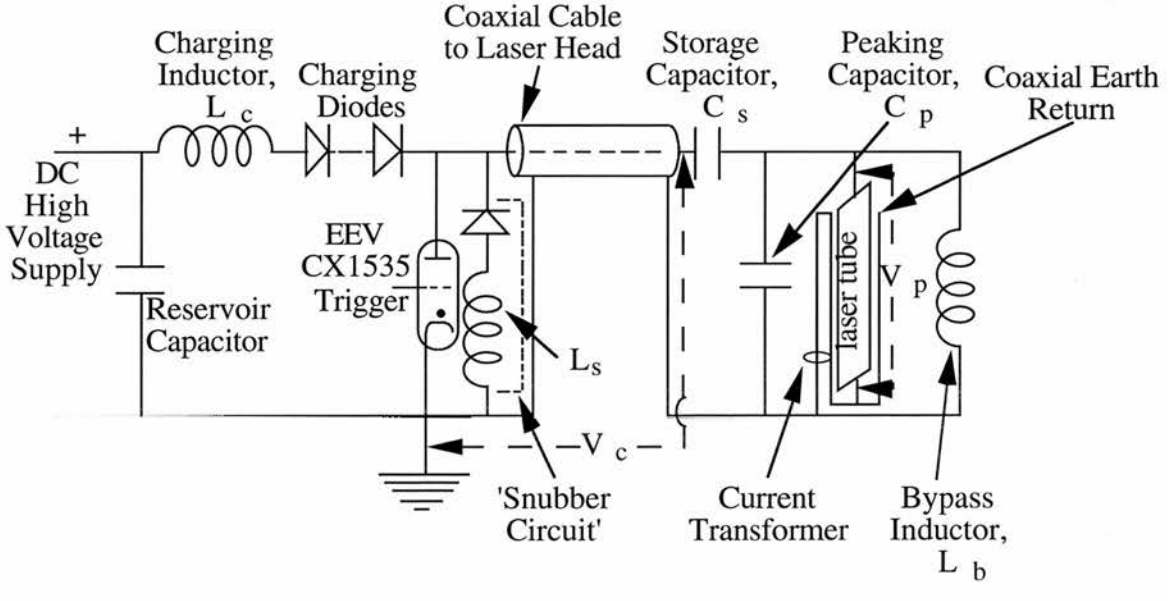

Figure 2.1: The resonant charging capacitor transfer circuit employed on the barium vapour laser.

The pulse recurrence frequency (PRF) is an important factor for the operation of BVLs since this determines the average output power, and also the interpulse period and

hence the time available for the buffer gas to cool the electrons effectively [5]. This is important for two main reasons. First, the PRF controls the degree to which the metastable lower laser levels may be depopulated by collisions with low energy electrons. This is believed to be one of the principal mechanisms limiting the upper PRF of the BVL. Second, the interpulse period controls the degree to which electron-ion recombination occurs and hence the overall laser tube impedance upon application of each excitation pulse. A longer interpulse period allows a longer period of time for collisional processes to cool the electrons and hence will decrease the prepulse metastable population and also decrease the preionisation density. The latter event would tend to increase the laser tube impedance prior to the following excitation pulse which is important for the generation of high energy electrons and hence effective upper level excitation. The PRF for BVLs varies typically from 5-30 kHz with the optimum PRF being dependent upon a number of other operating parameters.

Clearly, in order to be able to vary the PRF over such a wide range of frequencies, the resonant charging condition is insufficient to determine the operating PRF. Consequently a diode chain is often used in series with the charging inductor [1] as shown in Figure 2.1. This rectifies the voltage on C_s and hence allows the laser to be operated over a wide frequency range with an upper limit which is determined by the resonant charging condition. Figures 2.2a and 2.2b show theoretical waveforms which are typical of those obtained with and without a diode chain to rectify the voltage on C_s. In this example, the supply voltage is 6 kV and the waveforms are described by Equation 2.2 with V_1=0 (see below).

Due to the large impedance changes often associated with the breakdown of gas discharge tubes, voltages can ring between the circuit components. In this case, the voltage on C_s will oscillate and swing to a negative values which may typically vary between 0 and 1 kV. In general, thyratrons are unidirectional for current flow (ie similar to diodes) and hence any residual negative voltage will remain on C_s until the beginning of the following charging cycle. The voltage across the storage capacitor, V_s, may be described [1] as a function of time by Equation 2.2:

$$V_s(t) = (V_0 + V_1).[1 - \cos(\omega t)] \qquad (2.2)$$

where V_0 is the supply voltage, V_1 is the initial voltage on C_s, ω is the charging frequency (described by Equation 2.1) and t is the time. From Equation 2.2, it is apparent that if V_1 is non-zero, then C_s is charged to a value in excess of twice the charging voltage by V_1 when the $\cos(\omega t)$ term takes the value of -1, i.e. when the circuit is electrically resonant. The degree of overcharging is dependent upon the impedance of the discharge tube and hence on the discharge conditions (such as pressure). This can lead to voltage instabilities due to the fluctuations experienced with the initial value of V_1 on charging.

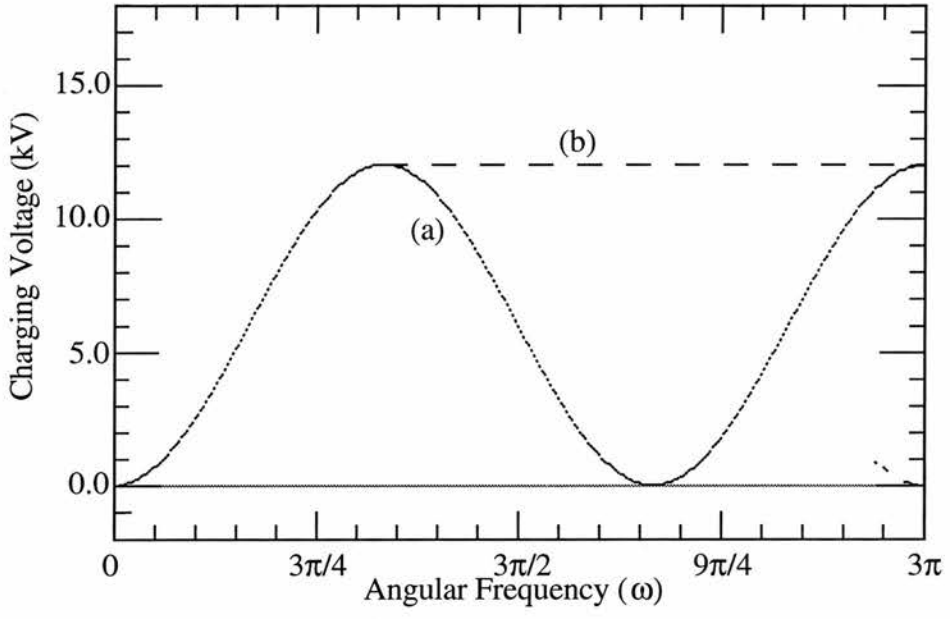

Figure 2.2: The resonant charging condition for a supply voltage of 6 kV. (a) V_1=0, (b) V_1=0 with rectifying diodes on C_s.

The incorporation of a 'snubber' circuit in the charging circuit [3] reduces charging voltage instabilities on C_s. The snubber is also shown in the circuit of Figure 2.1 and consists of a second high-voltage diode chain in series with an additional inductor, L_s. These are positioned in parallel with the thyratron as shown. With the inclusion of this circuit, the capacitor C_s is only discharged through the snubber circuit when there is a polarity reversal on the coaxial cable side of C_s. The upper value for L_s is governed by the

LC time constant for the snubber circuit which is also given by Equation 2.1 and must be significantly less than the time constant for the resonant charging condition. This is done so that C_s will be properly discharged before main charging begins each time. The ratio of L_c to L_s ranges typically between 3 and 5 to 1. The lower value for L_s is governed by the requirement for the thyratron anode to swing negative after forward conduction to enable the thyratron to recover properly. Under some discharge conditions, the impedances of the charging circuit and the discharge tube were well matched and the negative overswing on the thyratron was small, which tended to prevent the thyratron from recovering. When this occurred, the snubber circuit was removed, helping to extend the period of the negative overswing.

The resonant charging supply circuit used for the BVL is described as follows. A storage capacitor C_s was resonantly charged through a by-pass inductor, L_b, to a voltage $\sim 2V_o$, as described by Equation 2.2. This was then periodically discharged by electrically 'shorting' to ground by means of a thyratron switch. The purpose of the by-pass inductor was to keep to a minimum the current flow through the discharge tube during the resonant charging cycle (ie, the interpulse period). The correct selection of L_b is important since if it is too high then the possibility exists that current flowing through the laser tube in the interpulse (charging) period may begin to inhibit electron-ion recombination processes and hence reduce the discharge tube impedance [6]. The lower limit to the value of L_b is the value below which a significant proportion of the stored energy begins to pass through L_b instead of the laser tube during the discharge cycle. It was found that when the laser tube was cold or contaminated, the tube impedance was significantly higher, leading to an increased current flowing through L_b, causing it to heat. Under such conditions, the tube current was very small and the tube voltage oscillated with a time constant given by the values of C_p and L_b. As the laser tube warmed up and barium began to enter the discharge, the tube impedance fell, causing the tube current to increase and the current flowing through L_b to reduce. A variety of bypass inductances was tried under discharge conditions close to optimum for laser output power in order to establish a range of values for L_b. The results for this examination are discussed at length in Section 4.2.1. In summary,

however, no difference was observed in either the laser power or the laser tube impedance for values of L_b ranging between 100-300 μH.

2.3 Thyratron Considerations

Pulsed power driving circuits incorporating either spark gaps or thyratron switches for gas discharge lasers have been well documented over the years. For high repetition lasers such as CVLs and BVLs which operate between 5-20 kHz, spark gaps are inappropriate because the minimum interpulse period for such devices is only of order 250 μs, which is significantly higher than that required for efficient laser operation [7]. Most excitation circuits use a thyratron as the switch for which interpulse periods as short as 10 μs are possible.

2.3.1 Hydrogen Thyratrons [8]

The hydrogen thyratron consists of an anode and a cathode which are spatially separated and sealed within a vacuum-tight ceramic or glass envelope. A low-voltage external heater is used to heat a hydrogen reservoir contained within the envelope to establish a hydrogen pressure of several hundreds of millitorr between the anode and cathode region. In the non-conducting state, the thyratron operates to the left of the Paschen curve and thus there is electrical isolation between the anode and cathode for potential differences up to the breakdown potential, which is governed by both the anode-cathode spacing and the hydrogen pressure. Positioned between the cathode and anode are control grids which enable the conducting state of the thyratron to be controlled by the application of a pulsed 'triggering' voltage. This causes the gas to break down between the cathode and the grids which in turn allows the whole region between the anode and the cathode to become conducting. When the anode voltage has collapsed, rapid e^- / H^+ recombination returns the thyratron to its initial non-conducting state. The rate of recombination and hence the thyratron recovery may be enhanced by reverse biassing the anode with negative voltages on a time scale which is small compared to the resonant charging cycle.

2.3.2 The CX1535 Thyratron [9]

The thyratron used throughout the current work on the BVL was the type CX1535 manufactured by EEV Ltd. The high power, large voltage hold-off (up to 20 kV) and the high switching frequencies (up to 100 kHz) make it ideal for high repetition rate pulsed cyclic lasers. In order to maximise the reliability of the thyratron in terms of both failure to recover ('latching') and thyratron lifetime, the manufacturer's specified operating recommendations were carefully adhered to. These are shown in Appendix (I).

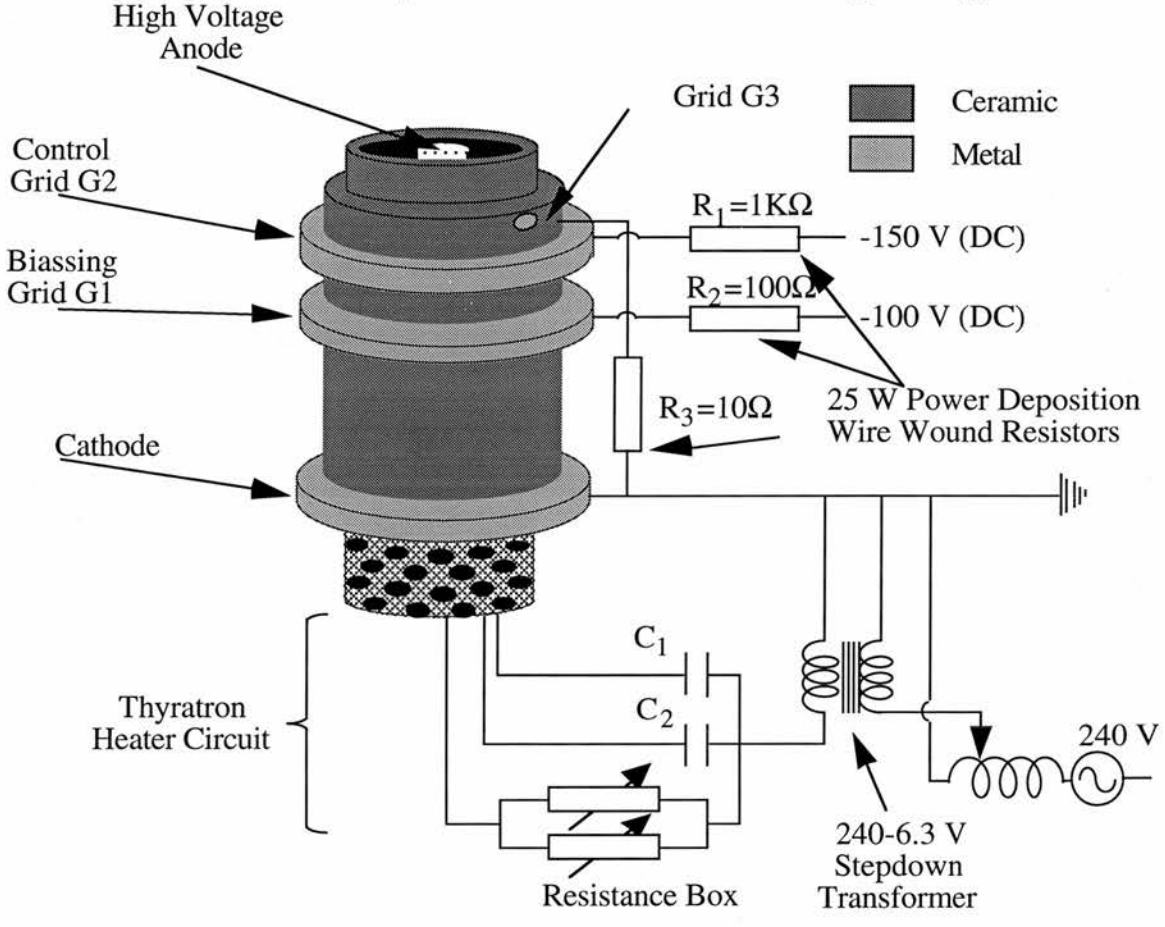

Figure 2.3: CX1535 thyratron showing the electrical connections to both the heater and the grids.

The CX1535 thyratron has a 3 grid structure. The first grid, G1, was maintained at a negative dc voltage with respect to the cathode at around -100 V, which created a dc discharge between G1 and the cathode of current ~0.1 A. The second grid G2 is known as the control grid. This was negatively biassed by -150 V which effectively shielded the region of plasma between G1 and the cathode from the positive anode voltage thereby ensuring that the thyratron remained non-conducting. When positive voltages in excess of

1000 V with a pulse duration greater than 0.5 μs were applied to G2, the thyratron was triggered into conduction by accelerating electrons from the plasma between the G1/cathode region towards the anode. The final grid, G3 was maintained at the cathode voltage by linking the two together with a 10 Ω resistor. G3 aids in high repetition rate operation by reducing the capacitance between the anode and G2.

An EEV sub-modulator unit was used to provide the voltage requirements for G1 and G2 and, as recommended, resistances of 1 kΩ and 100 Ω were used to link the sub-modulator unit to the grids G1 and G2 respectively. Figure 2.3 shows the electrical configuration used.

2.3.3 Thyratron Heater and Oil Cooling

The thyratron heater is required to heat a hydrogen reservoir bulb to control the hydrogen pressure within the vacuum tube. This vapour pressure dictates not only the voltage hold-off between the cathode and the anode, but also the overall conduction properties of the thyratron, which affects the anode fall time.

As recommended by EEV [9], the voltage supplied to the thyratron heater was maintained at 6.3 (±0.1) V and was supplied using a step-down transformer and variac. Both the transformer and variac were rated to 30 VA. On later CX1535 models, the heater current can be controlled separately from the supply voltage by means of a variable resistance box connected in parallel to the heater element. When the older model thyratron finally had to be replaced, the resistance box for the new thyratron was set to 6.4 Ω.

This additional external resistance box provides a better control of the hydrogen pressure and hence of the operating regime of the thyratron. For example, lower reservoir heater voltages and hence lower gas pressures increase the anode/cathode voltage hold-off, but reduce the recovery time. In addition, low gas pressures also restricts the maximum permissible rate of rise of current because of the reduced number of charge carriers. Higher reservoir heater voltages increase the maximum permissible rate of rise of current and increase the thyratron recovery time but reduce the voltage hold-off. Hence, there is a trade-off between all these parameters. As hydrogen was slowly lost through diffusion and other

processes, the value of the resistance box was changed in order to maintain the optimum hydrogen pressure for a given set of conditions. An indication of the need to change the heater resistance was when the thyratron anode fall time began to increase over the course of the thyratron lifetime (from 30 to 40 ns).

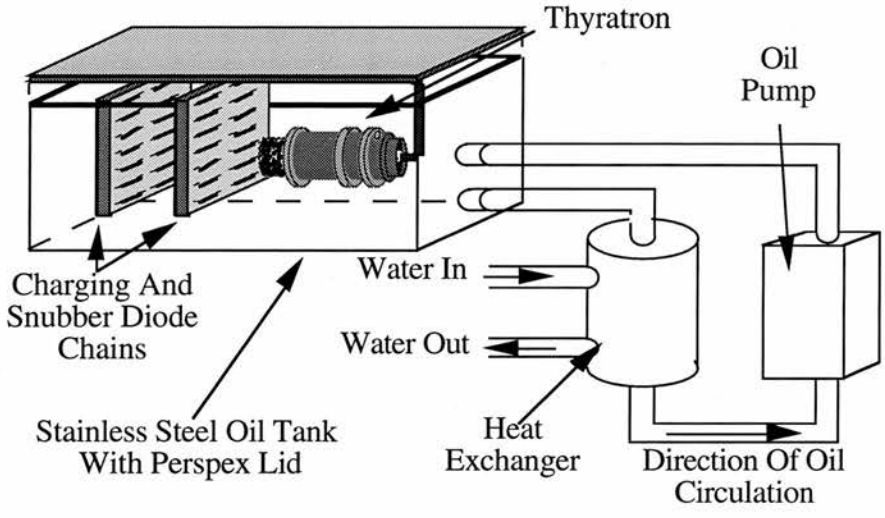

Figure 2.4: Oil tank used to cool the thyratron, charging and snubber diodes.

The thyratron accounted for up to 30 % of the electrical losses in the laser discharge loop, leading to significant heating of the thyratron anode. In the case of the CX1535, if the temperature of the anode were allowed to exceed 200°C, then the brazed anode could be damaged beyond repair. In order to prevent excessive anode heating, the thyratron, charging diodes and snubber diodes were all oil cooled by housing them within the oil tank which is shown schematically in Figure 2.4. The oil (Shell Diala BG) was circulated through the tank by a rotary pump (Totton Pumps) with the cool oil being directed into the anode 'cup' to prevent localised heating caused by 'stagnant' regions of oil. A water/oil heat exchanger was sufficient to cool the oil contained within the tank. Due to the relatively high dielectric constant of Diala BG, the oil also served as an effective medium to prevent electrical arcing from the high voltage components to ground.

2.3.4 Thyratron Recovery

Prior to each excitation pulse it is important for the thyratron to recover to its non-conducting state. As outlined in Section 2.2.1, if the thyratron anode is allowed to swing negative for a short period of time then recovery can be significantly enhanced. According to the manufacturer's specifications, the minimum time required for a CX1535 to recover is ~5 μs and consequently this governs the lower limit for the value of the charging inductor L_c, which needs be large enough to prevent the charging of C_s within this time period.

2.3.5 Capacitor Transfer Circuits

Due to the transient nature of the population inversion in BVLs, it is important to excite the laser using fast risetime current and voltage pulses. One method commonly [1] used to increase this risetime is to incorporate a peaking capacitor, C_p, in the resonant charging circuit, as shown in Figure 2.1. The ratio of the values for C_s to C_p commonly used with CVLs and BVLs typically ranges between 2:1 and 3:1. When the ratio is larger than 1:1, the efficiency of energy transfer from C_s to C_p decreases with increasing ratio. However, because the tube tube voltage enhancement increases with increasing ratio, there is a trade-off between the energy transfer efficiency and the current risetime. In addition to this, the optimum ratio for C_s:C_p is likely to depend upon the particular excitation conditions because of impedance matching. In order to keep the number of variable parameters to a minimum, the ratio was maintained at 2:1 throughout which is that found to be close to optimum for many other pulsed metal vapour lasers.

When there are two capacitors present in the excitation circuit, current is supplied to the laser tube from both C_s and C_p. This may cause a great deal of voltage oscillation due to resonances around both the discharge and thyratron loops, which often results in a characteristic double peaked current pulse [6]. The first peak is caused by energy being deposited from C_p and the second caused by energy deposition from C_s. They occur at different times because of the larger inductance path from C_s to the laser head compared with the C_p loop. Although the current in the second peak is sometimes quite significant, the energy being deposited is only small because the delay is such that the tube voltage has

(or has nearly) fully collapsed. The capacitor C_p is nearly always mounted as close to the laser tube as possible in order to keep the inductance of the discharge loop to a minimum and hence achieve the fastest risetimes.

2.4 Apparatus Design

2.4.1 Power Supply

The high voltage supply was a Converter Power RCS-6000 switch-mode unit, capable of producing up to 10 kV with a maximum 'continuous' power delivery of 6 kW. The supply was short circuit protected which prevented overload of the supply when the thyratron latched (failed to recover), and was also open circuit protected. The supply was used to charge a large reservoir capacitor (40 kV, 1 μF) through a 200 Ω charging resistor from which only small quantities of charge were drawn. The storage capacitor, C_s, was charged through a 150 mH charging choke (TEC Ltd) and the voltage rectified using BYW96E high-voltage diodes. A value of 150 mH was selected for the bypass inductor by considering the LC time constant and the required repetition frequency (9 kHz) for the laser (assuming a 2 nF storage capacitance). This is discussed more fully in Section 2.2.1. Since each diode was only rated to 800 V, 50 diodes were placed in series to rectify the voltage on C_s. These diodes were oil cooled in the same tank as the thyratron.

A 30 mH choke (TEC Ltd) in series with a further fifty BYW96E high-voltage diodes was used as the snubber, positioned in parallel with the CX1535 thyratron to ensure that C_s charged from zero volts each time. As discussed in Section 2.2.1 ,this value was selected to be a fifth of the value for the charging inductor.

A high-voltage coaxial cable of length 1.25 m linked the thyratron anode to the laser mounted storage capacitors. The storage and peaking capacitors (Murata) were rated to a maximum of 30 kV and were kept at a ratio of 2:1. After a period of time switching high voltages, the storage and peaking capacitors tended to become hot. This was found to reduce the values of the capacitances by as much as 20 to 30% (discussed in Section 3.7). It was these 'hot' capacitance values which were used to evaluate the input energy to the laser.

2.4.2 Laser Head Inductance

The requirement for fast (50-100 ns) current risetimes necessitated careful consideration of the geometrical design of the laser discharge circuit. In common with other electrical systems which have a time dependent current, the pulsed gas discharge tube used in BVLs has an inductance which is primarily governed by the geometry of the tube [10]. The most effective way of reducing this inductance (called the laser head inductance), L_{head}, is to use a coaxial earth return geometry as shown in Figure 2.5. The inductance of such an arrangement, L_{coax}, is given by

$$L_{coax} = \frac{\mu_0}{2\pi} \ln\left(\frac{r_2}{r_1}\right) \quad (Hm^{-1}), \tag{2.3}$$

where r_1 and r_2 are the radii of the inner and outer conductors respectively. It has been assumed in Equation 2.3 that there is uniform conductivity over the bore of the discharge tube, (a good approximation for high temperature CVLs and BVLs with relatively small bore tubes, where the skin depth is not a problem [11]). The diameter of the internal and external conductor diameters is r_1 and r_2 respectively.

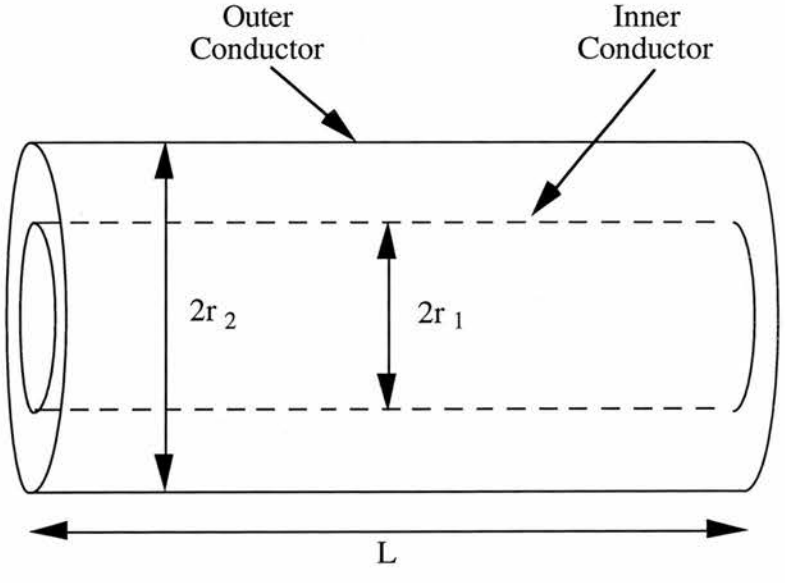

Figure 2.5: Coaxial geometry showing the inner and outer conductors.

This geometry (assuming uniform conductivity) gives the lowest value possible value for L_{head}; any variations from this arrangement lead to an increase in the value for the inductance.

2.4.3 Plasma Inductance

There is also an inductance associated with the plasma itself [10]. This inductance (the plasma inductance), L_p, is dependent upon the electron density n_e, as shown by Equation 2.4:

$$L_p = \frac{dm_e}{A e^2 n_e} \qquad (2.4)$$

where d and A are the discharge length and cross sectional area respectively; e and m_e are the charge and mass of an electron respectively. The inductance, L_p is time dependent because of the dependence on n_e. However, all the other factors are independent of time. The temporal dependence of n_e in the discharge tube for CVLs has been reported and varies typically by between 3 and 4, increasing from a minimum value of ~4.0×10^{19} m^{-3} in the interpulse period [12]. Substituting this value for n_e in Equation 2.4 gives a maximum plasma inductance of ~1 nH (where d=0.7 m and A=42×10^{-5} m^2 were used (see Section 2.5.5). This is small in comparison to the value of 200 nH estimated for L_{head} (by assuming a coaxial geometry) and hence was neglected in calculations involving L_{head}.

2.5 Laser Tube Designs

2.5.1 Introduction

A number of different BVL tubes were constructed before the final design discussed in Section 2.5.5 was implemented. In common with other studies [13] of the BVL, the main problem associated with each of the earlier designs was the lifetime of the laser tubes which typically varied between 10 and 20 hours of laser operation. The lasers described in Sections 2.5.2 and 2.5.3 only had lifetimes of approximately 3 hours.

2.5.2 Narrow-Bore BVL

The first laser constructed was a narrow-bore tube BVL which is shown schematically in Figure 2.6. This consisted of an alumina tube (Alsint 99.7% pure) of dimensions 12 mm internal diameter and 300 mm length which was used to confine the discharge. Copper wire was used to position the alumina tube centrally inside a quartz outer tube. The tube was insulated externally by wrapping Saffil alumina fibre mat around the quartz outer tube. The discharge tube was 'cleaned' by the discharge cleaning method using a fast buffer-gas flow rate, as discussed in Section 3.11.1. Once the tube was 'clean', small pieces of prepared barium (see Section 3.11.2) were positioned at regular intervals (~30 mm) along the length of the alumina tube.

2.5.3 Sapphire Laser Tubes

The second BVL constructed used sapphire tubes to contain the barium vapour. This design is shown schematically in Figure 2.7. At this stage the cracking of the alumina was believed to be due to the highly corrosive nature of the barium vapour on the alumina tube walls. Sapphire was used instead of alumina because of its increased resistance to chemical attack [14].

Two sapphire laser tubes, each of internal diameter 6 mm and 100 mm long, were positioned end to end inside a close fitting alumina tube which in turn was positioned centrally within an outer quartz tube. Saffil alumina fibre insulation was wrapped around the outside of the quartz tube. The laser tube was cleaned by the discharge cleaning technique discussed in Section 3.11.1. Pre-cleaned barium pieces were positioned at regular intervals (~30 mm) inside the sapphire tube. Unfortunately the lifetime of the sapphire laser tubes was considerably shorter than when alumina tubes were used. Figure 2.8 shows a photograph of the sapphire laser tubes used after only 2-3 hours of laser operation. A number of the cracks were believed to be due to thermal stress caused by temperature cycling. However, the pattern produced on the inner face of each sapphire tube was believed to be caused by chemical attack from the barium vapour, because a similar effect was caused by the action of barium vapour on quartz.

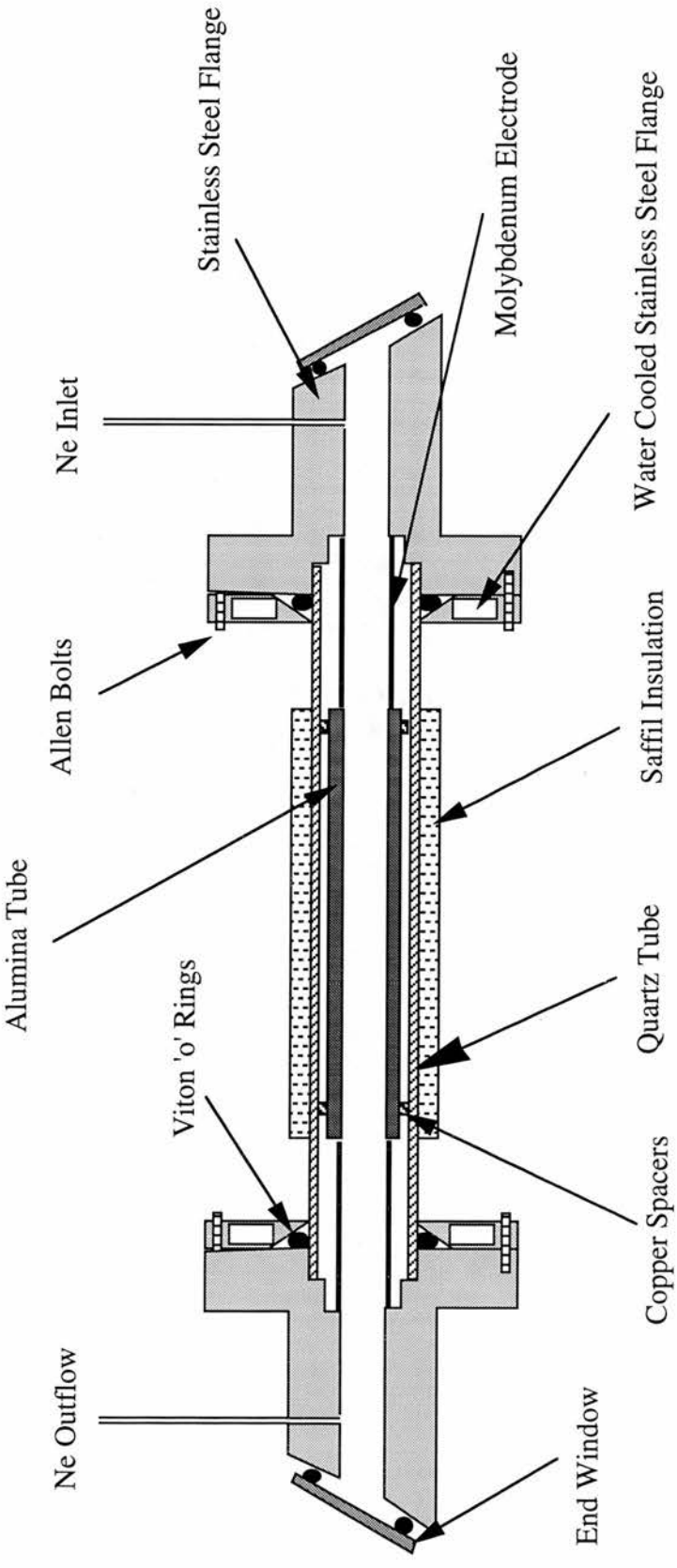

Figure 2.6: Narrow-bore barium vapour laser

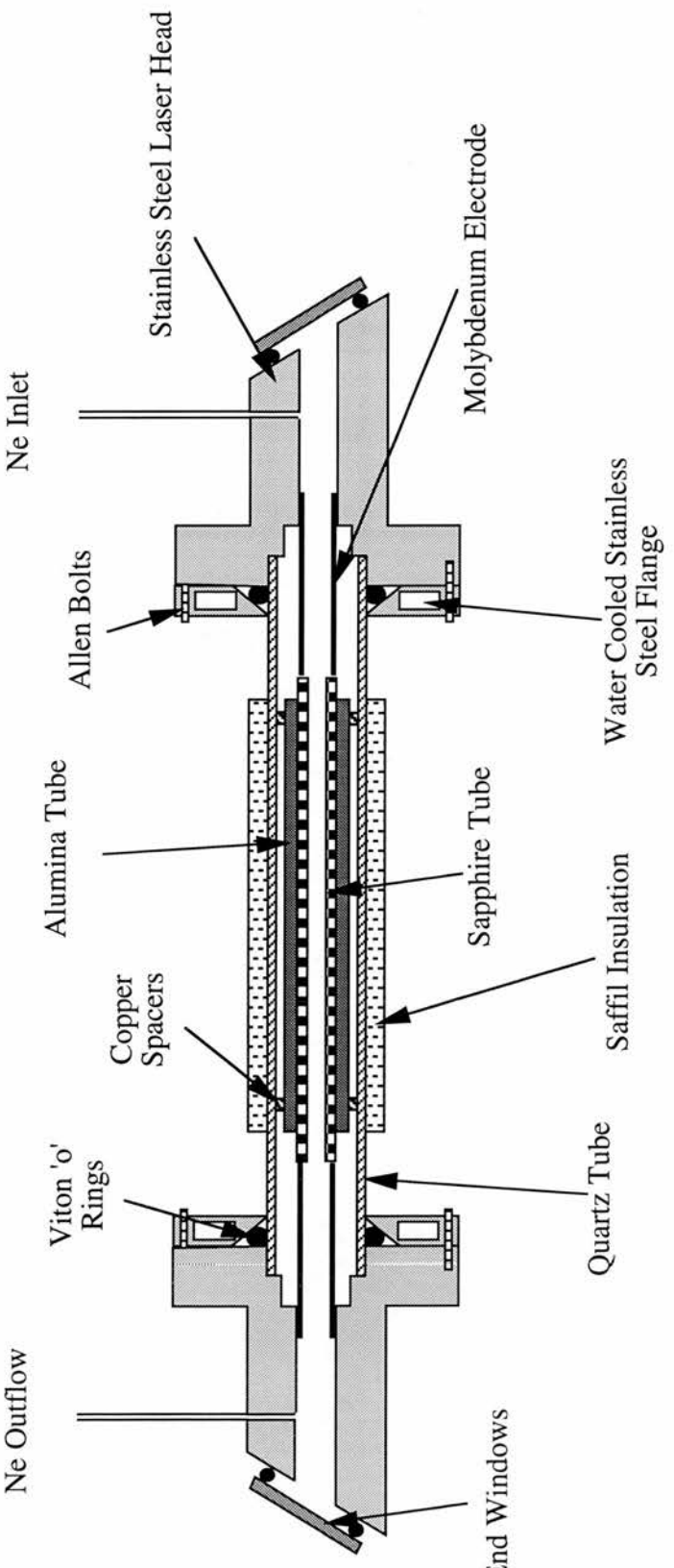

Figure 2.7: Barium vapour laser using sapphire laser tube

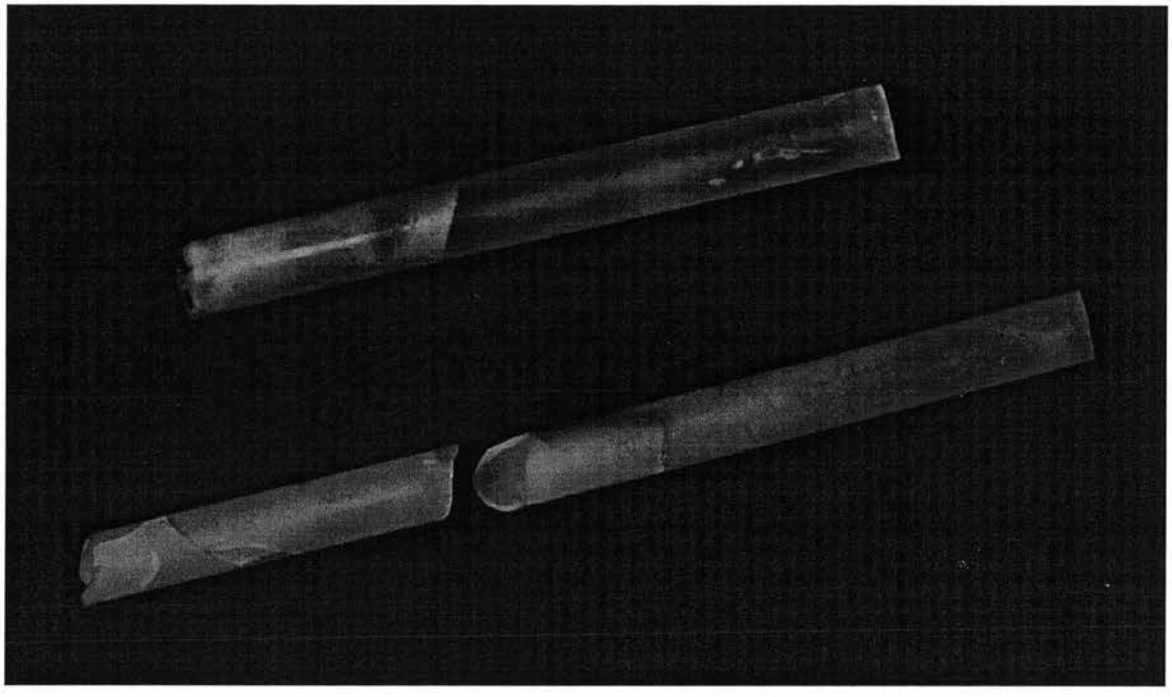

Figure 2.8: Photograph showing the sapphire laser tubes after 2-3 hours of laser operation.

2.5.4 BVL with Molybdenum Rings

Reports indicate that if the liquid barium is confined inside tantalum boats [15] which are regularly spaced along the inside of the alumina tube then the laser tube lifetime may be extended to up to 80 hours. This led to a third design consisting of 8 molybdenum rings each of length 15 mm, spaced equidistant along the inside of an alumina tube as shown in Figure 2.9. Each ring was cupped on the bottom to prevent liquid barium from spilling out onto the alumina. The alumina tube had an internal diameter of 23 mm, an external diameter of 31 mm and was 700 mm in length. Zirconia fibre insulation (discussed in Section 2.6.1) was wrapped around the outside and then centrally positioned inside an outer quartz tube. After the tube had been cleaned by discharge processing (discussed in Section 3.11.1), one piece of cleaned barium was positioned inside each ring. The main problems encountered with this design came from the difficulty of loading

the barium on to the rings. The barium either oxidised too quickly or was accidentally knocked out of the molybdenum boats during the loading process.

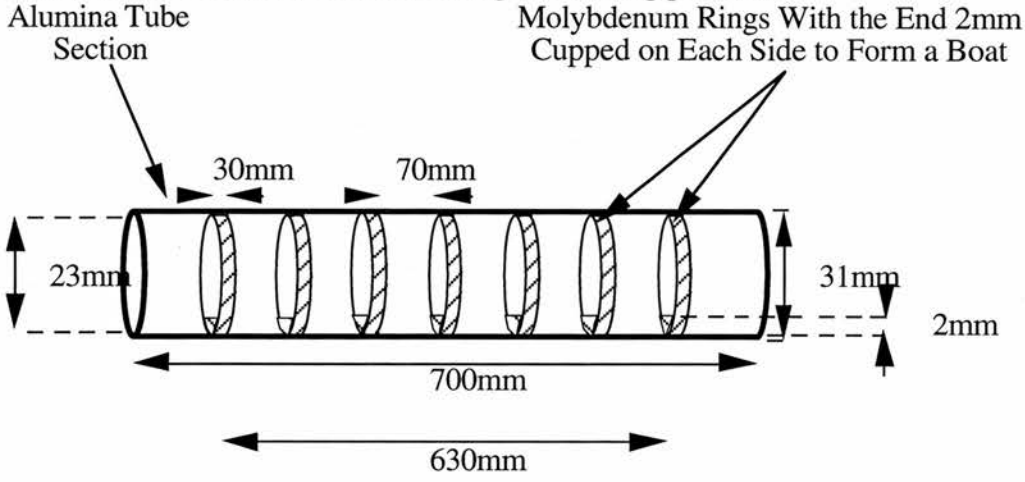

Figure 2.9: Diagram showing the design of the molybdenum ring laser tube.

2.5.5 BVL Seeded By Entrainment

In the preliminary laser designs discussed in Sections 2.5.2-4, the barium was regularly spaced along the length of the alumina in common with other metal vapour lasers. It was believed that the contact of the molten barium and also the condensing and solidification of barium onto the tube walls was the main reason for the cracking of the alumina tubes. Liquid barium is an excellent wetting agent [16] and consequently tended to permeate into fissures and micropores of the alumina. When the laser was turned off, barium solidified onto the tube walls whilst the tube was hot. It was the continued thermal contraction that caused the tube to crack, an example of which is shown in Figure 2.10. In the final BVL design, the barium was contained within a 30 mm long molybdenum boat positioned at the anode end of the laser tube. This prevented the liquid barium from coming into contact with the ceramic. The boat was made by tightly rolling a sheet of high purity molybdenum foil and folding the sides of the sheet in such a way as to prevent distortion (by twisting) of the boat under thermal cycling. The lower ends of the ring were cupped upwards and inwards by about 1-2 mm as for the rings described in Section 2.5.4 to form the boat and prevent liquid barium from spilling out over the ends.

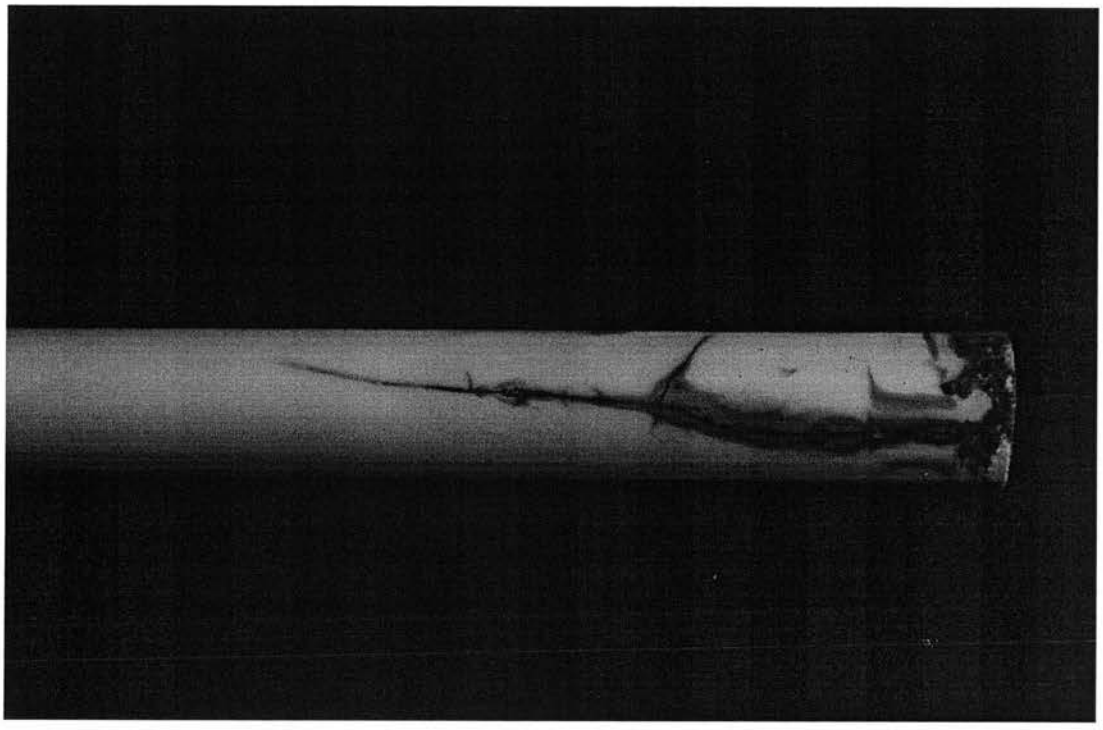

Figure 2.10: Photograph showing typical cracks in the alumina laser tube.

A further important feature of the final design was the use of ~50% less insulation over the region of the alumina which contained the molybdenum boat. This was a further attempt to reduce the damage caused by barium condensing on the alumina tube wall when the laser was slowly turned off. As the tube was slowly run down to switch off, the barium was purged from the alumina tube before it could condense and wet the tube walls. This was because the region of the alumina near the boat cooled faster than the rest of the active region when the laser input power was reduced to below threshold for oscillation. The inside of the alumina tube was white after the laser had been switched off, which indicated that the barium was effectively purged from the active region.

Once the laser tube reached the operating temperature (~1000°C) following switch on, the barium vapour filled the active volume by entrainment with a slow flow of buffer gas and/or by cataphoresis towards the cathode. Barium traps were positioned at both ends of the active region as shown in Figure 2.11 which prevented the barium vapour from

coming into contact with the quartz. This was an important feature because of the highly corrosive nature of barium to quartz. Each trap consisted of a wide bore alumina tube section with Zircar AL30AAH insulation at each end of the tube. The insulation was machined to provide a tight fit between the wide bore alumina and either the stainless steel electrode or the alumina confinement tube.

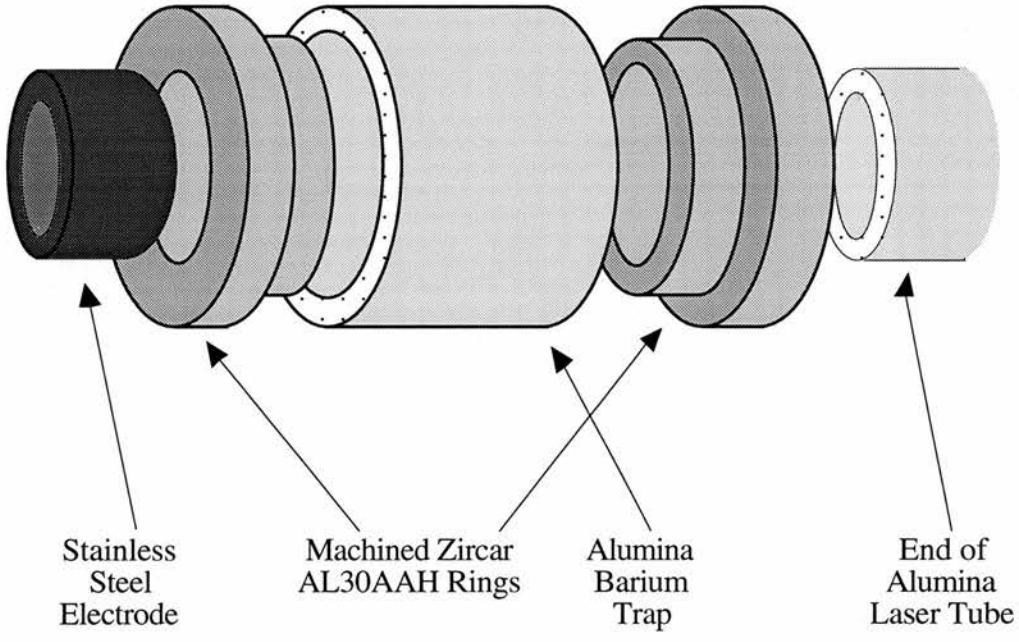

Figure 2.11: Barium traps used to confine the barium and protect the quartz outer tube from chemical attack.

Figure 2.12 shows the final design of the BVL for which laser tube lifetimes were extended up to ~500 hours of laser operation. This represented a marked improvement from the original designs discussed in Sections 2.5.2-4. A central high purity (99.7% Alsint) alumina tube of internal diameter 23 mm, external diameter 30 mm and 700 mm long was used to confine the barium vapour. This was sleeved inside Zircar AL30AAH high-purity alumina insulation which was centrally located inside an outer quartz tube. The AL30AAH was a soft fibrous alumina insulation and could be easily cut and machined to the required dimensions (see Table 2.1 for specifications). However, once the insulation had been 'baked out' at several hundred degrees, it changed its composition and became much harder and more brittle. There was a certain degree of shrinkage after the baking process, around 1% by volume. For other types of insulation (eg AL30AA), the shrinkage

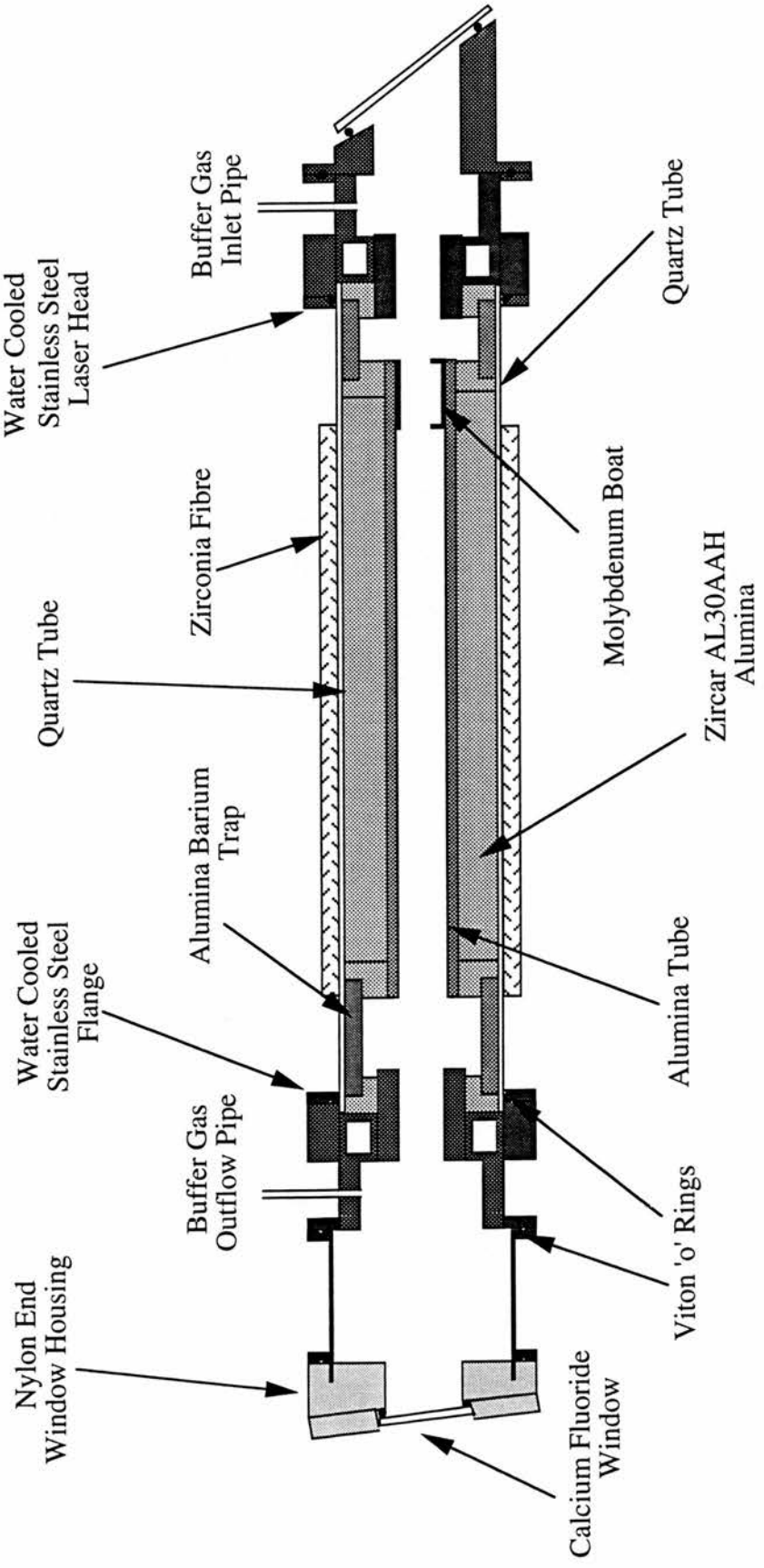

Figure 2.12: Diagram showing the final design for the BVL seeded by entrainment

could be as much as 2%. Consequently, the AL30AAH was machined to 1 mm larger than the central alumina tube to allow for this shrinkage.

Melting Point	>1871°C	
Specific Heat	1047 J/Kg°K	
Firing Shrinkage (isothermal soak 1 hr @1649°C)		
	Length	0.2 %
	Width	0.6 %
	Volume	1.0 %
Thermal		
Conductivity (W/m°K)	0.09 @ 250°F	0.12 @ 525°F
	0.16 @ 800°F	0.19 @ 1075°F
	0.23 @ 1350°F	0.27 @ 1650°F

Table 2.1: Thermal properties of Zircar AL30AAH insulation [17].

2.6 Additional Laser Design Considerations

2.6.1 Laser Tube Insulation

The first BVLs constructed using the design discussed in Section (2.5.5) used Zirconia fibre insulation. This was in the form of a ceramic fibre felt which could easily be wrapped around the central tube. The Zirconia fibre was originally used in preference to AL30AAH for three reasons. First, the thermal conductivity of Zirconia fibre was significantly lower (~50 %) and thus less insulation was required. Second, there was no linear shrinkage with temperature which was an undesirable phenomenon of the AL30AAH. Third, according to the manufacturer's specifications [17], there was less outgassing with Zirconia fibre than with the AL30AAH leading to a reduction in the processing time for discharge cleaning of the laser tube.

Once the laser was optimised for laser output power using a pure neon buffer gas, a preliminary investigation was made to observe the influence of hydrogen addition to the

laser power. The first few times that hydrogen was added to the laser, the laser power was found to increase significantly. However, the continued use of hydrogen on a day-to-day basis saw the laser power gradually decrease until laser oscillation ceased entirely with either neon or a neon/hydrogen buffer gas. This decrease in power was attributed to the high reducing properties of the hydrogen which caused the insulation to degrade. This was characterised by a change in the physical properties of the Zirconia fibre which was most pronounced with the fibre wrapped closest to the alumina tube. The insulation became inflexible and brittle, and crumbled when touched. There was also a marked change in colour, it turning from white to a distinct grey colour. The photograph in Figure 2.13 shows a comparison of insulation which was wrapped closest to the tube with some which was wrapped further away. Previously when only a neon buffer gas had been used, the

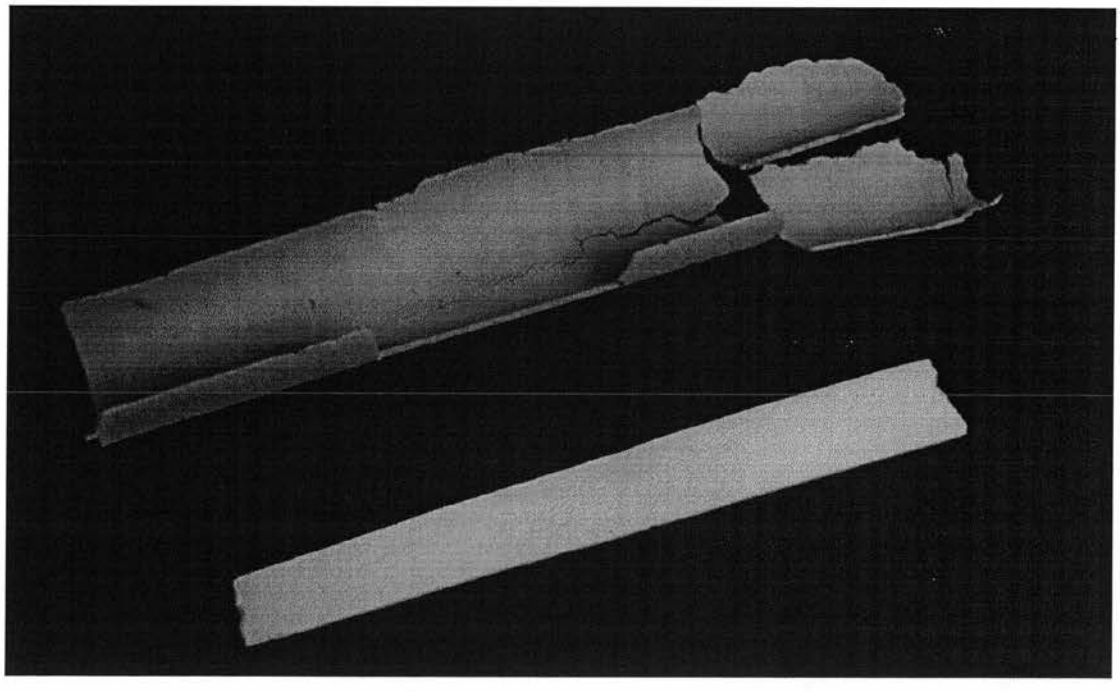

Figure 2.13: Photograph showing the difference between Zircar zirconia fibre insulation which had been positioned close to the alumina and similar insulation which had been positioned further away.

Zirconia fibre was not found to degrade nor the laser power to decrease with time. Only after this insulation was changed to Zircar AL30AAH were the problems with the insulation

eradicated. Zircar AL30AAH was used exclusively from then onwards. Due to the lower thermal conductivity of AL30AAH, extra insulation was required outside the quartz tube. This took the form of Saffil alumina fibre mat.

2.6.2 Laser Head Design

Figure 2.14 shows an enlarged diagram of the laser heads from Figure 2.12. The laser heads consisted of several stainless steel flanges, bolted together and sealed with Viton 'o' rings. Stainless steel electrodes were machined to a push-fit so as to protrude from the central flange. This flange was water cooled to prevent excessive heating of both the electrodes and the Viton 'o' rings. Gas inlet and exhaust pipes were also welded to this flange and connected to the vacuum system described in the following section. Dust traps were incorporated into the design, helping to prevent barium oxide and/or dust from the AL30AAH from reaching the end windows.

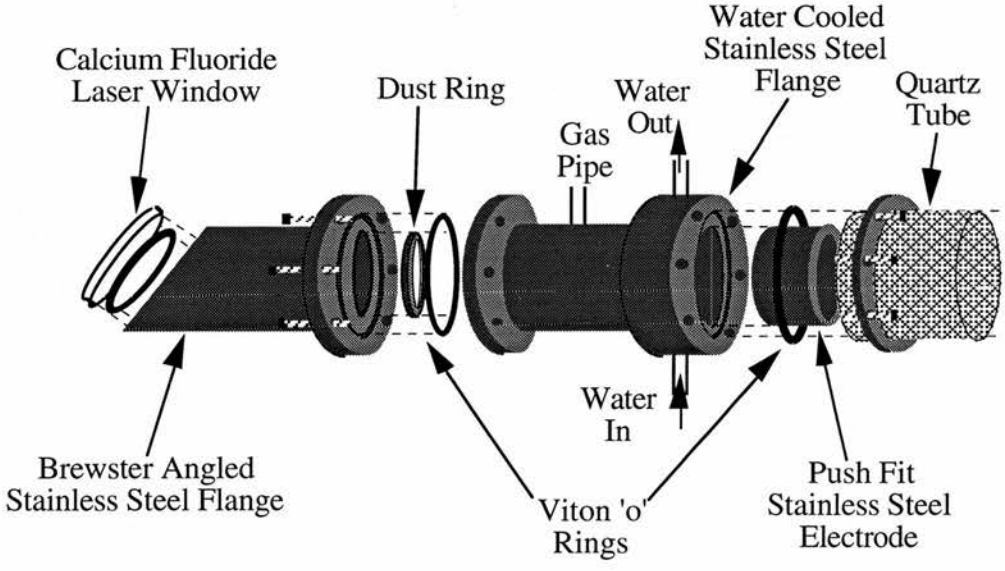

Figure 2.14: Enlarged view of one of the stainless steel laser head with an electrode and the quartz outer tube.

2.6.3 Vacuum / Gas Supply

The method of seeding the active volume by entrainment which was developed to overcome the problems outlined in Section 2.5.1-4 necessitated the use of a flowing buffer gas. Moreover, in common with high temperature CVLs, the slow flow of buffer gas helped to remove impurites from the active region. These impurities originated from either

the alumina confinement tube or the AL30AAH insulation when the laser tube was at the working temperature.

The vacuum system used is shown schematically in Figure 2.15. The buffer-gas flow rate was regulated through fine graduated needle valves (labelled (a) and (c) in Figure 2.15). The gas pressure was varied using a fine needle valve positioned between the cathode laser head and the Edwards E2M-12 2-stage rotary pump labelled (d) in Figure 2.15. The percentage of additive to the laser was controlled and measured by changing the relative flow rates through valves (a) and (c). This is discussed more fully in Section 3.2.

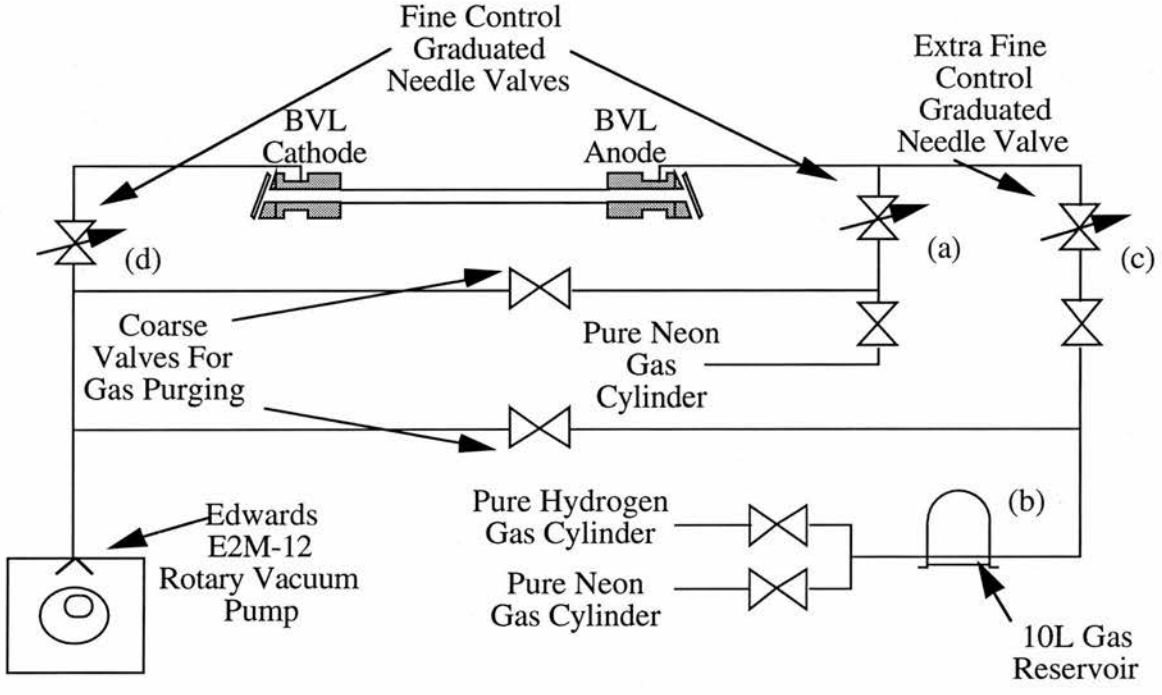

Figure 2.15: Gas supply connections to the barium vapour laser.

Stainless steel Swagelok 1/4" o.d. piping was used throughout with the exception of two glass coils (each 1.5 m length of tubing) mounted on the anode and cathode laser heads which were used for electrical isolation. The Swagelok unions, gas taps and 'o' ring fittings were all leak tested with a helium sensitive mass spectrometer to ensure that the complete vacuum system was leaktight. The rotary pump oil was a high-grade TW oil equivalent which greatly reduced the amount of backstreaming and hence oil contamination of the laser tube.

2.6.4 Laser Cavity Design

Due to the high gain (>10% cm^{-1}) of barium vapour lasers [18], the population of the upper laser level and hence the pulse duration is sufficiently short to make a high finesse cavity unnecessary and perhaps detrimental to the total laser output power. The cavity used was similar to those of other BVLs, consisting of a gold-coated high reflector and an uncoated calcium fluoride output coupler. The cavity was in a plane-plane geometry, thus the whole of the active volume was exploited. The separation of the two laser cavity mirrors was 1.5 m.

2.7 Summary

This chapter discusses the excitation circuit used throughout the present study of the BVL and also discusses in detail the laser design used. The excitation circuit was a resonant charging capacitor transfer circuit which used a thyratron to periodically switch the storage capacitor to ground. A peaking capacitor was incorporated into the circuit to speed up the tube current rise-time. This was mounted close to the laser in order to minimize the discharge circuit inductance. A coaxial earth-return geometry was also adopted to minimize the discharge circuit inductance.

The laser tube consisted of a central alumina tube of 23 mm diameter and 700 mm length which was sleeved inside Zircar AL30AAH alumina insulation. This was sleeved inside a quartz outer envelope which sealed onto stainless-steel end flanges. The barium was contained in a boat at the anode end of the laser tube which, at the operating temperature of the laser, seeded the active volume by entrainment using a slow-flow buffer gas. The laser cavity consisted of a gold-coated high reflector and a calcium fluoride flat as the output coupler.

2.8 References

[1] 'Metal Vapour and Metal Halide Vapour Lasers' ed. by G. G. Petrash, Proc. Lebedev Physics Institute, Nova Science, Commack (1987).

[2] N. K. Vuchkov, D. N. Astadjov, N. V. Sabotinov, IEEE J. Quantum Electron. **30** (3) pp 750-758 (1994).

[3] D. R. Jones, A. Maitland, C. E. Little, IEEE J. Quantum Electron. **30** (10) pp 2385-2390.

[4] 'Electromagnetism', I S Grant, W R Phillips, Wiley, Manchester Physics Series pp 269-274 (1975).

[5] P. A. Bokan, Sov. J. Quantum Electron. **15** (5) pp 622-626 (1985).

[6] G. L. Clarke, PhD Thesis, St Andrews (1988).

[7] A J Andrews, R C Tobin, C E Webb, J. Phys. D: Appl Phys **13** pp 1017-27 (1980).

[8] 'Hydrogen thyratron Preamble', English Electric Valve Ltd (1972).

[9] 'Hydrogen Thyratrons', EEV Product Data (1985).

[10] 'Transmission Lines', R A Chipman, Schaum's Outline Series in Physics McGraw Hill, New York (1968).

[11] M. J. Kushner, B. E. Warner, J. Appl. Phys. **54** (6) pp 2970-2982 (1983).

[12] G Hogan, PhD Thesis, Oxford University (1993).

[13] H. M. Pask, J. A. Piper, J. Appl. Phys. **72** (12) pp 5545-5554 (1992).

[14] O Marazov, I Kosadinov, J. Phys. E: Sci. Instrum. **22** pp 744-748 (1989).

[15] A. A. Isaev, G. Yu. Lemmerman, S. V. Markova, G. G. Petrash, Sov. J. Quantum Electron. **9** (9) pp 1144-1147 (1979).

[16] 'Metals Handbook' **2** American Society for Metals, 8th Edition, pp 525 (1967).

[17] Zircar inc Product Data (1990).

[18] K. I. Zemskov, M A. Kazaryan, G. G. Petrash, V. N. Smorchkov, V. P. Timofeev, S. A. Fridman, Sov. J. Quantum Electron. **10** (11) pp 1428-1431 (1980).

Chapter 3

Experimental Techniques, Measurements and Analysis

3.1 Introduction

In this chapter the various methods which have been used to measure discharge characteristics and the analysis of the results are discussed. This includes a discussion of the accuracy of the measurements made. Also discussed in this chapter is the preparation of the barium metal for loading into the laser and the discharge cleaning technique adopted, both of which were important for the reliable and consistent results.

3.2 Gas Flow Rate Calibration

As mentioned in Section 2.6.3, the needle valves were used to control the buffer-gas pressure, the buffer-gas flow rate and also the percentage of additive used. The values had to be carefully calibrated in order to be able to monitor the flow rates accurately, and hence to determine the percentage of additive to the laser. Automated and pre-calibrated atomic mass flow controllers would have provided easier methods for evaluating these parameters, but unfortunately these were not available at the time.

Before the needle valves could be calibrated, the total volume of the laser system first had to be estimated. This was carried out as follows: a reservoir bottle of fixed known volume (10 l) was connected to the laser by a short stretch of 1/4" pipe and isolated by a Nupro stop valve. The bottle was then filled with pure neon to a known pressure

(900 mbar). Once the laser had been pumped down to a low pressure (<0.1 torr) using a rotary pump, the laser was isolated from the pump before the valve to the reservoir bottle was opened. The resulting decrease in pressure of the reservoir bottle was measured and used to calculate the volume of the laser using the gas law at constant temperature given by Equation (3.1):

$$V_L = \frac{900x10}{P_F} - 10 \quad , \qquad (3.1)$$

where V_L and P_F are the laser volume and final pressure respectively. The laser volume was estimated to be (1.6 ±0.1) l, where the uncertainty was brought about by inaccuracies in measuring the pressure because of the dial gauge used.

Once the volume of the laser had been evaluated, the graduated needle valves were calibrated by measuring the increase in pressure per unit time (torr/s) for various positions of the valve when the laser tube was isolated from the vacuum pump. However, the calibration was complicated because for a given needle valve setting the rate of rise of pressure was found to be dependent upon the gas inlet pressure. For this reason the rate of rise of pressure was evaluated at a constant inlet pressure of 0.5 bar as measured at the cylinder regulator. This was maintained constant throughout the studies in the BVL. The flow rate was also found to be dependent upon the gas pressure inside the laser tube with the flow rate decreasing with increasing pressure. However, at low pressures (<100 torr) the effect was negligible and thus the flow rate was measured over the pressure regime in which the laser operated (20-60 torr).

The rate of rise of pressure was used to evaluate the flow rate in terms of the number of litre atmospheres which the laser would consume per hour (atm.l/hr) for each of the needle valve settings. Figure 3.1 shows the final calibration curves obtained for pure neon and pure helium for the valve marked (a) in Figure 2.15. For each of the curves, the degree of uncertainty shown in Figure 3.1 was evaluated by considering the uncertainty from both the volume of the laser tube estimated to be ±0.1 atm.l/hr and also the error in measuring the pressure increment estimated to be ±0.1 atm.l/hr.

The flow of H_2, D_2 and He additives into the laser was controlled using an extra-fine graduated needle valve (labelled (c) in Figure 2.15). This was particularly important when either H_2 or D_2 was used because the small size of the molecules made it difficult to regulate the flow rate using the standard valves. The additives were only required in small quantities and so were premixed inside a large (10 l) external reservoir which helped to further increase the reliability of the additive flow rate set. The premixes consisted of 10% H_2, 20% D_2 or 30% He in either neon or helium buffer gas.

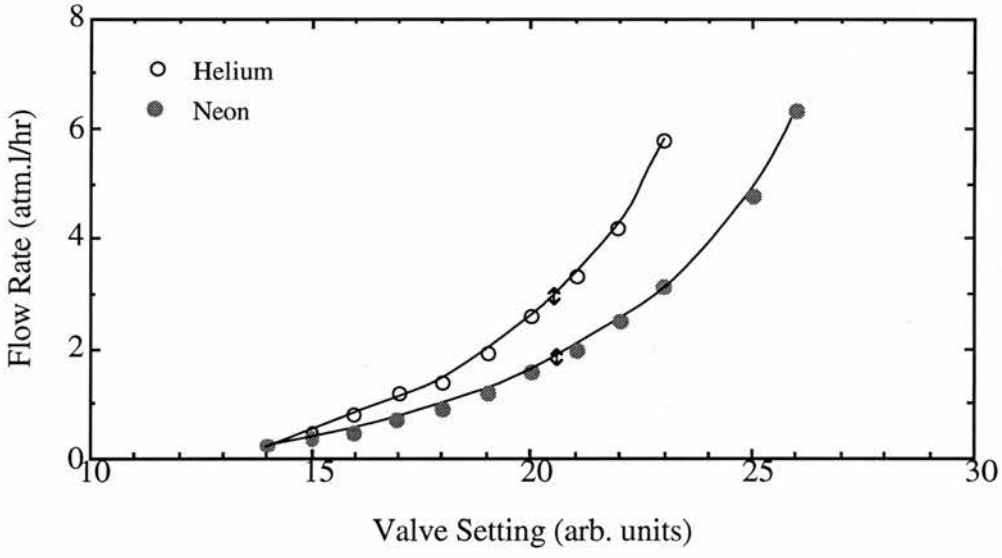

Figure 3.1: Flow rate as a function of needle valve setting with neon and helium.

The H_2, D_2 and He partial pressures within the laser tube were monitored and varied by changing the relative flow rates through the two needle valves (a) and (c) (see Figure 2.15). A constant total flow rate was maintained throughout the experiments by decreasing the flow rate through either valve (a) or (c) when the other valve was correspondingly increased such that a constant total pressure was maintained. The exhaust valve (valve (d) in Figure 2.15) which also regulated the pressure was left unchanged whilst results were being taken.

Valve (c), which regulated the percentage of additive to the laser, was also calibrated for flow rate using pure neon in an identical manner to that of valve (a) for various reservoir pressures, the results being shown in Figure 3.2. This provided another check on the relative flow rates between valves (a) and (c) and hence on the percentage of

additive in the laser mixture. A Ne/H_2 ratio of 90/10 was not found to significantly affect the calibrated flow rate values significantly for the extra-fine needle valve. All the buffer gases used (Ne, H_2 and He) were ultra-high grade, i.e. greater than 99.999 % purity.

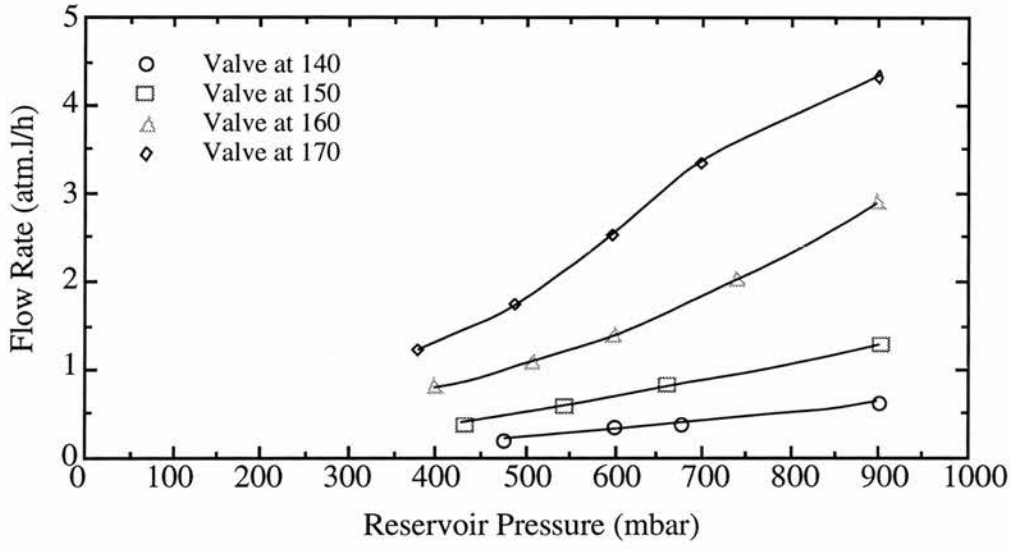

Figure 3.2: Flow rate through the extra-fine needle valve as a function of valve setting and reservoir pressure.

3.3 Voltage Measurements

High voltage measurements were made at three points on the laser circuit: the voltage on the charging capacitor, which enabled the input power (based on stored energy) to be evaluated; the laser tube cathode voltage and the laser tube anode voltage. These voltage measurements were made using high voltage probes (Tektronix models 6015 and 6015A) with the reference for each measurement having the common ground of the power supply/thyratron. The laser tube voltage, V_p, was measured by inverting and subtracting the voltage measured at the anode from the voltage measured at the cathode. This was considered important because although the anode laser head was grounded through the coaxial earth return, the anode voltage was found to swing to significant (≤3 kV) negative voltages during the early stages of the discharge cycle. The difference between the two measurements therefore gave a 'true' measurement of the voltage across the laser tube by eliminating the voltage drop across other circuit components, for example the wiring through the coaxial cable to ground (see Figure 2.1).

All the probes were checked for dc calibration with reference to the switch-mode power supply for voltages up to 10 kV. The ac signal for each probe was checked by comparing the waveform obtained at the cathode with the waveform measured using a new and calibrated probe direct from the suppliers. All the voltage probes used were found to give consistent and similar waveforms with reference to the common ground of the supply/thyratron. Uncertainties in the voltage measurements were therefore considered to be small ($\leq 5\%$).

3.4 Discharge Current Measurements

The discharge current was measured using a Rogowski coil current transformer (Ion Physics Company model) positioned at the cathode end of the coaxial earth return on the laser tube, as shown in Figure 2.1. The coaxial cable from the current transformer to the oscilloscope was made to be the same length as the leads from both the voltage probes to the oscilloscope to ensure that there was no time delay between the voltages measured and that of the tube current. The delay in signal for a length of coaxial cable was experimentally determined to be ~6 ns/m.

In order to be calibrated correctly, the current transformer requires termination into a 50 Ω load on the oscilloscope. Although the oscilloscope used (Tektronix model 2425) had 4 inputs, only two of them could be terminated with 50 Ω. It was also these two channels which had the subtraction facility enabelling the 'true' tube voltage to be determined. In order to enable all 3 traces to be observed simultaneously on the oscilloscope, a variable attenuator was used to convert the output from the current transformer such that the calibration was correct when terminated into a 1 MΩ load on the oscilloscope. This took the form of a 100 Ω multiturn trimmer in parallel to the output from the current transformer. The trimmer was calibrated to 20 A/volt and did not change the tube current risetime from the original calibrated value.

The output from the current transformer was compared to that from a different manufacturer's (Stangenes). Both the peak current and the current risetimes were found to be comparable between the two Rogowski coils.

3.5 Average Laser Output Power Measurements

The average laser power was measured using a thermal detector (Scientech 461 model). It had a uniform spectral response over the full range of wavelengths emitted by the BVL. The power meter was calibrated with reference to another power meter (Laser Control) which had been previously calibrated to within 5% of NPL standards. Figure 3.3 shows the calibration curves for the Scientech power meter. On the 10 W power scale the laser power was found to be approximately 5% higher than the measured value and approximately 10% higher on the 30 W scale. The manufacturer's estimated uncertainty in the power measurements was ±5%.

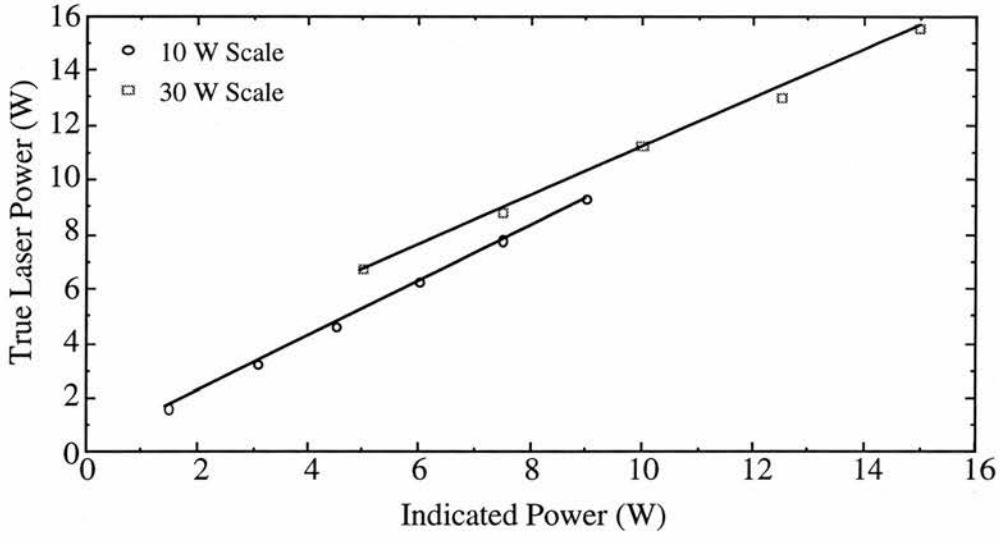

Figure 3.3: Calibration curve of Scientech 461 power meter.

There was found to be some day-to-day variability in the laser output power. For example, variations in discharge operating conditions such as input power (based on stored energy) could vary by around 5% because of the dependence of the storage capacitance on temperature (discussed in Section 3.7). According to results from Section 5.2.2, input power variations of 5% from the optimum value of 1800 W (using a neon-H_2 (97:3) buffer gas) would lead to an output power variation of around 5%. The effect would be more pronounced when the discharge conditions were off optimum.

Other factors which may be responsible for day-to-day fluctuations in the laser output power include variations in the barium distribution within the tube and the discharge cleanliness (cleanliness increases with increasing time of laser operation) which both alter

the tube impedance. An estimate of ±10% of the power measured was taken as the uncertainty. Random fluctuations in the power meter caused by either air turbulence (because of the large detector head used and the absorption of some of the wavelengths by atmospheric water) or electrical noise from the pulsed power environment caused problems in measuring low power levels (<0.2 W) and is the main reason why laser oscillation at 2.92 μm and 4.72 μm was not characterised for various discharge parameters.

3.6 Laser Pulse Intensity Measurements

The temporal evolution of each of the laser pulses was measured using a HgCdTe detector (Vago PCI-L-3 model). The spectral response of this detector was highly non-uniform with the detectivity varying by up to a factor of 5 across the wavelength range of interest (1-6 μm). The typical spectral dependence of the detectivity lies in the region

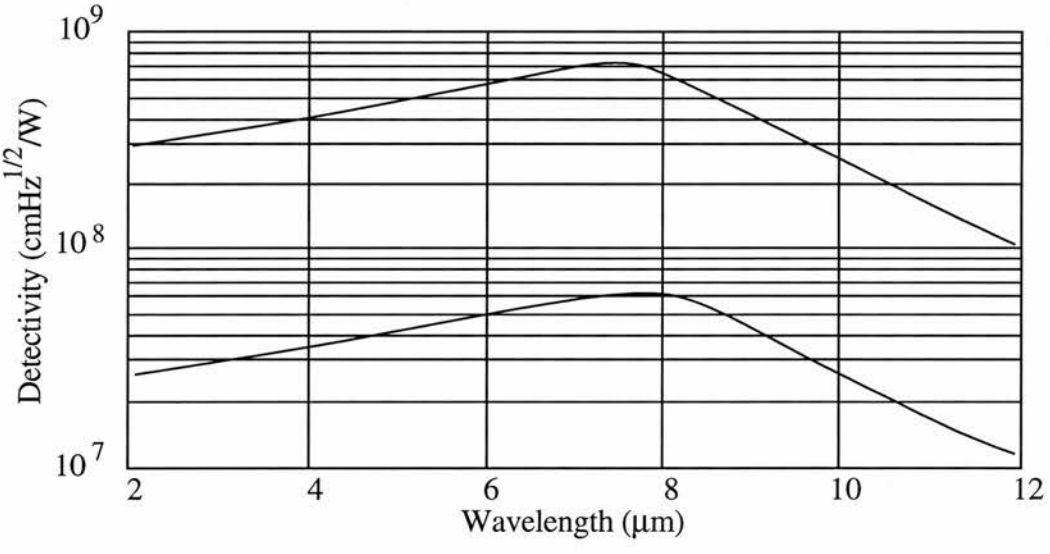

Figure 3.4: Spectral dependence of the detectivity for the HgCdTe detector.

between the two lines in Figure 3.4. The peak response was at 10.6 μm for this particular model. Below ~2 μm the detectivity was very poor, but due to the relatively high power of the 1.13 and 1.50 μm laser transitions, measurement of the laser pulse intensity at these wavelengths was not a problem. However, because of the non-uniform spectral response of the HgCdTe detector, a comparison of laser pulses to evaluate the power at each wavelength was not possible because a precise calibration curve for the spectral response for this particular detector could not be accurately determined.

The HgCdTe detector was housed inside a diecast box with the aim of reducing the problems commonly associated with electrical noise from a pulsed power environment. Also contained within the box were the biassing electronics for the detector which provided a maximum current of 10 mA from a 6 V battery. Figure 3.5 shows the electrical biassing arrangement used. The recommended maximum current rating for the detector was 20 mA.

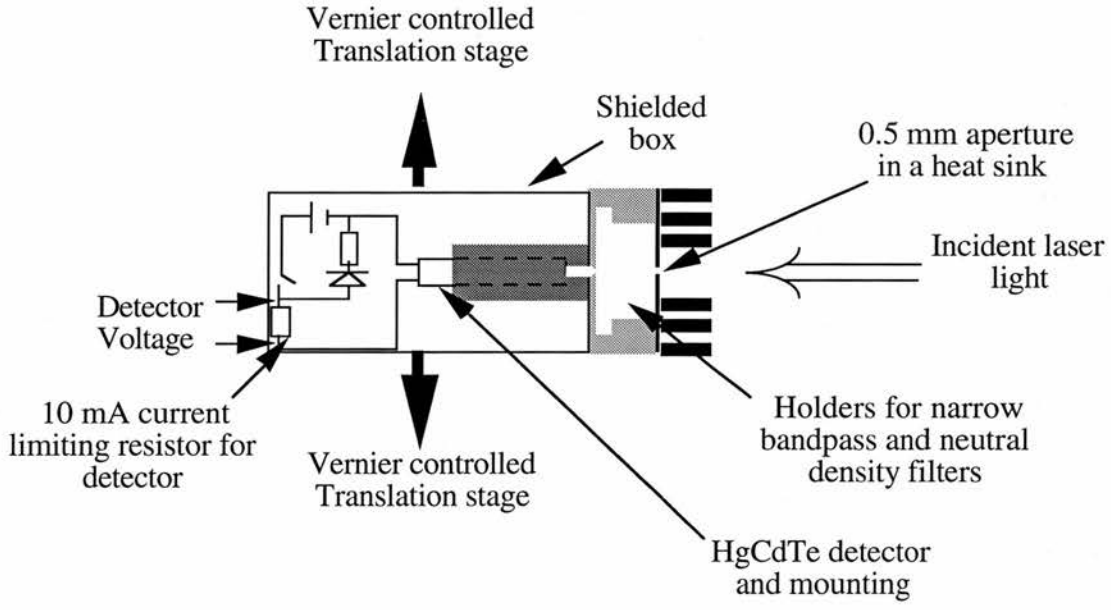

Figure 3.5 : Schematic view of the apparatus used to measure beam profiles at selected wavelengths, also shown are the biassing electronics used for the detector.

For each oscillogram taken of the laser pulse intensity, oscillograms were also taken of the background intensity waveform from the detector in the absence of laser radiation. The background noise was then subtracted from the laser pulse intensity to obtain the laser pulse waveform. Before the background could be subtracted, both the waveforms first had to be digitised and interpolated. Fortran 77 programs were written for the background subtraction; these are listed in Appendix II. The program required a computer with NAG® (numerical algorithm) libraries installed. A fuller discussion of the digitising method used can be found in Section 3.12. Figure 3.6 shows an example of the 1.50 μm laser pulse intensity before and after background subtraction along with the background waveform.

Specific wavelengths (1.13, 1.50, 2.55, 2.92 and 4.72 μm) were individually selected using narrow bandpass filters. The spectral response for each filter is shown in Figure 3.7 and was taken in to account when the contribution of the total power from each

wavelength was evaluated. The filters were only 21 mm in diameter and so it was necessary to aperture the laser beam to the 50% total laser power level prior to each measurement in order to prevent the filters from aperturing the laser beam output.

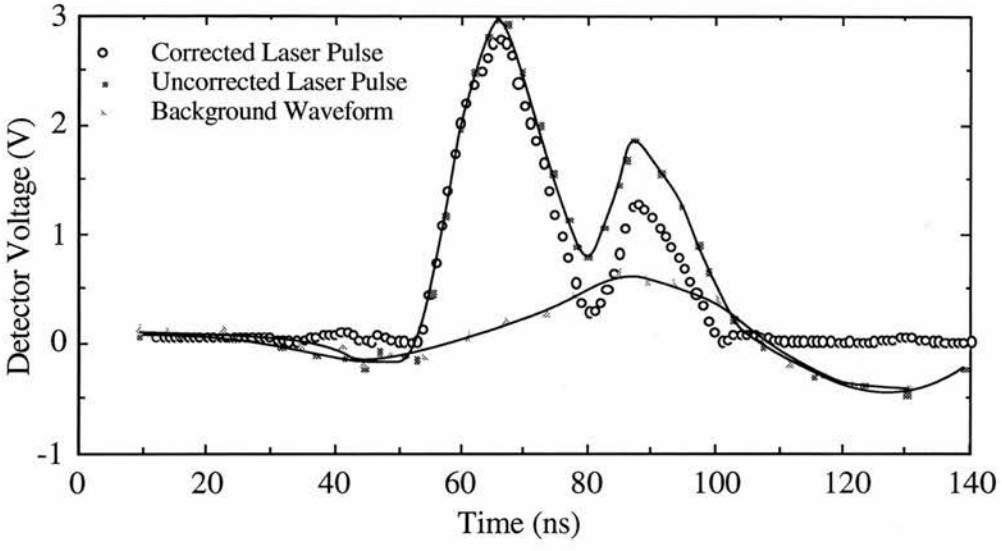

Figure 3.6: Background subtraction from the 1.50 μm laser pulse intensity.

3.6.1 Laser Beam Intensity Profile Measurements

The temporal and spatial evolutions of the laser intensity at both 1.13 μm and 1.50 μm were investigated for various discharge conditions. The laser intensities were measured using the HgCdTe detector as described in Section 3.6. However, in this case the mounted detector was positioned behind a narrow 0.5 mm diameter hole as shown schematically in Figure 3.5. The pin-hole and detector assembly were carefully aligned such that the pinhole and the detector were in a direction parallel to the incident laser beam. A nylon mounting behind the pinhole enabled narrow band-pass filters to be inserted in front of the detector for wavelength selection. The whole system was mounted on a bench rail, which enabled the pinhole to be moved perpendicularly across the laser beam, and a radial dependence for laser pulse intensity to be measured. The position of the pinhole was measured with respect to the beam centre using a mounted Vernier caliper gauge.

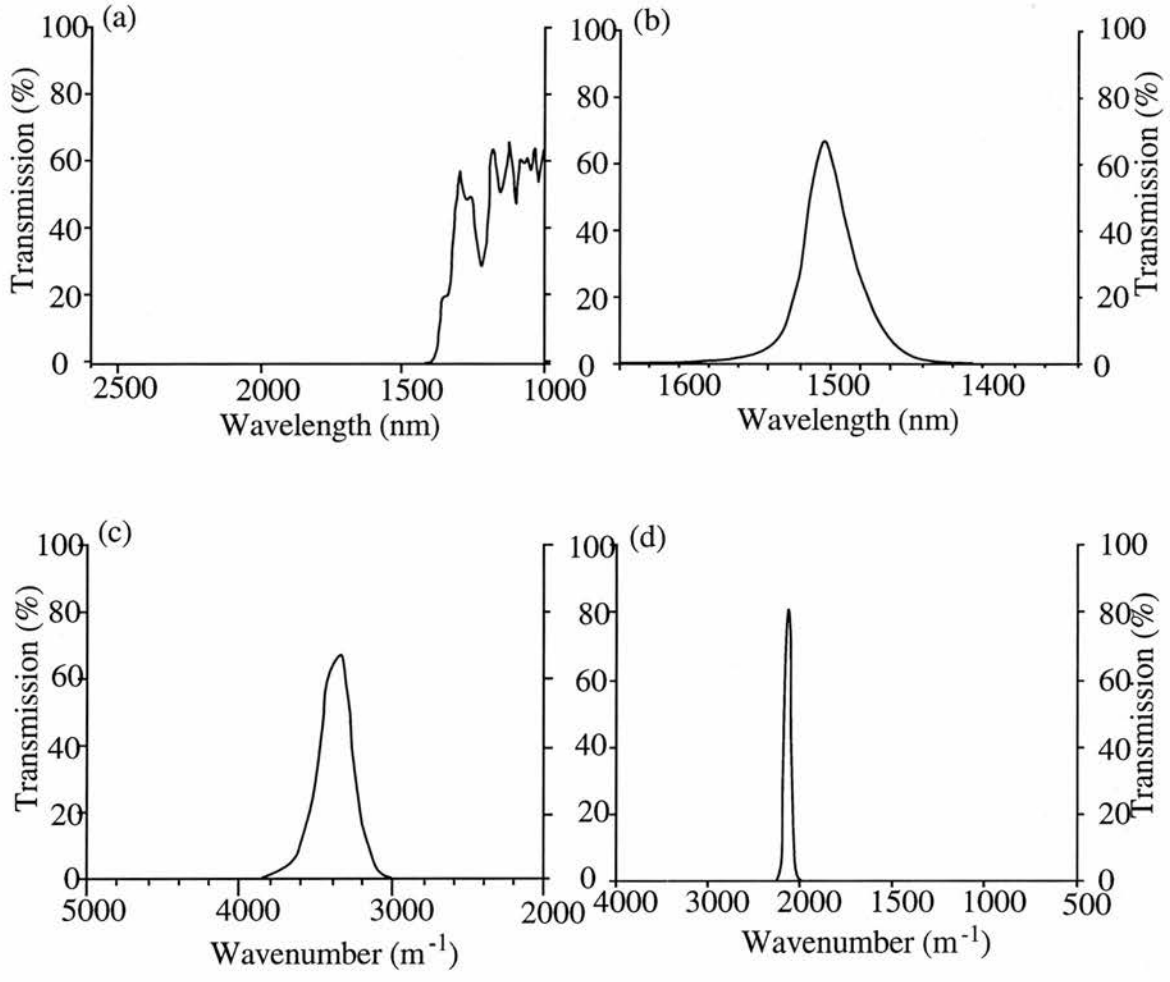

Figure 3.7: Transmission characteristics of (a) the 1.13 μm, (b) the 1.50 μm, (c) 2.92 μm and (d) 4.72 μm bandpass filters used to select individual laser transitions.

3.7 Capacitance Measurements

As was outlined in Section 2.4.1, high voltage (>30 kV) capacitors manufactured by Murata were used exclusively for both the storage and peaking capacitors. These were mounted close to the laser head in order to keep the inductance of the discharge circuit to a minimum. One unfortunate property of these capacitors was that the value of the capacitance was found to decrease with increasing temperature. An example of the dependence of capacitance of a Murata 202M capacitor wth temperature is shown in Figure 3.8.

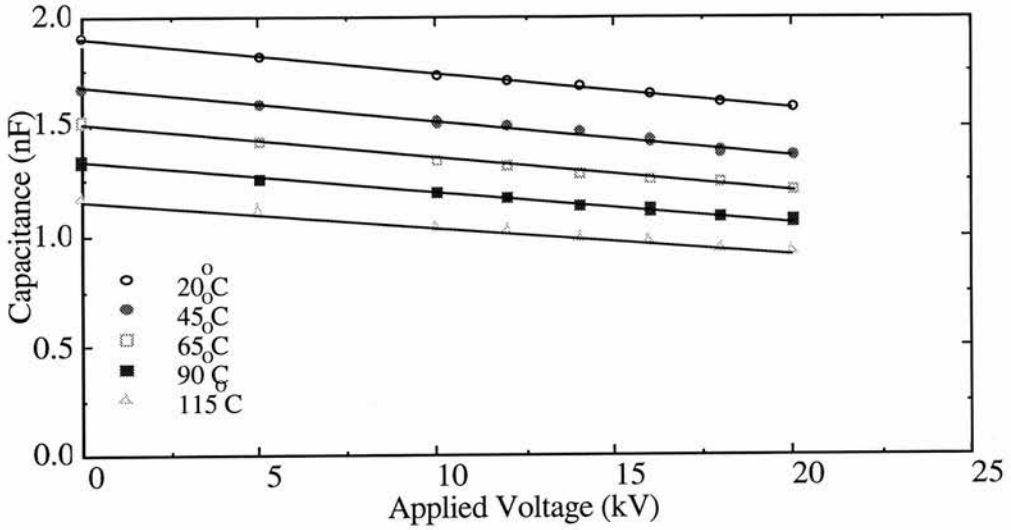

Figure 3.8: Capacitance as a function of temperature and applied voltage for a Murata 202M high voltage capacitor [1].

The temperature which the capacitor reached during the operation of the laser depended upon both the relative position of the capacitor with the hot discharge tube, and also the particular charging voltage selected and the PRF at which the laser was operated (the last because of lossy dipole oscillations within the dielectric material). The PRF of operation was believed to contribute most to the temperature increase. In all cases the capacitance quoted was the 'hot' value which was measured after results had been taken by momentarily turning off the laser and removing the capacitor from the circuit before measuring its capacitance.

The capacitance was also found to vary with applied voltage as is also shown in Figure 3.7. However, this decrease in capacitance with increasing voltage stress was not taken into account when the input power and efficiency were evaluated in Chapters 4-6.

Another source of capacitance in the circuit was the distributed capacitance present in the coaxial cable which linked the thyratron anode to the charging capacitor. The value of the capacitance was evaluated to be 0.13 nF and was taken into account when the input power and the overall laser efficiency were evaluated although it remained unclear whether this circuit component behaved as a capacitance or solely as a discrete inductance.

3.8 Evaluation of Laser Tube Circuit Inductance

With any electrical system which has a time varying current, the driving voltage comprises an inductive component and a resistive component. However, it is the resistive component of the voltage which contributes to the energy deposition, the inductive component merely temporarily stores energy in the electrical circuit. In order to be able to evaluate the energy deposition, and indeed the electron density from the tube current and tube voltage waveforms, it is essential to include the effects of inductance on the measured voltage. This section addresses the methods used to evaluate this inductance.

The analysis of the inductance, L_{head}, of the laser tube, the coaxial return and the peaking capacitor loop, purely from a geometrical aspect would be a difficult task. An easier and more reliable method for evaluating L_{head} was to use the tube current and tube voltage waveforms measured over the duration of the excitation pulse. The measured tube voltage, V_{meas}, comprises two components [6], a resistive component V_{res}, and an inductive component V_{ind}, as shown in Equation 3.2:

$$Vmeas = Vres + Vind, \tag{3.2}$$

which may also be written as

$$V_{meas} = I_d R + L_{head} \times \frac{d(I_d)}{d(t)}, \tag{3.3}$$

where I_d and R are the tube current and tube resistance, both of which are time dependent.

When $$I_d = 0, \tag{3.4}$$

Equation 3.3 becomes

$$V_{meas} = V_{ind} = L_{head} \times \frac{d(I_d)}{d(t)}, \tag{3.5}$$

and hence from Equation 3.5, L_{head} may be evaluated when the current is zero by determining V_{meas} and the rate of change of current with respect to time.

Another method of evaluating L_{head} is to consider the apparent power, W_{app}, being deposited into the laser tube, as shown in Equation 3.6:

$$W_{app} = V_{meas} I_d . \tag{3.6}$$

Using Equation 3.3, Equation 3.6 may be rewritten as

$$W_{app} = \left(I_d R + L_{head} \, x \frac{d(I_d)}{d(t)} \right) I_d , \tag{3.7}$$

taking the first derivative of Equation 3.7 with respect to time and evaluating it at the peak of the current pulse where the first derivative is zero gives Equation 3.8:

$$\left. \frac{d(W_{app})}{d(t)} \right|_{I_d = 0} = L_{head} I_d x \frac{d^2(I_d)}{d(t)^2} , \tag{3.8}$$

from which the inductance could also be evaluated. In the derevation of Equation 3.8 it has been assumed that the rate of change of tube resistance with respect to time is zero. This is approximately true over the majority of the excitation pulse, as shown in Figure 3.9d where the time dependence of the derivative of the quotient between the resistive tube voltage (assuming a constant laser head inductance of 200 nH) and the tube current is plotted, i.e. the derivative of the tube resistance as a function of time. Fortran programs listed in Appendices III and IV were written to evaluate L_{head} using Equations 3.5 and 3.8 respectively. These were designed to run on SPARC stations equipped with NAG® (numerical algorithm) libraries [2]. The first method for evaluating L_{head} proved to be much easier and more reliable than the second.

Whichever method was adopted, the tube current and tube voltage waveforms first had to be manually digitised from oscilloscope photographs; this is described in Section 3.12. The data were then transferred from a PC to an Apple Macintosh computer and edited so that it was in the correct format to transfer onto a Sun computer. However, before L_{head} could be evaluated, a number of Fortran 77 programs were first written to modify each of the data sets. This was necessary because the tube current and tube voltage waveforms were digitised independently from each other and hence although they had the same zero point (defined as the onset of the tube current), the time intervals for both data sets were irregular, making evaluation of the current and the voltage at specific times impossible. Both the programs listed in Appendices III and IV first interpolated and curve fitted the data points for the tube current and tube voltage waveforms before re-drawing using new data sets with regular time intervals of 1 second. Because of the sometimes complex shape of the waveforms, the only curve fitting and interpolating routines which were found to describe the waveform accurately were NAG® numerical algorithms, which is the reason why the data had to be transferred onto a Sun computer. These routines also had the distinct advantage that they could be used to differentiate and integrate the curves accurately.

For the second method, the turning points of the tube current waveform were accurately evaluated by a series of successive approximations. The first derivative of the apparent power and the second derivative of the tube current waveform were subsequently evaluated at this turning point. The complex shape of the tube current waveform made it difficult for the program to reliably pinpoint the turning point corresponding to the peak current, this was identified manually from a selection of calculated turning points. Equation 3.8 was used to evaluate L_{head} once the correct turning point was selected. The main problem with the evaluation of L_{head} using this particular method was the margin of error which came from the digitising of the current pulse data. This was predominantly caused by the finite thickness of the waveforms on the oscillogram photographs which caused some degree of uncertainty in the digitising process. After differentiating the interpolated current trace twice, this error was found to be significantly increased and could

cause large fluctuations in the value of the second derivative and hence in the resistive component of the tube voltage. The degree of uncertainty originating from the voltage was much less than that from the current since the W_{app} term in Equation 3.8 was only dependent upon the first derivative, (ie the first derivative of the product of the tube current with the tube voltage).

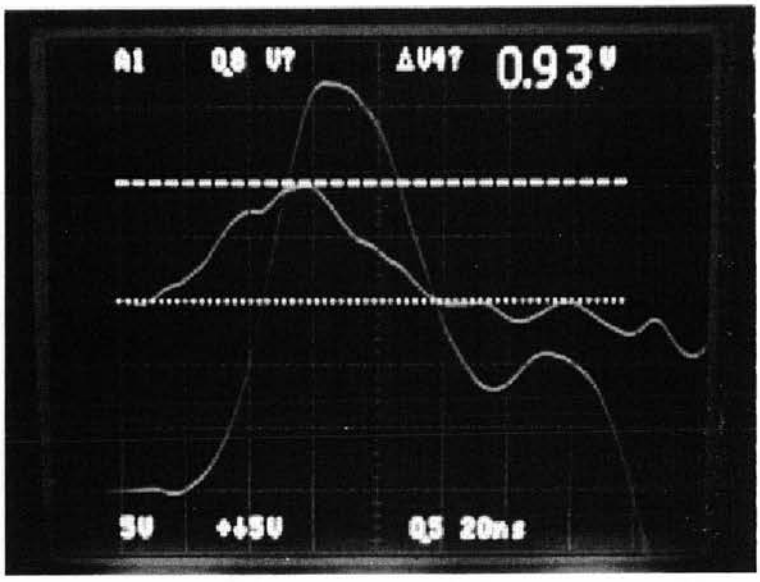

Figure 3.9a: Oscilloscope photograph of the tube current and tube voltage waveforms.

The uncertainty in the digitised waveforms was reduced to a large extent by modifying the interpolation routines to enable the original data to be smoothed. An example of the effect of smoothing is shown in Figure 3.9 where (a) shows the original oscilloscope photograph for the tube voltage and tube current, (b) shows the same tube current waveform which had been digitised and interpolated using both unsmoothed and smoothed data points, (c) shows the second derivative of the tube current for unsmoothed and smoothed data, and finally (d) shows the evaluated resistive tube voltage for unsmoothed and smoothed tube current data (where L_{head} was taken to be 200 nH for reasons discussed shortly). Although the degree of smoothing used in the above example was kept to a minimum and hardly made any change to the original tube current waveform, smoothing the current data made a significant difference to the second derivative and hence

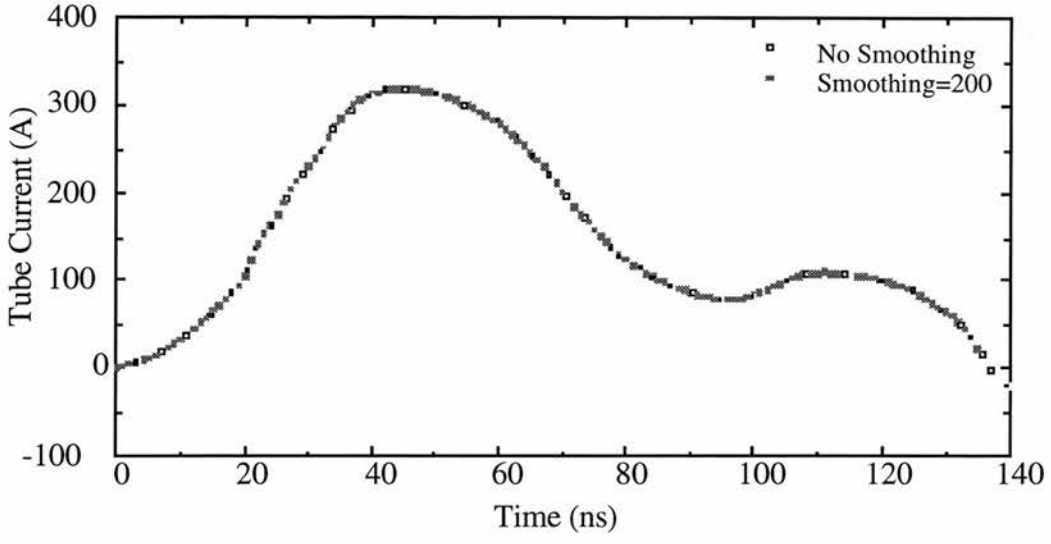

Figure 3.9b: Digitised and interpolated tube current waveform without and with data smoothing.

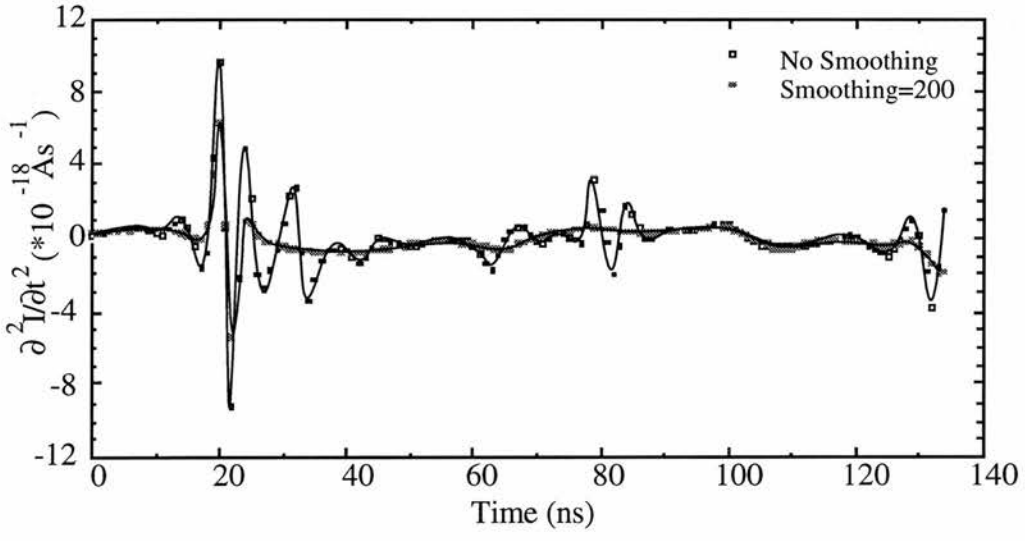

Figure 3.9c: Second derivative of the tube current for smoothed and unsmoothed data.

to both the resistive tube voltage and the evaluated value of L_{head}. After considerable experimentation with the weighted smoothing program, the smoothing factors which were found to give a consistant value for L_{head} using Equation 3.8 whilst maintaining the shapes of the tube current and tube voltage waveforms were found to be 0 for the tube voltage and 200 for the tube current. These values were used exclusively for all the digitised waveforms used to calculate L_{head} using Equation 3.8. It should be noted that some

problems arose when the tube current waveform was particularly 'broad' about the maximum tube current. Under these circumstances, L_{head} tended to infinity as the second derivative of the current in Equation 3.8 tended to zero.

Although the first method for the evaluation of L_{head} (Equation 3.5) also required the tube current and tube voltage waveforms to be digitised and interpolated, the current waveform only needed to be differentiated once and hence smoothing of the data was not required. This greatly simplified the evaluation of L_{head}. Because L_{head} is dependent solely upon the geometry of the discharge tube (assuming no discharge constriction during the current pulse), the value of L_{head} should be the same using either method.

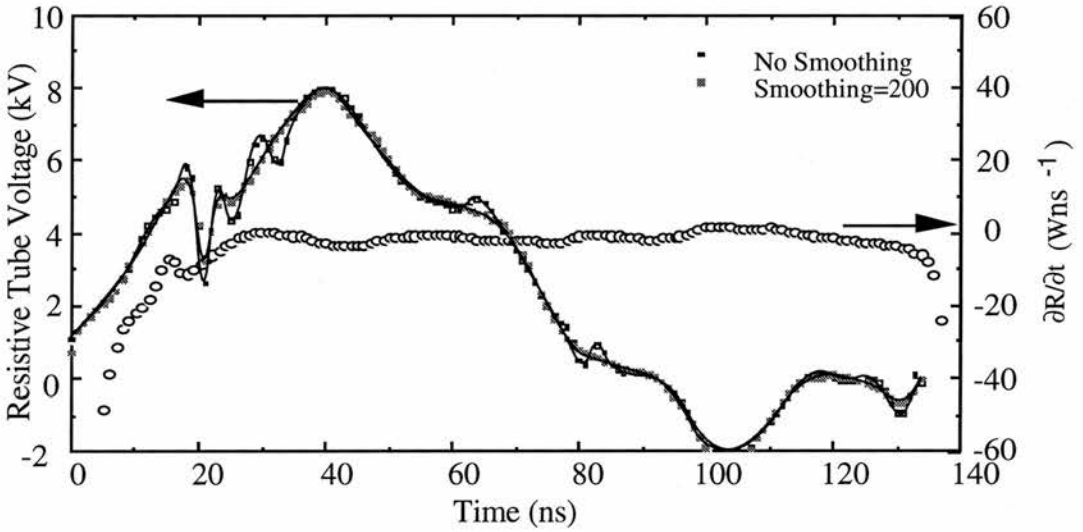

Figure 3.9d: Evaluated resistive tube voltage (without and with smoothing in the digitised tube current waveform) and evaluated rate of change of tube resistance with respect to time.

The oscillograms used for the evaluation of L_{head} were taken under the conditions described in Section 5.2.5. Oscilloscope photographs were taken at charging voltages ranging from 14 kV to 18 kV inclusive, while correspondingly varying the PRF to maintain the total input power (based on stored energy) at 1800 W, both with and without 3% added hydrogen. The charging capacitance and pressure were maintained at 1.2 nF (hot) and 54 torr respectively. The inductance was evaluated by the two methods discussed earlier with only two points discarded because of the symmetrical shape of the tube current waveform. An average value for L_{head} was taken for all the conditions with the uncertainty being taken as the statistical variation from a mean value. In this way L_{head} was evaluated to

be 200±120 nH. Figure 3.10 shows the complete breakdown of the results for both the methods discussed at each of the charging voltages. This compares well with the minimum value of L_{head} estimated from the coaxial geometry which is described by Equation 2.3 which gave a value of L_{head} of ~220 nH (taking r_1=11.5 mm and r_2= 50 mm and a length of 0.75 m). The variation in the values for L_{head} was believed to result from the variation in the discharge conditions (e.g. changes in tube impedance and discharge constriction) which occurred on a day-to-day basis. The variation in the values for L_{head} were considerably more reliable when Equation 3.5 was used for the evaluation than when Equation 3.8 was used. This is possibly because in the derrevation of Equation 3.8 the rate of change of the tube resistance was assumed to be negligable when infact it is not. Inclusion of the rate of change of tube resistance with time into Equation 3.8 would greatly complicate the evaluation for L_{head} by introducing a second order differential equation which would require numerically solving at each time interval. It was for this reason that the resistive component was assumed to be independent of time (over the duration of the excitation pulse).

Charging Voltage (kV)	L_{head} Using Equation (3.5)		L_{head} Using Equation (3.8)	
	No H_2	3% H_2	No H_2	3% H_2
14	287	165	3092*	93
15	442	159	318	40
16	232	343	8793*	91
17	256	166	240	48
18	299	-	56	59

- Data set out of range

* Discarded results

Figure 3.10: Results for the evaluation of L_{head} for various charging voltages without and with hydrogen additives using Equations 3.5 and 3.8.

3.9 Temporal Energy Deposition Calculation

Once L_{head} had been evaluated, then the temporal course of the energy deposition, E_{dep}, and hence of the power being deposited into the laser tube could be calculated. This was done by multiplying the resistive component, V_{res}, of the measured voltage by the tube current, I_d [1]:

$$E_{dep} = V_{res} I_d = \left(V_{meas} - L_{head} \times \frac{d(I_d)}{d(t)} \right) I_d . \qquad (3.9)$$

The Fortran 77 program listed in Appendix V was written to enable E_{dep} to be evaluated from I_d and V_{meas} waveforms, but would only work on systems with NAG® routines installed. Furthermore, the program also allowed the integral of E_{dep} to be evaluated between any two time intervals.

The product of the integral of E_{dep} with the PRF over the duration of the excitation pulse was used to evaluate the power delivered, P_{del}, to the laser tube. This value, when compared with the calculated value based on the stored energy, enabled the losses in the circuit to be evaluated and compared for a variety of different discharge conditions. The integration of P_{del} over time intervals was useful because it provided a measure of the temporal match of power deposition and the gain period. Any energy deposition after the gain period was effectively wasted, and lowered the laser operating efficiency.

3.10 Electron Density Calculation

An estimate was made of the temporal evolution of the electron density in the excitation pulse by considering the conductivity of the laser tube [3] from the measured tube current and tube voltage waveforms. This could only be attempted once the inductive component of V_{meas} was taken into account. The objective of such an analysis is to determine whether the addition of hydrogen to the buffer gas had any effect upon the temporal course of the total electron density. There is, however, a large degree of uncertainty (>50%) using this particular method because it provided a measure of the

average electron density across the bore of the tube, whereas in reality there is a strong radial dependence [4].

The conductivity of a plasma, σ, [5] may be expressed in terms of the electron density, n_e, the charge on an electron, e, the electron mass, m_e, the electron collision frequency with all species within the buffer gas, ν_c, the current density, J, and the electric field, E, by the relationship

$$\sigma = \frac{J}{E} = \left(\frac{n_e e^2}{m_e \upsilon_c} \right). \qquad (3.10)$$

Because the collision cross-section for momentum transfer (and consequently the buffer gas collision frequency) is strongly dependent on the electron energy, it is important to make a consideration for the electron energy in the analysis of the conductivity described by Equation 3.10. The average electron energy, Q_e, may be expressed in terms of a time dependent exponential decay [6]:

$$Q_e = Q_0 \exp\left(\frac{-t}{\tau_c} \right), \qquad (3.11)$$

where the time constant τ_c approximates to be the full width of the current pulse and Q_0 represents the electron energy at the time of onset of the current pulse. For efficient excitation of the upper laser levels of barium this was nominally estimated to be around 5 eV, an identical value to that used in [6] for a similar analysis of the electron density in copper halide vapour lasers.

The electron collision cross sections, σ_m, in neon, atomic hydrogen and molecular hydrogen are given by the empirical Equations 3.12-14 respectively [6], where the electron energy is in electron volts and σ_m is in Å^2. These data compared favorably with those from other sources [7].

$$\sigma_m = 1.6 Q_e^{1/6}, \qquad (3.12)$$

$$\sigma_m = 27 Q_e^{-1/2}, \text{ and} \tag{3.13}$$

$$\sigma_m = \frac{46.21 \ln(Q_e + 1.46)}{Q_e + 1.46}. \tag{3.14}$$

The collision frequency, υ_c, used in Equation 3.10 is related to σ_m by the relationship [8] shown by Equation 3.15, where p is the pressure in torr:

$$\upsilon_c = 21.0 \times 10^7 Q_e^{1/2} p \sigma_m. \tag{3.15}$$

Substituting Equations 3.11, 3.12 and 3.15 into Equation 3.10 gives the following expression for pure neon:

$$n(\text{neon})_e = \frac{3.36 \times 10^8 m_e p J Q_o^{2/3} \exp\left(\frac{-2t}{3\tau_c}\right)}{e^2 E}. \tag{3.16}$$

Substituting Equations 3.11, 3.12, 3.13 and 3.15 into Equation 3.10 gives

$$n(3\%\ H)_e = \frac{p J m_e}{e^2 E}\left(1.70 \times 10^8 + 3.26 \times 10^8 Q_o^{2/3} \exp\left(\frac{-2t}{3\tau_c}\right)\right), \tag{3.17}$$

for a mixture of 97% neon and 3% atomic hydrogen. Here it is assumed that the total collision cross section for electron collisions, σ_m(total), for the gas mix of 3% hydrogen and 97% neon was equal to the sum of the contributions of the collision frequency for each constituent gas species, i.e.

$$\sigma_m(\text{total}) = \frac{97}{100} 1.6 Q_e^{1/6} + \frac{3}{100} 27 Q_e^{-1/2}. \tag{3.18}$$

The proportions of atomic and molecular hydrogen present within the buffer gas during the excitation pulse were unknown. However, since the difference between the collisional cross section for atomic and molecular hydrogen was small (around 10% over electron energy ranges from 2-6 eV), the data from Equation 3.13 were used exclusively (and hence Equation 3.17 could be used) for the gas mix containing hydrogen.

3.11 Laser Tube Preparation

3.11.1 Discharge Cleaning

The laser power was found to be very sensitive to impurities within the discharge which originated from either the alumina tube/insulation, or poor seals allowing minute quantities of air to enter the discharge. Water vapour was a particular problem and took a great deal of thermal processing to be removed from the ceramic. Impurities were removed by operating the laser at tube wall temperatures above that normally required for efficient laser oscillation. Cleaning the laser by operating at elevated tube wall temperatures ensured that when the laser was operated under normal conditions, impurities were less likely to enter the discharge from the tube wall.

Although there were large quantities of water vapour present in the ceramic when either a new alumina tube or insulation was used, the majority of the water vapour could be removed by using a rotary pump to pump the laser tube under vacuum whilst the laser tube was warm (200-500^{o}C). However, a residual amount of water vapour remained 'locked' inside the ceramic, and could only be removed by heating the laser to very high temperatures [9].

The impurities within the discharge tube were measured in two ways and are discussed as follows:

First, an optical spectrum analyser (EG &G model) was used to observe the spectrum of the discharge. This could be used to identify and monitor molecular impurities, such as air, and atomic impurities present in the discharge. The vast majority of the spectra observed when the laser tube was clean were those of neon only with a notable exception occurring at ~550 nm corresponding to a hydrogen transition. This particular transition

was monitored on a day-to-day basis until the relative intensity became constant. It was found to be impossible to remove all the hydrogen from the laser tube using techniques at our disposal, probably as a result of internal bonding of impurities within the alumina which caused hydrogen to slowly diffuse out with time.

Secondly, the tube current and measured tube voltage waveforms were used to monitor the impurities in the discharge indirectly by measuring the discharge tube impedance [10]. The tube impedance was high when the laser tube had a large number of impurities present, corresponding to a high peak tube voltage and low peak tube current. As the laser tube was discharge cleaned over a period of hours, the peak tube voltage was found to decrease gradually and the peak tube current to increase gradually. These trends continued until most of the impurities had been removed, at which point there was no further change in the shape of the current and voltage waveforms when monitored on a day to day basis, even with a sealed off laser tube. Discharge cleaning generally took several tens of hours of operation at high tube wall temperatures, particularly when either new insulation and/or a new alumina tube was fitted.

3.11.2 Barium Preparation

Barium is a very reactive metal and is usually stored either under paraffin oil or in an inert environment such as argon. The barium used throughout this work was stored under paraffin oil. Problems were not encountered with impurities from the paraffin oil provided that care was taken to remove it all beforehand. The barium came in the form of a rod ~1/2" diameter and had a thick white-grey oxide layer on the outside which had to be removed before it could be used inside the laser. This section describes the method adopted for the cleaning of the barium and the removal of the oxide layer.

Surplus deposits of paraffin on the barium rod were first removed with absorbant cloth before placing inside a specimen jar filled with 40-60°C petroleum spirits (low water content). A lid was used on the jar to prevent absorption of water vapour in to the spirits. The jar was then placed in an ultrasonic bath for around 20 munutes to ensure that as much

as possible of the paraffin had been dissolved. The rod was then placed inside another specimen jar containing clean petroleum spirits.

Once cleaned in this manner, the barium was cut into lumps using a large pair of tin-snips and flattened using a 6" vice to a thickness of ~1-2 mm between pre-cleaned copper plates. The edges of the resulting barium disc were trimmed to expose a clean metallic surface. The flat surfaces were then scraped using a scalpel and/or a needle file to remove the oxide layer. The size of the disc which was eventually loaded into the laser was around 10 mm diameter (corresponding to a total mass of ~1.5 g).

Most of the preparation and cutting of the barium was carried out under petroleum spirits with the exception of the flattening of the barium in the vice. However, the time required for this process was short, resulting in only minimal oxidation of the surface. The barium had to be quickly loaded onto the molybdenum boat because in a matter of around 20 seconds the clean metallic surface would oxidise in air. The boat could not be removed once barium had been used in the laser tube because it was found to weld to the tube walls and hence the laser had to be loaded by first removing the anode window and then using a loading rod to position the barium piece inside the boat. A purging buffer-gas flow helped to reduce both oxidation of the barium and also contamination of the laser tube from air and water vapour. The laser was then pumped under vacuum for a number of hours before operation. This allowed plenty of time for the outgassing of small deposits of petroleum spirits from the barium.

3.12 Digitising Oscillograms

Unfortunately, a digitising oscilloscope was not available during experiments in order to measure and store the waveforms from the high-voltage probes, current transformer and the HgCdTe detector, and hence the only hard copies of the output were oscillogram photographs. In that form, mathematical manipulation of the recorded waveforms was not possible and therefore each of the oscillogram photographs had to be digitised such that each waveform was described by a set of data points. A Cherry graphics tablet interfaced with a computer was used for this purpose. The software was written by a

member of staff [11] at the University as part of an undergraduate experiment and enabled a waveform to be digitised and described by up to 500 data points to a precision of ±0.1 mm. The data points could be directly copied from the PC into a graphing package to re-create the waveforms.

In order to manipulate the waveforms (for example, subtracting the background noise from the laser pulse as described in Section 3.6), measurements at identical times were required for both of the waveforms. This could not be achieved with the digitising package since each waveform had to be digitised independently. This was overcome by accurately curve fitting each waveform and then creating a new data set with regular time intervals to describe the waveform. The only effective curve fitting routines which could accurately describe the sometimes complex waveforms were from NAG libraries [2]. Once the waveforms had been curve fitted, manipulation of the data was simple and quick, enabling background subtraction from laser pulses, calculation of the laser head inductance (Section 3.8), and the temporal analysis of both the energy deposition in the discharge tube (Section 3.9) and the electron density (Section 3.10).

3.13 Gas Temperature Evaluation

One possible mechanism to explain observed increases in laser power and efficiency when hydrogen is added to a neon buffer gas of a CVL and CHL is the reduction in the gas temperature with the addition of hydrogen because of the increased thermal conductivity of the buffer gas. This is one possible explanation for the particularly marked increase in laser power on the tube axis (see Section 4.5). However, thermal modelling of CHLs [6] suggests that small (2%) percentages of hydrogen additive to the buffer gas of is insufficient to make any significant change to the on-axis gas temperature and consequently is not a viable mechanism to explain the observed increases in laser power.

In Section 1.3.3 it was suggested that the electron temperature decreased exponentially with time and that if a sufficient amount of time were allowed between the interpulse period then the electron temperature eventually reaches the average gas temperature of the buffer gas. Because MVLs are excited by a pulsed electrical discharge,

the gas temperature also exhibits a time dependency, i.e. the buffer gas temperature decrreases as the interpulse period is increased. This raises another mechanism which may influence the performance of metal vapour lasers, i.e. the degree to which the gas temperature reduces in the interpulse period.

It is the purpose of this section to determine the effect of the addition of small percentages of additive on the radial gas temperature profile, and also to evaluate whether interpulse cooling of the buffer gas is likely to contribute to a significant reduction in the electron temperature.

3.13.1 Gas Cooling in the Interpulse Period

Using an identical analysis to that used in Reference [12], the increase in gas temperature, ΔT, accompanying the energy pulse is related to the input pulse energy, ΔE, through the gas molar heat capacity at constant volume, $C_{V,m}$, according to:

$$\Delta E = mC_{V,m}\Delta T. \tag{3.19}$$

Substituting m from the ideal gas equation (Equation 3.20), and $C_{V,m}$ from the molar heat capacity at constant volume (Equation 3.21), into Equation 3.19 and re-arranging to evaluate the fractional increase in gas temperatue for a given energy input gives Equation 3.22 shown below:

$$PV = mRT \tag{3.20}$$

$$C_{V,m} = \tfrac{3}{2}R \tag{3.21}$$

$$\frac{\Delta T}{T} = \frac{2\Delta E}{3PV} \tag{3.22}$$

where T is the gas temperature (K), ΔT is the change in the gas temperature (K), ΔE is the pulse energy input (J), V is the volume of the laser tube (m^3) and P is the buffer gas pressure (Pa).

In Section 5.2.3 it was found that the optimum input power to the laser was approximately 1800 W. This corresponds to a pulse energy of approximately 160 mJ (assuming a PRF of 11.5 kHz). Substituting in to Equation 3.22 the values of 160 mJ for the pulse energy, 6500 Pa for the pressure (corresponding to 50 torr) and $3x10^{-4}$ m^3 for the laser volume gives a fractional change in temperature of only approximately 5%. This assumes that all the stored energy is used to heat the gas which in reality is not the case. In Section 4.4.4 the power deposition from the storage capacitor to the laser tube was experimentally determined to be between 60% and 70% efficient and consequently the fractional change in gas temperature decreases by a corresponding figure, i.e. from 5% to approximately 3%. It is for this reason that gas cooling in the interpulse period was not considered to be an important factor and the justification as to why a steady state approximation could be made for the radial temperature profile analysis in Section 3.13.2.

3.13.2 Radial Gas Temperature Dependence

The steady-state radial conduction of heat through a cylinder [6] of radius r (assuming infinite length) is given by:

$$\frac{1}{r}\frac{d}{dr}\left[r\lambda\frac{dT}{dr}\right]+q=0 \qquad (3.23)$$

where q is power deposited per unit volume, T is the gas temperature and λ is the thermal conductivity which is temperature dependent, as shown in Equation 3.24,. The values for the constants a and B are dependent on the type of buffer gas.

$$\lambda(T)=BT^{a} \qquad (3.24)$$

Typical values for a and B for neon, hydrogen, helium, and a mix of 2% hydrogen and 98% neon gases are shown in Table 3.11.

Gas	Temperature (K)	B ($Wm^{-1}K^{-1}$)	a ($Wm^{-1}K^{-1}$)	Reference
Ne	800-3000	$9.7x10^{-4}$	0.685	[6]
H_2	800-1600	$4.4x10^{-4}$	1	[6]
H_2	1600-2600	$4.4x10^{-25}$	7.56	[6]
He	800-3000	$24x10^{-4}$	0.73	[12]
Ne:H_2 (98:2)	800-1600	$9.3x10^{-4}$	0.695	[6]
Ne:H_2 (98:2)	1600-2600	$1.84x10^{-6}$	1.54	[6]

Table 3.11: Typical values for the thermal conductivity coefficients a and B

Equation 3.23 may be solved for T(r) using the boundary conditions:

(i) $dT/dr = 0$ at $r=0$, and

(ii) $T=T_w$ when $r=R$

where R is the tube radius and T_w is the tube wall temperature, as shown in Equation 3.25:

$$T(r) = \left[T_w^{1+a} + \frac{1+a}{4B} q(R^2 - r^2) \right]^{\frac{1}{1+a}} \qquad (3.25)$$

Figure 3.12 shows how the gas temperature varies with radial position for neon, neon and hydrogen (ratio of 98:2), helium and hydrogen gas, assuming a fixed wall temperature of 1300 K (approximately optimum for the BVL) and the optimum input power of 1800 W founf in Section 5.2.3 (corresponding to a specific input power of 6 Wcm^{-3}). Clearly the on-axis gas temperature is greatest when neon is used giving on-axis temperatures of

approximately 2400 K, and significantly lower when either helium or hydrogen are used, giving on-axis temperatures of approximately 1700 K and 1600 K respectively.

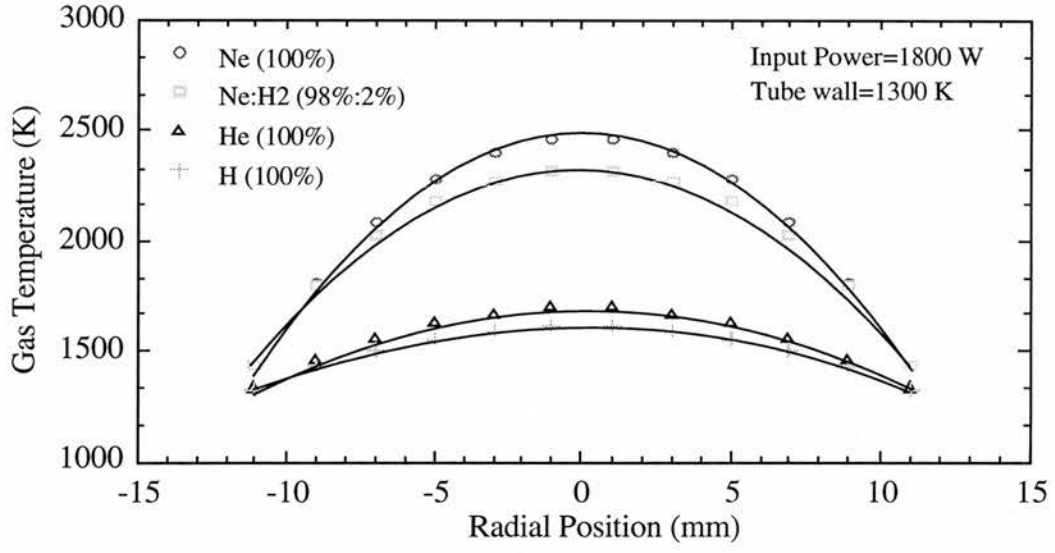

Figure 3.12: Dependence of gas temperature on radial position in discharge tube.

Although an input power of 1800 W was found to be the optimum input power using either neon or a premix of neon and 3% hydrogen was used (see Section 5.2.3), the actual power delivered to the discharge tube was experimentally determined to be approximately 40% less when neon was used and approximately 30% less when a neon/hydrogen (ratio 97:3) gas mix was used (see Section 4.4.4). The radial dependence of gas temperature was re-evaluated using the measued values for the power deposited (i.e. 3.7 Wcm^{-3} and 4.3 Wcm^{-3} for neon and a neon/hydrogen gas mix respectively). This is shown in Figure 3.13.

It is clear from Figure 3.13 that the on-axis gas temperature decreased for all the buffer gases because of the decrease in the specific power delivered to the tube. However, because the power delivered to the tube was greater when a pre-mix of neon and hydrogen was used compared to when only neon was used, the increase in the thermal conductivity with hydrogen addition (which would normally result in a reduced on-axis gas temperature) is off-set by the increase in the power delivered to the tube. The net result of this is that the

on-axis gas temperature is approximately the same using neon as when using a neon/hydrogen gas mix (ratio 98:2).

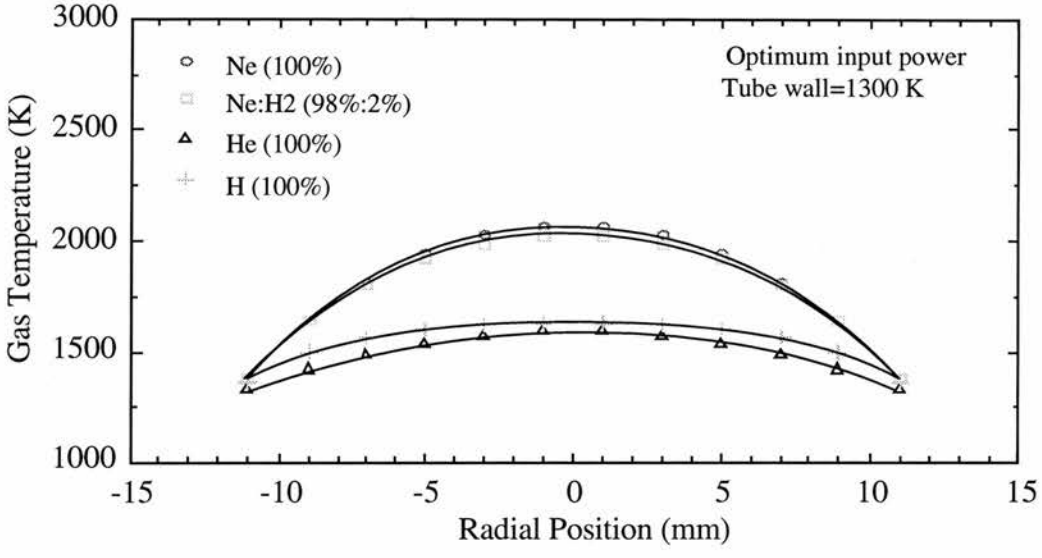

Figure 3.13: Dependence of gas temperature on radial position in discharge tube.

It is interesting to note that even though the input power for maximum total laser power was considerably higher when helium was used as the buffer gas (at approximately 2400 W, see Chapter 6) compared to when either neon or a premix of neon and hydrogen were used (both approximately 1800 W), the on-axis gas temperature was evaluated to be 1800 K which is still considerably lower when either neon or neon and hydrogen was used.

3.14 Summary

The needle valves which controlled the buffer-gas flow rate were calibrated which enabled the percentage of additive to the laser tube to be determined. The laser power meter was also calibrated with reference to a previously calibrated power meter. The laser pulse intensity waveforms were measured using a HgCdTe detector which was mounted behind a pin hole and on a translation stage which enabled the profile of the laser pulse intensity to be measured. The discharge tube inductance was determined experimentally to be 200±120 nH. This was used to evaluate the resistive component to the measured tube voltage which enabled the power delivery to the laser tube and the temporal course of the electron density during the excitation pulse to be determined.

A simple gas heating model has been developed to estimate the radial dependence of gas temperature for various buffer gas types. Using a steady-state approximation it has been shown that the addition of small percentages of hydrogen to a neon buffer gas is unlikely to significantly change the on-axis gas temperature. This is because the decrease in the on-axis gas temperature which would result from the increased gas conductivity with the addition of 2% hydrogen to a neon buffer gas is off-set by an increase in the specific power delivered to the tube.

3.15 References

[1] Work Undertaken by Dr S. Fairlie, University of St Andrews (1993).

[2] NAG® Fortran Library, Dept mathematics, University of St Andrews (1993).

[3] 'Conductance of multicomponent gas mixtures', Yu. G. Chernov, High Temp (1970), **8** (5) pp 881-885.

[4] E. Le Guyadec, C. Chamouard, J. P. Goosens, D. Gilbert, P. Lemaire, Opt. Comm. **100** (5,6) pp 461-466 (1993).

[5] M. J. Kushner, B. E. Warner, J. Appl. Phys. **54** (6) pp 2970-2982 (1983).

[6] D. N. Astajov, N. K. Vuchkov, N. V. Sabotinov, IEEE J. Quantum Electron. **24** (9) pp 1927-1935 (1988).

[7] 'Plasma Physics', J. L. Delcrouix, **2**, Wiley, New York pp 163 & 167 (1968).

[8] 'Microwave Discharge Phenomena in Gases', A. D. MacDonald, Wiley, New York P 25 (1966).

[9] O.Marazof, I.Kostadinov, J.Phys.E:Sci Instrum. **22** pp 744 (1989).

[10] G. L. Clarke, PhD Thesis, St. Andrews University (1988).

[11] Software written by J. Armitage, University of St Andrews (1990).

[12] T.R. Pugsley PhD Thesis, St Andrews University (1994).

Chapter 4

Influence of H_2, D_2 and He Additives on BVL Operation with a Ne Buffer Gas

4.1 Introduction

In this chapter, the dependence of the laser power (all lines), and the laser power at 1.13 μm and 1.50 μm have been investigated for various percentages of H_2, D_2 and He added to the neon buffer gas of a BVL. The findings for the temporal dependence of the 1.13 μm and 1.50 μm transitions, the temporal dependence of the tube current and the tube voltage waveforms have also been investigated for various percentages of H_2, D_2 and He added to a neon buffer gas. Also discussed in this chapter is the analysis of the power deposition in the laser tube and its dependence upon the percentage of H_2, D_2 and He added.

A number of factors were kept constant throughout this section with the aim of keeping the number of varied parameters to a minimum. Such parameters include the choice of the by-pass inductance, the ratio of storage to peaking capacitance and the buffer-gas flow rate. In the first part of this chapter, the choice for the selection of each is briefly discussed.

4.2 Fixed Parameter Values

4.2.1 The Bypass Inductor, L_b

During the charging cycle, the majority of the current used to charge the storage capacitor flowed through the by-pass inductor, L_b, and only a small fraction flowed through the partially ionized discharge tube. The degree to which either current path contributes to the charging process was governed by the value of L_b and the laser tube conductance during the charging cycle. As was discussed in Section 2.2.2, if the value of L_b were too large then the electron/ion recombination which occurs in the interpulse period could be hindered because of the current flowing through the tube during the charging cycle. This would tend to increase the preionisation density within the tube and hence reduce the discharge tube impedance before the following excitation pulse. It was therefore important to establish the dependence of the by-pass inductance on both the total laser power and also the tube conductivity in order to determine whether or not the maximum laser power was being hindered by too high a current flowing through the discharge tube during this charging cycle.

Using a neon buffer gas only, the dependence of the laser power, the tube current and the tube voltage waveforms were measured for various by-pass inductances. The measurements were all taken on the same day in order to remove the possibility of any random day to day variations. The change was made by first turning off the supply, swapping the inductors, and turning the supply back on; the whole process took around 10-15 seconds to perform. A short period of time was then allowed for the laser to restabilise before the laser power, the tube current and tube voltage waveforms were measured. By keeping the process as short as possible, the thermal shock etc on the laser tube was also kept to a minimum.

The laser was maintained at an input power of 1800 W (based on stored energy); the charging voltage, PRF and pressure were maintained at 16 kV, 11.5 kHz and 54 torr respectively. These discharge conditions were found to correspond to maximum total laser power. The by-pass inductances were made by evenly winding 18 s.w.g. insulated copper wire around glass tubing in the form of a coil to the values of 280, 140, 70 and 40 μH.

The total laser power, laser power at 1.13 μm and at 1.50 μm were measured for each of these by-pass inductors. Oscillograms of the tube current and tube voltage were also taken.

Figure 4.1 shows how the total laser power, the laser power at 1.13 μm and at 1.50 μm varied as functions of the value of L_b. Figure 4.2 shows the corresponding tube current and tube voltage waveforms obtained for each of the by-pass inductors. Despite the wide range of inductance values selected, the laser power at both 1.13 μm and 1.50 μm showed little or no variation with the value of L_b. The tube voltage and tube current waveforms also appeared to show little or no variation with the value of L_b.

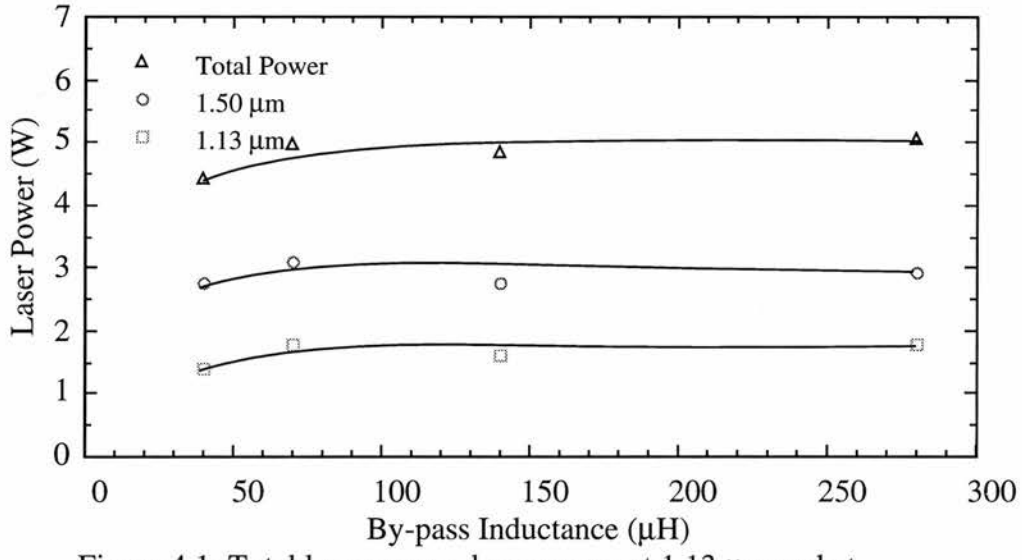

Figure 4.1: Total laser power, laser power at 1.13 μm and at 1.50 μm as a function of by-pass inductance.

If variation of the by-pass inductance were to make any difference to the preionisation density and hence to the tube impedance, then it would be reflected in either the laser power or the tube voltage and tube current waveforms. A decrease in the preionisation density would tend to cause the peak tube voltage to increase and the peak tube current to decrease. In addition, the step which often occurred in the tube current waveform (see Section 4.4.3) would tend to decrease with a decreasing preionisation density. No increases or decreases were observed in the laser power, the tube current waveform, the tube voltage waveform or the characteristic step in the tube current, thus it was concluded that over the range of by-pass inductances selected, negligible charging current passes through the laser tube under these conditions and consequently the

preionisation density within the tube remained unaffected by the selection of the value for the by-pass inductor within the range investigated.

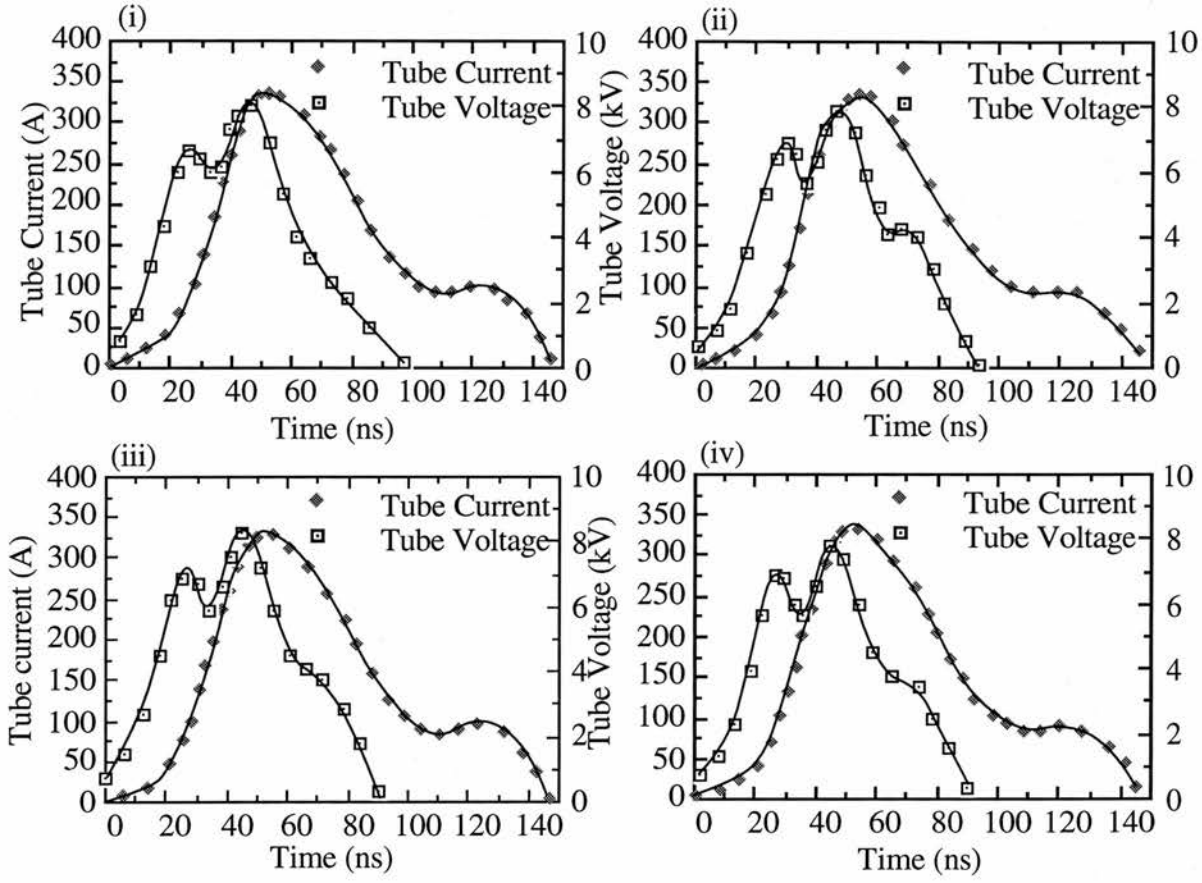

Figure 4.2: Tube current and tube voltage waveforms using various different bypass inductors (i) 280 μII, (ii)140 μH, (iii) 70 μH and (iv) 40 μH.

4.2.2 Buffer Gas Flow Rate

In many high-temperature laser systems, for example CVLs, a buffer gas flow is important to remove impurities from the discharge region. These impurities usually enter the discharge zone from either the central laser tube and/or the insulation material surrounding this tube, because of the high temperatures which are required for laser oscillation. Sealed-off high temperature lasers such as CVLs have been demonstrated [1], and with such devices, laser tube cleanliness becomes a very important design feature.

The design of the BVL used in the present studies required a flowing buffer gas in order to seed the active volume with barium vapour. It was not designed as a slow flow or sealed off BVL. In addition, it would be difficult to purge the laser tube of barium vapour

prior to turning off the laser or indeed to control small percentages of additives to the buffer gas if the tube were sealed off.

As with other high temperature lasers, a flowing buffer gas helped to remove both trace impurites and residual traces of additives from the laser tube. There was, however, found to be an upper limit to the flow rate. This was governed in part by considerations of a reduction in the lifetime of each load of barium, but also by the influence of the low temperature of the buffer gas as it entered the region of the laser tube close to the molybdenum boat and the finite rate of barium evaporation (entrainment).

Figure 4.3 shows experimentally how the laser power varied with buffer gas flow rate using only a neon buffer gas. Under these discharge conditions the optimum buffer-gas flow rate was found to be 1-3 atm.l/hr. The flow rate was thereafter maintained throughout all the studies of the BVL at 3 atm.l/hr.

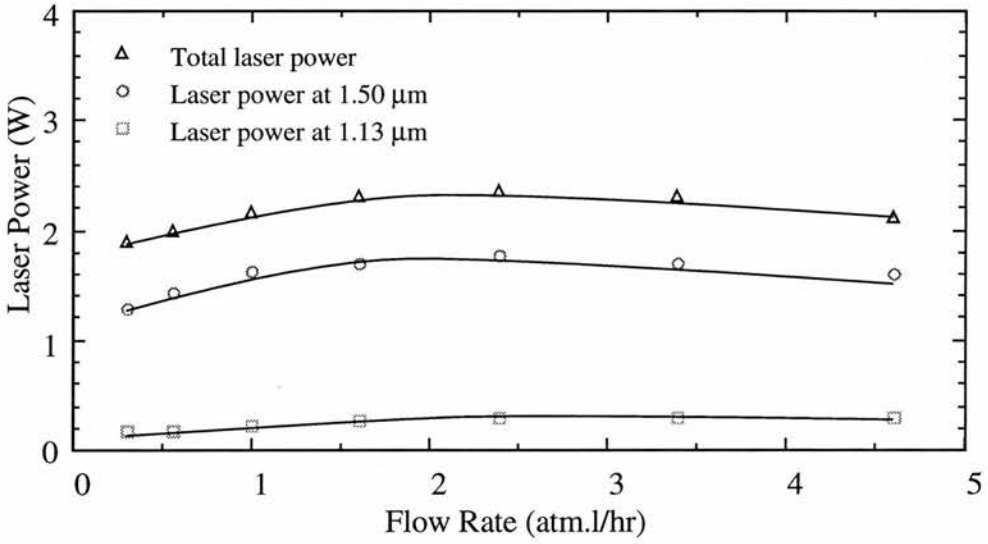

Figure 4.3: Total laser power, laser power at 1.13 μm and 1.50 μm as a function of buffer gas flow rate.

4.2.3 Storage and Peaking Capacitors

As discussed in Section 2.3.5, the electrical excitation circuit is an important consideration when designing pulsed self-terminating lasers because of the requirement for a fast risetime (50-100 ns) tube current. One method often adopted to reduce the risetime is the inclusion of a peaking capacitor in the discharge circuit, with a value typically one half to one third the value of the storage capacitor. The optimum ratio is likely to depend upon the particular discharge conditions and so a fixed ratio of 1:2 was selected.

Figure 4.4 shows the effect of introducing a peaking capacitor on the tube current and tube voltage waveforms. The value of the peaking capacitor was approximately half the value of the storage capacitor, corresponding to 0.8 nF and 1.6 nF respectively (hot values). The operating conditions of the driving circuit were identical in both cases with a charging voltage, PRF and pressure of 14 kV, 15 kHz and 52 torr respectively.

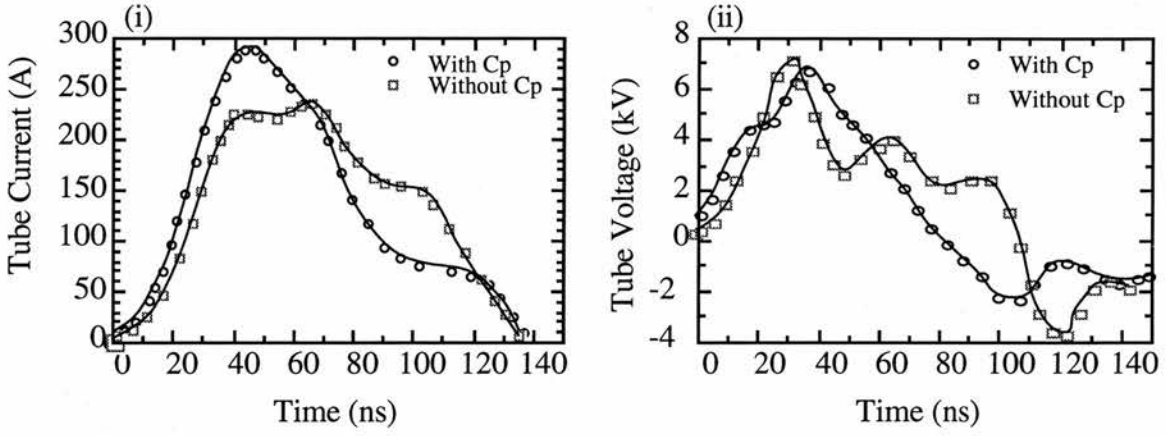

Figure 4.4: Effects of including a peaking capacitor on (i) the tube current and (ii) the tube voltage waveforms.

One distinct feature of the introduction of a peaking capacitor was the increase in the peak tube current from 220 A to 290 A. Another distinct feature was that the peak tube voltage noticeably shifted to coincide more with the peak tube current, shifting from a 30 ns delay to only 8 ns with the inclusion of a peaking capacitor. This represented a significant difference because in both cases the onset of laser oscillation began at approximately the peak of the tube current. The enhanced electric field at this point with the inclusion of a peaking capacitor favours upper level excitation because of the generation of higher energy electrons.

The tube current was enhanced when a peaking capacitor was included in the circuit, since the energy stored in the peaking capacitor could be quickly transferred to the laser tube due to the low inductance discharge loop. This resulted in an increased tube current risetime. Contributions from the storage capacitor were believed to occur later in the tube current waveform because of the higher inductance path between it and the laser tube. This is the explanation for the double peaked tube current waveform often obtained (see Section 5.2.5).

4.3 Variation of Additive Percentages

4.3.1 Laser Power Dependence on H_2

The laser was repeatedly operated on a daily basis using a neon buffer gas under identical conditions until the laser power, tube current and the tube voltage stabilised to constant values. The buffer gas pressure, charging voltage, PRF and charging capacitance were maintained at 52 torr, 13 kV, 10 kHz and 1.3 nF respectively. A premix of neon and hydrogen was added to the laser from a 10 l reservoir bottle (ratio of 10:1 Ne:H_2) through a calibrated fine-control metering valve. As the valve from the reservoir bottle was opened then the metering valve from the pure neon supply was correspondingly closed in order to maintain a constant flow-rate. The exhaust valve to the vacuum pump (valve (d) in Figure 2.15) which controlled the pressure was left untouched during the measurements. The total laser power and the laser power at the principal wavelengths of 1.13 μm and 1.50 μm were measured as functions of the percentage of hydrogen added in the range 0-9%. The peak tube voltage and tube current measurements were also measured.

At temperatures below ~200°C, hydrogen reacts with barium to form barium hydride, which in the absence of air is a stable compound. Failure to remove the hydrogen from the laser tube whilst the laser was hot resulted in the formation of BaH_2 when the tube cooled down. It was therefore important at each time to purge as much of the hydrogen as possible from the laser tube before the laser was turned off. This was achieved by closing the neon/hydrogen metering valve and correspondingly opening the needle valve for the pure neon (to maintain the pressure and flow rate) and allowing time for the hydrogen to purge from the system to re-establish the conditions for laser power, tube current and tube voltage before H_2 was added. Only when hydrogen had been purged was the input power then slowly reduced over the course of approximately an hour before finally being turned off when the tube wall temperature was between 400°C and 600°C. The laser was then vacuum pumped to remove residual traces of hydrogen. When the laser was restarted, the conditions using only a neon buffer gas were re-established before any further experiments were undertaken.

It should be noted that it was found difficult to remove the hydrogen from the laser when the percentage of hydrogen additive was large (>10%). It was then found necessary to discharge clean the laser for perhaps several hours and to vacuum pump the laser overnight.

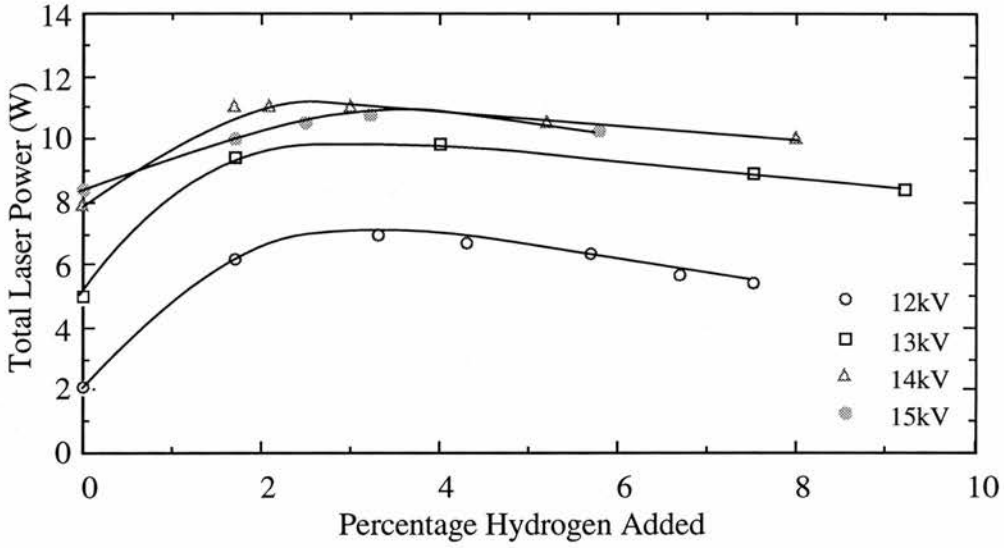

Figure 4.5a: Total laser power as a function of percentage hydrogen added for various charging voltages.

Figure 4.5 shows how (a) the total laser power (b) laser power at 1.13 μm and (c) laser power at 1.50 μm varied with percentage of added H_2 for various charging voltages ranging from 12 to 15 kV. In the absence of added H_2, the total laser power and laser powers at 1.13 μm and 1.50 μm increased with charging voltage, although at higher charging voltages the increase in laser power at 1.13 μm was only minimal, increasing from 3.4 W at 14 kV to 3.6 W at 15 kV.

The addition of small amounts of H_2 significantly increased the laser power at both wavelengths over all the charging voltages selected. The laser power at 1.13 μm peaked when the percentage added hydrogen was between 2% and 4%. Any further increase in the H_2 percentage above this caused the laser power at 1.13 μm to decrease rapidly from the peak value. The laser power at 1.50 μm also increased with increasing H_2 percentage, peaking with between 5% and 6% added H_2. At higher percentages, the laser power at 1.50 μm began to decrease, but at a much slower rate than occurred at 1.13 μm. In all cases, the laser powers at both 1.13 μm and 1.50 μm were higher when H_2 was present in the tube (up to 9%) than with only neon. The total laser power (which predominantly

had contributions from the 1.13 μm and 1.50 μm transitions) peaked at 9.8 W with a H_2 percentage of between 2% and 4%. This represented an increase of ~95% in laser power from the case when only neon was used as the buffer gas.

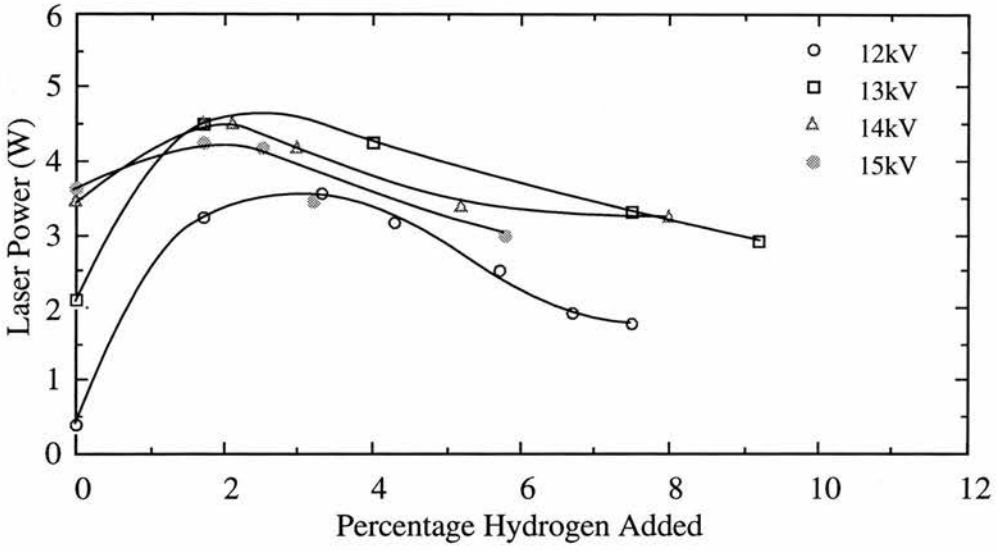

Figure 4.5b: Laser power at 1.13 μm as a function of percentage hydrogen added for various charging voltages.

Figures 4.5b and 4.5c indicate that the 1.13 μm laser transition is much more dependent upon the percentage of added H_2 than the 1.50 μm laser transition. At 1.50 μm, the laser power increased with increasing charging voltage for all H_2 percentages. However, at 1.13 μm the charging voltage which gave the maximum power for a given H_2 percentage decreased with increasing percentage. For example, in the absence of H_2, the charging voltage which gave maximum power at 1.13 μm was 15 kV. With 3% added H_2 the charging voltage for maximum output at 1.13 μm decreased to 14 kV and with 6% added H_2, the optimum charging voltage decreased further to 13 kV. Addition of H_2 to the laser tended to cause the peak tube current to decrease and the peak tube voltage to increase with increasing percentage of additive.

There are two likely mechanisms for the increase in laser power at 1.13 μm and 1.50 μm with the addition of H_2 to the neon buffer gas. These are discussed as follows.

First, at low charging voltages, the increase in laser power at 1.13 μm and at 1.50 μm with the addition of small quantities of H_2 to the discharge may be caused by an increase in upper level excitation. This enhanced upper level excitation is caused by an

increase in the tube impedance resulting from enhanced electron cooling and increased electron-ion recombination (see Section 1.3.5).

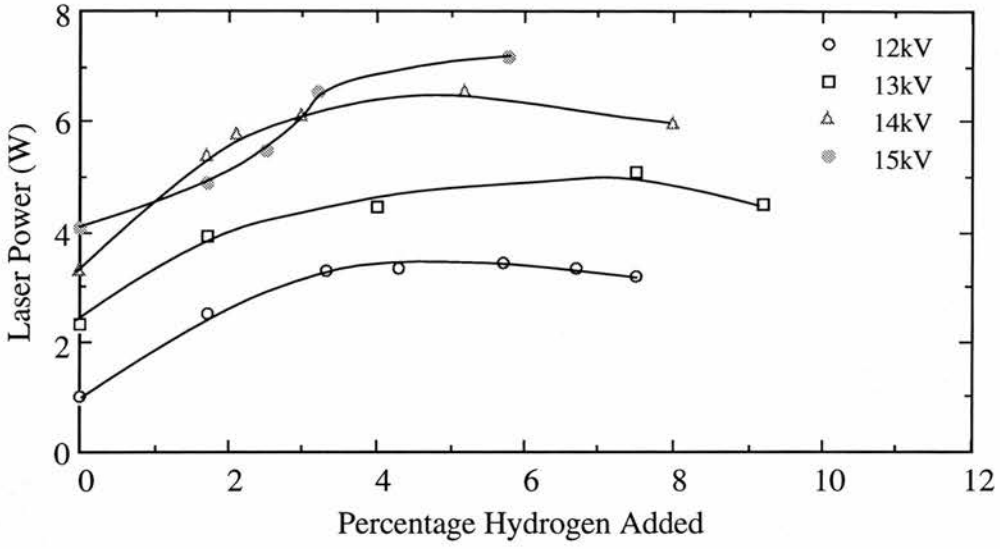

Figure 4.5c: Laser power at 1.50 μm as a function of percentage added hydrogen for various charging voltages.

Second, the increase in laser power at 1.13 μm and 1.50 μm with H_2 addition may be due to a decrease in the metastable population in the interpulse period caused by the enhanced electron cooling in the interpulse period because of the presence of additives (see Section 1.3.5).

In the absence of any added H_2, and indeed for small (<3%) percentages of added H_2, the laser powers at 1.13 μm and 1.50 μm generally increased with increasing charging voltage. However, at larger H_2 percentages the laser power at 1.13 μm increased with increasing charging voltage for charging voltages up to 13 kV, but then decreased when the charging voltage was increased further. Conversely, the laser power at 1.50 μm increased with increasing charging voltage regardless of the percentage of added H_2. There are two likely mechanisms which explain the observed trends which are outlined as follows.

First, the $5d^3D_2$ lower laser level for the 1.13 μm transition has a very low energy (~1.2 eV) and consequently thermal/relaxed population of this level is much more likely to become a problem than the thermal population of the 1.50 μm lower laser level. Although increasing the input power by increasing the charging voltage enhanced the excitation to the upper laser level, the increase in input power also increases the thermal population of the

lower laser levels. This would have an effect upon the 1.13 μm transition at lower input powers than the 1.50 μm transition. Increasing the hydrogen percentage could exacerbate the problem by increasing the power deposition into the laser tube (characterised by an increase in the tube wall temperature), because the increased tube impedance gives better matching of the discharging circuit to the laser tube. This would explain why the charging voltage which gave maximum power at 1.13 μm tended to decrease with increasing H_2 percentage.

Second, the decrease in power of the 1.13 μm laser transition with increasing high H_2 percentage may be caused by increased competition between the 1.13 μm and 1.50 μm transitions because of the shared upper laser level (see Section 1.3.5). This phenomenon is discussed more fully in Section 4.4.

4.4 Comparison of H_2, D_2 and He Additives

4.4.1 Laser Power

In order to gain more insight into the mechanisms involved when H_2 is added to the neon buffer gas of the BVL, it is helpful to establish whether any other additives to the buffer gas also increase the laser power and efficiency. Other gases of interest are D_2 and He. A comparison of D_2 and H_2 is particularly interesting because both exhibit the same chemical activity and only differ in their molecular masses. Both H and D may form electronegative ions in the discharge afterglow but because of the relative molecular masses, the efficiency of electron cooling will be lower for D_2 than for H_2. Helium does not form electronegative species and hence an increase in laser power with helium additives identifies an improvement in laser performance as due to an increase in either the degree of electron cooling, and hence in discharge tube impedance, and/or metastable depopulation of the lower laser levels.

The dependences of the total laser power, and laser powers at 1.13 μm and at 1.50 μm were investigated as functions of H_2, D_2 and He additive concentrations in a neon buffer gas. The percentages of each were controlled by considering the relative flow rates through calibrated needle valves in much the same way as described in the preceding

section (Section 4.3.1), with the exception that when D_2 and He were used, the reservoir bottle was premixed with 20% D_2 and 33% He respectively and not 10%. In each case the remaining balance within the bottle was pure neon. Larger percentages of D_2 and He were required because 10% of either added to the laser was found to be insufficient to cause either the total laser power or the laser power at 1.13 μm to peak or saturate. As also discussed in Section 4.3.1, prior to reducing the input power and turning off the laser, the H_2 and D_2 were purged from the laser to regain the conditions before either were added. This was not found to be necessary when He additives were used because helium is inert to barium and hence could be easily and simply removed by pumping under vacuum once the laser was turned off.

The laser input power was kept constant at 1800 W (based on stored energy) which corresponded to a charging voltage, PRF, pressure and storage capacitance of 16 kV, 11.5 kHz, 52 torr and 1.2 nF (hot value) respectively. These represented the conditions which gave both the maximum total laser power when 3% H_2 was added to the laser, as discussed in Section 5.2.3, and also the conditions which gave maximum laser power in the absence of added H_2 for this capacitance value. Measured quantities of H_2, D_2 or He were added to the buffer gas in increasing percentages. For each percentage, time was allowed for the laser power to stabilise before taking measurements of the total laser power, and the laser powers at 1.13 μm and at 1.50 μm. Oscillograph photographs for the laser pulses at both 1.13 μm and 1.50 μm were taken for each percentage along with the tube current and the tube voltage waveforms.

Figure 4.6 shows how (a) the total laser power, (b) the laser power at 1.13 μm and (c) the laser power at 1.50 μm varied as functions of the percentage of H_2, D_2 and He added. Figure 4.6a shows that the total laser power peaked at 12.5 W when 5% H_2 was added to the laser. A comparable laser power could be obtained when the D_2 percentage was approximately double at 10%. However, a similar laser power could not be obtained for any percentage of helium up to at least 33%. The total laser power was larger for any of the additives and for any percentage of additive examined than when only neon was used as the buffer gas.

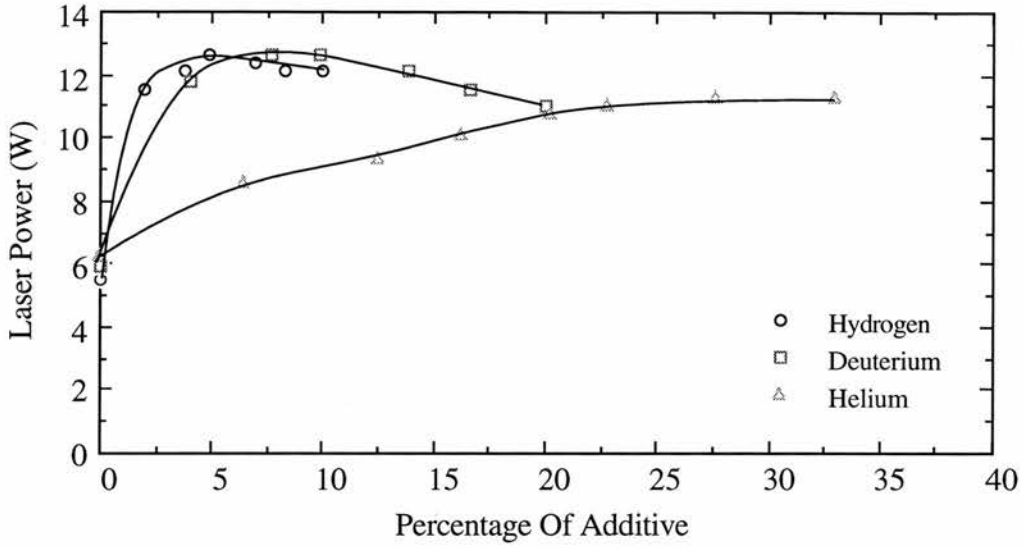

Figure 4.6a: Total laser power as a function ofpercentage of additive to the buffer gas.

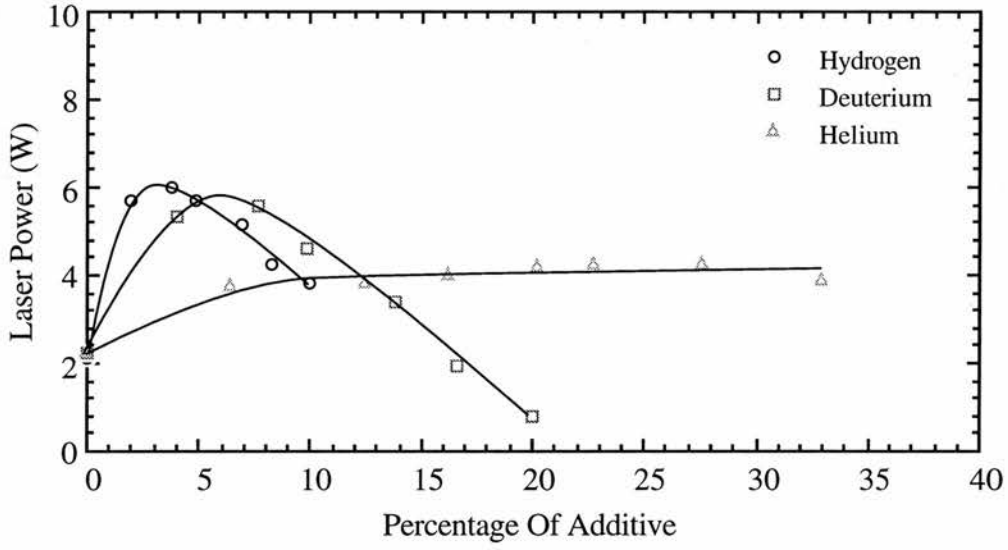

Figure 4.6b: Laser power at 1.13 μm as a function of percentage of additive to the buffer gas.

Figures 4.6b and 4.6c show the contributions to the total laser power from the 1.13 μm and the 1.50 μm transitions respectively. The laser power at 1.13 μm increased when both H_2 and D_2 were added to the laser, with the laser power peaking with 3% H_2 and with 6% D_2 added to the laser. The maximum laser power which could be obtained at 1.13 μm using either H_2 or D_2 was approximately the same at 6.0 W and 5.8 W for H_2 and D_2 additives respectively. The laser power at 1.50 μm increased with increasing percentage of additive and did not reach an optimum value, as was the case with the

1.13 μm transition. The laser power at 1.50 μm was approximately the same for comparable amounts of H_2 and D_2 added to the laser.

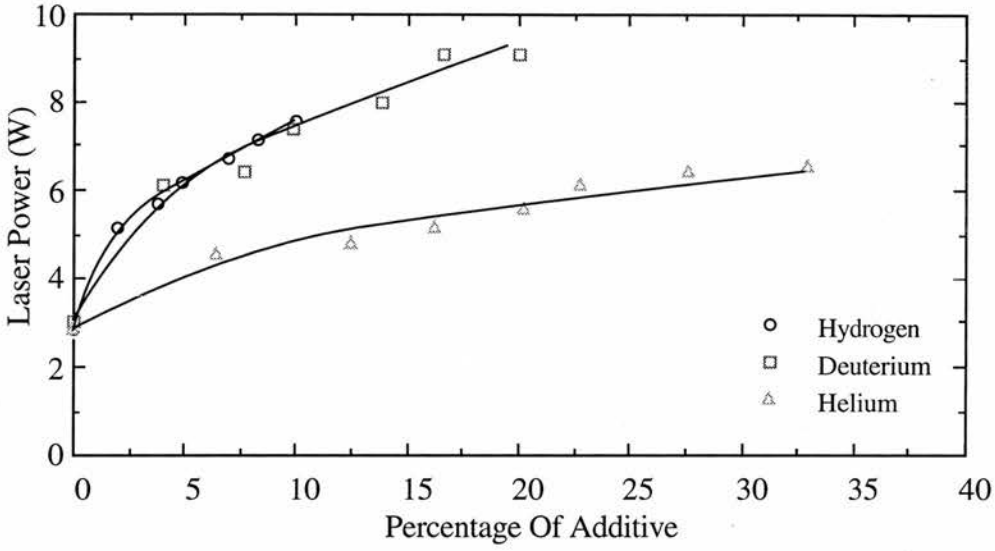

Figure 4.6c: Laser power at 1.50 μm as a function of percentage of additive to the buffer gas.

4.4.2 1.13 μm and 1.50 μm Laser Pulse Intensities

Figure 4.7 shows a number of contour plots of how laser pulse intensity at (i) the 1.13 μm and (ii) the 1.50 μm (measured at the beam centre) varied with the addition of various percentages of (a) H_2, (b) D_2 and (c) He. The input power (based on stored energy) P_{in}, PRF, charging voltage, buffer gas pressure, storage and peaking capacitances (hot values) were maintained at 1800 W, 11.5 kHz, 16 kV, 54 torr, 1.2 nF and 0.6 nF respectively.

In each case laser oscillation began first at 1.50 μm and was then followed by laser oscillation at 1.13 μm some 10-20 ns later. Furthermore, the addition of any of the three additives caused the laser pulse to occur earlier with respect to the onset of the current pulse than when only neon was used as the buffer gas. The time delay between the beginning of the current pulse and the onset of laser oscillation was also found to be dependent upon the type of additive used. In general, the laser pulse occurred earlier with increasing percentage of additive with the effect being most pronounced with H_2 additives, followed by D_2 and least with He.

Figure 4.7a: 1.13 μm laser pulse as a function of time and percentage of hydrogen added.

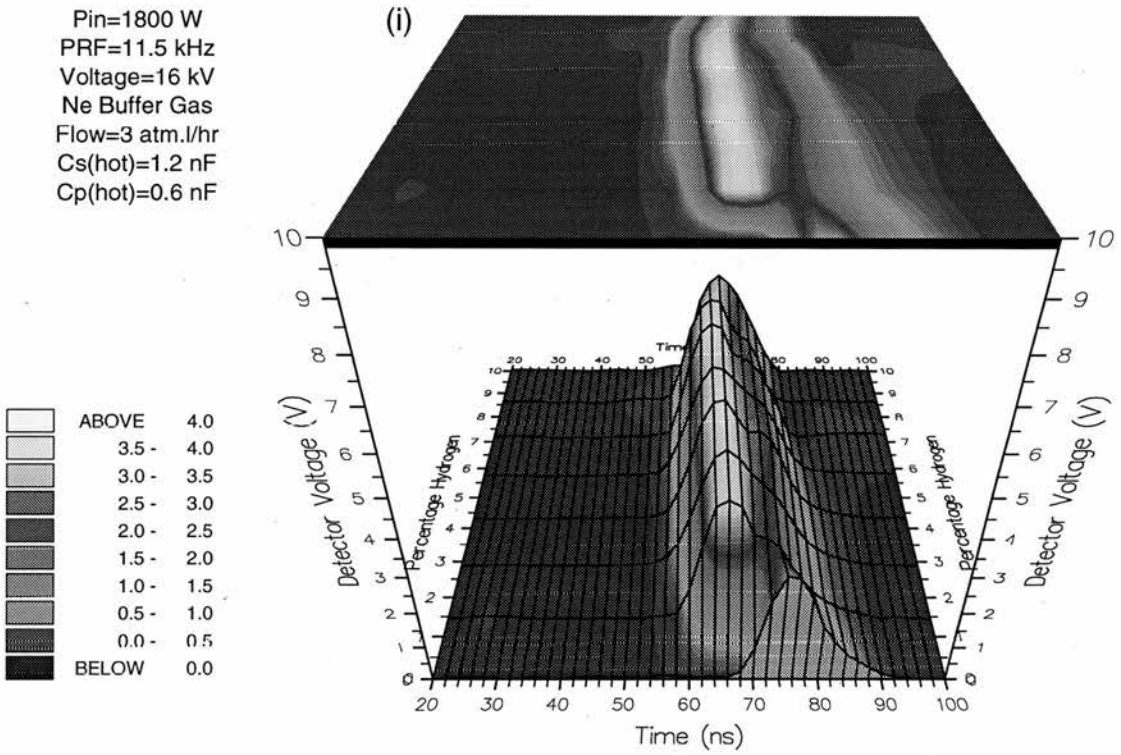

1.50 μm laser pulse as a function of time and percentage of hydrogen added.

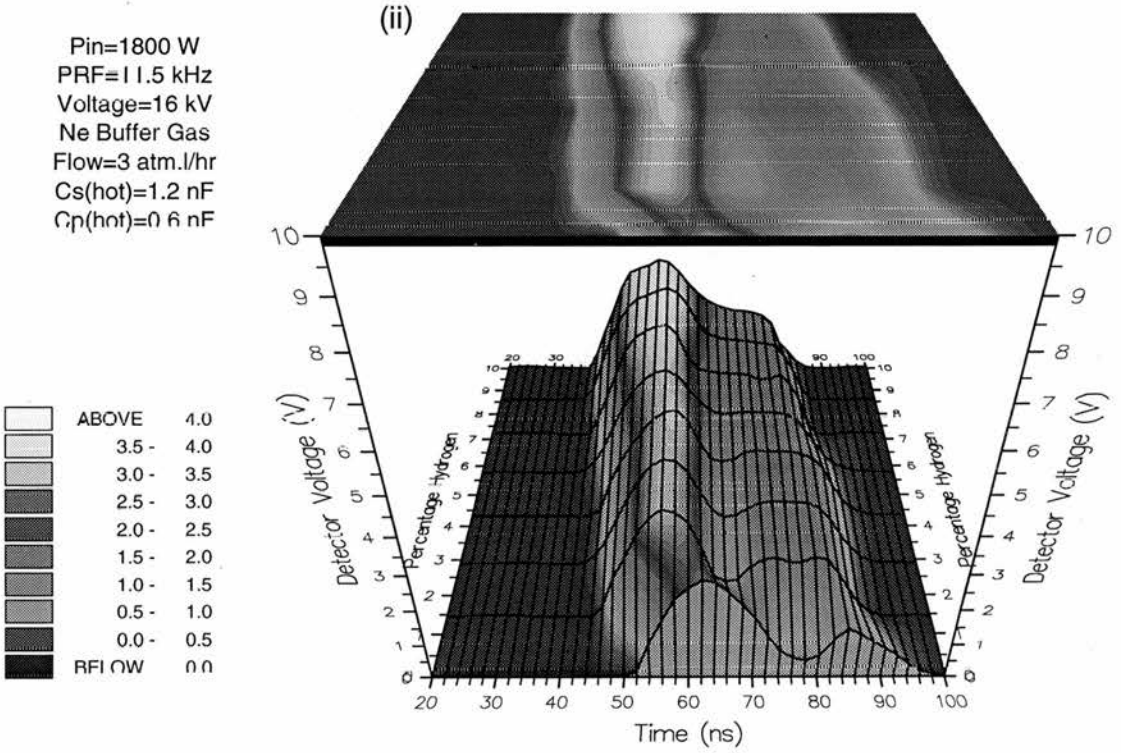

Figure 4.7b: 1.13 μm laser pulse as a function of time and percentage of deuterium added.

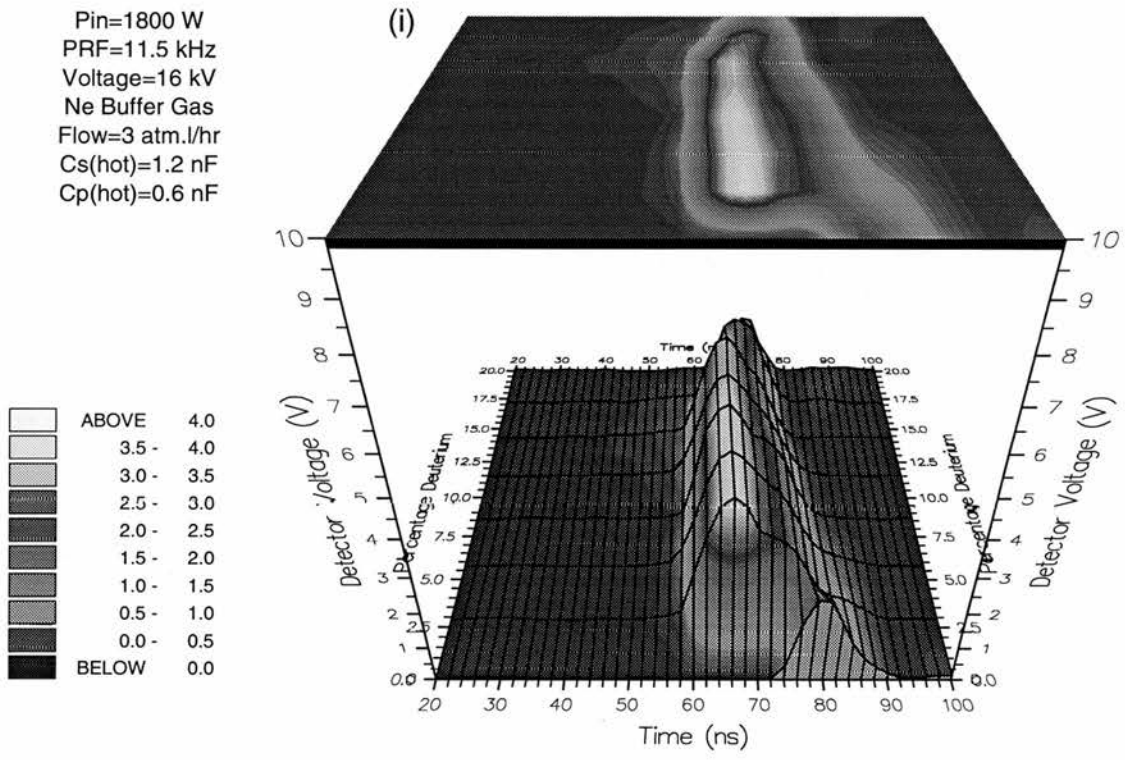

1.50 μm laser pulse as a function of time and percentage of deuterium added.

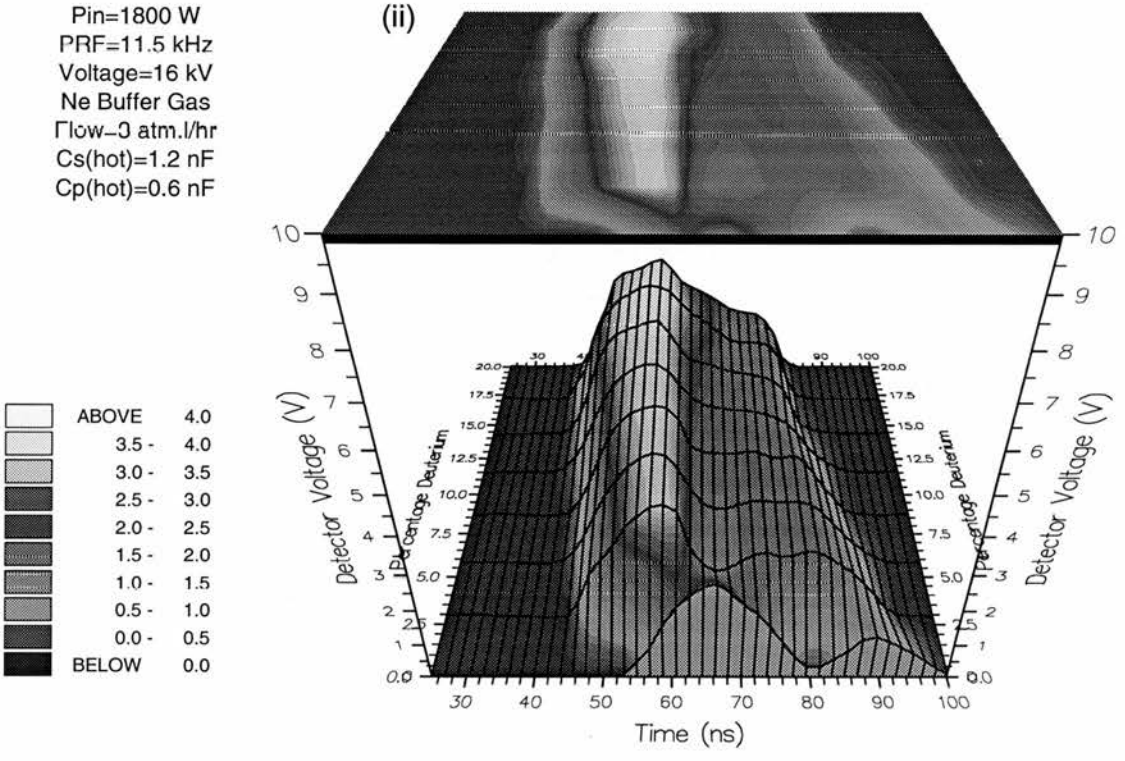

Figure 4.7c: 1.13 μm laser pulse as a function of time and percentage of helium added.

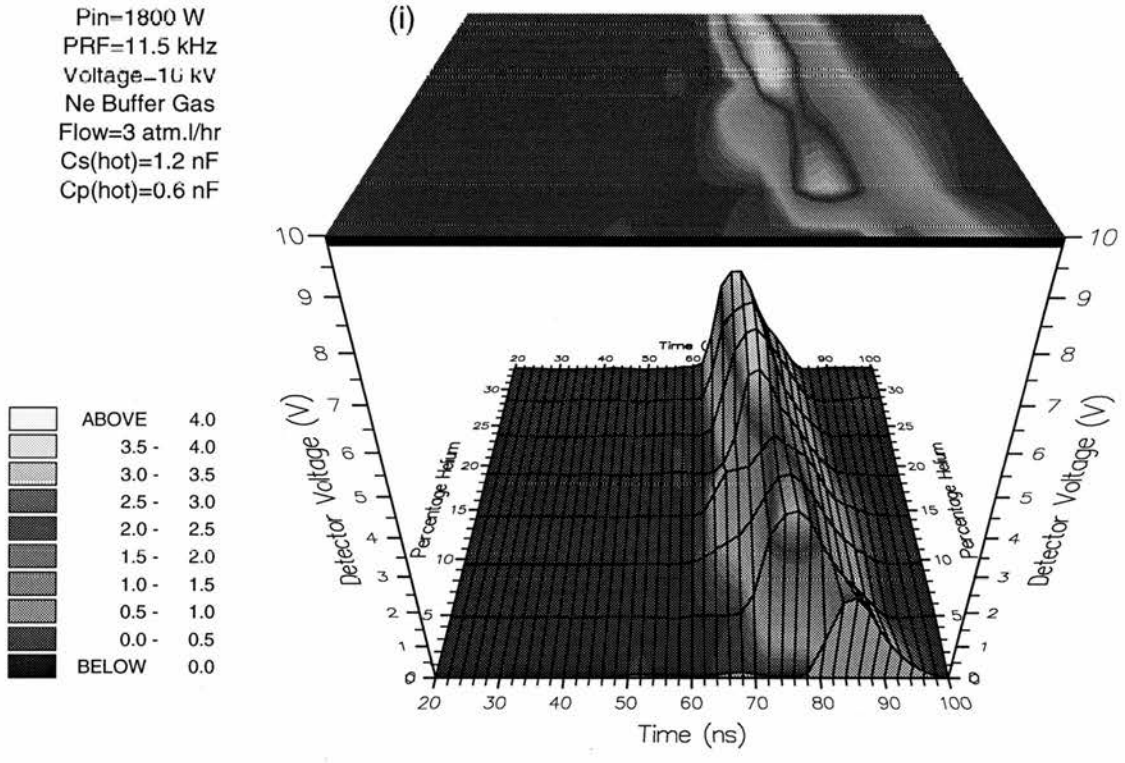

1.50 μm laser pulse as a function of time and percentage of helium added.

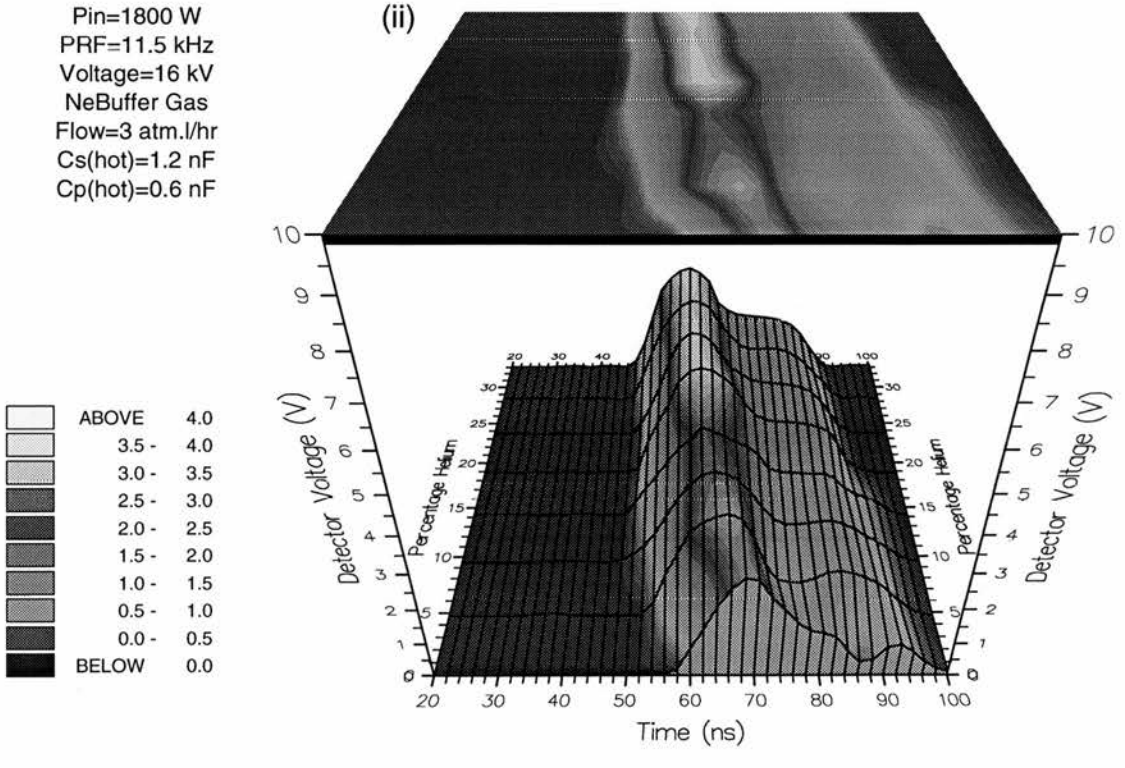

The temporal dependence of the onset of the laser oscillation with respect to the beginning of the current pulse can be explained in terms of the metastable population level. The chief mechanism by which the metastable lower laser level is depopulated is by electron collision in the interpulse period. For reasons discussed in Section 1.3.5, the presence of H_2, D_2 or He additives in the buffer gas may result in a reduction in the metastable population during the interpulse period and thereby enabling a threshold population inversion to be established earlier in the excitation pulse.

Although the metastable population determines the point at which a threshold inversion may be established, this is not the only mechanism which can determine the onset of laser oscillation. The excitation mechanism must also be taken into account and can also be used to explain the observed trends, as follows. The enhanced electron cooling which results from the addition of additives is likely to lead to increased tube impedance (see Section 1.3.5) and thereby enhance the conditions for upper laser level excitation. The effect of additives on the tube impedance, breakdown potential and the resulting excitation pulse are discussed in Section 4.4.3 and 4.4.4 respectively.

Figure 4.7 clearly shows a minimum in intensity which occurs in the 1.50 μm laser pulse some 10-20 ns after the onset of the laser pulse. This was particularly interesting since this corresponded to the peak of the 1.13 μm laser pulse and was believed to be caused by competition between the two laser transitions, which occurs because the two transitions share a common upper level [2]. The inclusion of additives to the neon buffer gas tended to enhance the laser power at 1.50 μm at this minimum, and hence the laser power at 1.50 μm increased at the expense of the 1.13 μm transition. The competition which exists between these two transitions showed a strong dependence upon both the percentage and the type of additive used. For similar percentages of H_2, D_2 and He, the most effective additive at reducing this minimum was H_2, followed by D_2 and finally He. Larger percentages of D_2 and still larger percentages of He were required before a laser pulse intensity waveform at 1.50 μm could be obtained similar to that obtained when H_2 was used.

It is not surprising that H_2 addition to the buffer gas tended to show the greatest effect on reducing the competition between these two transitions followed by D_2 and then He. As mentioned above, one of the principal mechanisms limiting the laser power of self-terminating lasers such as BVLs is the metastable lower laser level population. Increasing the percentage of additive to the buffer gas would directly increase the electron buffer gas collision frequency (as given by Equations 3.12-14 and discussed in Section 1.3.9), and consequently increase metastable deactivation (see Section 1.3.5). The type of additive in the buffer gas is equally as important as the percentage of additive used. For reasons discussed in Section 1.3.5, for comparable percentages of H_2, D_2 and He, the metastable lower laser level depopulation rate would be fastest with H_2 and slowest with He.

The competition between the two transitions provided an insight into the mechanism which limited the laser power at 1.13 μm with increasing percentage of additive. Laser oscillation occurred first at 1.50 μm, because of the high gain of the transition. It was only when the population of the 1.50 μm metastable lower laser level became sufficiently high that laser oscillation at 1.13 μm could begin. Laser oscillation continued at 1.13 μm until either its lower laser level also became sufficiently populated or the population of the upper laser level increased enough such that the higher gain 1.50 μm transition could begin again.

As is discussed more fully in Section 4.4.3, the breakdown potential of the laser tube tended to increase with increasing percentage of additive. This would lead to an enhancement in the excitation of the upper laser level and would partially explain why the laser power at 1.50 μm increased for all the percentages of H_2 and D_2 selected. However, this enhanced upper laser level should also result in the increase in laser power at 1.13 μm, which is clearly not the case at high percentages of H_2 and D_2, as shown in Figure 4.6b.

The only mechanism by which the 1.50 μm transition could be enhanced at the expense of the 1.13 μm transition would be if there were an increase in the population of the 1.13 μm lower laser level relative to that of the 1.50 μm transition lower level. However, from previous discussions, there should be a decrease in the population of the 1.13 μm lower laser level with increasing percentage of additive, which would have the

reverse effect from that observed and would increase the laser power. This indicates that there is a mechanism by which the population of the 1.50 μm lower laser level can be transferred to the 1.13 μm lower laser level.

The fact that the competition was much less pronounced when He additives were used than with either of the others, and that the laser power at 1.13 μm merely saturated with increasing He percentage, would suggest that the effect was either a molecular phenomenon or an electron attachment phenomenon. It is possible that rotational and vibrational modes of H_2 and D_2 were excited in transferring of population from the higher metastable level (1.50 μm) to the lower metastable level (1.13 μm) by molecular collisions. An enhanced electron cooling rate (which would promote population transfer) because of a molecular process between pulses was ruled out in Section 1.3.8. Likewise it is difficult to see how electron attachment to H or D could promote transfer between lower levels. The molecular energy transfer mechanism is plausible, since the energy difference between the two metastable levels is ~0.5 eV which corresponds closely to a vibrational mode of excitation for H_2. This redistribution of lower level populations would occur predominantly during the interpulse period.

4.4.3 Tube Current and Tube Voltage Waveforms

Figure 4.8 shows how (a) the peak tube current and (b) the peak tube voltage varied with the percentage of H_2, D_2 and He added to the neon buffer gas. The discharge conditions were similar to those described in Section 4.4.1. In each case, increasing the percentage of additives increased the peak tube voltage and decreased the peak tube current. The increase in the peak tube voltage was most pronounced when the additive was either H_2 or D_2 with comparable percentages of each giving approximately the same peak tube voltage. Large percentages of helium (>15%) were required before there was any significant increase in the peak tube voltage. Similar trends with the peak tube current were observed with comparable percentages of H_2 and D_2, resulting in approximately the same decrease in the peak values. Adding helium to the buffer gas had much less of an effect.

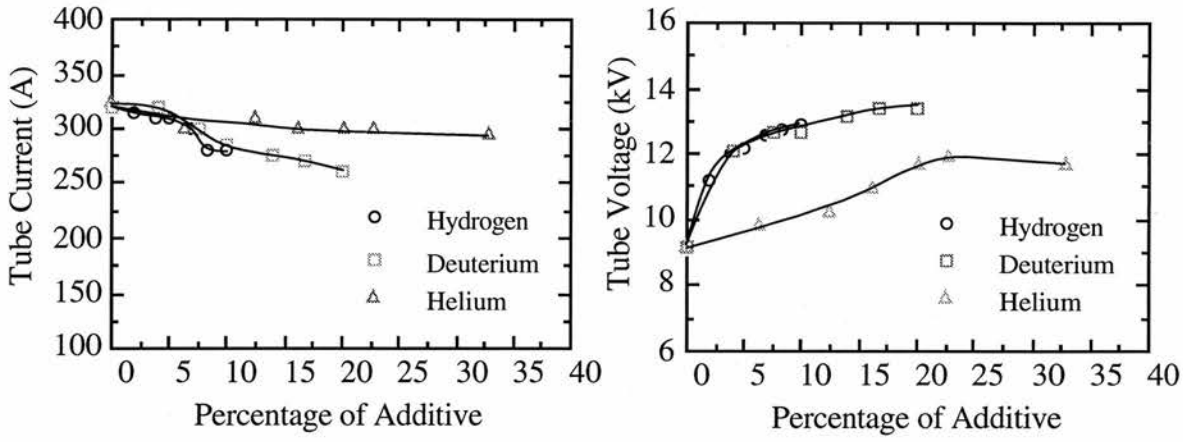

Figure 4.8: Peak tube current and peak tube voltage as functions of percentage of additive.

The increase in the peak tube voltage and the decrease in the peak tube current with increasing percentage of additive suggested that the discharge tube impedance increased with increasing percentage of additive. In addition, for comparable percentages of additive, the increase in tube impedance was found to be greatest when H_2 was used followed by D_2 and then He. The observed increase in tube impedance and its dependence of the type of additive could be explained in terms of the enhanced electron cooling resulting from the addition of additives (see Section 1.3.5). The ability of H and D to form electronegative species may further reduce the pre-pulse free electron density and accelerate recombination.

Figure 4.9 shows how the current waveform changed with various percentages of (a) H_2 (b) D_2 and (c) He additives. As shown above, one effect of increasing the percentage of additives was to cause the peak current to decrease. Another effect was the change in the overall shape of the current waveform with the addition of additives. There appeared to be a characteristic 'step' on the leading edge of each of the current pulse waveforms which tended to decrease in height with an increase in the percentage of additive. Figure 4.9 also shows that the step was found to be dependent upon the particular additive used. For a given fixed percentage of additive, the step occurred earliest with respect to the onset of the current pulse when H_2 was used. This was then followed by D_2 and finally He.

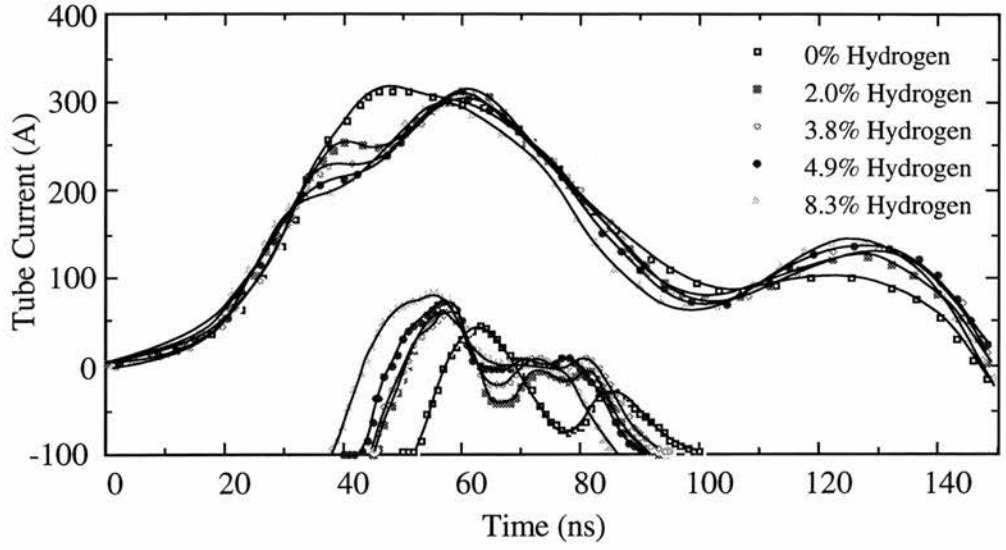

Figure 4.9a: Tube current and the 1.50 μm laser pulse intensity as functions of time for various percentages of hydrogen.

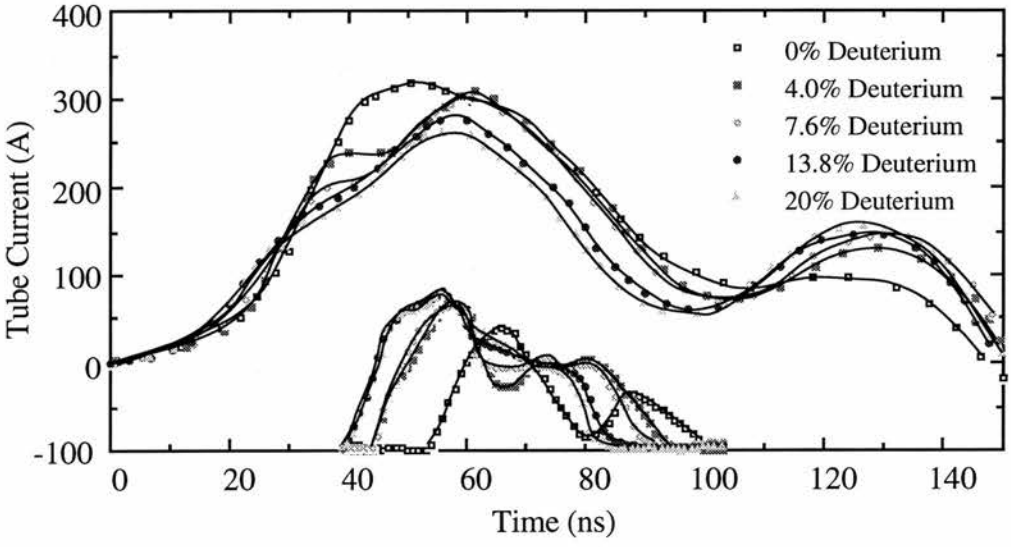

Figure 4.9b: Tube current and the 1.50 μm laser pulse intensity as functions of time for various percentages of deuterium.

A similar step in the tube current waveform has been observed to occur in high temperature CVLs [3] and CHLs [4]. The decrease in the step with increasing percentage is believed to give an indication of the preionisation density within the laser tube, for the following reason. At the beginning of the excitation pulse, the current is carried predominantly by electrons which remain from the previous pulse - the so-called phantom current [3]. The tube current increases as the electric field across the tube grows. However, there comes a point at which the tube voltage is sufficiently high that the current which

could be carried in the tube is limited by the number of charge carriers. This point corresponds to the decrease in the gradient on the leading edge of the tube current waveform. As the electric field increases further, the average electron energy in the tube also increases so that collisional ionisation processes greatly accelerate, increasing the electron number density. At this point, the tube current is no longer limited by the number of charge carriers and hence rapidly increases. Hence the step in the tube current waveform gives an indication of the preionisation density within the tube.

The lower the electron preionisation density, the lower down the current pulse the step appears. From observations of the step in the tube current waveform, preionisation appeared to decrease with increasing percentage of H_2 additive. As shown in Figures 4.9b and 4.9c, a similar effect was observed when D_2 and He additives were used with a neon buffer gas, but in these cases the percentages required were higher to obtain a similar decrease in the step. This reflected the ability of the additive to cool the electrons in the discharge afterglow effectively and hence raise the electron-ion recombination rate.

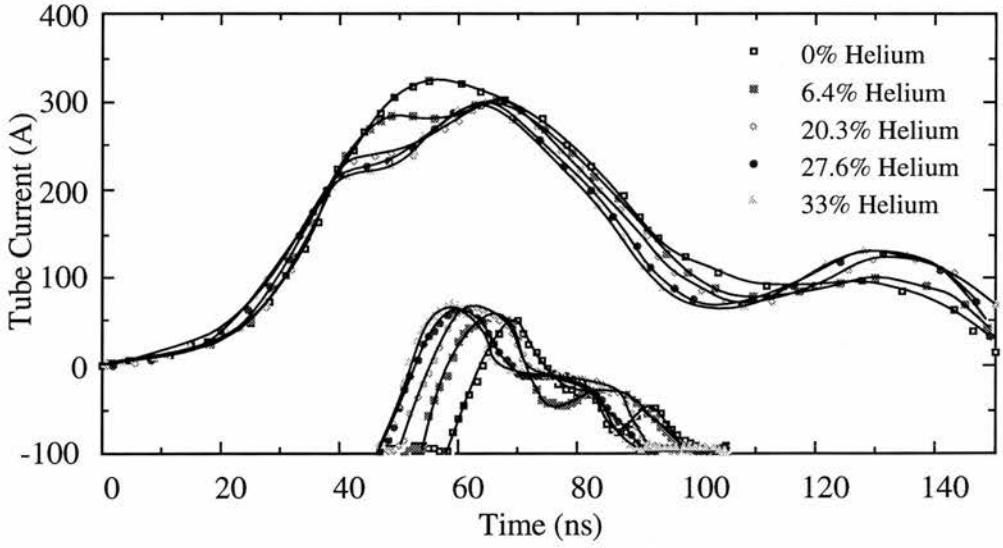

Figure 4.9c: Tube current and 1.50 μm laser pulse intensities as functions of time for various percentages of helium.

Also shown in Figure 4.9 is the 1.50 μm laser pulse for various percentages of (a) H_2, (b) D_2 and (c) He additives. The onset of the 1.50 μm laser pulse tended to occur at earlier times as the percentage of any of the additives was increased and correlated reasonably well with the step in the tube current waveform. At this point, the average

electron energy is increasing and becomes sufficiently high for efficient collisional excitation to the upper laser level.

Although the discharge tube was already a conductive plasma and hence could not 'breakdown', a tube breakdown potential can be defined as the point at which secondary collisional ionisation processes begin to be important within the discharge tube. Thus, the tube breakdown potential was considered to be the tube voltage which corresponded to the end of the step in the tube current waveform.

Figure 4.10 shows how the tube 'breakdown' potential varied with various percentages of H_2, D_2 and He additives to the neon buffer gas. In each case the effect of additives to the neon buffer gas was to increase the tube breakdown potential. The effect was most pronounced with H_2 and D_2 where the tube 'breakdown' potential increased from approximately 6 kV to between 11.0 and 11.5 kV with 5% additives of H_2 and D_2 and to only 8 kV with 5% He additives. The increase in the tube 'breakdown' potential was approximately the same for comparable percentages of H_2 and D_2. However, for He additives, considerably higher percentages were required before a similar breakdown potential could be obtained.

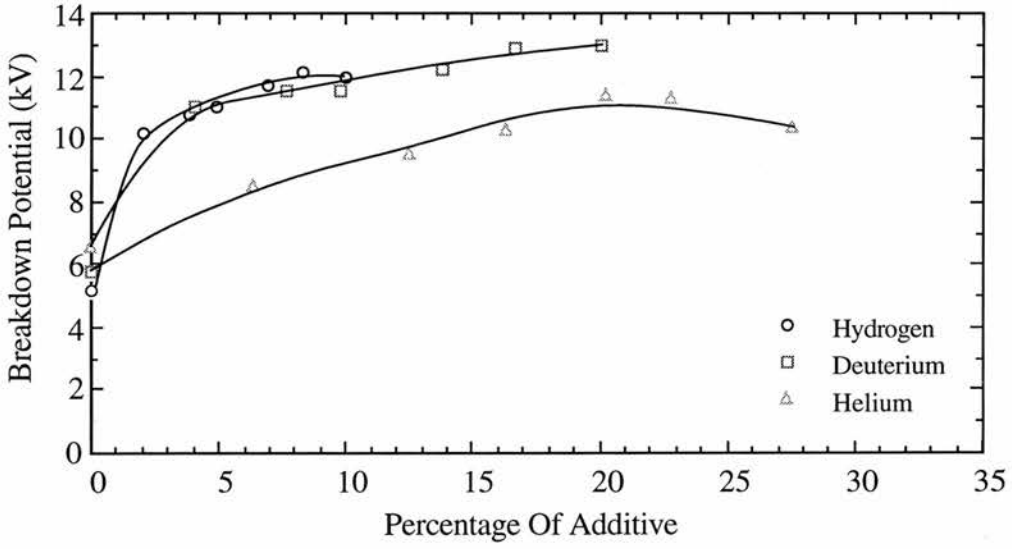

Figure 4.10: Tube breakdown potential as a function of percentage of additive.

The enhanced applied electric field which resulted from the addition of H_2, D_2 and He additives to the neon buffer gas is likely to enhance excitation to the upper laser level and lead to increased laser output power (see Section 1.3.5). The electric fields were

enhanced the most with H_2 additives and least with He which explains why the largest laser output powers were obtained using H_2 additives, followed by D_2 and then He.

4.4.4 Temporal Energy Deposition

In Section 5.2.4 it was found that the laser power at both 1.13 μm and 1.50 μm was strongly dependent upon the input power (based on stored energy), with the laser power at 1.13 μm peaking at a lower input power than at 1.50 μm. One possible explanation was that this was influenced by the thermal population of the low lying metastable energy levels. In Section 5.2.4 it was also found that H_2 addition slightly reduced the input power (based on stored energy) corresponding to the maximum laser power at 1.13 μm. This could be caused either by an increase in the thermal conductivity of the buffer gas because of the presence of H_2 and/or the increased power deposition because of the increased tube impedance. In this section, the effects of H_2, D_2 and He additives on the temporal energy deposition into the laser tube of a BVL have been investigated by considering the tube current and tube voltage waveforms in order to establish whether there is an increase in the power deposition with additives to the buffer gas.

The method by which the energy deposition into the laser tube was evaluated is discussed at length in Section 3.9, and in summary as follows. First, the laser head inductance was experimentally determined (as discussed in Section 3.8) and this value used to modify the measured tube voltage in order to determine the resistive component. This enabled the temporal evolution of the energy deposition to be evaluated by multiplying the resistive component of the tube voltage by the measured tube current.

The total power deposition was evaluated by integrating the temporal energy distribution over the whole region of the excitation pulse and multiplying by the PRF. The power deposition was also determined over select regions of the excitation pulse, including regions before the onset of the 1.50 μm laser pulse and also over the duration of the 1.50 μm laser pulse. This was achieved by restricting the limits of integration to the relevent time intervals and once again multiplying the result by the PRF.

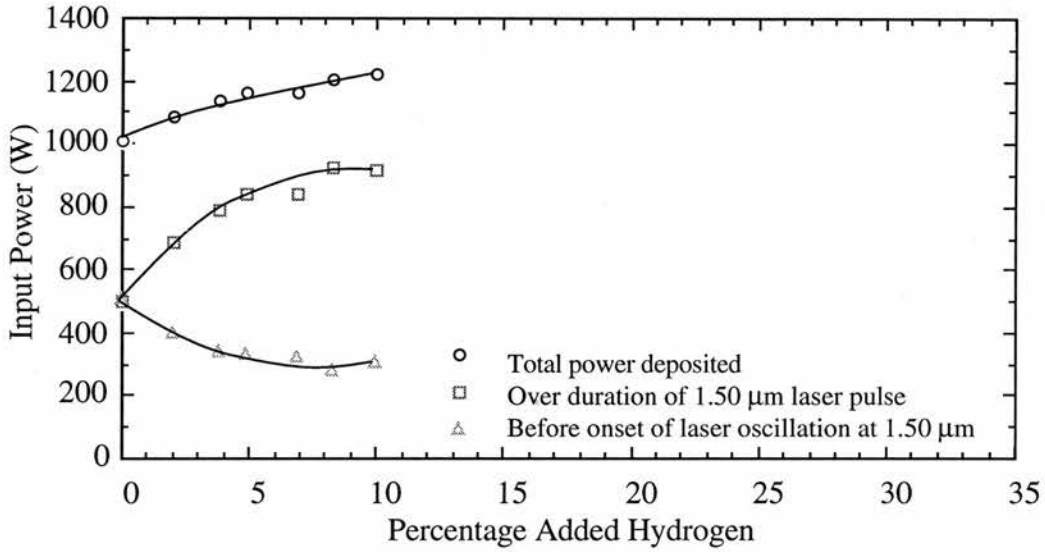

Figure 4.11a: Power deposited into laser tube as a function of percentage added hydrogen.

Figure 4.11 shows how the total power deposition, the power deposition over the 1.50 μm laser pulse and the power deposition before the 1.50 μm laser pulse varied as a function of percentage of additive using (a) H_2, (b) D_2 and (c) He as the additive. It is clear that in all cases the effect of additives to the neon buffer gas was to increase the overall power deposition in the laser tube. In addition to this, the inclusion of additives also increased the power deposition over the duration of the 1.50 μm laser pulse and reduced the power deposition before the onset of laser oscillation at 1.50 μm. The effect was most pronounced when either H_2 or D_2 was used with only small percentages being required to significantly increase the actual power deposition. Higher percentages of He were required for the power deposition to be significantly different from when a pure neon buffer gas was used.

The trends observed in the power deposition reflected the ability of the buffer gas to cool the electrons effectively and hence to reduce the pre-ionisation density (see Section 1.3.5). The increase in power deposition with increasing percentage of additive was believed to be chiefly due to the increased tube impedance. The increased tube voltage hold-off was believed to improve the matching of the discharge tube to the circuit thereby increasing the energy transfer efficiency.

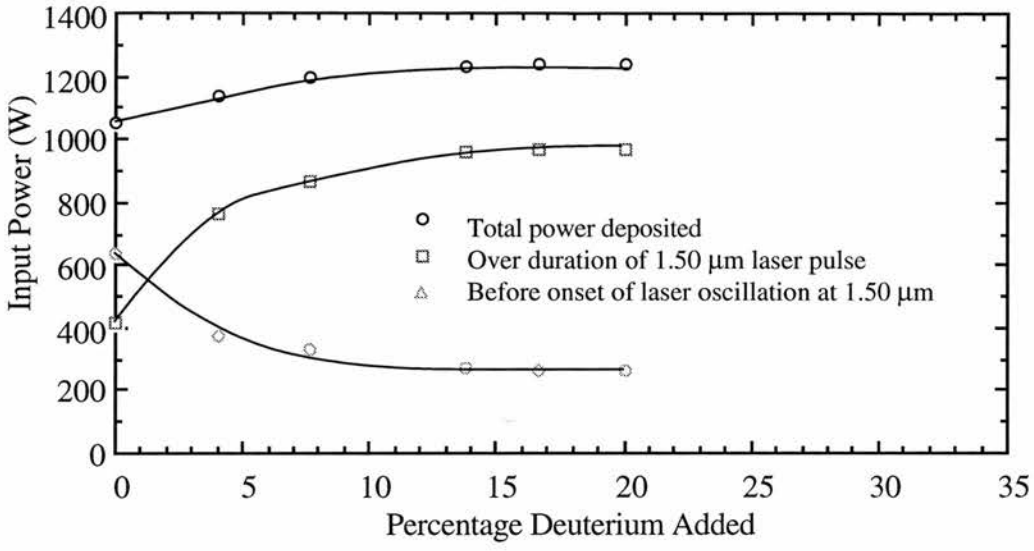

Figure 4.11b: Power deposited into laser tube as a function of percentage deuterium added.

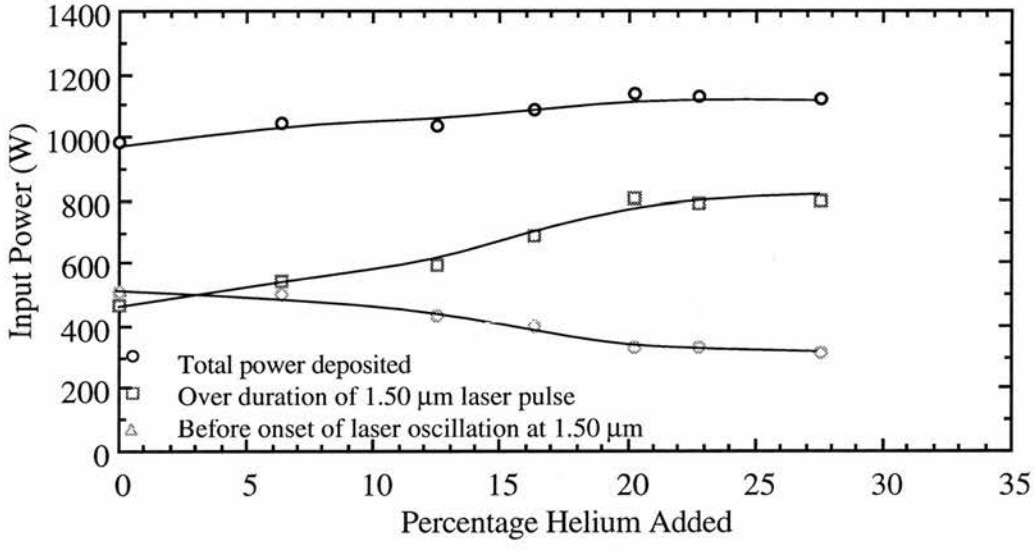

Figure(4.11c): Power deposited into laser tube as a function of percentage helium added.

4.5 Beam Profiles

In this section, an analysis was made of both the temporal and spatial evolution of the 1.13 μm and 1.50 μm laser pulses. The discharge conditions were optimum for maximum laser power with 3% added hydrogen (see Chapter 5), with the charging voltage (V_c), PRF, neon pressure, and storage and peaking capacitances of 15 kV, 12 kHz,

54 torr, 1.2 nF and 0.6 nF respectively. Laser pulse intensity measurements were made using a HgCdTe detector mounted on a translation stage such that intensity measurements for the laser output could be taken at various transverse positions across the beam. This is discussed in greater detail in Section 3.6, and the experimental layout is shown in Figure 3.5.

Figures 4.12 and 4.13 show the temporal and spatial evolution of (a) the 1.50 μm and (b) 1.13 μm laser pulses without and with 3% added H_2 respectively. In the absence of any added hydrogen, the 1.50 μm transition showed a characteristic minimum in the temporal evolution of the waveform. This occurred at the onset of laser oscillation at 1.13 μm and was due to gain competition (Section 4.4.2). Spatially, the waveform had a 'flat top' intensity profile similar to that of many high temperature CVLs [5]. Figure 4.14 shows the temporal evolution of the 1.13 μm and 1.50 μm laser pulses for identical discharge conditions but with 3% H_2 added to the neon buffer gas. The effect of H_2 addition was to enhance laser oscillation at both 1.13 μm and 1.50 μm, particularly on the tube axis (ie at the beam centre), where the intensity profile for both transitions changed from being flat-top to more Gaussian-like. The addition of hydrogen also significantly reduced the minimum which occurred in the 1.50 μm laser pulse waveform.

The 'flat top' intensity profile shown in Figure 4.12a is typical of high temperature metal vapour lasers. It is brought about by the non-uniform gas temperature (gas density), non uniform current and electron energy distribution across the bore of the laser tube [2].

In Section 5.2.1, a phosphor card was used to observe the laser beam profile. It was found that when the laser was operated at low buffer gas pressures, the laser beam profile at both 1.13 μm and 1.50 μm was annular (doughnut shape). This is evident in Figures 4.14, 4.15 and 4.16 which show the temporal and spatial evolution of the 1.13 μm and 1.50 μm laser pulses using only neon, a premix of neon and 3% H_2 and a premix of neon and 3% He respectively. In each case, the discharge conditions were identical, with the exception that the neon buffer gas pressure was maintained at 20 torr. At this pressure, the increase in laser power at both 1.13 μm and 1.50 μm with either 3% H_2 or 3% He addition was much larger than when the buffer gas pressure was

Figure 4.12a: Temporal and spatial evolution of the 1.50 μm laser pulse without 3% added hydrogen or helium.

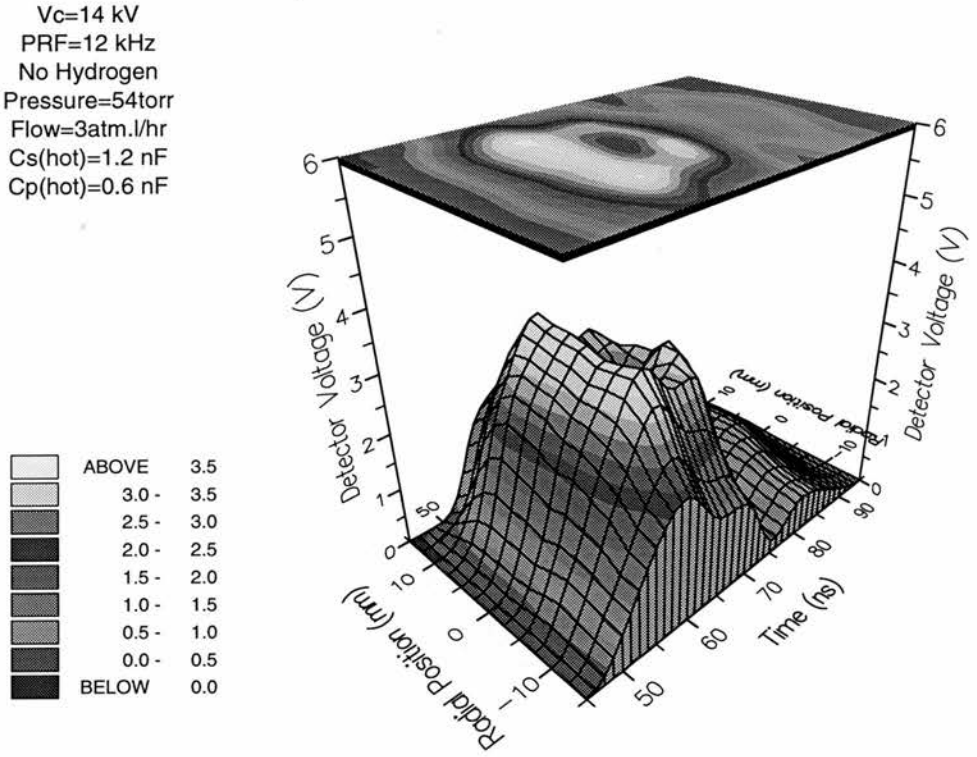

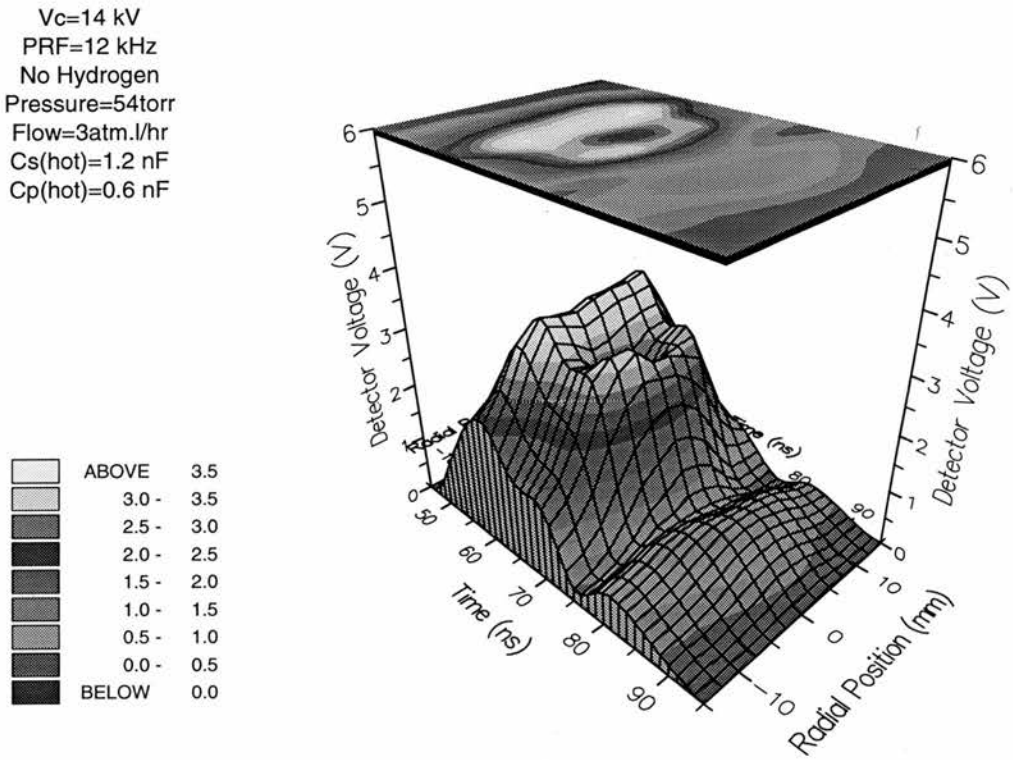

Figure 4.12b: Temporal and spatial evolution of the 1.13 μm laser pulse without 3% added hydrogen or helium.

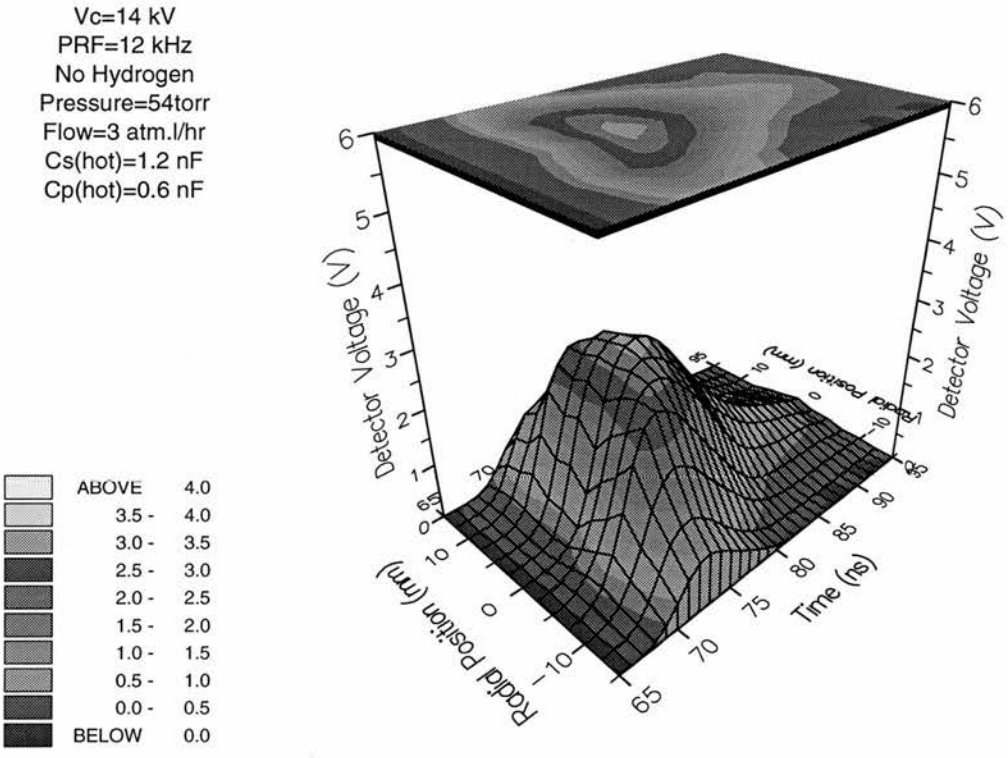

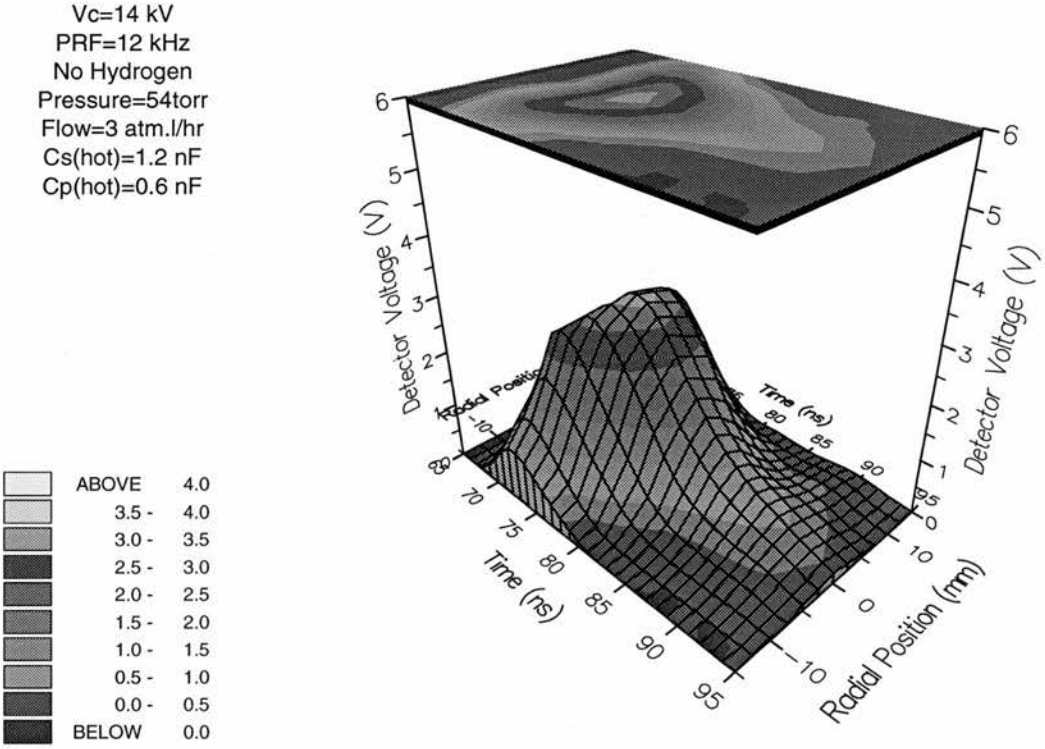

Figure 4.13a: Temporal and spatial evolution of the 1.50 μm laser pulse with 3% added hydrogen.

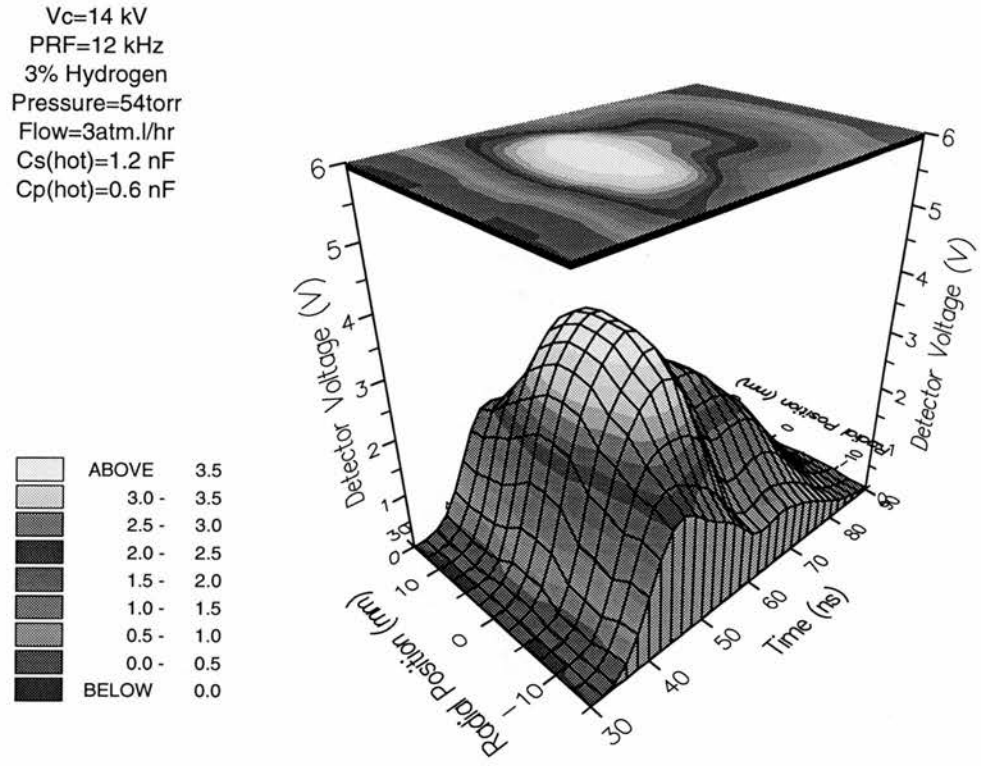

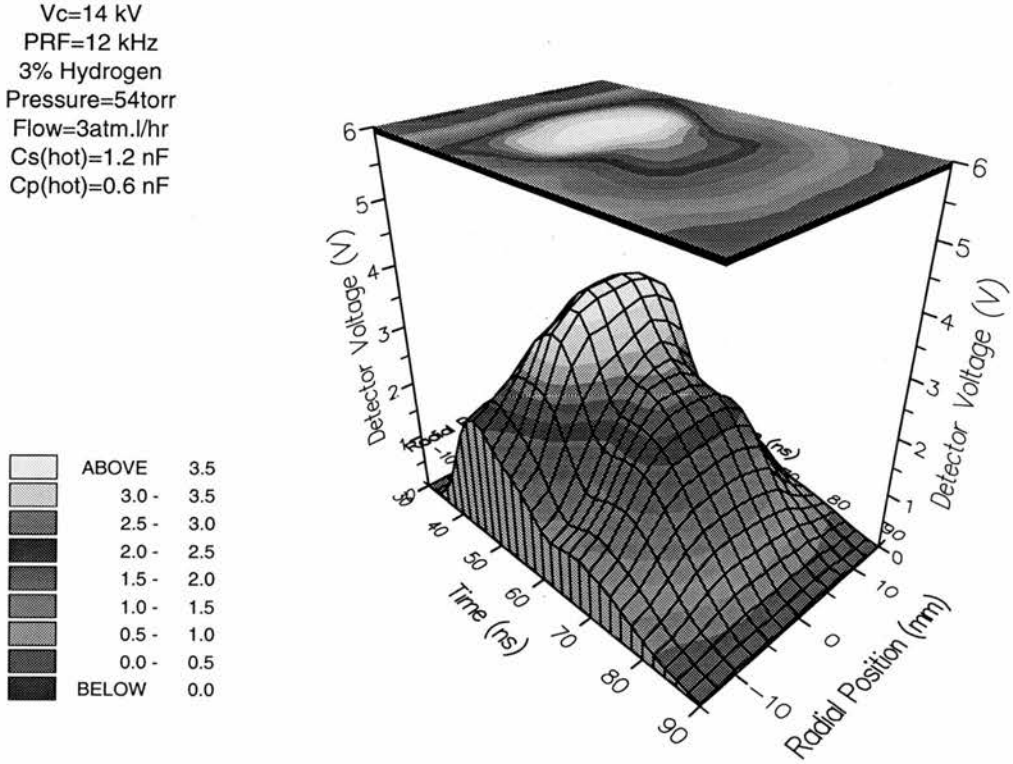

Figure 4.13b: Temporal and spatial evolution of the 1.13 μm laser pulse with 3% added hydrogen.

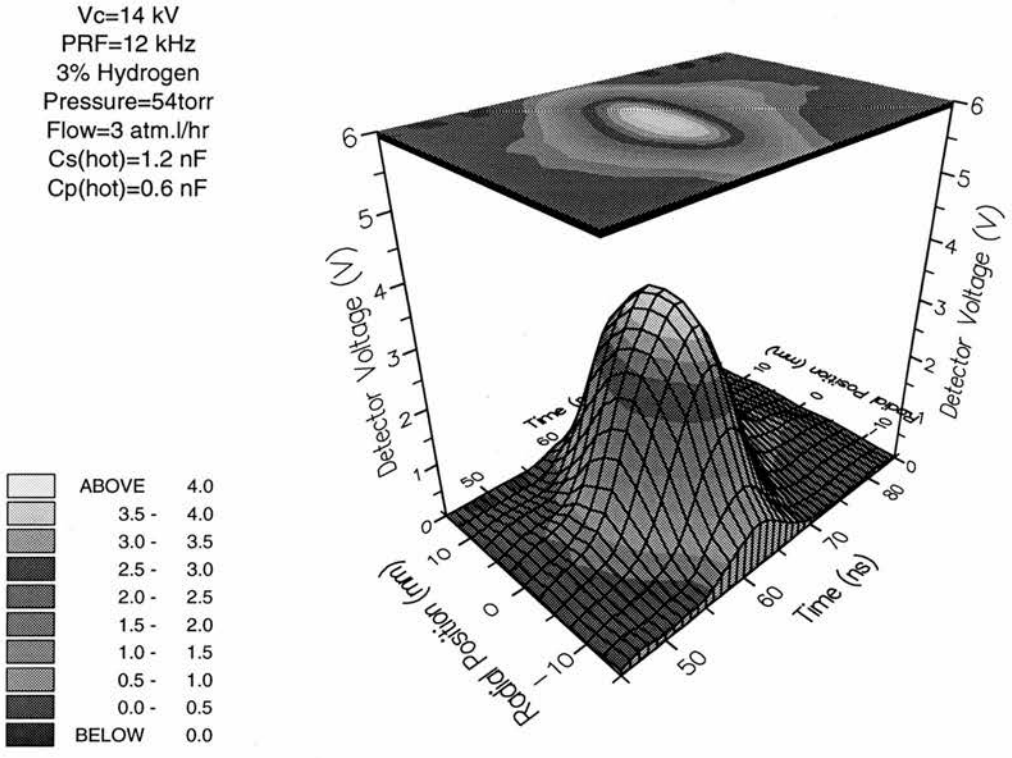

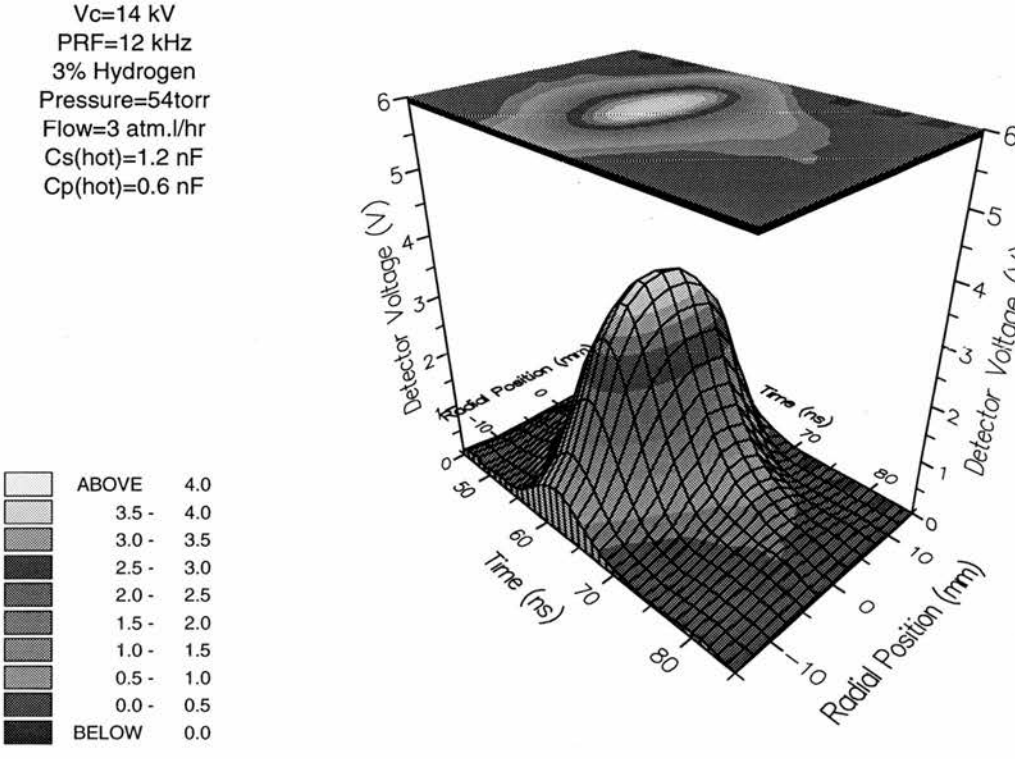

Figure 4.14a: Temporal and spatial evolution of the 1.50 μm laser pulse without 3% added hydrogen or helium.

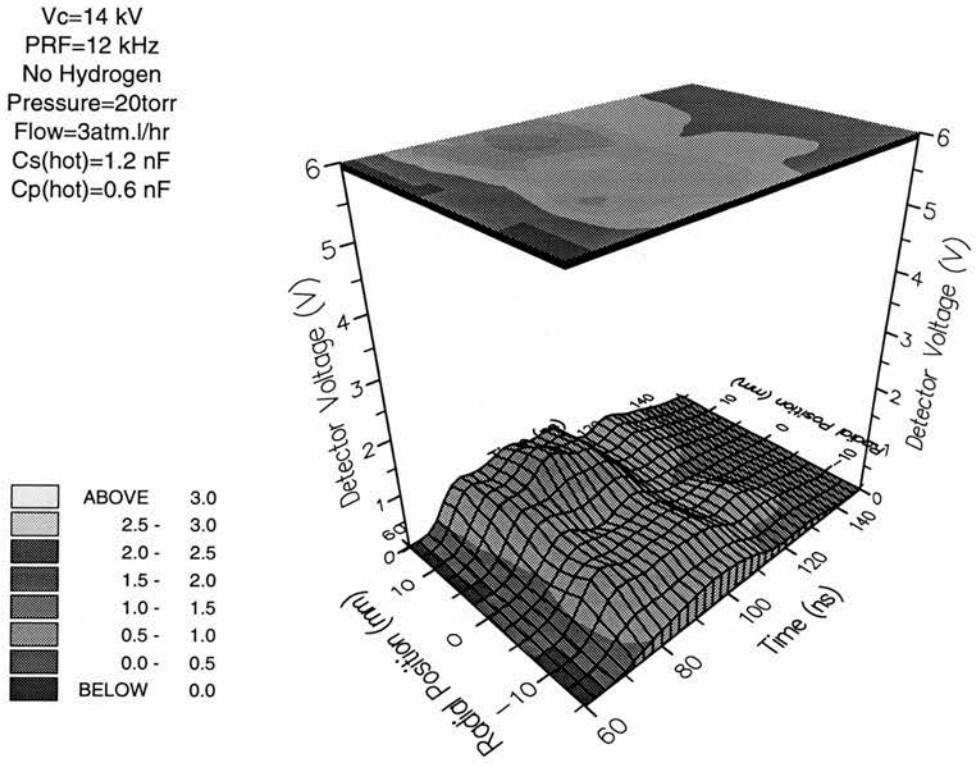

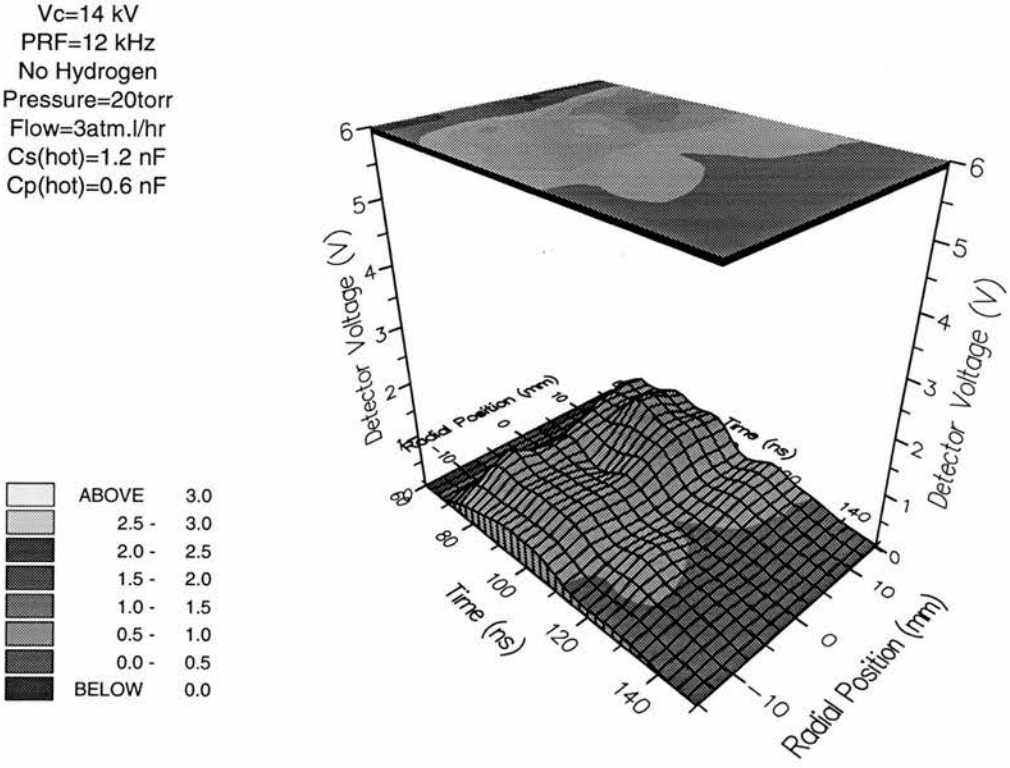

Figure 4.14b: Temporal and spatial evolution of the 1.13 μm laser pulse without added hydrogen or helium.

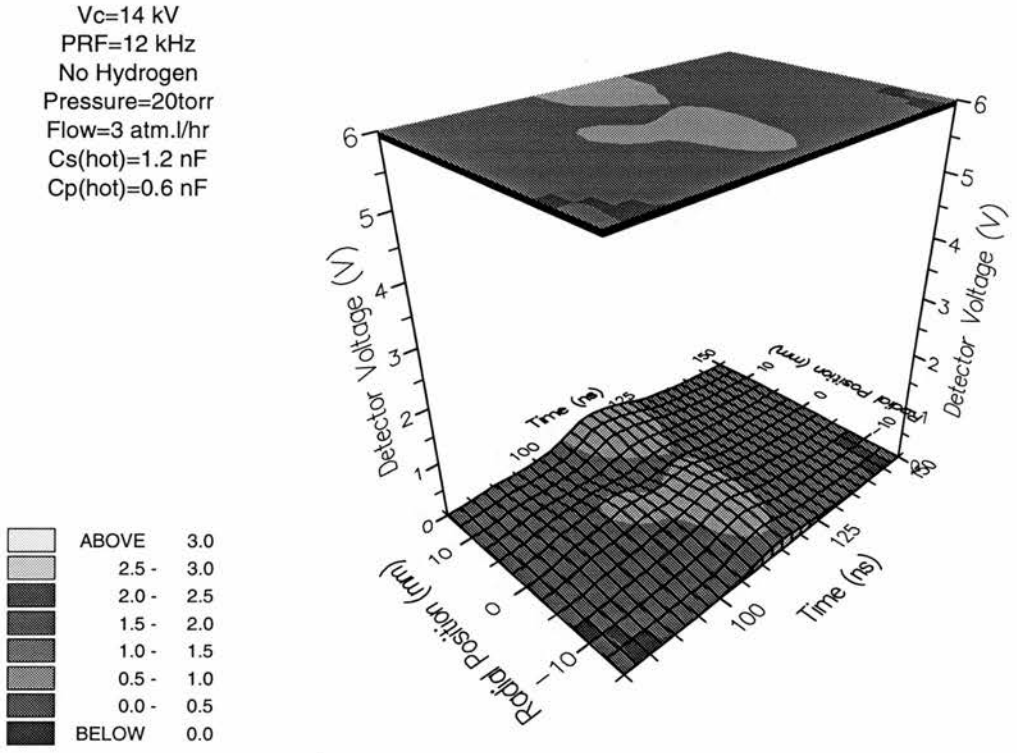

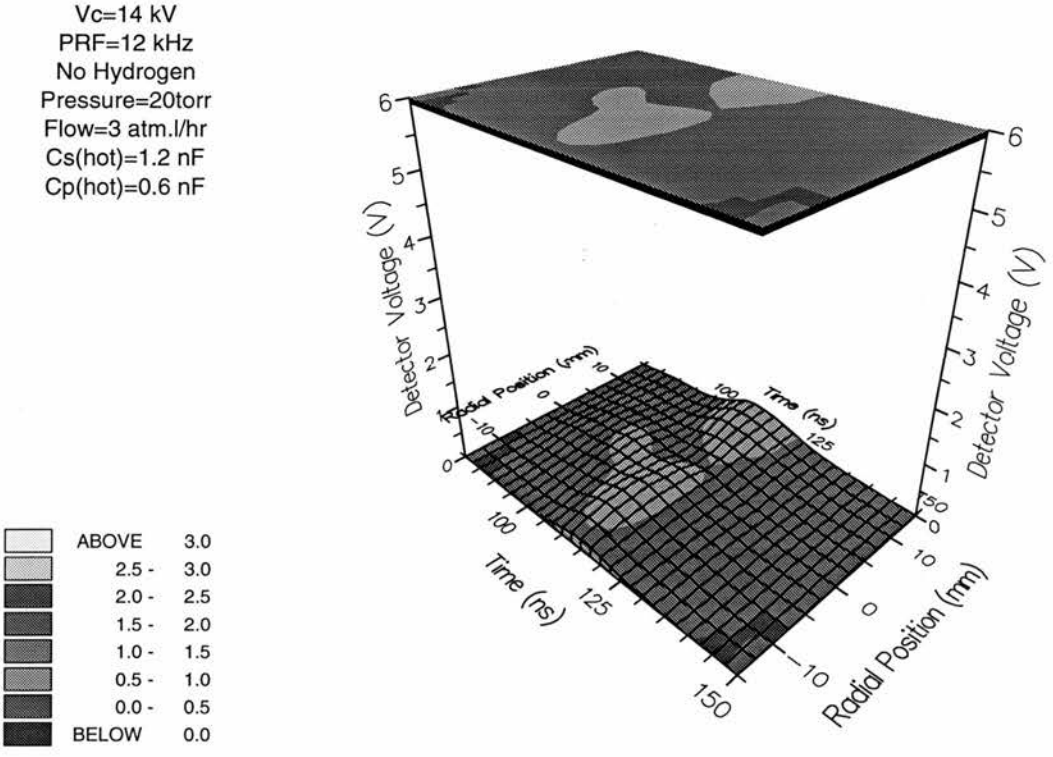

Figure 4.15a: Temporal and spatial evolution of the 1.50 μm laser pulse with 3% added hydrogen.

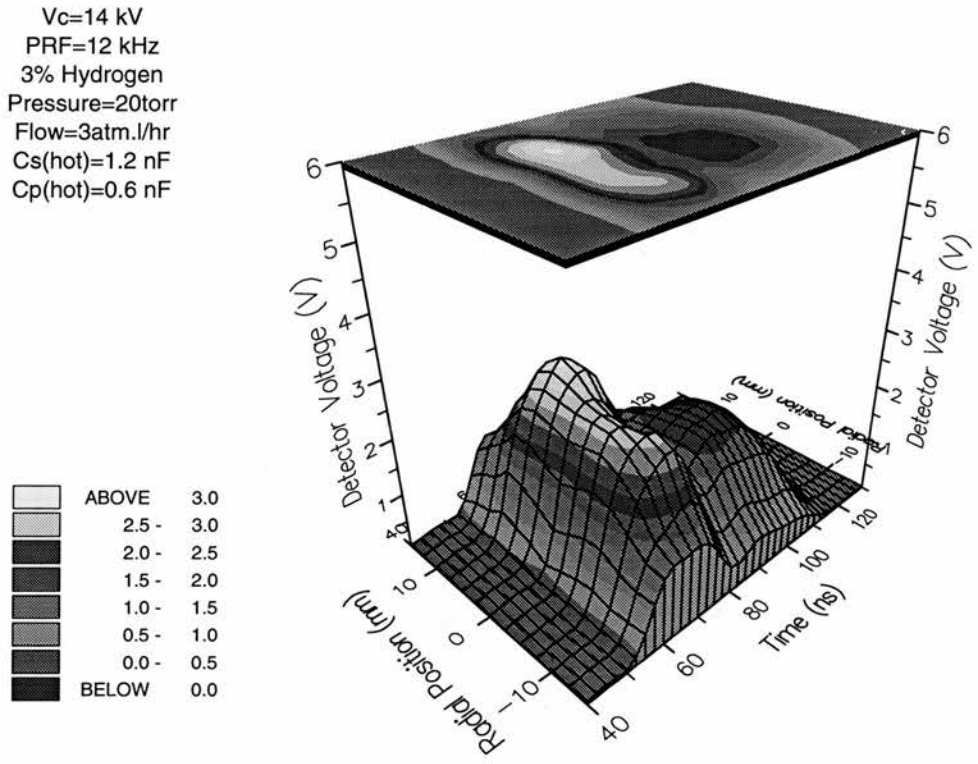

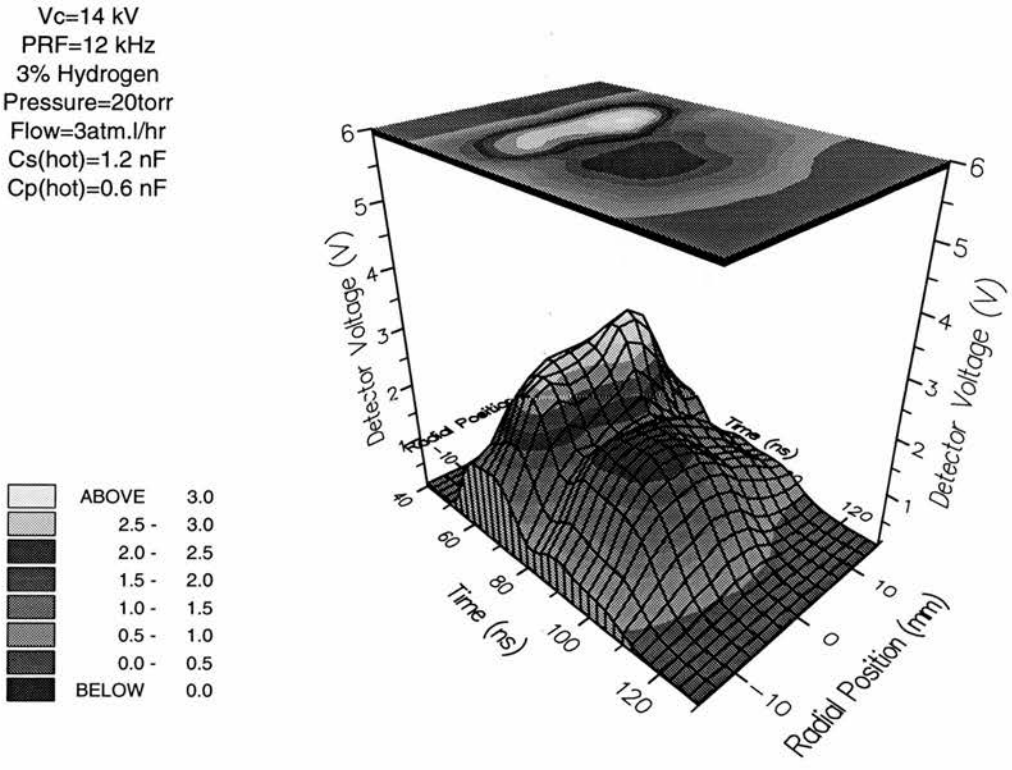

Figure 4.15b: Temporal and spatial evolution of the 1.13 μm laser pulse with 3% added hydrogen.

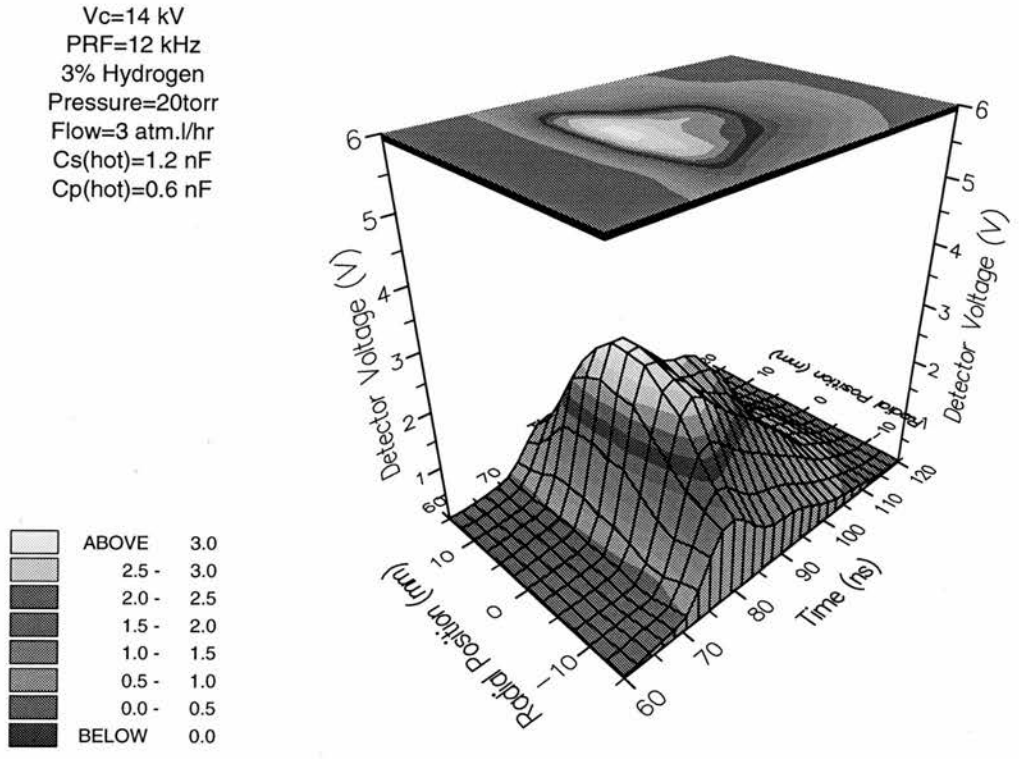

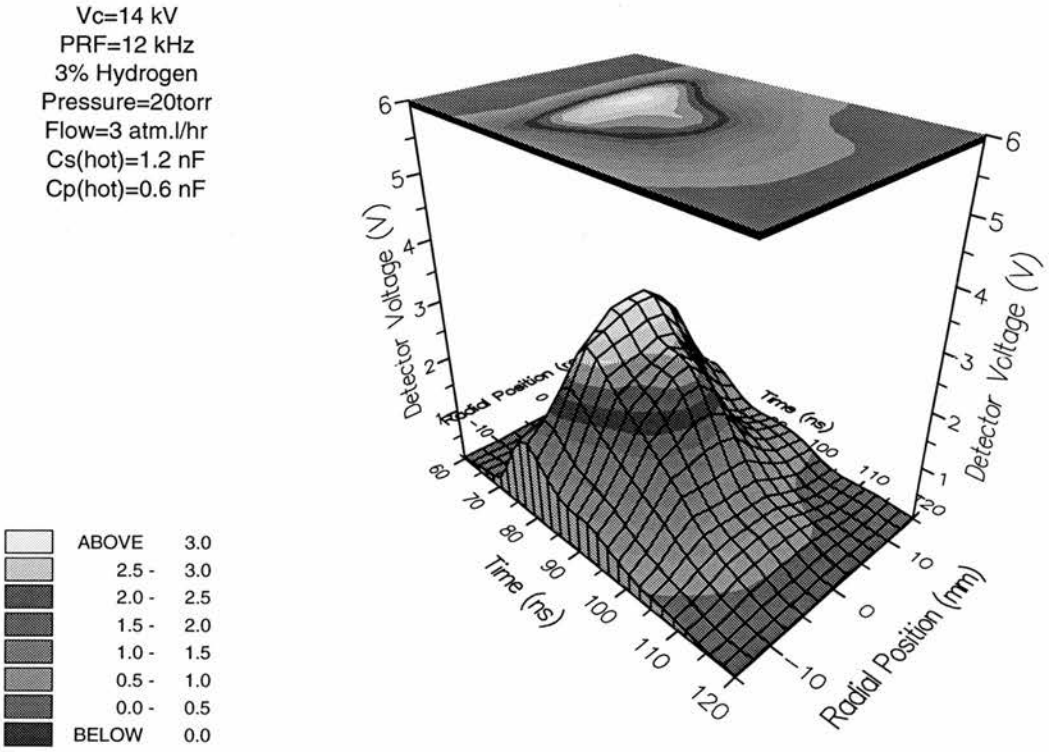

Figure 4.16a: Temporal and spatial evolution of the 1.50 μm laser pulse with 3% added helium.

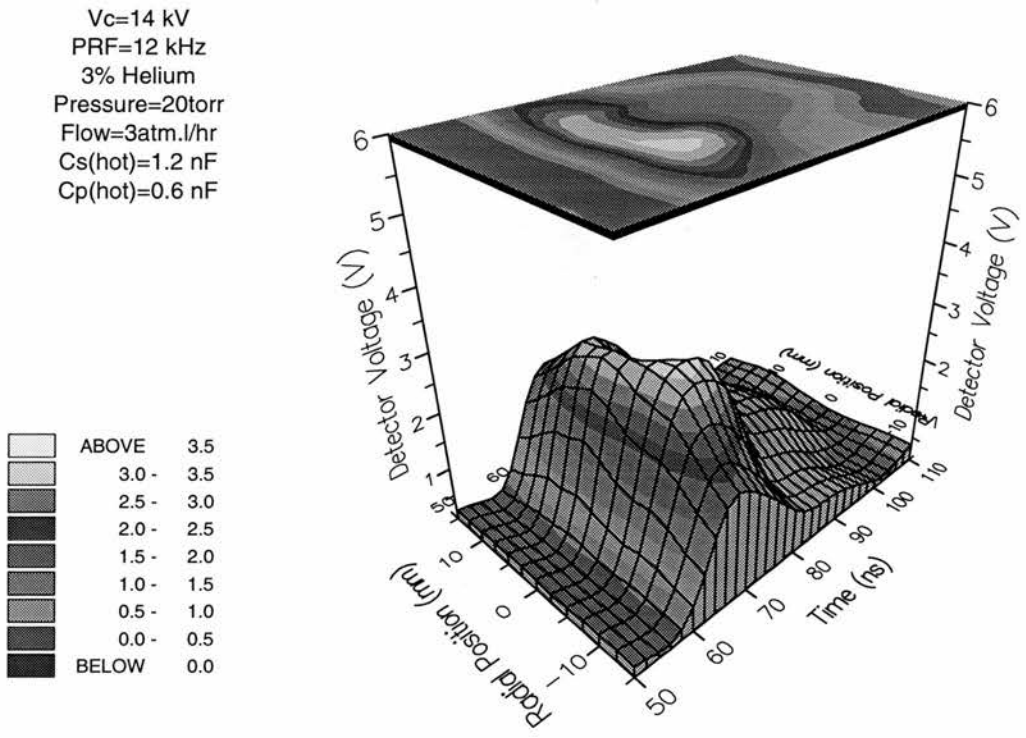

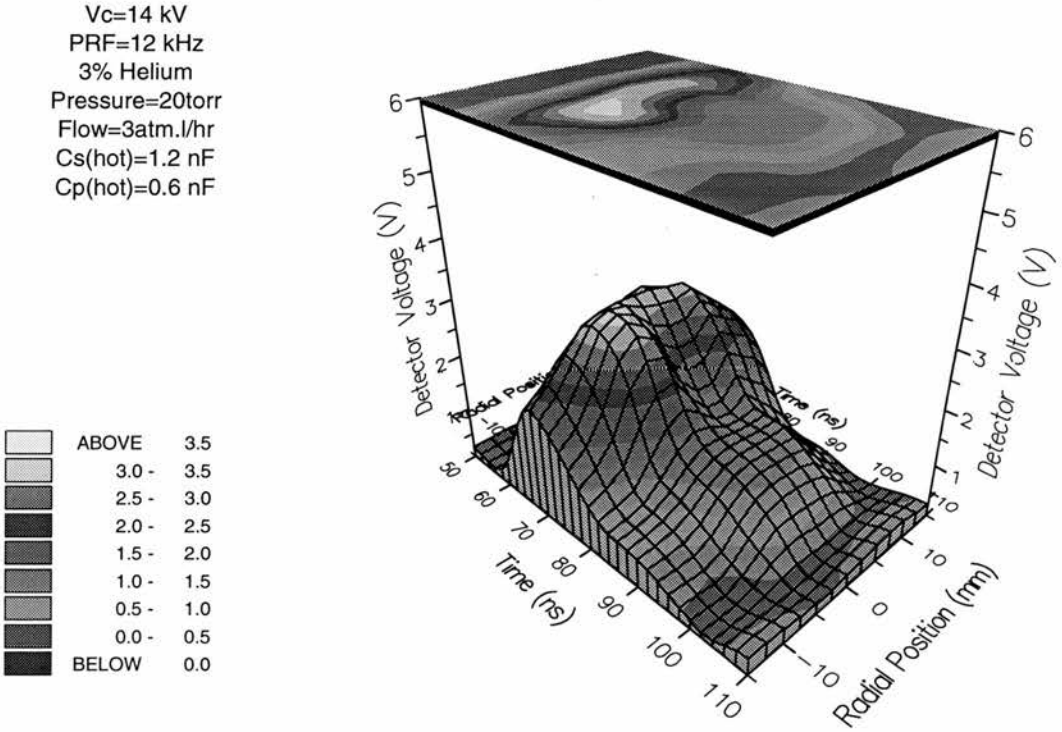

Figure 4.16b: Temporal and spatial evolution of the 1.13 μm laser pulse with 3% added helium.

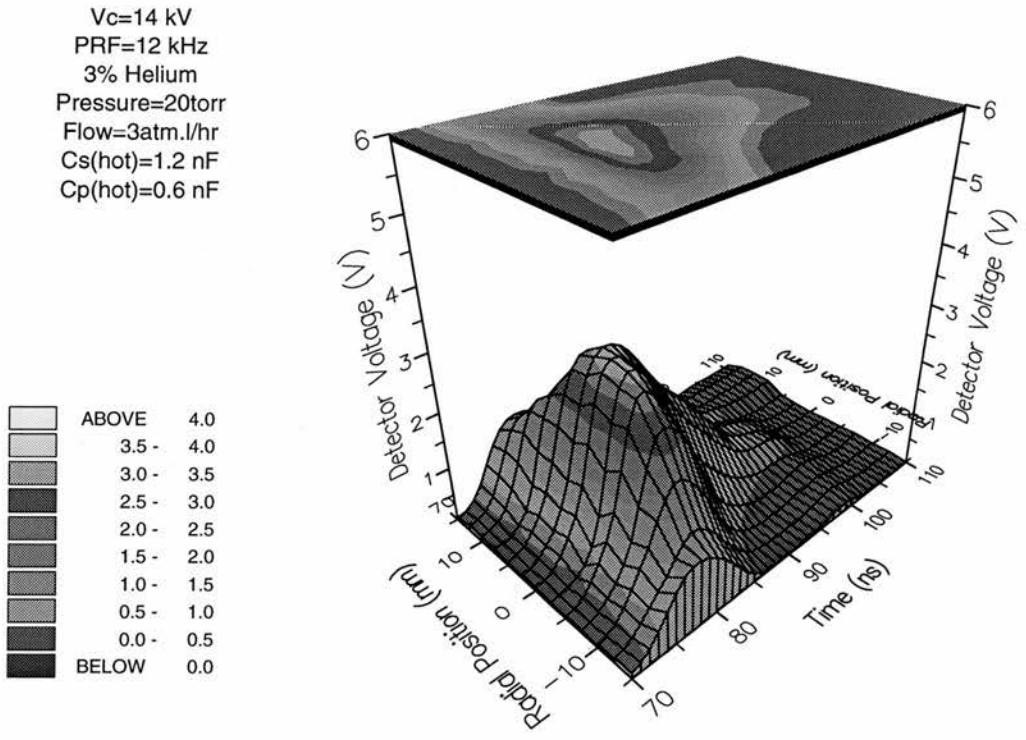

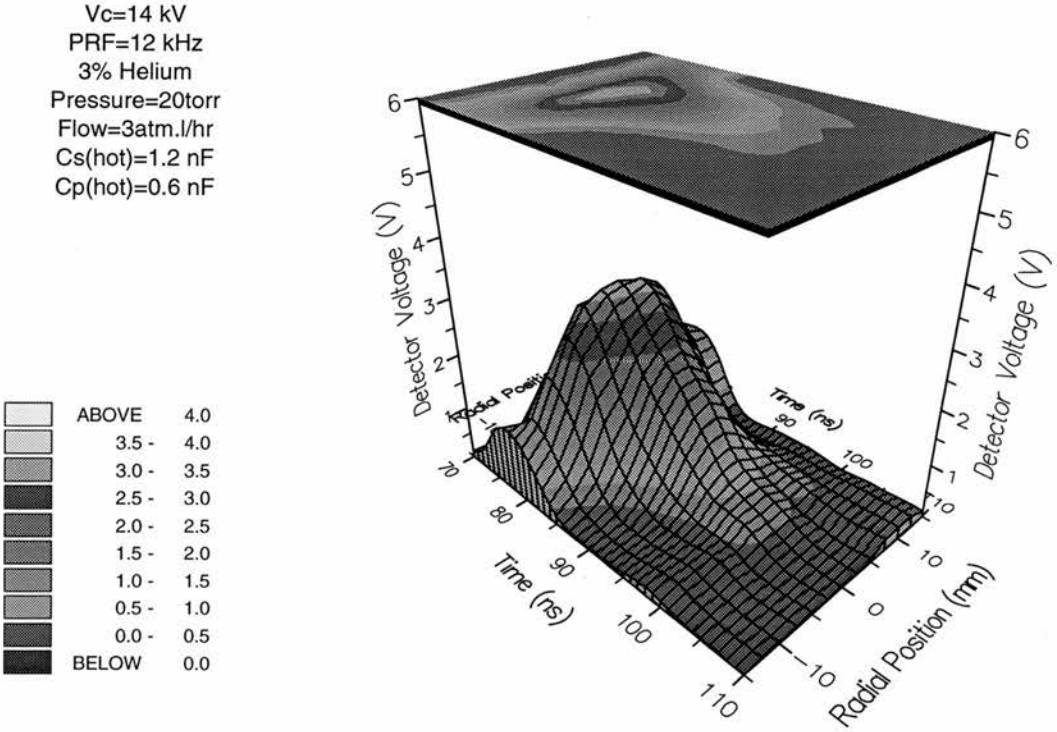

54 torr. When only neon was used as the buffer gas, the laser pulse intensity at 1.13 μm and 1.50 μm was greater nearer the tube wall than on the tube axis. The effect of either additive was to significantly enhance laser oscillation of both transitions on beam axis relative to that near the wall.

4.6 Temporal Evolution of the Electron Density

In this section the temporal course of the electron density, n_e, was evaluated by considering the conductivity of the laser tube, i.e. from the tube current and tube voltage waveforms [6]. Although the electron density is dependent upon the radial position, this method gave a time resolved indication of the average electron density over the duration of the excitation pulse. However, it should be stressed that the uncertainties using this method to evaluate the electron density may be large [7] (typically ~50%), and thus only give an indication of the trends for the temporal evolution of the electron density, and the effect of hydrogen addition on the electron density. The method by which n_e was evaluated is discussed in detail in Section 3.10, with Equation 3.16 being used to evaluate the electron density using only neon as the buffer gas. When various percentages of hydrogen were added to the buffer gas, modifications were made to Equation 3.16 in order to account for the increased electron collision cross-section when hydrogen was present in the laser tube. An example of such a modification is shown in Equation 3.17 where 3% H_2 was added to the neon buffer gas. A Fortran 77 computer program was written to evaluate the temporal evolution of the electron density from the digitised tube current and tube voltage waveforms. This is listed in Appendix VI and requires a computer with NAG routines installed. The average electron energy at the beginning of the excitation pulse (Q_o in Equations 3.16 and 3.17), was assumed to be constant at 5 eV and the laser head inductance (used to evaluate the resistive tube voltage component of the measured tube voltage) was assumed to be 200 nH (see Section 3.8).

Figures 4.17a and 4.17b show the temporal course of the electron density for various percentages of hydrogen added to a neon buffer gas. The input power, charging voltage, PRF, buffer gas pressure and charging capacitance were maintained at 1800 W,

16 kV, 10.2 kHz, 52 torr and 1.2 nF (hot value) respectively. These had previously been found to be optimum conditions for maximum total laser power when 3% H_2 had been added to the buffer gas. The hydrogen was added to the laser in an identical manner to that discussed in Section 4.4, with percentages ranging from 0-10%. In the absence of any

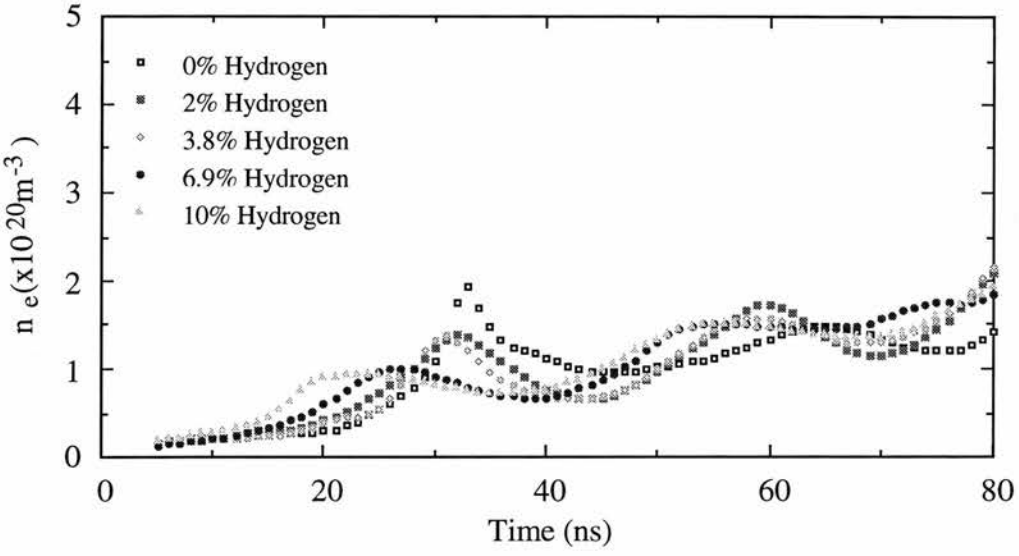

Figure 4.17a: Temporal course of the electron density for various percentages of added hydrogen.

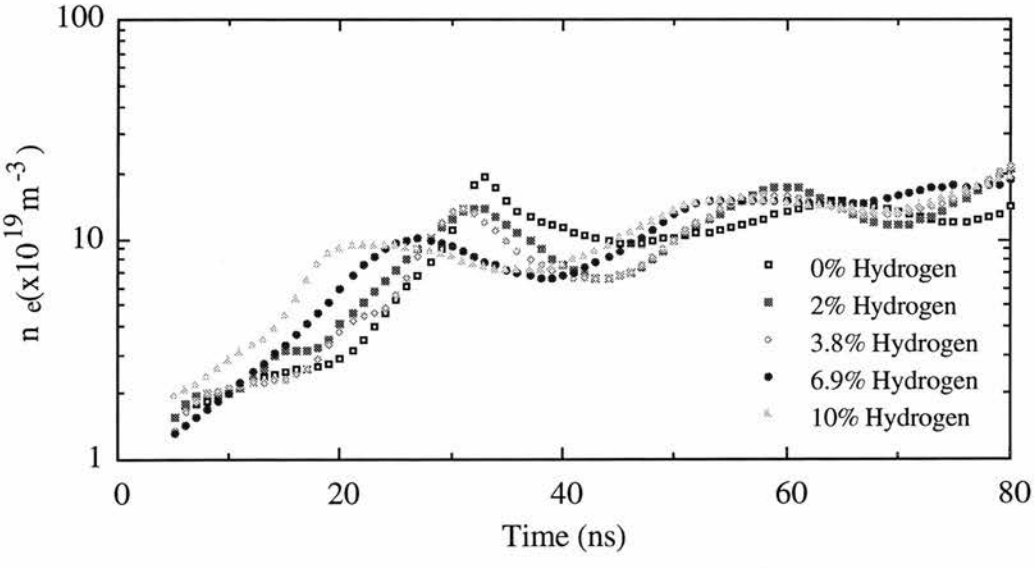

Figure 4.17b: Temporal course of the electron density for various percentages of added hydrogen.

added hydrogen, the electron density appeared to increase from approximately $2x10^{19}$ m^{-3}, at the beginning of the current pulse, to approximately $2x10^{20}$ m^{-3} some 30 ns later, these figures are comparable to those typically obtained for CVLs [3]. This peak in the electron

density appeared to decrease with increasing percentage of added H_2. For example, with 10% added hydrogen, the equivalent peak corresponded to an electron density of approximately $4x10^{19}$ m^{-3} which occurred 20 ns after the onset of the current pulse. In general, for any given time during the excitation pulse, the electron density appeared to decrease with increasing percentage of added hydrogen. However, one exception to this occurred early on in the excitation pulse, where increasing the percentage of hydrogen appeared to increase the electron density. This could be explained in terms of the enhanced electric fields obtained when hydrogen was present in the discharge which is likely to lead to ionisation occurring earlier in the excitation pulse because of the higher average electron energy. Possibly at later times, when the electric field was beginning to collapse, the presence of the hydrogen caused the average electron energy to decrease which in turn would reduce the rate of collisional ionisation (and hence electron density).

4.7 Summary

In this chapter the influence of H_2, D_2 and He additives on the total laser power, the laser power at 1.13 μm and the laser power at 1.50 μm using a neon buffer-gas was discussed. Also discussed in this chapter was the effect that these additives had on the temporal evolution of the 1.13 μm and 1.50 μm laser pulse intensities and the temporal evolutions of the tube current and tube voltage waveforms. The tube current and tube voltage waveforms were used to evaluate the dependences of the temporal power delivered to the laser tube and the temporal evolution of the electron density on the percentage of additive.

The laser power at 1.50 μm increased with increasing percentage of additive to the buffer-gas, with H_2 and D_2 additives giving larger increases in laser power than He additives. The laser power at 1.13 μm was found to increase with small percentages of additive, peak and then decrease as the percentage of additive was inceased further. Larger percentages of D_2 than H_2 and even larger percentages of He than H_2 were required for the laser power at 1.13 μm to peak.

The increase in laser power with the addition of H_2, D_2 and He additives was attributed in part to an increase in excitation to the upper laser level caused by an increase in the tube impedance (characterised by an increase in tube voltage and a decrease in the tube current) and hence in E/N (see Section 1.3.5). The increase in tube impedance was found to be greatest when either H_2 or D_2 was used as the additive. The increased tube impedance with additive addition was also reflected by a decrease in the step which occurred in the tube current waveform. The position of the step relative to the onset of the current pulse gave a measure of the preionisation density at the beginning of the following excitation pulse [3,4]. Hydrogen additives were found to cause the step to decrease by the largest amount followed by D_2 and finally He. This trend reflected the relative abilities of each of the additives to cool electrons in the interpulse period (see Section 1.3.5), i.e. H_2 cools electrons faster than D_2 and He and consequently electron-ion recombination is most rapid with H_2 additives and least rapid with He additives.

The decrease in laser power at 1.13 μm with large percentages of additives could only be explained in terms of a lower level effect. This is because the 1.13 μm and 1.50 μm laser transitions share a common upper laser level and consequently an increase in upper level excitation should enhance laser oscillation of both transitions equally which was not found to be the case for large percentages of additives. The increase in laser power at 1.50 μm and the corresponding decrease in the laser power at 1.13 μm with increasing percentage of additive was attributed to the decrease in the 1.50 μm metastable lower laser level population in the interpulse period. The fact that the laser power at 1.13 μm peaked for lower percentages of H_2 than for D_2 again reflected the ability of the additive to effectively cool the electrons and hence reduce the metastable lower laser level for the 1.50 μm transition in the interpulse period. The laser power at 1.13 μm did not peak in the same manner when He was used compared to when either H_2 or D_2 were used which suggested that there may be a phenomenon which is peculiar to H_2 and D_2, i.e. a transfer of population from the 1.50 μm metastable level to the 1.13 μm metastable level due to a molecular process.

It is likely that the increase in laser power at 1.13 μm and 1.50 μm with the addition of H_2, D_2 and He additives to the buffer-gas is due to a combined effect of increased excitation to the upper laser level and increased metastable depopulation in the interpulse period.

The addition of additives to the buffer gas was found to significantly change the power delivery from the circuit to the laser tube. As the percentage of additive was increased, the total power delivered to the laser tube and the power delivered over the duration of the 1.50 μm laser pulse increased whilst the power deposited before the onset of laser oscillation at 1.50 μm decreased. The effect was most pronounced with H_2 additives followed by D_2 and then He. The increased tube impedance was responsible for the increased power delivery and the change in the temporal delivery of power to the tube. There was improved matching of the charging circuit to the laser tube.

4.8 References

[1] English Electric Valve Ltd (1994).

[2] H. M. Pask, J. A. Piper, IEEE J. Quantum Electron. **30** (10) pp 2376-2384 (1994).

[3] G. Hogan, PhD Thesis, Oxford University (1993).

[4] D. R. Jones, S. N. Halliwell, C. E. Little, Optics Comm.**111** pp 394-402 (1994).

[5] J. J. Chang, Appl. Opt. **33** (12) pp 2255-2265 (1994).

[6] V. M. Batenin, V. A. Burmakin, P. A. Vokhmin, A. I. Evtyunin, I. I. Klimovskii, M. A. Lesnoi, L. A. Selezneva, Sov. J. Quantum Electron. **7** (7) pp 891-893 (1977).

[7] Yu. G. Chernov, High Temp. **8** (5) pp 881-885 (1970).

Chapter 5

Hydrogen Addition to a BVL with a Neon Buffer Gas

5.1 Introduction

In this chapter, the effects of hydrogen addition to the neon buffer gas of a BVL upon the total average laser power, the laser power at 1.13 μm, the laser power at 1.50 μm, the temporal evolution of the 1.13 μm and 1.50 μm laser pulses, and the tube current and tube voltage waveforms are discussed. Furthermore, the dependences of these characteristics upon the discharge conditions (for example, the buffer gas pressure, charging voltage, PRF and storage capacitance) are also discussed. The BVL used throughout these investigations is discussed in detail in Section 2.5.5. It consisted of an alumina confinement tube (dimensions of i.d. 23 mm, o.d. 31 mm and length of 700 mm) which was sleeved inside Zircar AL30AAH insulation and contained within an outer quartz tube as shown in Figure 2.11. The laser was leak tested using a mass spectrometer before discharge cleaning using a neon buffer gas (see Section 3.11.1). Clean barium pieces (see Section 3.11.2) were loaded onto a molybdenum boat positioned at the anode end of the laser and a purging buffer gas was used to prevent contamination of the tube. Once the laser tube reached the operating temperature of between 800-1000°C, the barium began to seed the active volume by entrainment with a slow flow Ne/NeH_2 buffer gas.

The dependences of total laser power, laser power at 1.13 μm and laser power at 1.50 μm on the charging voltage were investigated for various PRFs and buffer gas pressures for fixed storage capacitance values. The buffer gas used was alternated between neon and a premix of neon and 3% H_2 which had previously been found to be optimum for maximum laser power (see Section 4.3). Hydrogen was sometimes found to be difficult to remove from the laser tube, so care had to be taken to ensure that measurements made using only neon additives were consistent with those obtained before any hydrogen had been added to the laser tube. The dependences of laser power on operating conditions such as buffer gas pressure, charging voltage, PRF, storage capacitance and input power are discussed in Sections 5.2.1, 5.2.2, 5.2.3 and 5.2.3 respectively.

The effects of hydrogen addition on the temporal evolution of both the 1.13 μm and 1.50 μm laser pulses, the tube current and tube voltages were also investigated as functions of the above mentioned parameters. The results for these are discussed in Sections 5.3 and 5.4 respectively.

A study was made using a monochromator to investigate whether hydrogen addition had any effect upon the full range of laser transitions. Results from this investigation are discussed in Section 5.5.

The dependence of energy deposition on the charging voltage and the input power was investigated both with and without 3% added hydrogen, which is discussed in Section 5.6.

5.2 Dependence of Laser Power on Discharge Conditions

5.2.1 Buffer Gas Pressure Dependence

The dependences of the total laser power, laser power at 1.13 μm and laser power at 1.50 μm were investigated as functions of buffer-gas pressure both with and without added H_2. The percentage of added H_2 was maintained at 3%, which corresponded to the optimum value for both the total laser power and the 1.13 μm laser transition (see Section 4.3.1). The charging voltage and storage capacitance were maintained constant throughout at 12 kV and 1.2 nF (hot value).

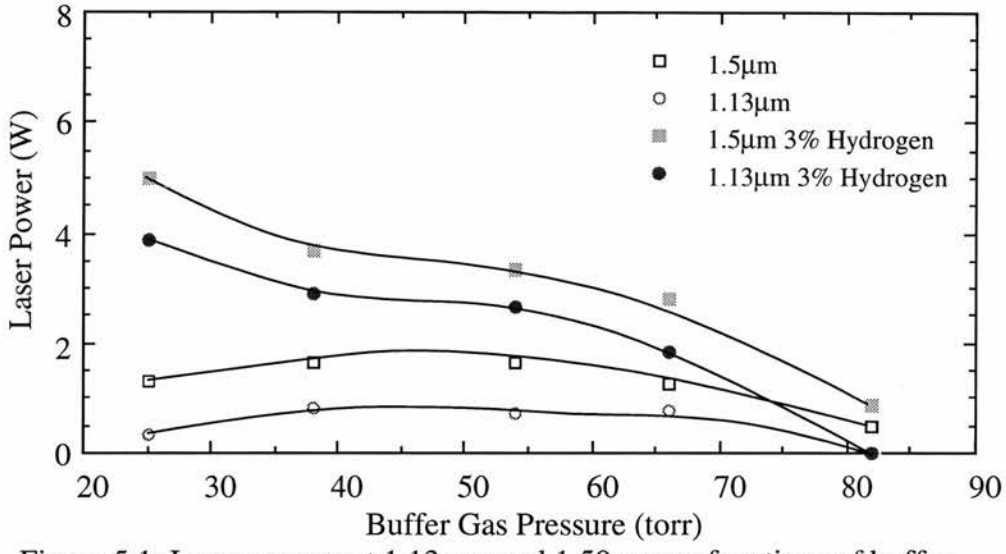

Figure 5.1: Laser powers at 1.13 μm and 1.50 μm as functions of buffer gas pressure at a PRF of 11 kHz with and without 3% added hydrogen.

The laser powers were measured individually at each pressure, first without H_2, then with 3% added H_2. This was found to be a more reliable method than, for example, taking measurements for various pressures first without H_2, then with 3% added H_2. Figures 5.1, 5.2 and 5.3 show how the laser powers at 1.13 μm and 1.50 μm varied with buffer gas pressure with and without 3% added hydrogen at 11 kHz, 13 kHz and 15 kHz respectively. It should be pointed out that at low buffer-gas pressures, problems were encountered with the lifetime of each barium load. This was due either to diffusion to the cold regions and/or the high gas flow rate which carried the barium vapour quickly to the cathode barium trap.

The addition of 3% H_2 to the neon buffer gas increased the laser power at both 1.13 μm and 1.50 μm at all the PRFs and buffer gas pressures selected (ranging from 20 to 82 torr). At 11 kHz, the proportionate increase in laser power at 20 torr was much higher than at all the other pressures, increasing from 0.3 W to 3.9 W at 1.13 μm and from 1.5 W to 5.0 W at 1.50 μm with the addition of 3% H_2. At a pressure of 20 torr, the laser power at both 1.13 μm and 1.50 μm decreased with increasing PRF, a phenomenon observed both with and without H_2. Indeed, at 13 kHz, laser oscillation at 1.13 μm ceased altogether whilst at other pressures laser oscillation continued. In contrast, at higher pressures, the laser power at 1.50 μm always increased with increasing PRF

both with and without added H_2. The laser power at 1.13 μm also increased with increasing PRF, from 11 kHz to 13 kHz, but almost ceased when the PRF was increased further to 15 kHz.

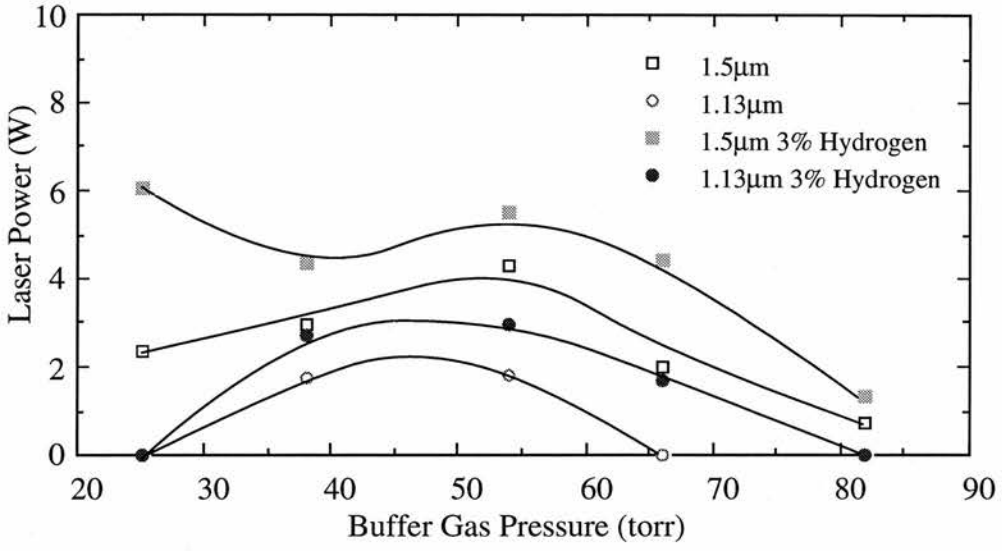

Figure 5.2: Laser powers at 1.13 μm and 1.50 μm as functions of buffer gas pressure at a PRF of 13 kHz with and without 3% added hydrogen.

With the exception of the results at 20 torr, the pressure which gave the maximum power at 1.13 μm and 1.50 μm was approximately the same both with and without 3% added H_2. This was around 50 torr for both laser transitions, giving peak powers at 1.13 μm of 2.0 W and 3.0 W without and with 3% added H_2 respectively at a PRF of 13 kHz, and peak powers at 1.50 μm of 5.8 W and 7.0 W without and with 3% added H_2 at a PRF of 15 kHz. This was consistent with the trends found in Section 5.2.3, i.e. that the laser power at 1.50 μm peaked at higher input powers than at 1.13 μm.

Using a phosphor card to allow visual indication of the near infrared laser radiation, the radial beam intensity profiles at both 1.13 μm and 1.50 μm were observed at a pressure of 20 torr. In the absence of any added H_2, the laser beam profile at both wavelengths appeared annular (ie laser oscillation occurred predominantly near the tube wall and not on the tube axis). When 3% H_2 was added to the buffer gas, laser oscillation on the tube axis appeared to be significantly enhanced for both the 1.13 μm and 1.50 μm transitions. This effect was not observed to the same extent at higher pressures. In Section (4.5), a more detailed analysis was undertaken concerning the effects of H_2 and

He additives on the temporal and spatial evolution of both the 1.13 μm and 1.50 μm laser pulses at both an optimum pressure and a low pressure of neon buffer gas.

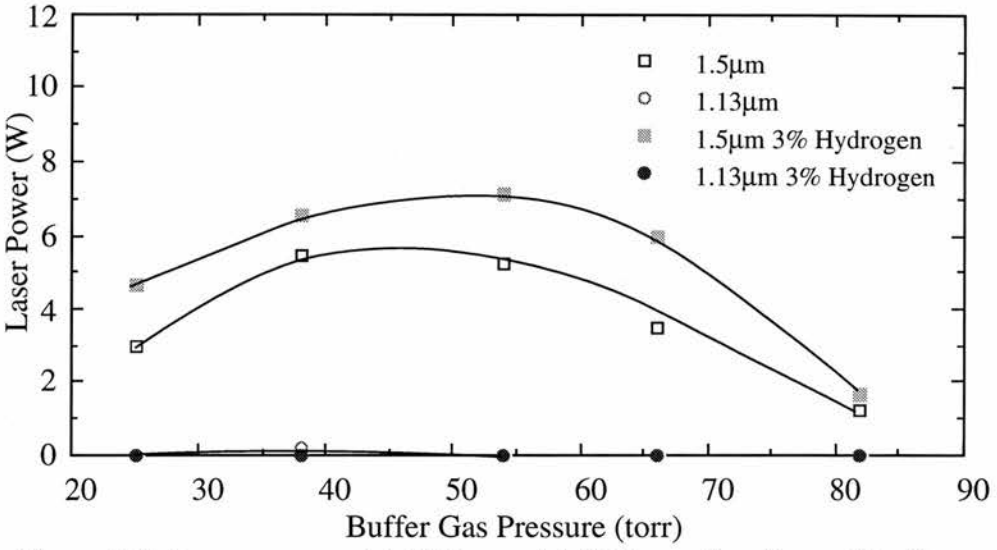

Figure 5.3: Laser powers at 1.13 μm and 1.50 μm as functions of buffer gas pressure at a PRF of 15 kHz with and without 3% added hydrogen.

The change in the radial intensity distribution with the addition of hydrogen, when operating the laser at low (20 torr) pressures, may be explained in terms of improved matching of the charging supply to the discharge tube, faster depopulation of the lower metastable laser levels and lower remanent electron density.

Lower gas pressures generally favour the generation of higher electron energies because of the increased E/N ratio [4]. However, lower gas pressures also result in a lower laser tube impedance. As the PRF is increased, the decrease in time available for recombination reduced causes the prepulse free electron density to increase, hence reducing further the tube impedance. For reasons discussed in Section 1.3.5, this reduces excitation to the upper laser level. The addition of H_2 to the laser tube increases the laser tube impedance (characterised by an increase in the tube voltage and a decrease in the tube current) resulting in more efficient excitation.

Increasing the PRF also reduces the time for which the metastable lower laser levels can be depopulated by electron collision, and hence reduces the population inversion in the following excitation pulse. The addition of H_2 can largely compensate for the decrease in time available by increasing the electron cooling rate in the interpulse period.

At moderate (40-60 torr) buffer gas pressures, the increase in tube impedance resulting from enhanced electron-ion recombination leads to more efficient excitation to the upper laser level. This is reflected by an increase in laser power at both 1.13 μm and 1.50 μm when the buffer gas pressure is increased from 20 torr to between 40 torr and 60 torr. The addition of H_2 further increases the tube impedance and hence the laser output power. At these pressures, as the PRF is increased, the prepulse free electron density correspondingly increases, hence reducing the excitation of the upper laser levels. However, this is largely offset by the increase in the deposited input power and hence in barium vapour density. At higher PRFs, the laser power at 1.13 μm is significantly reduced, which could be as a result of metastable depopulation caused either by inefficient electron cooling or by thermal population of the lower level (see Section 1.3.5).

At high (80 torr) buffer gas pressures, the high tube impedance is compromised by the reduced E/N ratio which does not favour efficient excitation to the upper levels (see Section 1.3.5). The addition of H_2 in this regime may enhance upper laser level excitation by virtue of an increase in the E/N ratio (characterised by an increase in the tube voltage with H_2 addition), or reduce the prepulse metastable population because of more efficient electron cooling. Because the tube impedance is already relatively high, the influence of hydrogen at higher buffer-gas pressures is only limited.

5.2.2 PRF and Charging Voltage Dependence

Figures 5.4, 5.5 and 5.6 show how the laser powers at 1.13 μm and 1.50 μm varied with PRF for charging voltages of 12 kV, 14 kV and 16 kV respectively, both with and without the addition of 3% H_2. The pressure and charging capacitance were maintained at 54 torr and 1.2 nF (hot values) respectively. The following trends were observed: first, the laser powers at both 1.13 μm and 1.50 μm increased with the addition of 3% H_2 over all the discharge conditions selected. Second, the power of the 1.13 μm line reached a maximum at lower PRFs than the 1.50 μm line (12-13 kHz *cf.* 15-16 kHz respectively, in the absence of H_2; 12-13 kHz *cf.* 18-19 kHz respectively, in its presence). Third, the upper PRF was extended for the 1.50 μm line when H_2 was added, but no such

PRF advantage was obtained for the 1.13 μm line. Although not shown in these figures, laser oscillation at 1.50 μm has also been achieved at a PRF of 25 kHz when, in the absence of H_2, laser oscillation would normally cease at 18-19 kHz. Once again, the PRF was not extended for the 1.13 μm transition with the addition of H_2.

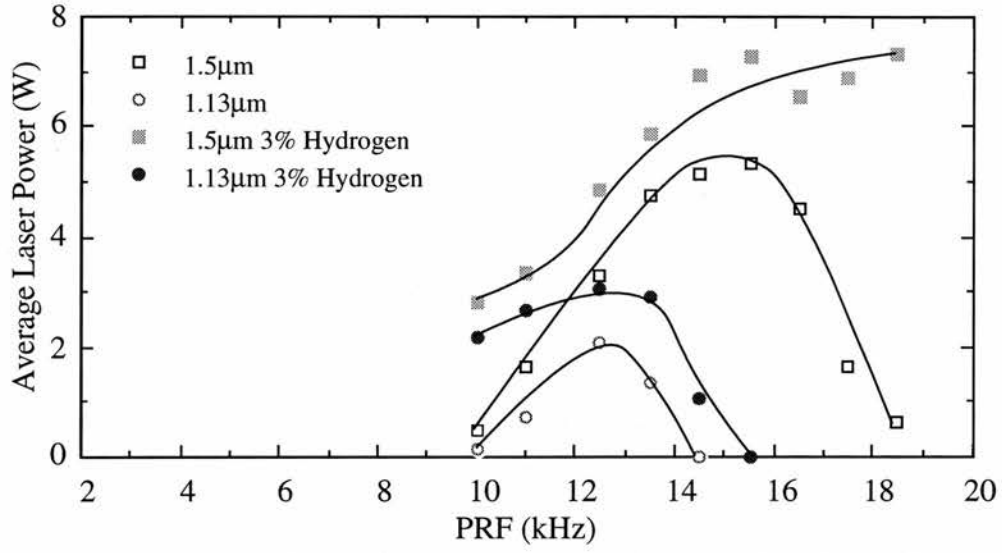

Figure 5.4: Average laser powers at 1.13 μm &1.50 μm as functions of PRF at a charging voltage of 12 kV with and without 3% added hydrogen.

At low charging voltages, the laser power at 1.13 μm increased with increasing PRF, reached a peak, then decreased as the PRF was increased further. In contrast, at low charging voltages, the laser power at 1.50 μm increased with increasing PRF. Indeed, it was only at higher charging voltages that the laser power at 1.50 μm began to peak with increasing PRF. These trends can be explained by considering the principal factors which limit the PRF to BVLs, i.e. the metastable population and the prepulse free electron density.

Increasing the PRF generally led to an increased metastable population since less time was available for collisional depopulation to occur. The lower energy of the 1.13 μm metastable level suggests that that level would become over populated at lower PRFs than the lower metastable level of the 1.50 μm transition. Hence, the 1.13 μm transition should extend to a lower upper limit in PRF relative to the 1.50 μm transition, as observed in Figure 5.4. The addition of H_2 would tend to accelerate the depopulation of the metastable

level (see Section 1.3.5) which explains the observed increase in laser power of both transitions with H_2 addition.

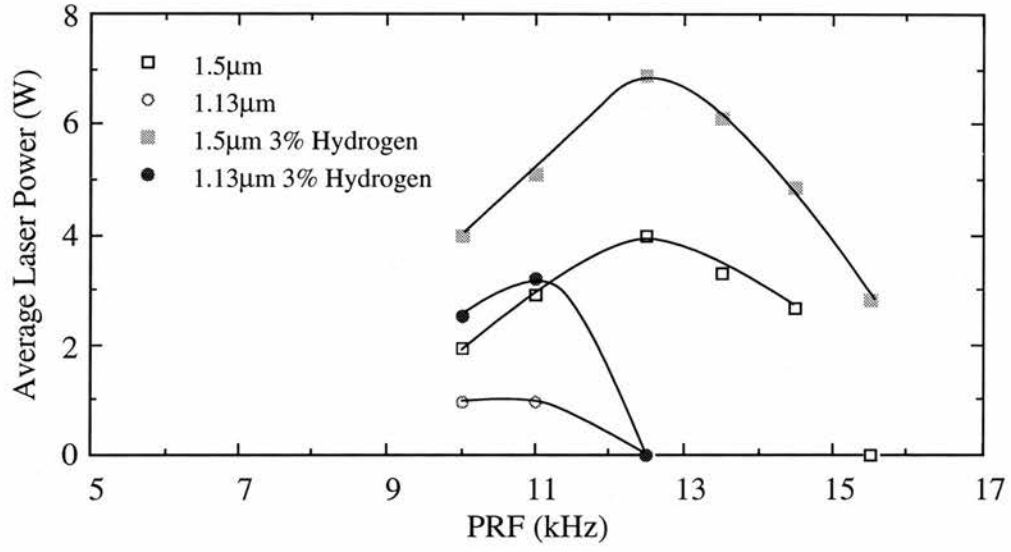

Figure 5.5: Average laser powers at 1.13 μm and 1.50 μm as functions of PRF at a charging voltage of 14 kV with and without 3% added hydrogen.

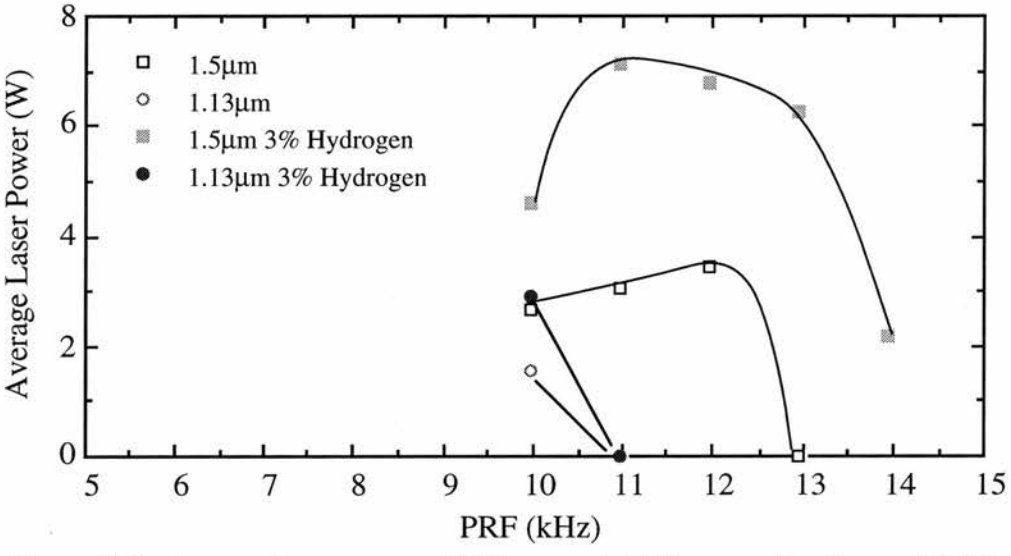

Figure 5.6: Average laser powers 1.13 μm and 1.50 μm as functions of PRF at a charging voltage of 16 kV with and without 3% added hydrogen.

The enhanced electric fields arising from an increased charging voltage should increase excitation to the upper laser level, thereby increasing laser power at both 1.13 μm and 1.50 μm. However, this was only observed to occur at low PRFs. It is possible that at higher PRFs, increasing the charging voltage (and hence the input power) resulted in significant thermal population of the metastable levels, which countered any beneficial effect of the increased applied voltage.

Increasing the PRF also increases the preionisation density, which reduces the overall tube impedance and hence reduces excitation to the upper laser level (see Section 1.3.5). However, since the two transitions share a common upper level, any decrease in upper level excitation should affect the laser powers at both transitions. The reverse is in fact observed, i.e. the laser power increased at 1.50 μm with increasing PRF, whilst the laser power at 1.13 μm decreased. This would suggest that, under these conditions, the preionisation density was not the dominant mechanism limiting the laser power at 1.13 μm.

A further possible mechanism limiting laser output power is an excessively high barium vapour density. When this occurs, the tube impedance is strongly reduced. Under such conditions, increasing the charging voltage would exacerbate the problem, since it would increase the input power and thereby raise the barium vapour density which would lead to a further lowering of the tube impedance.

5.2.3 Storage Capacitance Dependence

The effect of varying the storage capacitance on the total laser power, the laser power at 1.13 μm and the laser power at 1.50 μm was investigated for conditions both with and without 3% added H_2. Storage capacitance values ranged from between 0.9 nF anf 2.7 nF (hot values) at approximately regular intervals (0.9, 1.2, 1.7, 2.2, 2.4 and 2.7 nF). For each capacitance value, the total laser power was optimised by varying both the charging voltage and the PRF. Generally speaking, the charging voltage ranged from 12-18 kV and the PRF from 5-14 kHz. The PRF which gave maximum laser power decreased with increasing storage capacitance. Some problems were encountered with the thyratron latching, which, in some cases, prevented a full range of voltage measurements from being made. This was found to occur most frequently when small storage capacitances were used.

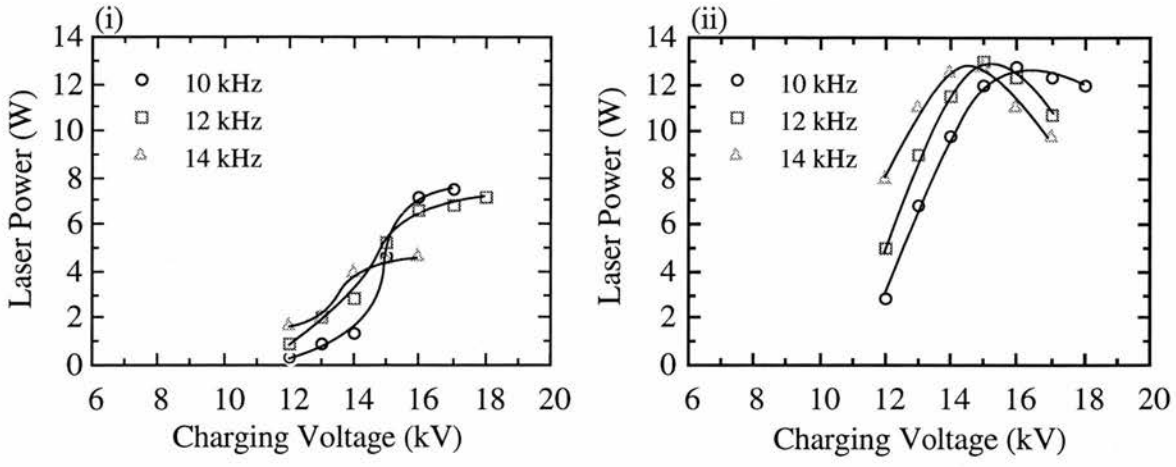

Figure 5.7a: Total laser power as a function of charging voltage and PRF (i) without added hydrogen and (ii) with 3% added hydrogen for a storage capacitance of 1.2 nF.

Figure 5.7a,b,c shows how the total laser power, the laser power at 1.13 μm and the laser power at 1.50 μm varied with charging voltage at PRFs of 10, 12 and 14 kHz respectively for a fixed storage capacitance of 1.2 nF (hot value).

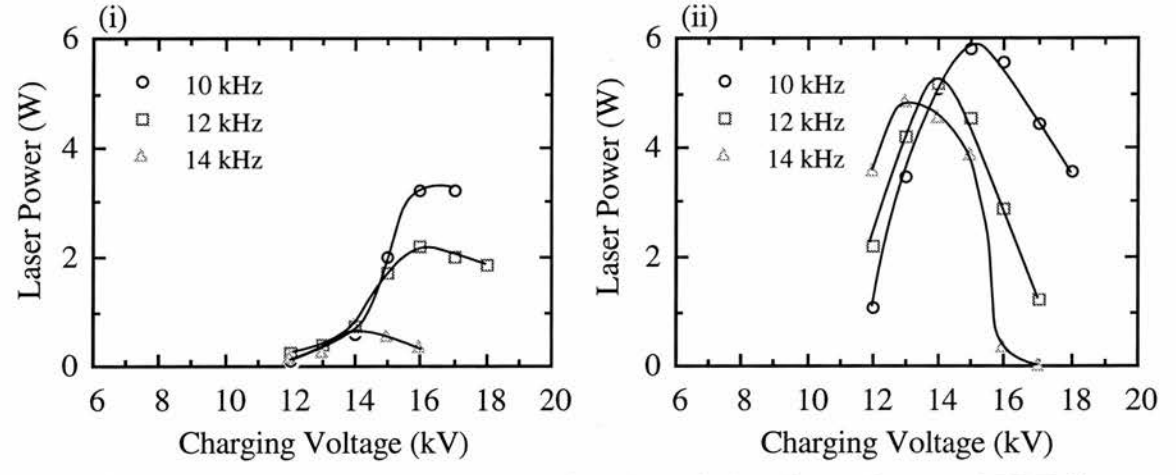

Figure 5.7b: Laser power at 1.13 μm as a function of charging voltage and PRF (i) without added hydrogen and (ii) with 3% added hydrogen for a storage capacitance of 1.2 nF.

In the absence of any added H_2, the laser power at 1.50 μm monotonically increased with charging voltage, and hence with input power, for all the PRFs selected. In addition, for a given charging voltage the laser power at 1.50 μm generally increased with increasing PRF. At a constant PRF, the laser power at 1.13 μm also increased with increasing charging voltage but reached a peak, above which the laser power decreased with a further increase in the charging voltage. The optimum voltage for maximum laser power at 1.13 μm tended to decrease with increasing PRF, as shown in Figure 5.7b,

thereby maintaining an approximately constant input power (based on stored energy). For example, the optimum voltage decreased from ~17 kV at 10 kHz to ~16 kV at 12 kHz and ~14 kV at 14 kHz, thereby maintaining a constant input power of 1.7 (±0.1) kW. At higher, and fixed charging voltages, the laser power at 1.13 μm generally decreased with increasing PRF, and hence increasing input power. For both laser transitions, the highest laser powers were obtained when high charging voltages were employed (also shown in Figure 5.12).

In the absence of any added H_2, the maximum total laser power which could be obtained increased with increasing charging capacitance for values up to ~2.4 nF (hot value). Above this value, the maximum achievable total laser power began to decrease. The upper limit to the charging capacitance was likely to be caused by excessive ionisation of the barium vapour in the excitation pulse. This is because in order to maintain the optimum input power for laser oscillation at 1.13 μm (see below), the PRF had to be decreased as the capacitance was increased. For each capacitance value, the maximum total laser power occurred at high charging voltages. Generally speaking, as the capacitance was increased, the optimum PRF for maximum total laser power decreased whilst maintaining a high charging voltage and consequently, the pulse energy (discharge current) increased with increasing capacitance [1]. In this way it was established that there existed an optimum input power for the laser which remained constant (for a given amount of insulation) and hence an optimum tube wall temperature [1]. The optimum input powers for the 1.13 μm and 1.50 μm laser transitions were approximately 1.7 kW and 2.1 kW respectively.

One effect of H_2 addition to the 1.13 μm laser transition was to decrease the optimum charging voltage for maximum laser power for a given PRF. For example, the optimum charging voltage decreased from ≥17 kV to ~15 kV at 10 kHz, ~16 kV to 14 kV at 12 kHz and from ~14 kV to 13 kV at 14 kHz with the addition of 3% H_2 as shown in Figure 5.7b. At a PRF of 14 kHz, the laser power at 1.50 μm decreased only as the charging voltage was increased from 16 kV to 17 kV with 3% added H_2. Unfortunately, results could not be taken under similar conditions without any added H_2 because of problems with the thyratron latching. However, when larger storage capacitance

values were used, an optimum charging voltage was also found to exist for the 1.50 μm laser transition, with charging voltages above this optimum tending to reduce the laser power at 1.50 μm.

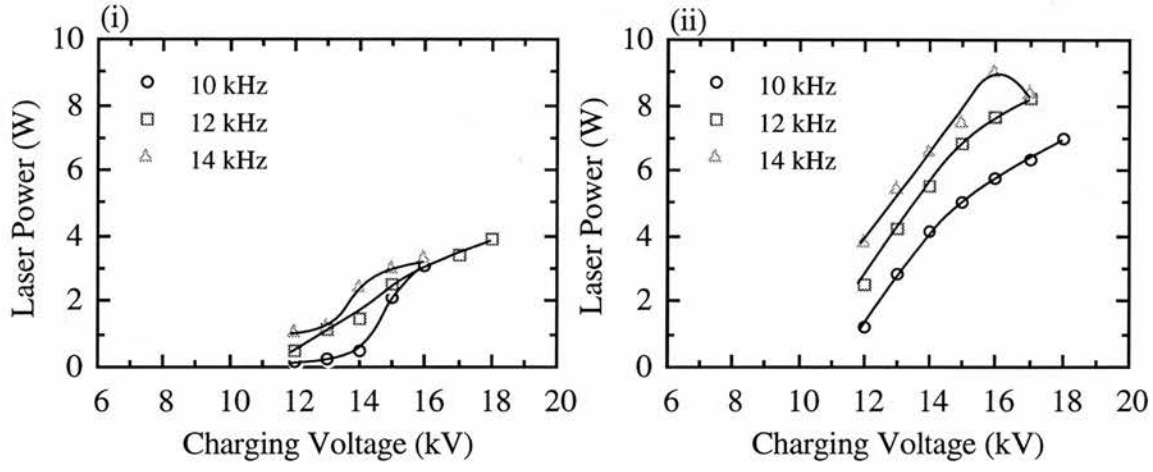

Figure 5.7c: Laser power at 1.50 μm as a function of charging voltage and PRF (i) without hydrogen and (ii) with 3% added hydrogen for a storage capacitance of 1.2 nF.

The addition of 3% H_2 to the buffer gas increased the total laser power for all the storage capacitors, charging voltages and PRFs selected. However, the most marked increase occurred when the charging capacitance, charging voltage and PRF were 1.2 nF (hot value), 15 kV and 10 kHz respectively. Under these conditions, the total laser power increased from 5.2 W to 14.3 W with the addition of 3% H_2. This corresponded to an increase of ~180% in the overall laser efficiency (based on stored energy), which increased to 1.0%. These values were significantly higher than the highest previously reported total laser power and efficiency of 12.5 W and 0.72% (non-simultaneous values) respectively [2]. The optimum charging capacitance for maximum laser power when 3% H_2 was added to the buffer gas was 1.2 nF (hot value). As the capacitance was increased beyond this, the maximum laser power which could be obtained for each capacitance value gradually decreased. Nevertheless the total laser power always remained at least 20% above the maximum input power which could be obtained when only neon was used. The maximum laser power obtained with 3% added H_2 was also achieved at high charging voltages but at smaller storage capacitance values. Hence, in order to maintain a constant input power, the PRF which corresponded to the maximum laser power was significantly higher when H_2

was added to the buffer gas than when only neon was used (10 kHz at 1.2 nF as opposed to 6 kHz at 2.4 nF using pure neon).

As outlined previously, there were optimum average input powers (based on stored energy) for both the 1.13 μm and 1.50 μm laser transitions. In the absence of added H_2, these were around 1.7 kW and 2.1 kW for 1.13 μm and 1.50 μm respectively. The optimum input power for maximum laser power was a compromise between these two values. Input powers above this optimum tended to cause the laser power at 1.13 μm to decrease, and the laser power at 1.50 μm to increase. The addition of H_2 to the laser appeared to reduce the optimum average input power (based on stored energy) slightly for both transitions. This reduction in average power in the circuit was attributed to an increase in the energy transfer efficiency from the storage capacitor to the laser tube with the addition of H_2 (see Section 5.6). Furthermore, for a given input power, the total laser power was much less dependent upon the particular excitation conditions with H_2 present in the discharge than in its absence. Figure 5.8 shows how, with 3% added H_2, the maximum laser power could be readily obtained for a variety of charging voltages and PRFs provided that the total input power remained around 1.6 kW using a storage capacitance of 1.2 nF. In the absence of H_2, the maximum laser power which could be obtained was much more dependent upon the PRF. Figure 5.9 shows the dependence of the total laser power on input power (based on stored energy) using a charging capacitance of 2.4 nF (hot value) both with and without 3% added H_2. At this higher capacitance value, with 3% added H_2, the maximum laser power could still be obtained over a broad band of PRFs. However, in the absence of added H_2, there existed only a narrow band of PRFs (ranging from 6-8 kHz) over which the optimum power could be obtained. This suggested that a long interpulse period was essential when using a neon buffer gas, particularly for the 1.13 μm transition, and that when H_2 is added to the laser, the upper limit to the PRF may be significantly raised (in this case doubled).

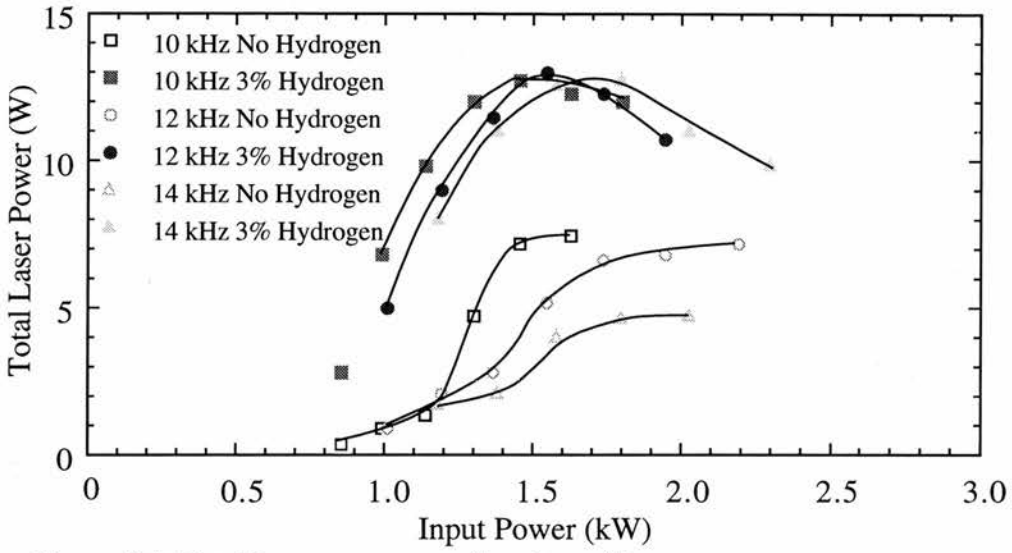

Figure 5.8: Total laser power as a function of input power at a storage capacitance of 1.2 nF with and without 3% added hydrogen.

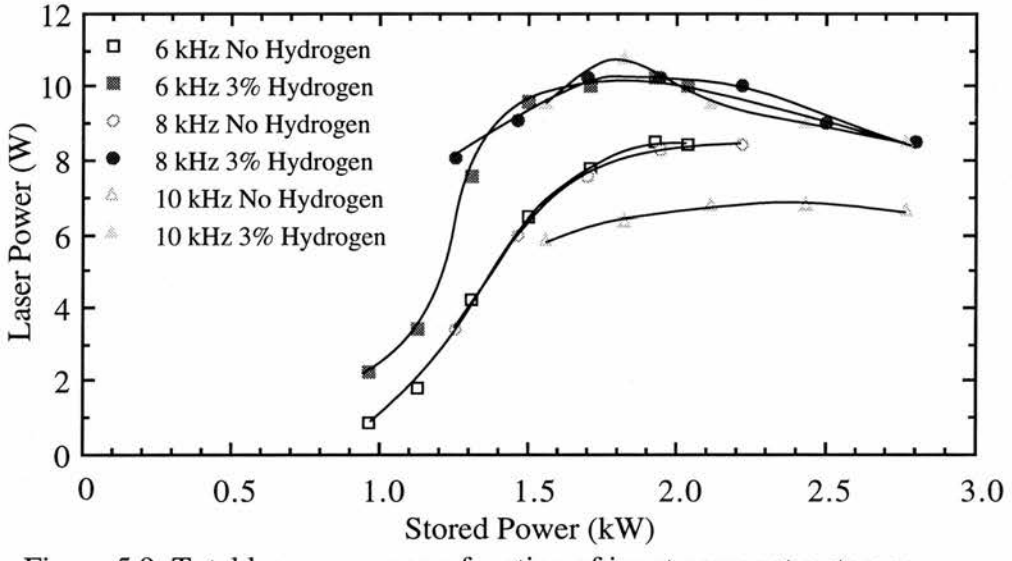

Figure 5.9: Total laser power as a function of input power at a storage capacitance of 2.4 nF with and without 3% added hydrogen.

The decreased dependence of PRF on the optimum laser input power with the addition of H_2 and also in the absence of H_2, the decreased dependence of PRF on the total laser output power with increasing charging capacitance would suggest that one of the chief mechanisms dictating the total laser power of the BVL is the degree of electron cooling in the discharge afterglow. In addition to this, the marginal decrease in the optimum input power with the addition of hydrogen to the laser indicates that the laser tube was better matched to the charging circuit. The increased tube impedance with hydrogen addition (see

Section 5.4) indicates that the prepulse free electron density (and hence the electron-ion recombination) is an important factor limiting the laser output power of BVLs using a neon buffer gas.

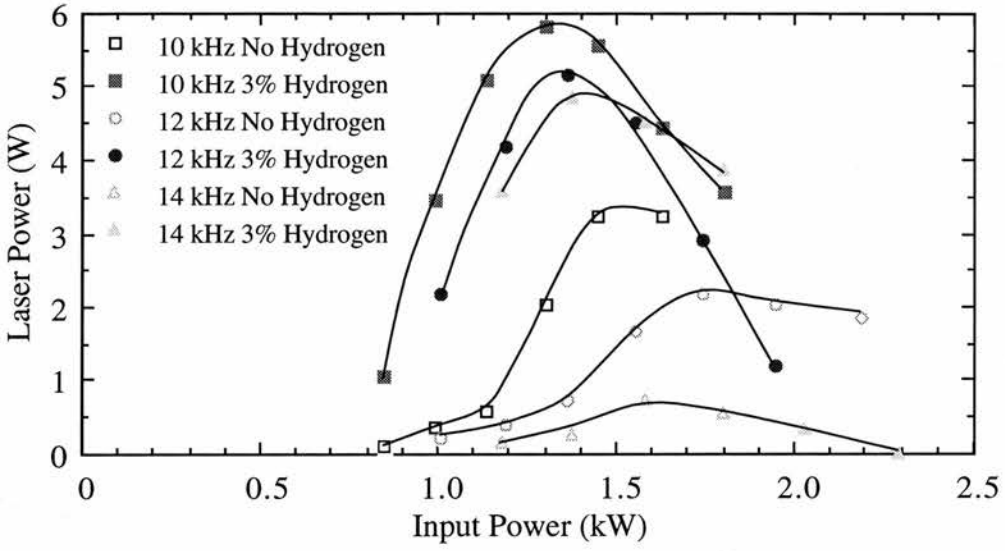

Figure 5.10a: Laser power at 1.13 μm as a function of input power at a storage capacitance of 1.2 nF with and without 3% added hydrogen.

Figures 5.10a,b show how (a) the laser power at 1.13 μm and (b) the laser power at 1.50 μm varied with the input power for the optimum storage capacitance value of 1.2 nF with added H_2. Figures 5.11a,b show how the laser power at (a) 1.13 μm and

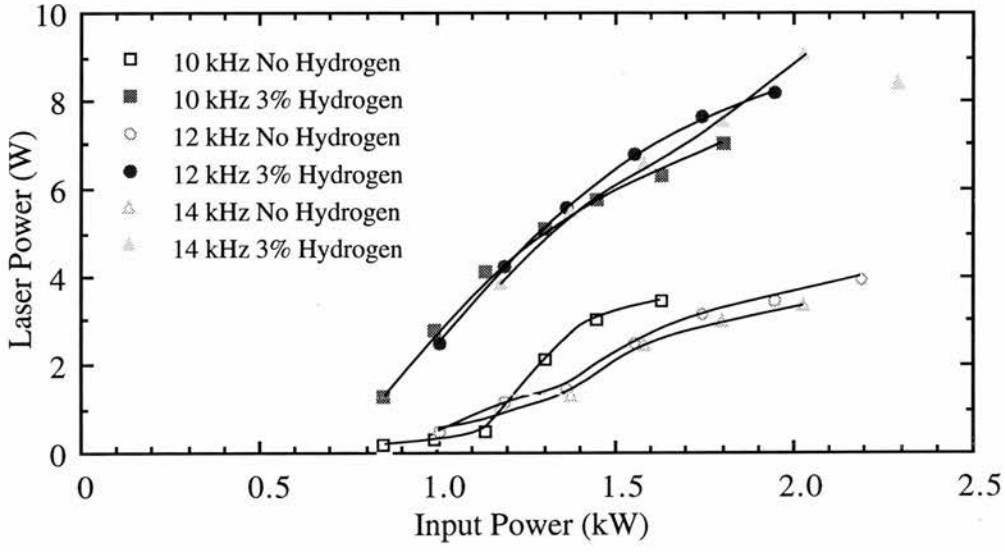

Figure 5.10b: Laser power at 1.50 μm as a function of input power at a storage capacitance of 1.2 nF with and without 3% added hydrogen.

(b) 1.50 μm respectively varied with input power for the optimum storage capacitance of 2.4 nF without added H_2. The optimum input power for laser power at 1.13 μm

decreased with the addition of H_2. The result of a more detailed study of laser power as a function of input power, PRF and charging voltage are shown in Figures 5.12, 5.13 and 5.14, and discussed below.

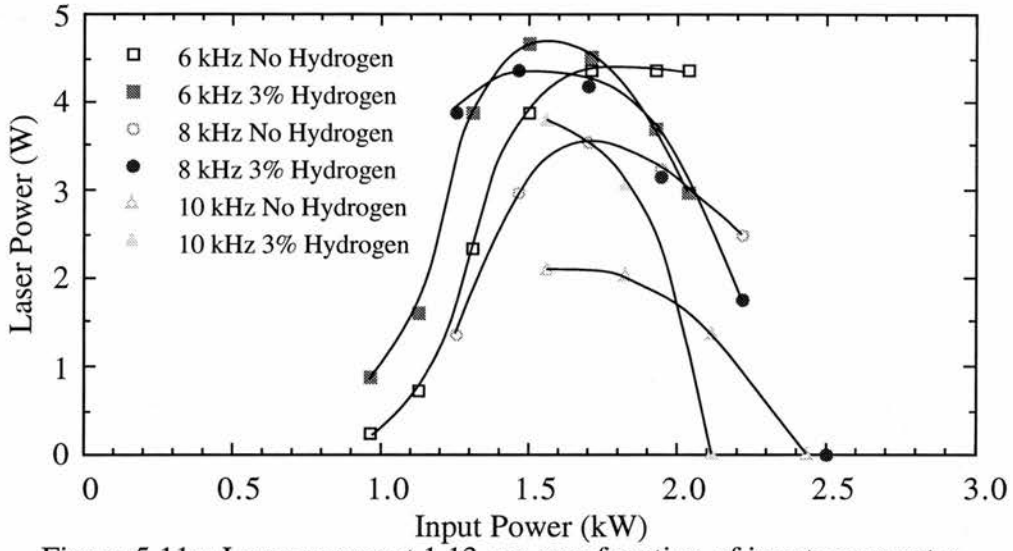

Figure 5.11a: Laser power at 1.13 μm as a function of input power at a storage capacitance of 2.4 nF with and without 3% added hydrogen.

The total laser power and laser power at 1.13 μm and 1.50 μm were also measured as functions of charging voltage for constant input powers (based on stored energy) by correspondingly decreasing the PRF when the charging voltage was increased. Charging voltages ranged from 14-18 kV inclusive, in 1 kV increments. Oscillograms of the tube voltage, tube current and both the laser pulse intensities at 1.13 μm and 1.50 μm were taken at each charging voltage. After each set of charging voltage measurements, the charging voltage was decreased to 14 kV and the previous discharge conditions re-established before the PRF (and hence the input power) was increased further. The input power (based on stored energy) was varied between 1.2 kW and 2.7 kW, in 0.3 kW increments. This particular method of taking results proved to be particularly fast, chiefly because less time was required to take each voltage measurement since no time was required for the wall temperature to stabilize between readings. An identical procedure was adopted when H_2 was added to the laser, but, this time the original conditions (ie laser power, tube current and tube voltage waveforms) were re-established before any H_2 was added. This ensured that results with H_2 could be compared with those without any added

H_2. Additional measurements, both without and with added H_2 were later taken to check for continuity of results. The storage capacitance was maintained at 1.2 nF (hot value) throughout.

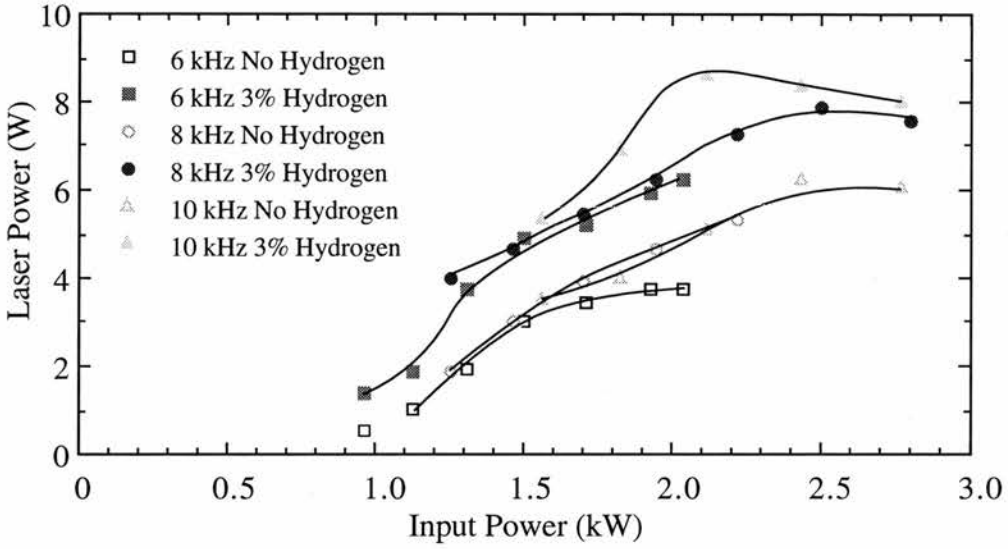

Figure 5.11b: Laser power at 1.50 μm as a function of input power at a storage capacitance of 2.4 nF with and without 3% added hydrogen.

Figures 5.12a,b,c shows how (a) the total laser power, (b) laser power at 1.13 μm and (c) the laser power at 1.50 μm varied as functions of charging voltage and input power with and without 3% added H_2. In this case, maximum total laser power occurred at similar input powers with and without H_2, at around 1.8 kW. The addition of 3% H_2 caused the total laser power, laser power at 1.13 μm and laser power at 1.50 μm all to increase for all the charging voltages and input powers selected. In addition, the range of values of the PRF and charging voltage which gave the maximum total laser output power increased greatly, provided that the input power was maintained at around 1.8 kW. This was again caused chiefly by the decrease in the dependence of laser power at 1.13 μm on the PRF with the addition of H_2. The discharge conditions at which maximum laser power was obtained at 1.50 μm also appeared to shift to lower charging voltages, and consequently to higher PRFs when H_2 was added to the laser.

Figure 5.12a: Total laser power as a function of charging voltage and input power without added hydrogen.

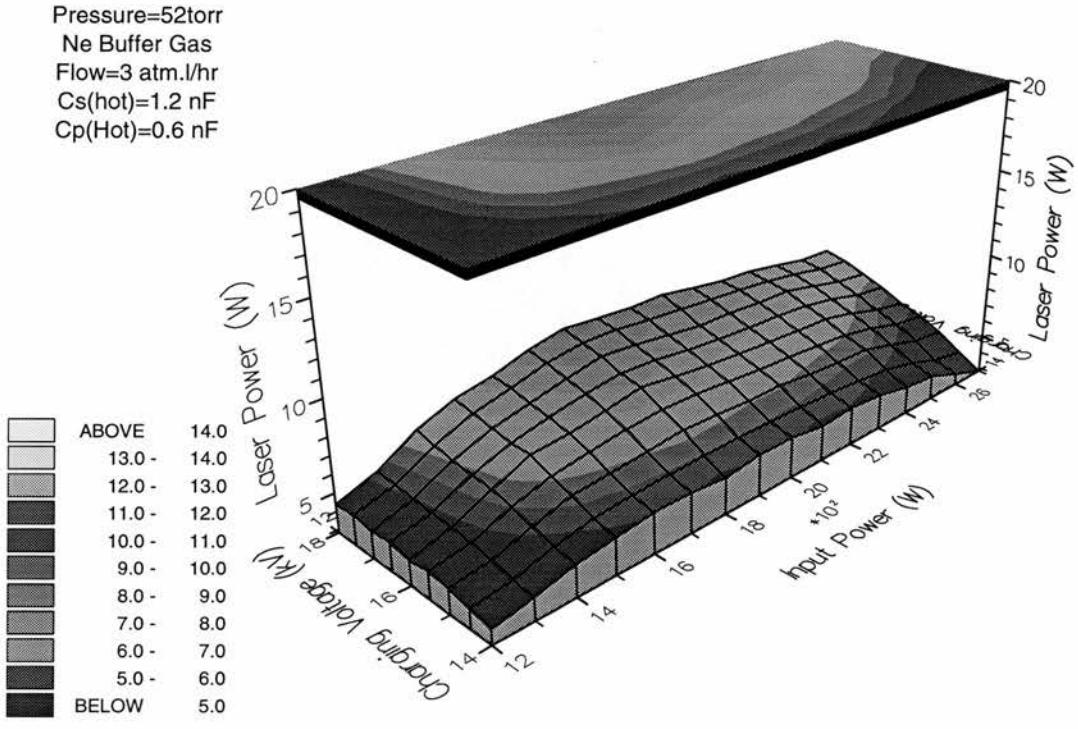

Total laser power as a function of charging voltage and input power with 3% added hydrogen.

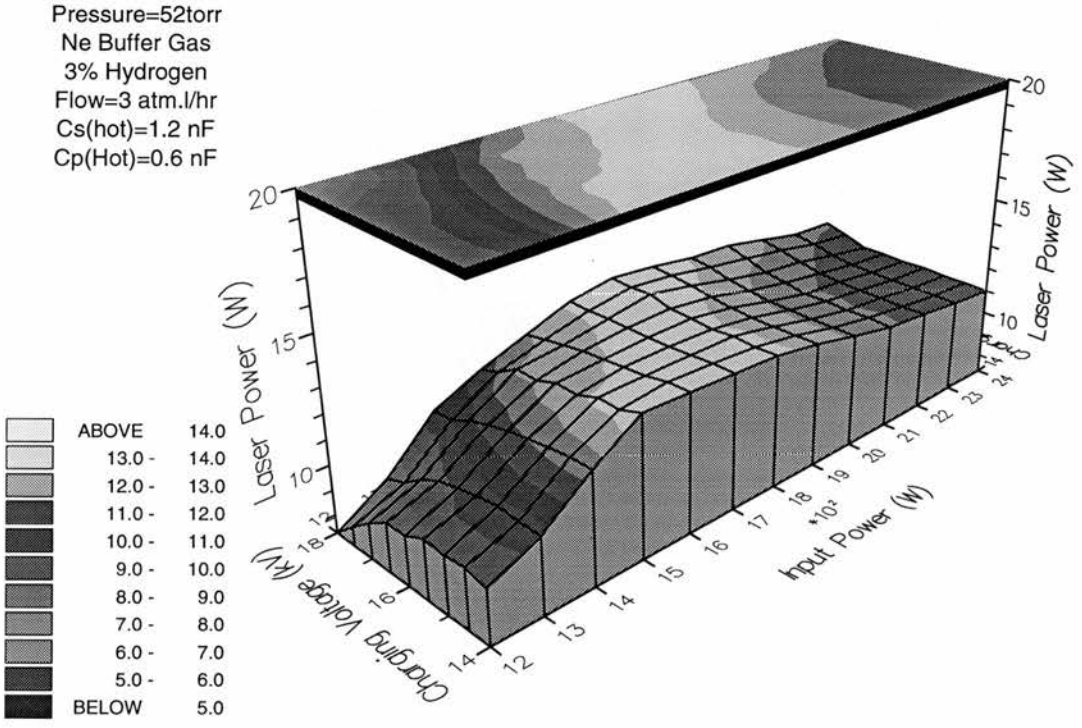

Figure 5.12b: Laser power at 1.13 μm as a function of charging voltage and input power without added hydrogen.

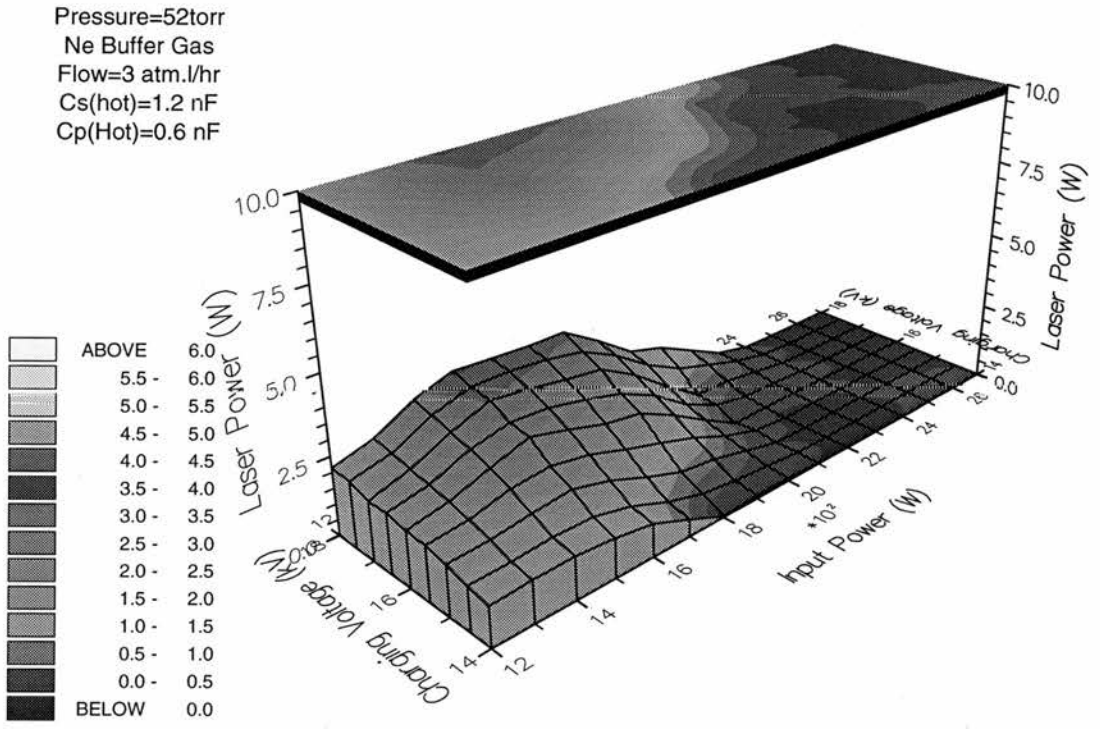

Laser power at 1.13 μm as a function of charging voltage and input power with 3% added hydrogen.

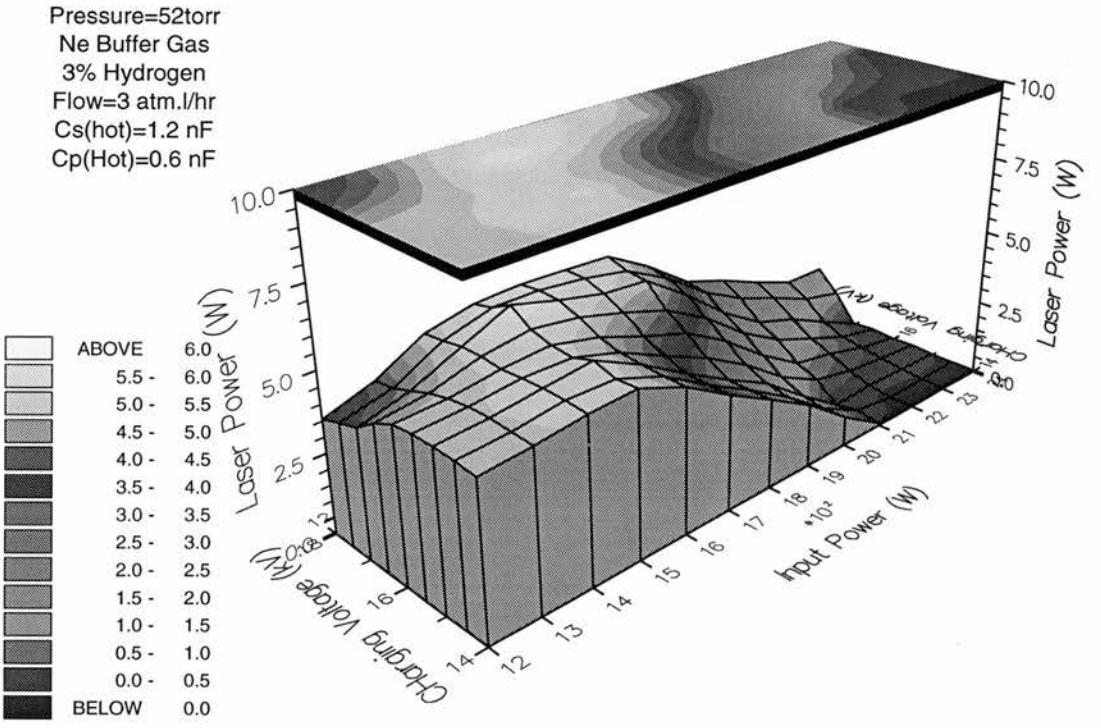

Figure 5.12c: Laser power at 1.50 μm as a function of charging voltage and input power without added hydrogen.

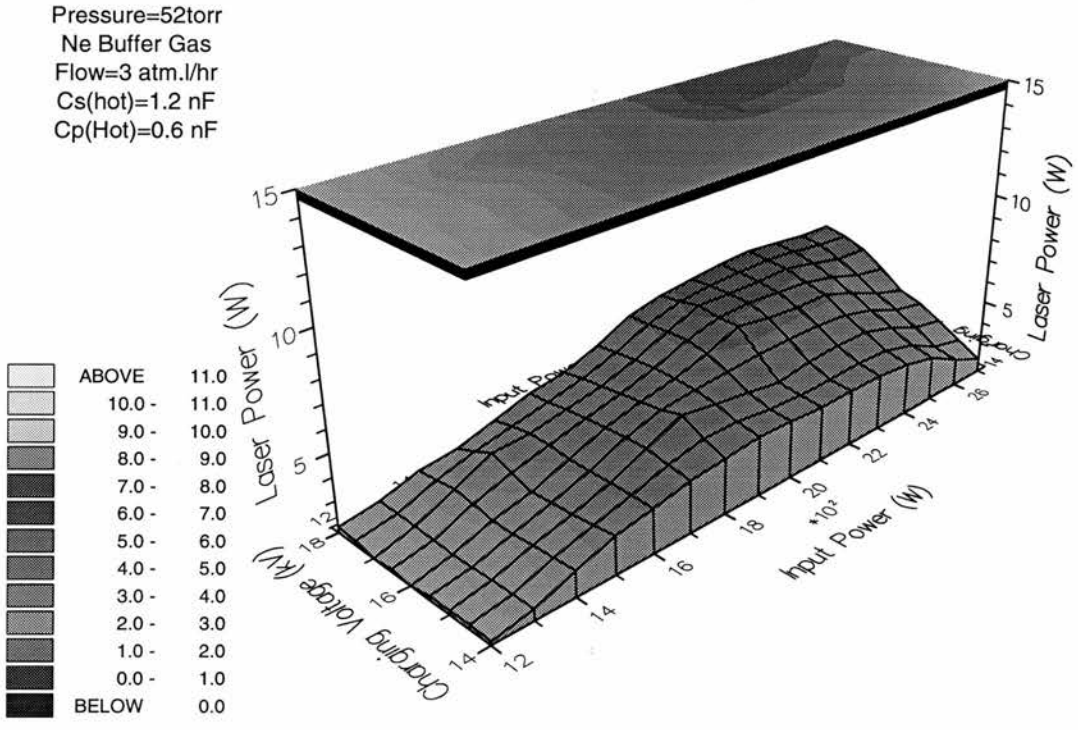

Laser power at 1.50 μm as a function of charging voltage and input power with 3% added hydrogen.

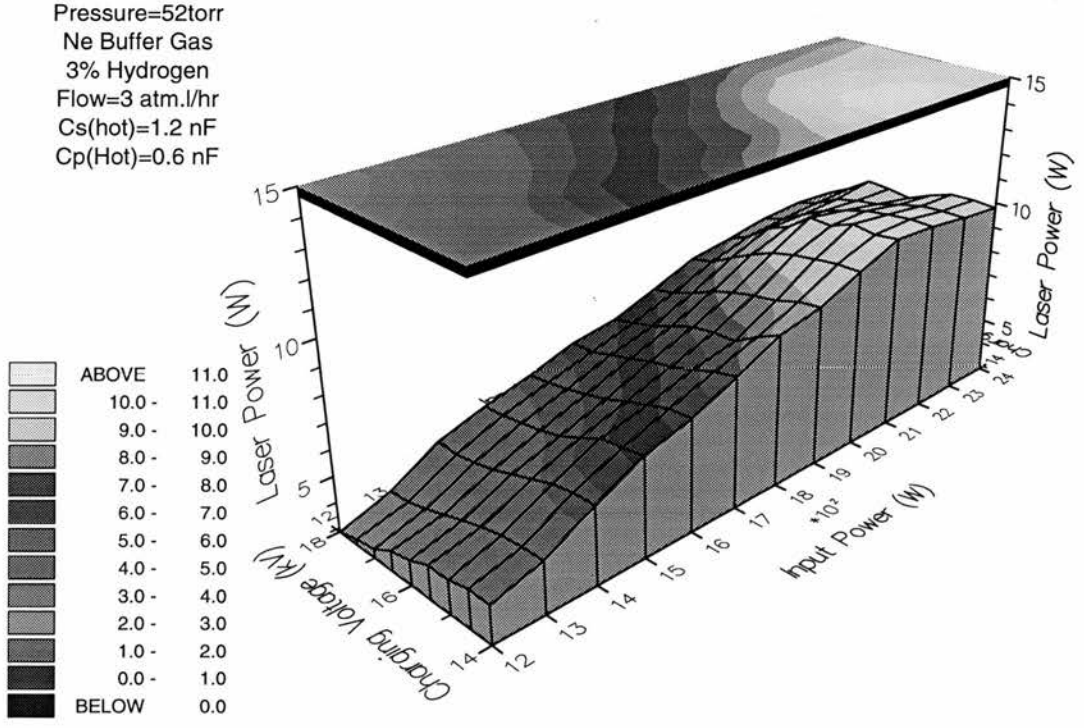

It should be noted that the absolute laser powers obtained in this section (Section 4.2.4) were somewhat different from some of the previous results (eg. Sections 4.2.1, 4.2.2 and 4.2.3). This is because these results were taken using a new thyratron. The anode fall time for this new thyratron was considerably shorter than the old one, and consequently changed the conditions for excitation (for example, the tube current risetime). This led to more efficient pumping of the upper laser levels. Despite this, the overall operating dependences on parameters such as the optimum storage capacitance and pressure were unchanged.

5.3 Temporal Evolution of the Laser Pulse

Figures 5.13a,b show how (a) the threshold tube current and (b) the threshold tube voltage for onset of the 1.50 μm laser transition varied with charging voltage both without and with added H_2. The input power (based on stored energy) was maintained at 1800 W by decreasing the PRF as the charging voltage was increased. The charging capacitance was 1.2 nF (hot value) which was previously found to be that which gave the maximum laser putput power with 3% added H_2 (see Section 5.2.3). Although the

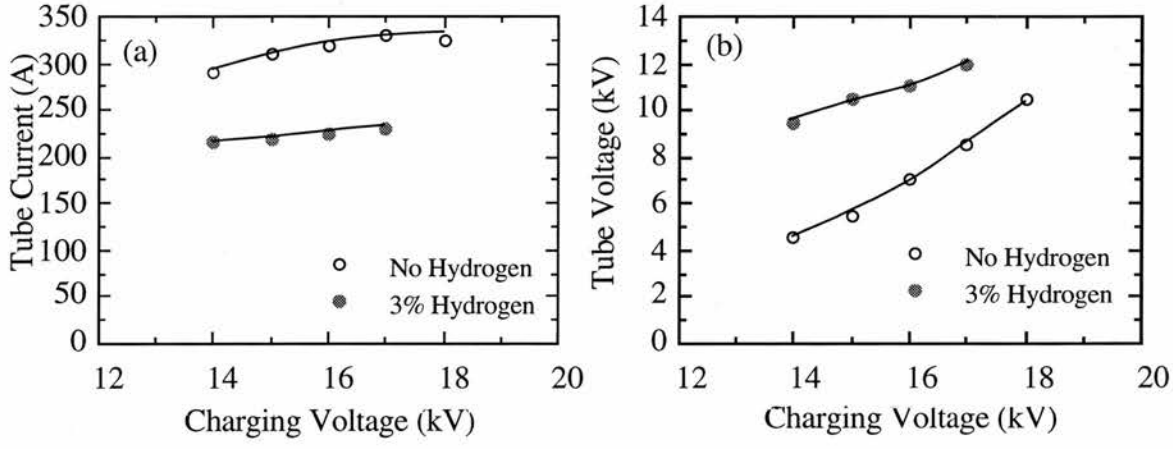

Figure 5.13: (a) threshold tube current and (b) threshold tube voltage at 1.50 μm as a function of charging voltage for a constant input power of 1.8 kW with and without 3% added hydrogen.

threshold current required for laser oscillation at 1.50 μm remained unaffected by the increasing charging voltage (and hence the decreasing PRF), the addition of 3% H_2 to the laser did cause a significant reduction, as shown in Figure 5.13a. The threshold voltage,

which tended to increase with charging voltage, *increased* with H_2 addition, as shown in Figure 5.13b.

The threshold current decreased and the threshold voltage increased with the addition of hydrogen principally because of the increased electron collision frequency resulting from H_2 addition. This would lead to faster electron cooling and hence would tend to decrease both the metastable population and the electron density during the interpulse period. In either case, this would result in a threshold inversion being established earlier in the excitation pulse, and hence a decrease in the delay between the excitation pulse and the laser oscillation would result, as observed. However, neither of these arguments can be used to explain why the delay between the onset of the tube current and the laser pulse does not decrease when the charging voltage was increased while the corresponding PRF was decreased. Increasing the charging voltage whilst maintaining a constant input power should both enhance excitation to the upper laser level (higher E/N) and also reduce the metastable population (because of the increased time interval between pulses).

Figure 5.14 shows how the delay between the beginning of the excitation pulse and the onset of laser oscillation at 1.50 μm decreased when the storage capacitance was increased to 2.4 nF. The addition of 3% H_2 caused this delay to decrease further, for each of the storage capacitances selected. The charging voltage, PRF and input power were chosen to give maximum laser power for each of the capacitance values for which the conditions had previously been found in Section 5.2.3: i.e. ~16 kV and 1.7 kW for the charging voltage and input power respectively. As the capacitance was increased, the PRF was decreased in order to maintain a constant input power of ~1.7 kW. In this example, the trends expected were observed, i.e. the decrease in the interpulse period resulted in more time available for electron collisions which is believed to have aided metastable depopulation, and electron-ion recombination.

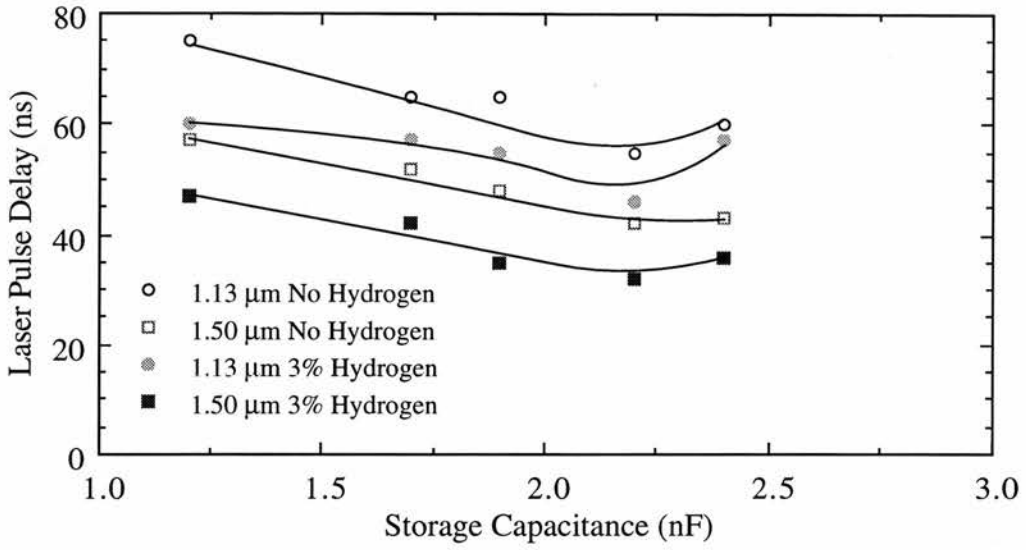

Figure 5.14: Laser pulse delay between the beginning of the excitation pulse and the 1.13 μm and 1.50 μm laser pulses as a function of storage capacitance, with and without 3% added hydrogen, for a constant input power and charging voltage.

5.4 Tube Current and Tube Voltage Waveforms

In general, the addition of H_2 to the buffer gas tended to cause the peak tube current to decrease and the peak tube voltage to increase. This was by no means the only effect that the addition of H_2 caused. Other effects included: the delay between the peak of the tube current and that of the tube voltage increased; the 'tube breakdown potential' (defined as tube voltage corresponding to the step on the tube current waveform, as discussed in Section 4.4.3) increased; the step on the tube current waveform occurred at earlier times.

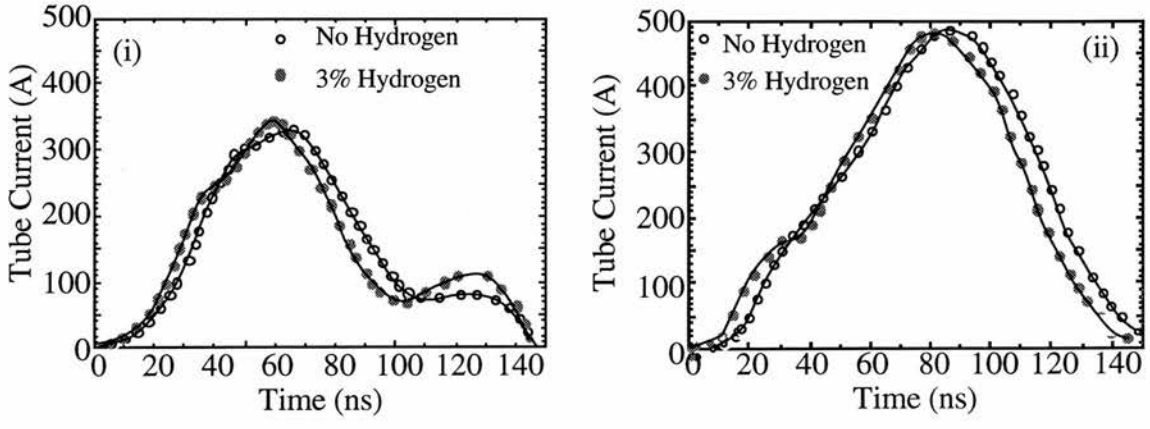

Figure 5.15a: Tube current waveforms using storage capacitances of (i) 1.2 nF and (ii) 2.4 nF with and without 3% added hydrogen.

Figures 5.15a,b show the effect of H_2 addition on (a) the tube current and (b) the tube voltage waveforms for maximum power conditions both with and without 3% added

H_2. For optimum conditions with H_2, the storage capacitance, charging voltage and PRF were 1.40 nF, 16 kV and 11.5 kHz respectively. For maximum power conditions without any added H_2, the storage capacitance, charging voltage and PRF were 2.4 nF, 16 kV and 6 kHz respectively.

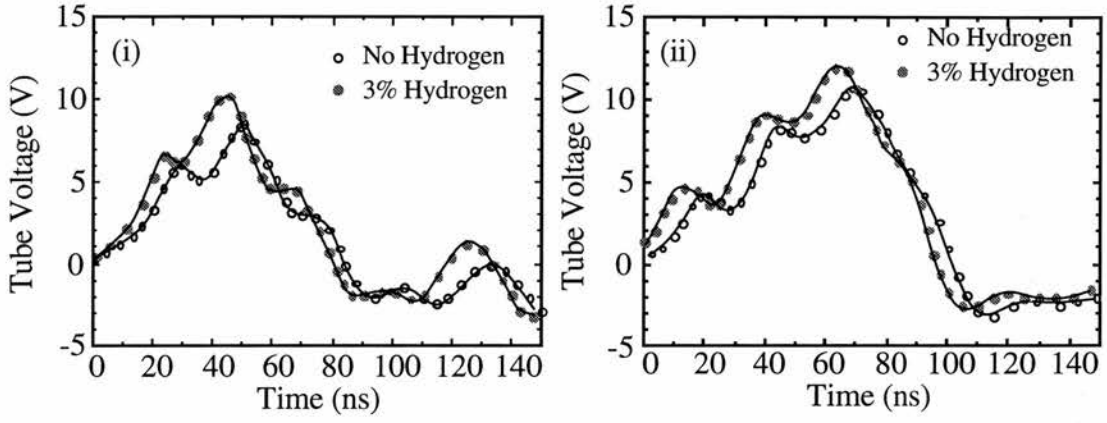

Figure 5.15b: Tube voltage waveforms using storage capacitances of (i) 1.2 nF and (ii) 2.4 nF with and without 3% added hydrogen.

When the charging capacitance was 1.2 nF (hot value), the addition of hydrogen caused the position of the step in the current pulse to decrease from ~56 ns to ~42 ns with respect to the onset of the pulse. The tube voltage which corresponded to these steps increased from 8.5 kV to 10 kV. When the charging capacitance was 2.4 nF (hot value), the addition of hydrogen caused the step to occur ~8 ns earlier, at ~34 ns from the onset of the current pulse. The tube voltages which corresponded to the step with 2.4 nF were both around 6.5 kV. In the absence of added H_2, the step in the tube current waveform occurred at much earlier times for the larger capacitances than for smaller capacitances. In addition, the tube voltage was significantly larger when the larger capacitance value was used.

Figures 5.16a,b show a contour plot of how (a) the tube current and (b) the tube voltage varied with the charging voltage for a constant input power of 1800 W (based on stored energy) without and with 3% added H_2. As the tube voltage was increased, the corresponding PRF was decreased (to maintain contant input power), the step in the current pulse occurred at earlier times with respect to the onset of the current pulse. Furthermore, the tube voltage increased with increasing charging voltage, indicating an increase in tube

Figure 5.16a: Tube current as a function of time and charging voltage without added hydrogen.

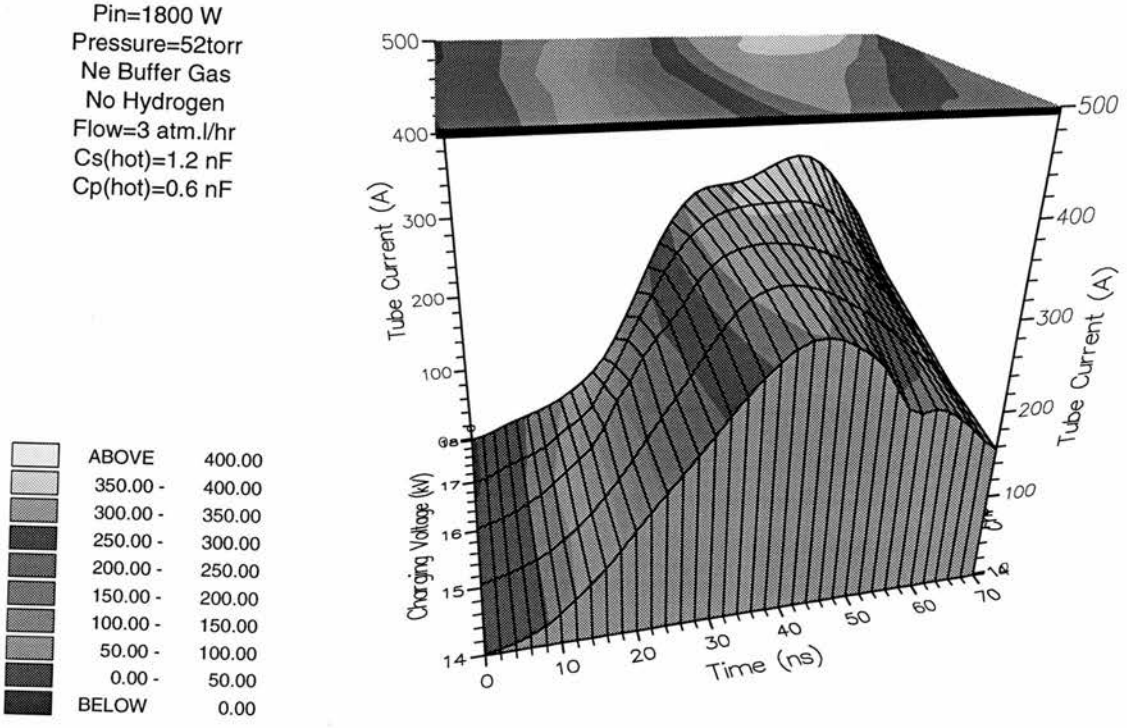

Tube current as a function of time and charging voltage with 3% added hydrogen.

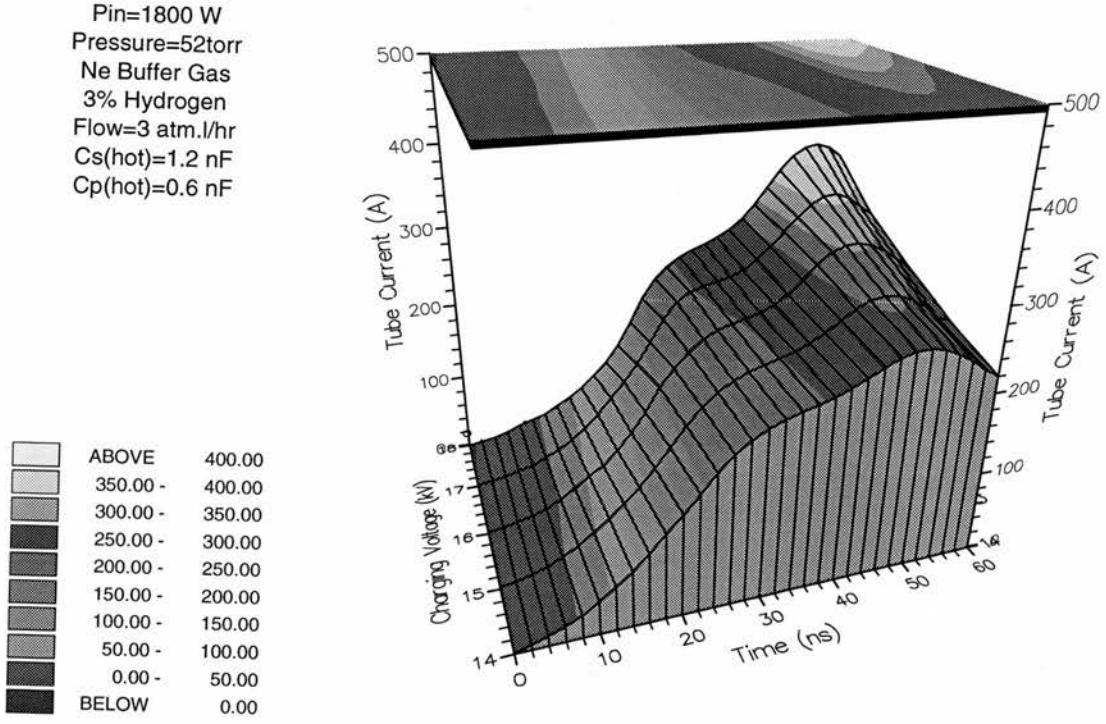

Figure 5.16b: Tube voltage as a function of time and charging voltage without added hydrogen.

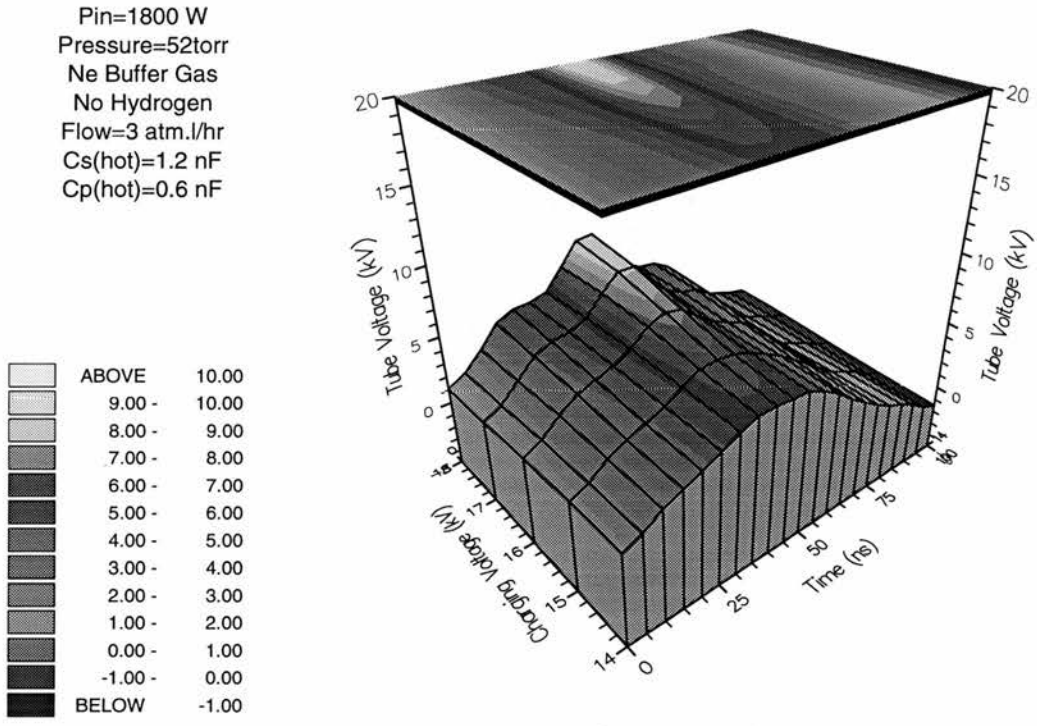

Tube voltage as a function of time and charging voltage with 3% added hydrogen.

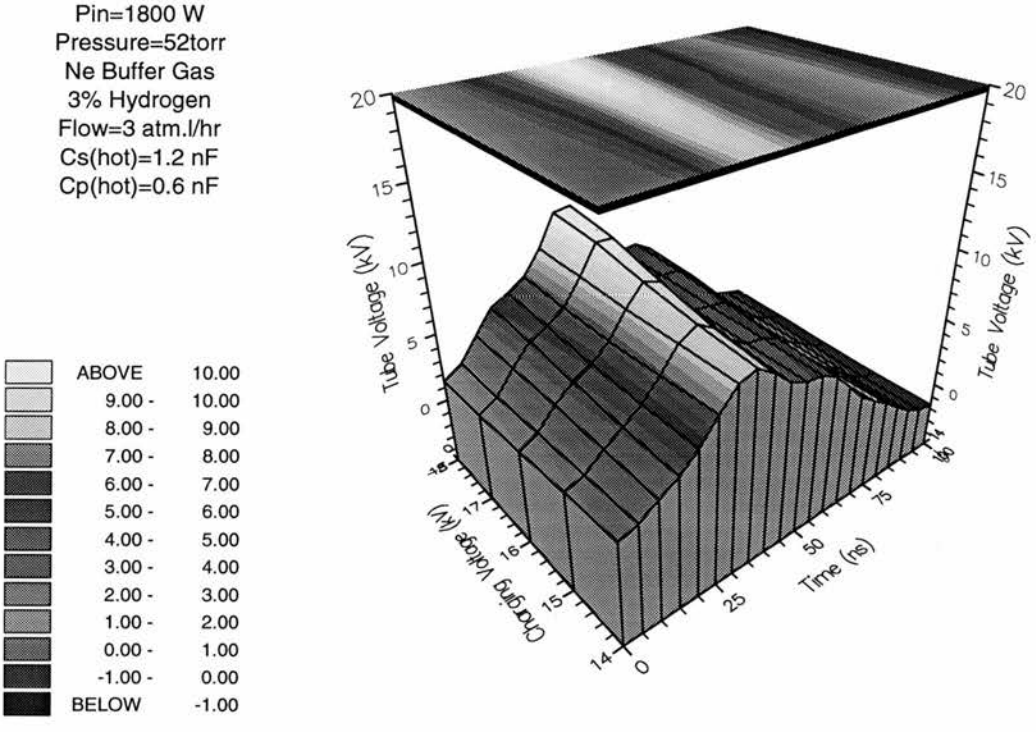

impedance. In each case, the addition of H_2 caused this step to occur earlier.

The relative position of the step under various conditions both with and without added H_2 can be explained in terms of the preionisation density of the laser tube [4]. As the capacitance was increased from 1.2 to 2.4 nF, the PRF had to be correspondingly decreased from 11.5 to 6 kHz whilst maintaining a constant charging voltage. This considerably increased the interpulse period, which enabled more efficient electron cooling and hence faster and more complete electron-ion recombination. Similarly, for the results taken at a constant input power, as the charging voltage was increased (and the corresponding PRF was decreased), the degree of electron cooling in the longer interpulse period increased. In each case, the addition of H_2 further reduced the preionisation density by increasing the degree of electron cooling, and hence recombination, leading to an increased tube impedance [3].

5.5 Specific Wavelength Transitions

There is a number of transitions which occur only when a helium buffer gas is used. Collisional coupling between resonance levels induced by the buffer gas is a likely reason for this [5]. In this section, H_2 was added to a neon buffer gas in order to determine whether or not H_2, when added to a neon buffer gas, could induce laser transitions which normally only take place using a helium buffer gas.

Specific wavelengths were selected using a monochromator (Jobin-Yvon) with the laser pulses being measured using a HgCdTe detector, as discussed in Section 3.6. The monochromator was carefully aligned using a He-Ne laser such that the laser beam was incident perpendicular to the entrance/exit slits. In this way it was ensured that the wavelength gauge and the transmission characteristics of the monochromator correlated well with the calibrated dial. A calcium fluoride lens was used to focus the output from the laser onto the entrance slits in order to increase the laser intensity and hence raise the signal-to-noise ratio of the detector. Because the monochromator used a diffraction grating, care was taken to identify correctly those wavelengths which had undergone multiple orders of diffraction. Although there was a large number of orders when the monochromator was

scanned from 1-9 μm, particularly for the 1.13 μm and 1.50 μm transitions, they enabled the wavelength transmission dial to be well calibrated over the complete scale range of the monochromator. Two sets of discharge conditions were selected, (a) the maximum power conditions without added H_2 and (b) the maximum power conditions with 3% added H_2. The wavelengths which contributed to the total laser power for the various conditions selected were identified as 1.13, 1.50, 2.16, 2.92, 4.67, 4.72, 5.89 and 6.45 μm. With the exception of the 6.45 μm transition (experimentally determined to be 6.46±0.01 μm), all could be identified from the energy level diagrams shown in Figures 1.1a and 1.1b. There is only one other report of laser oscillation at 6.45 μm [6]; the investigators were also unable to identify the particular transition. It is interesting to note that laser oscillation does occur at 6.45 μm using strontium and that one of the major impurities contained within barium metal is strontium, which may contribute to between 1-3% of the total mass of barium metal. In general, the addition of H_2 increased the laser power for all the laser transitions observed. Under these discharge conditions, no laser transitions were observed when H_2 was added to the laser which could not be obtained using only neon.

5.6 Temporal Energy Deposition

The temporal evolution of the energy deposition was evaluated as a function of charging voltage at the input powers of 1.2, 1.5 and 1.8 kW, both with and without 3% added H_2. This was used to evaluate the power delivered to the laser tube from the charging circuit by multiplying the energy deposited with the PRF. The analysis used for this is discussed in detail in Sections 3.8 and 3.9. Figures 5.17a,b,c show how (a) the total power delivered into the laser, (b) the power delivered over the duration of the 1.50 μm laser transition and (c) the power delivered before the 1.50 μm transition varied with charging voltage, for constant input powers of 1.2, 1.5 and 1.8 kW (based on stored energy) without and with 3% added H_2. Under all conditions, the total power delivered to the discharge increased with the addition of H_2 to the laser (shown in Figure 5.17a). The increase was particularly large at a charging voltage of 14 kV, when the interpulse period was short and hence the discharge impedance low. This was presumably caused by a high

preionisation density, which was reduced when H_2 was added because of the increased electron collision frequency [3] (see Section 1.3.5).

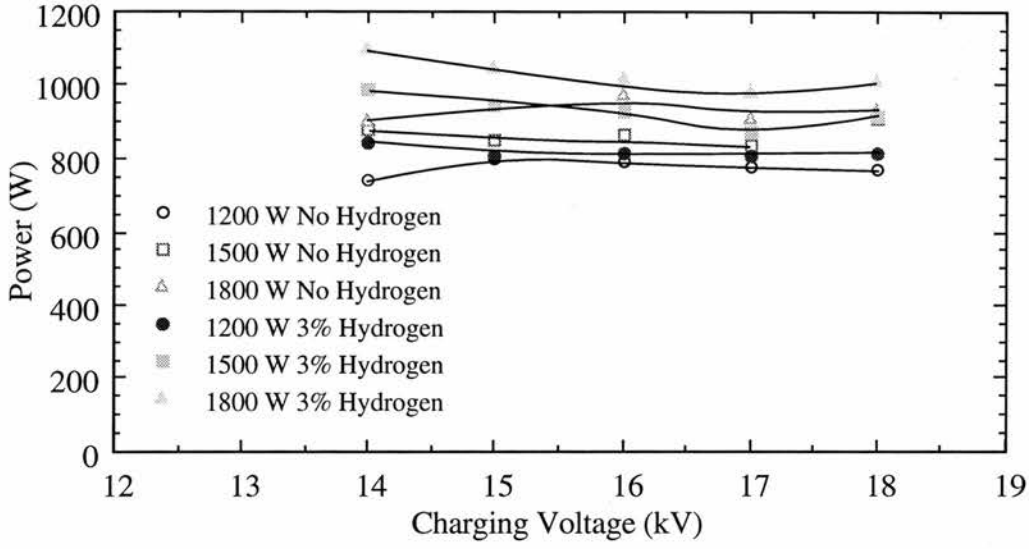

Figure 5.17a: Total power delivered to the laser tube as a function of charging voltage, at various input powers (based on stored energy), with and without 3% added hydrogen.

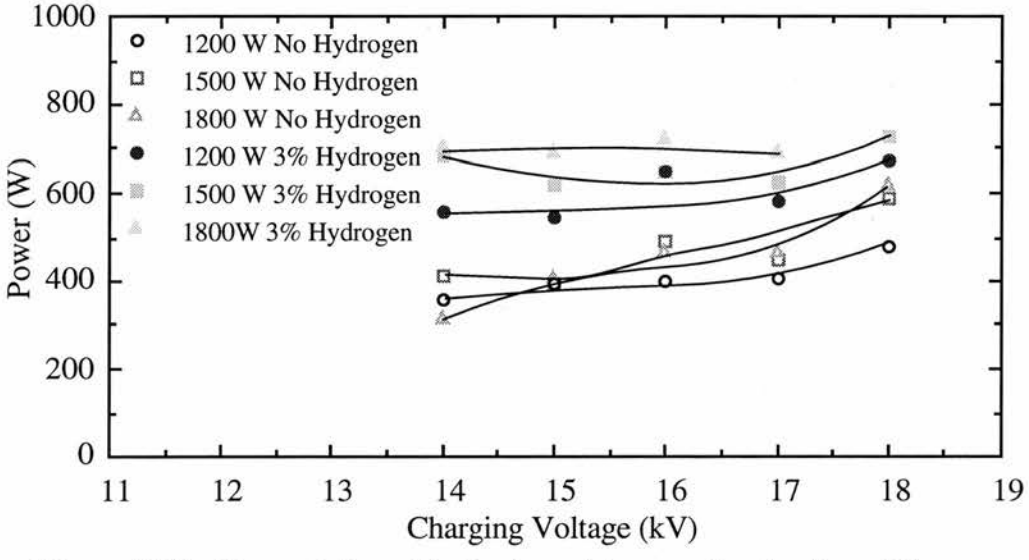

Figure 5.17b: Power delivered to the laser tube over the duration of the 1.50 μm laser pulse as a function of charging voltage, at various input powers (based on stored energy) with and without 3% added hydrogen.

The increase in the power delivered to the discharge with H_2 addition was not found to be uniform over the duration of the excitation pulse. This is shown in Figure 5.17b and 5.17c. Here the increase in power delivered was principally over the duration of the 1.50 μm laser pulse. Indeed, the power delivered before the onset of the 1.50 μm laser pulse decreased by over 30% with H_2 addition. Although increasing the

tube voltage (and decreasing the PRF) did not significantly change the total power delivered to the tube, increasing the voltage did cause the power deposition to decrease before the onset of laser oscillation at 1.50 μm, and to increase over the duration of the laser pulse (as shown). This could be caused by a reduction in the conductivity, which in turn would cause the breakdown potential of the laser tube to increase (see Section 5.4 and 1.3.5). The effect would be enhanced with H_2 addition because of the increased tube impedance.

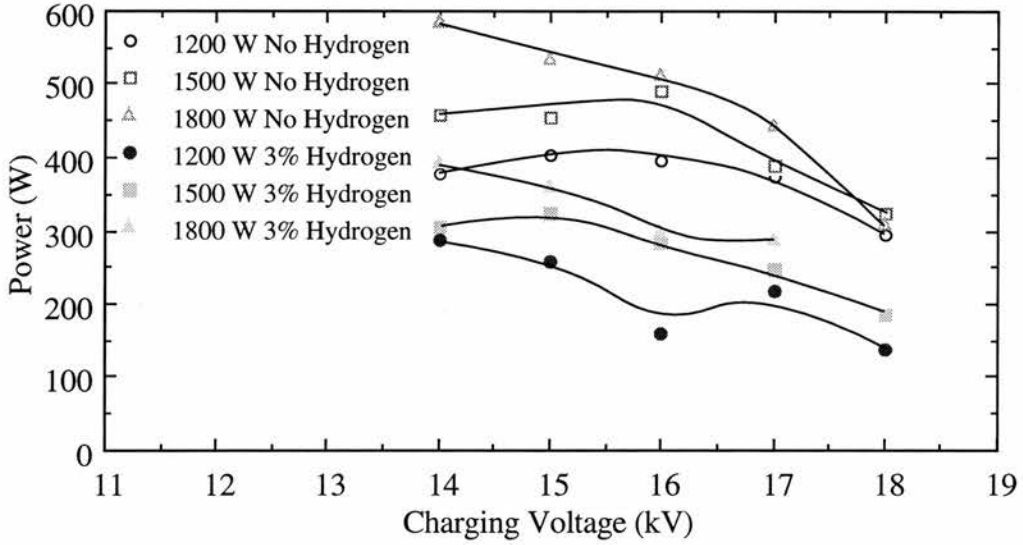

Figure 5.17c: Power delivered to the laser tube before the onset of the 1.50 μm laser pulse as a function of charging voltage, at various input powers, with and without 3% added hydrogen.

5.7 Summary

In this chapter a detailed comparison was made between the conditions which favoured laser oscillation at 1.13 μm and 1.50 μm using a neon buffer-gas without any additives and the conditions which favoured laser oscillation at 1.13 μm and 1.50 μm using a neon buffer-gas with 3% added H_2.

There was found to be an optimum input power (based on stored energy) for both the 1.13 μm and 1.50 μm laser transitions of approximately 1700 W and 2100 W respectively using a neon buffer-gas only. The addition of H_2 to the buffer-gas caused the optimum input power for these transitions to decrease by approximately 200 W for both the 1.13 μm and 1.50 μm laser transitions. An analysis of the tube current and tube voltage waveforms suggested that this was caused by an increase in the actual power delivered to the laser tube with the addition of H_2 for a given voltage.

For a given storage capacitance value, the laser power at 1.13 μm and 1.50 μm was found to be less dependent on the PRF when 3% H_2 was present in the buffer-gas than when only neon was used provided that the input power was maintained at that for maximum laser power. In addition, the optimum storage capacitance was significantly lower and consequently the optimum PRF was much higher when H_2 was present in the discharge tube. Indeed, laser oscillation at 1.50 μm has been achieved at PRFs when, in the absence of H_2, laser oscillation could not be supported. Previous studies of BVLs suggest that the upper limit to the PRF may be caused by either a high metastable population [7], or a high remanent free electron density in the interpulse period [8]. It remains unclear what the limiting factor is in this case, since the effect of H_2 is to enhance electron cooling in the interpulse period which can cause a reduction in the metastable population and a reduction in the prepulse free electron density (see Section 1.3.5).

5.8 References

[1] H. M. Pask, J. A. Piper, J Appl. Phys **72** (12) pp 5545-5554 (1992).

[2] A. A. Isaev, G. Yu. Lemmerman, S. V. Markova, G. G. Petrash, Sov. J. Quantum Electron. **9** (9) pp 1144-1147 (1979).

[3] M. J. Withford, D. J. W. Brown, J. A. Piper, Opt. Comm. **110** pp 699-707 (1994).

[4] G. Hogan, PhD Thesis, Oxford University (1993).

[5] H. M. Pask, J. A. Piper, IEEE J. Quantum Electron. **29** (9) pp 2540-2546 (1993).

[6] Ph. Cahuzac, Phys. Lett. **32A** (3) (1970) pp 150-151.

[7] V. V. Kazakov, S. V. Markova, G. G. Petrash, Sov. J. Quantum Electron. **14** (5) pp 642-646 (1984).

[8] P. A. Bokan, Sov. J. Quantum Electron. **16** (8) pp 1041-1046 (1986).

Chapter 6

Helium Buffer Gas

6.1 Introduction

Though not essential for laser oscillation, the buffer gas in pulsed cyclic metal vapour lasers has several important roles. It raises the tube impedance, thereby increasing the energy transfer efficiency from the charging circuit to the discharge loop. The buffer gas also indirectly aids in reducing the metastable population in the interpulse period. This is brought about by elastic collisions between electrons and the buffer gas atoms in the interpulse period, which reduce the electron energy during that time; the cooler electrons enhance the rate of deactivation of metastable levels by superelastic electron collisions. Finally, the buffer gas helps to increase the lifetime of each load of metal, by reducing the diffusion of metal vapour to the cold regions, ie outside the active region and onto the windows.

In Chapters 4 and 5, the results are concerned mainly with the addition of H_2, D_2 and He additives to a neon buffer gas. In this chapter, a complete characterisation is presented of the laser power, laser pulse intensities, tube current and tube voltage waveforms, using a helium buffer gas. The charging voltage, PRF, buffer gas pressure and storage capacitance have all been varied. Experiments have also been undertaken to measure effects of H_2 and D_2 addition under otherwise optimum conditions for maximum laser power using a helium buffer gas. The results for this are discussed with reference to

the similar investigation undertaken using only a neon buffer gas which is discussed in detail in Chapter 4.

6.2 Helium Pressure Dependence

6.2.1 Laser Power

Laser power measurements were taken at regular (1 kV) increments of the charging voltage, ranging typically between 12 kV and 18 kV. The PRF was decreased for each increase in the charging voltage, such that a constant input power (based on stored energy) was maintained. In each case, the input power was calculated using hot capacitance values, which were assumed to be constant over all the charging voltages and input powers used. The dependence of laser power on charging voltage was determined at first using low input powers. The input power was incremented (by raising the PRF) once measurements for a complete range of charging voltages had been measured and the process of measuring the laser power on charging voltage (whilst maintaining a fixed input power) was repeated. This was continued until results had been obtained for a range of input powers. Using this method for investigating the trends in laser power (ie measuring the dependence of laser power on charging voltage whilst maintaining a constant input power, instead of increasing the charging voltage for fixed PRF) greatly increased the rate at which measurements could be taken. This was primarily because, for each set of charging voltage measurements, the tube wall temperature remained approximately constant, so less time was required for the temperature of the discharge tube to restabilise when the discharge conditions were changed. In addition, the lifetime for each barium load was found to be increased, because of the reduced temperature cycling of the laser tube. Typical input powers (based on stored energy) ranged from 1.2 kW to 2.6 kW.

Figures 6.1, 6.2 and 6.3 show how the total laser power, the laser power at 1.13 μm and the laser power at 1.50 μm, respectively, varied with charging voltage and input power (based on stored energy), for helium buffer-gas pressures of (a) 20, (b) 38, (c) 52 and (d) 70 torr. For all the charging voltages and buffer gas pressures selected, laser oscillation only began once the input power reached a threshold, between

Figure 6.1a: Total laser power as a function of charging voltage and input power at a pressure of 20 torr.

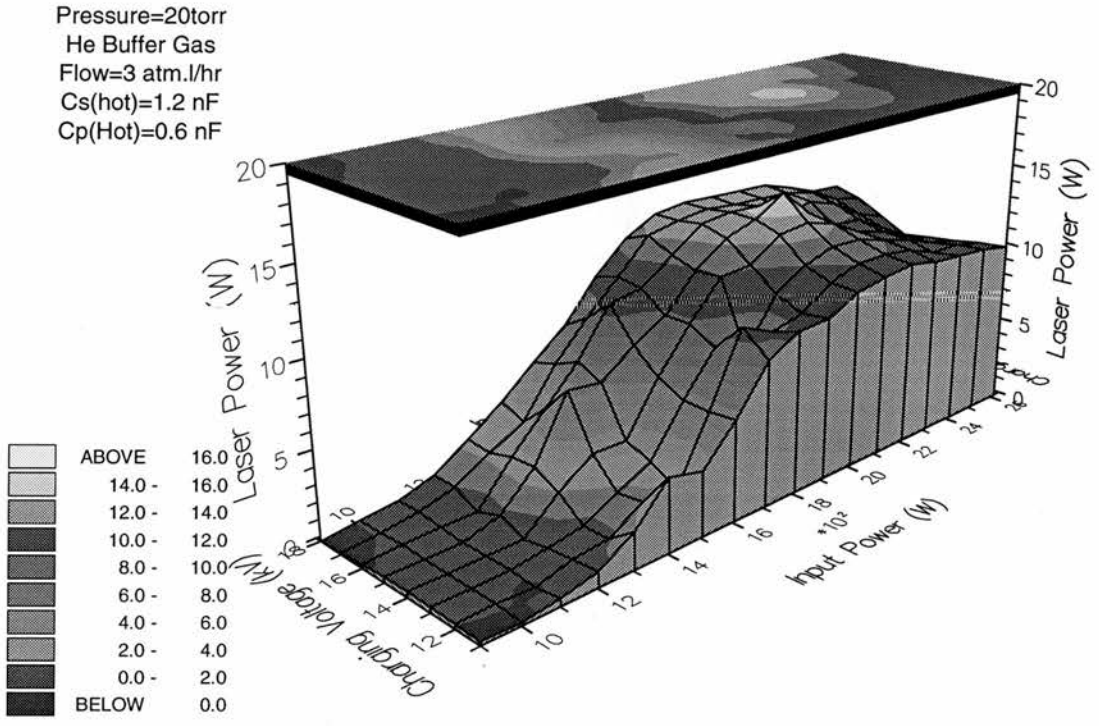

Figure 6.1b: Total laser power as a function of charging voltage and input power at a pressure of 38 torr.

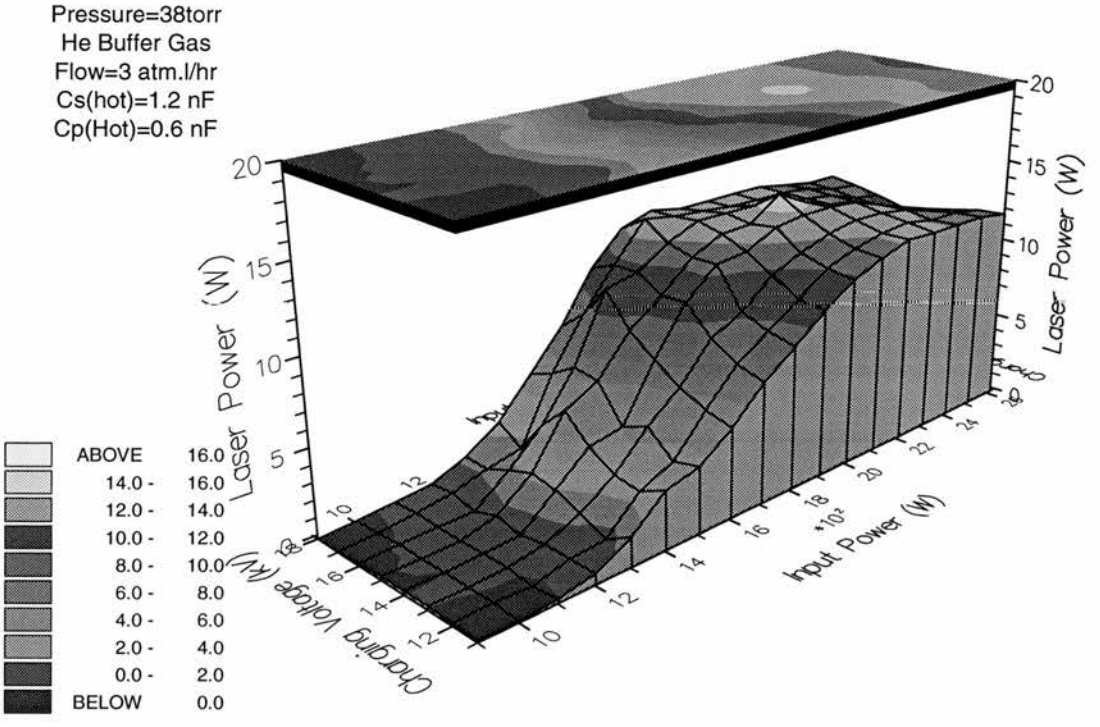

Figure 6.1c: Total laser power as a function of charging voltage and input power at a pressure of 52 torr.

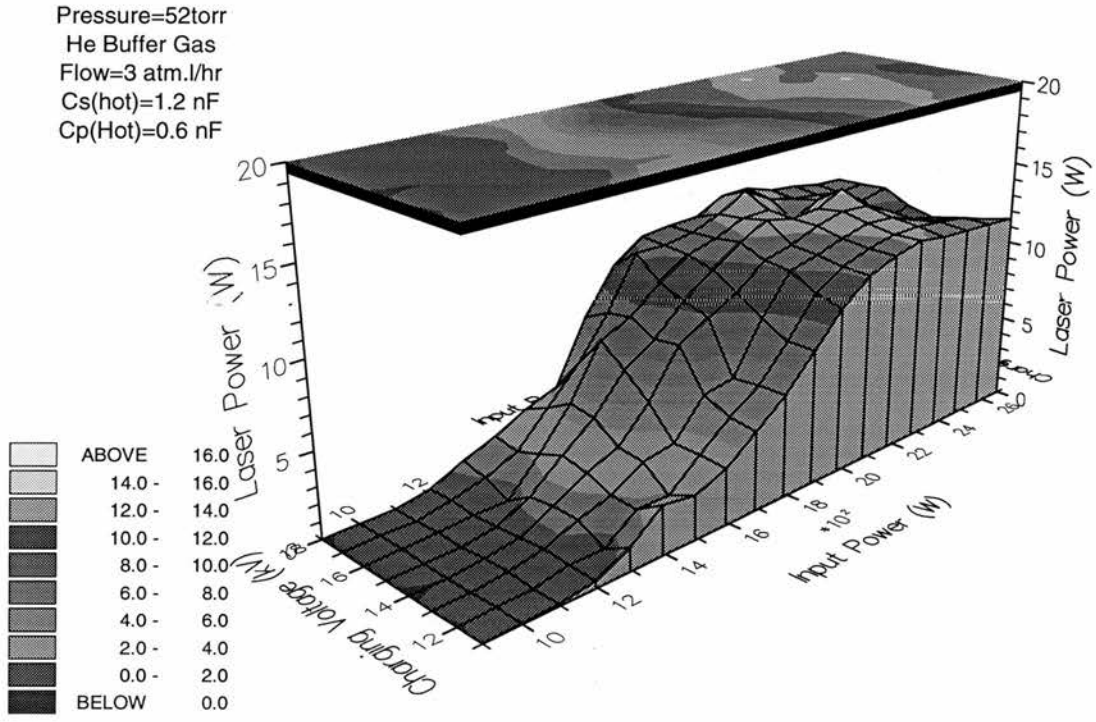

Figure 6.1d: Total laser power as a function of charging voltage and input power at a pressure of 70 torr.

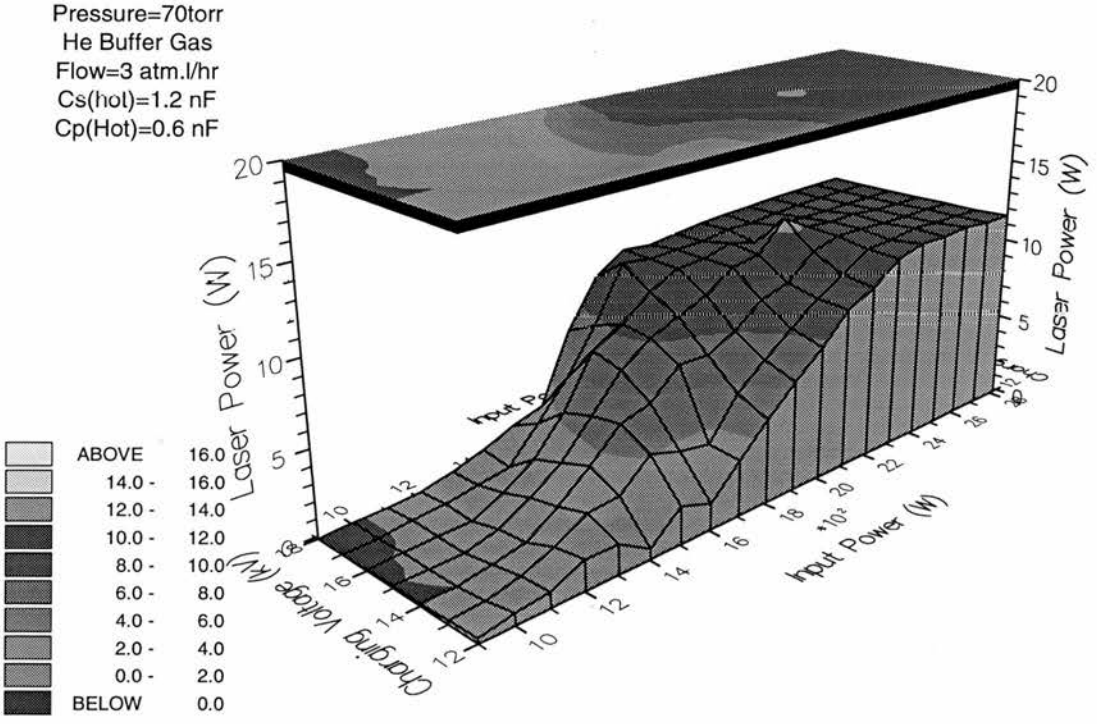

1.2 kW and 1.3 kW. This probably reflected the minimum barium vapour density required for radiation trapping to occur. The total laser power reached a broad peak for an input power of 2.0 kW to 2.1 kW and a charging voltage of approximately 15 kV. Although the total laser power was comparable to that obtained when a premix of neon and 3% H_2 was used as the buffer gas (giving an average laser output power of 12.7 W with 20 torr of helium), the overall laser efficiency was substantially lower at 0.65% (based on stored energy) compared to 1.0% using neon with 3% added H_2 (see Section 5.2.3). The transitions which contributed to the majority of the total laser power using a helium buffer gas also came from the 1.13 μm and 1.50 μm transitions, giving average powers of 4.0 W and 7.5 W respectively. The discharge conditions for maximum total laser power were a compromise between the optimum conditions for maximum laser power at 1.13 μm and those at 1.50 μm. The pressure which gave the maximum laser power was substantially lower using a neon buffer gas rather than helium. This was also found to be the case with other studies of BVLs [1].

As in Section 5.2.3 when a neon buffer gas was used, the discharge conditions under which the 1.13 μm and 1.50 μm transitions individually optimised when using a helium buffer gas were also found to be very different. The input power corresponding to the maximum laser power at 1.13 μm (1.8 kW) was much lower than the input power which gave maximum laser power at 1.50 μm (2.4 kW). The laser power at 1.13 μm was found to be particularly sensitive to both the input power and the charging voltage. The optimum charging voltages were also found to differ, with maximum laser power at 1.13 μm being obtained at high charging voltages (and consequently at lower PRFs), typically between 16 kV and 18 kV, and laser power at 1.50 μm being obtained at lower charging voltages (and higher PRFs), typically between 12 kV and 14 kV.

The effect of competition between the two transitions increased as the charging voltage was increased (and the corresponding PRF decreased). This was reflected in the laser pulse waveforms: there was a reduction in the 1.50 μm transition pulse intensity at the onset of laser oscillation of the 1.13 μm transition, which became more pronounced as the charging voltage was increased (discussed further in Section 6.2.2). In Chapter 4, the

Figure 6.2a: Laser power at 1.50 μm as a function of charging voltage and input power at a pressure of 20 torr.

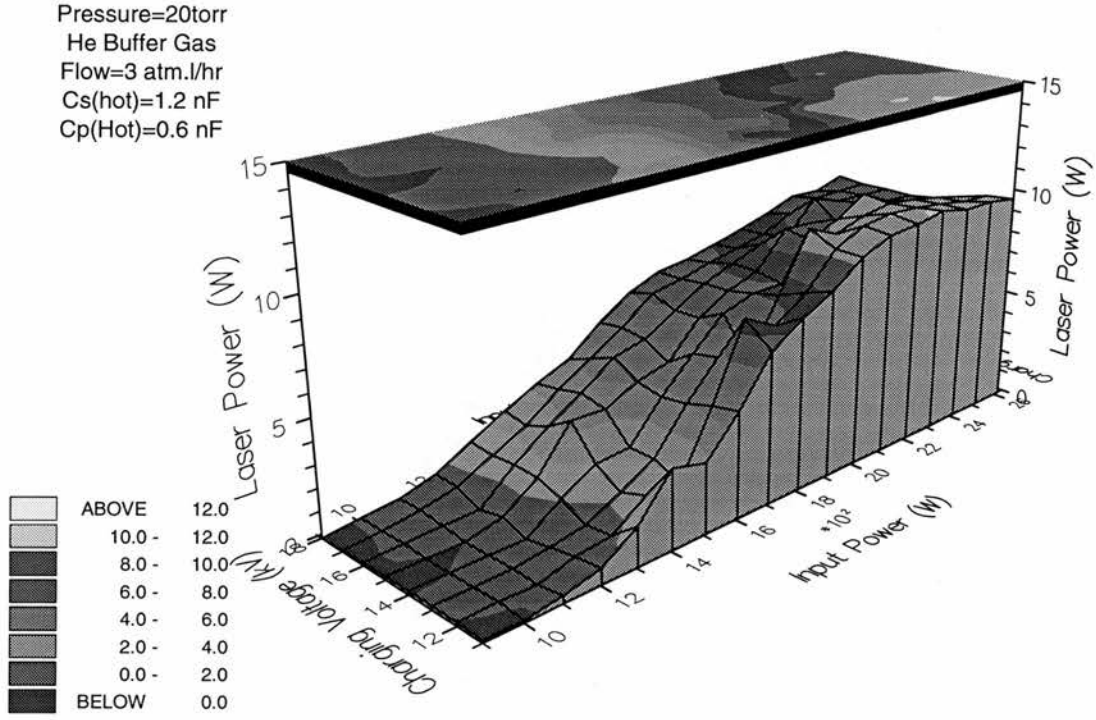

Figure 6.2b: Laser power at 1.50 μm as a function of charging voltage and input power at a pressure of 38 torr.

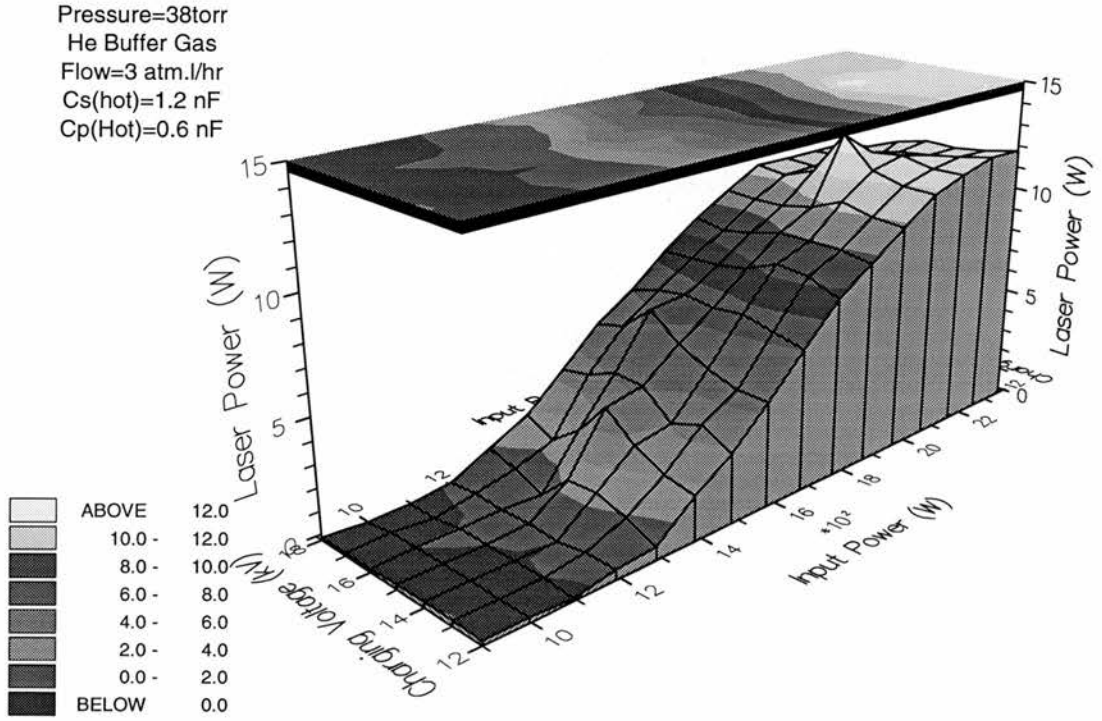

Figure 6.2c: Laser power at 1.50 μm as a function of charging voltage and input power at a pressure of 52 torr.

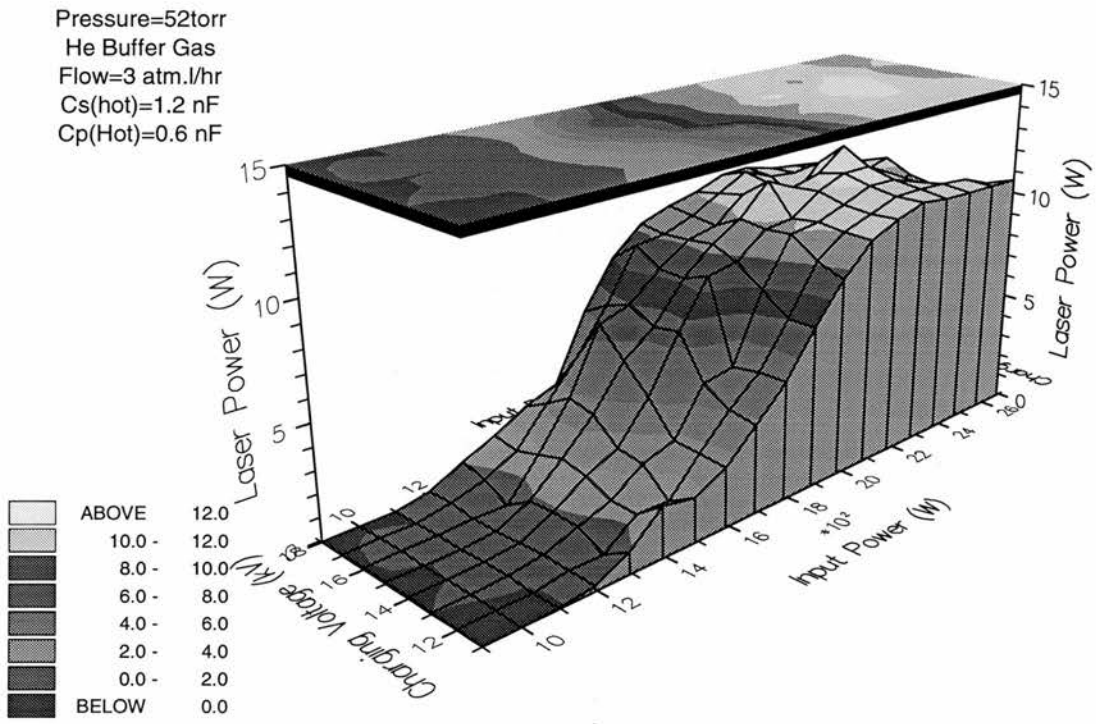

Figure 6.2d: Laser power at 1.50 μm as a function of charging voltage and input power at a pressure of 70 torr.

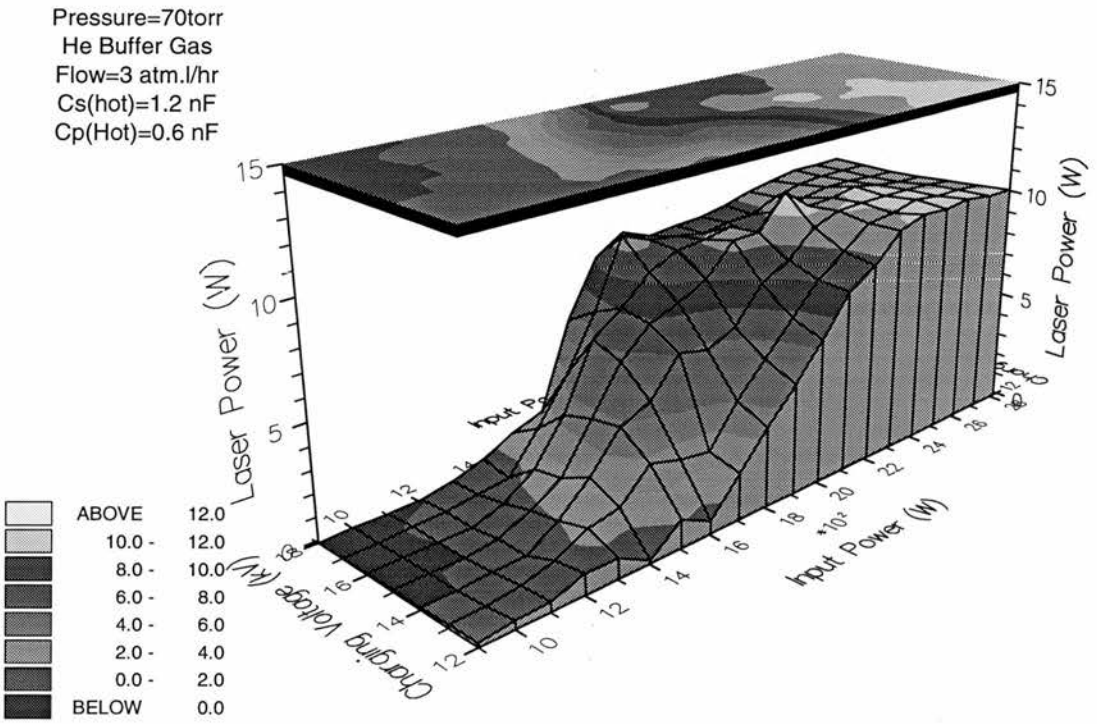

increase in the competition between the two transitions was associated with enhanced electron cooling in the interpulse period, which aided both metastable depopulation and electron-ion recombination. The latter is unlikely to explain the observed trends, since the step in the tube current waveform and hence the preionisation density appeared to remain unchanged under these conditions, despite the large variations in both the charging voltage and PRF (see Section 6.2.3). This suggests that the increase in the laser power at 1.13 μm was a result of a decrease in the population of the metastable lower laser level.

Increasing the PRF (and hence the input power) above the optimum conditions for laser oscillation at 1.13 μm tended to cause the laser power at 1.13 μm to decrease and the laser power at 1.50 μm to increase. Because the 1.13 μm and 1.50 μm transitions share a common upper level, any increase in upper level excitation should enhance both transitions equally. It was for this reason that the observed changes in laser power could only be explained in terms of the metastable lower laser level populations. As outlined in Section (1.3.5), a high metastable level population could be caused by either inefficient electron deactivation in the interpulse period or by a thermal population of the level caused by a high gas temperature. If the observed decrease in laser power at 1.13 μm was caused by inefficient electron cooling then, for a given charging voltage, the optimum input power for the 1.13 μm transition should be higher when using helium as the buffer gas instead of neon. This is because helium has a much larger electron collision cross section for momentum transfer than neon. Electron cooling (and hence metastable deactivation and electron ion recombination) is therefore greater with helium as the buffer gas rather than with neon. However, the optimum input powers for helium and neon were found to be the same, so it was concluded that, under these conditions, the upper limit to the 1.13 μm transition was limited by the thermal population of the metastable level rather than rate of deactivation of the metastables.

The optimum gas pressures for maximum total laser power, laser power at 1.13 μm and laser power at 1.50 μm were also found to be different. The laser power at 1.13 μm decreased when the pressure was increased above 20 torr, whilst the laser power at 1.50 μm first increased with increasing buffer gas pressure (up to between 38 torr and

Figure 6.3a: Laser power at 1.13 μm as a function of charging voltage and input power at a pressure of 20 torr.

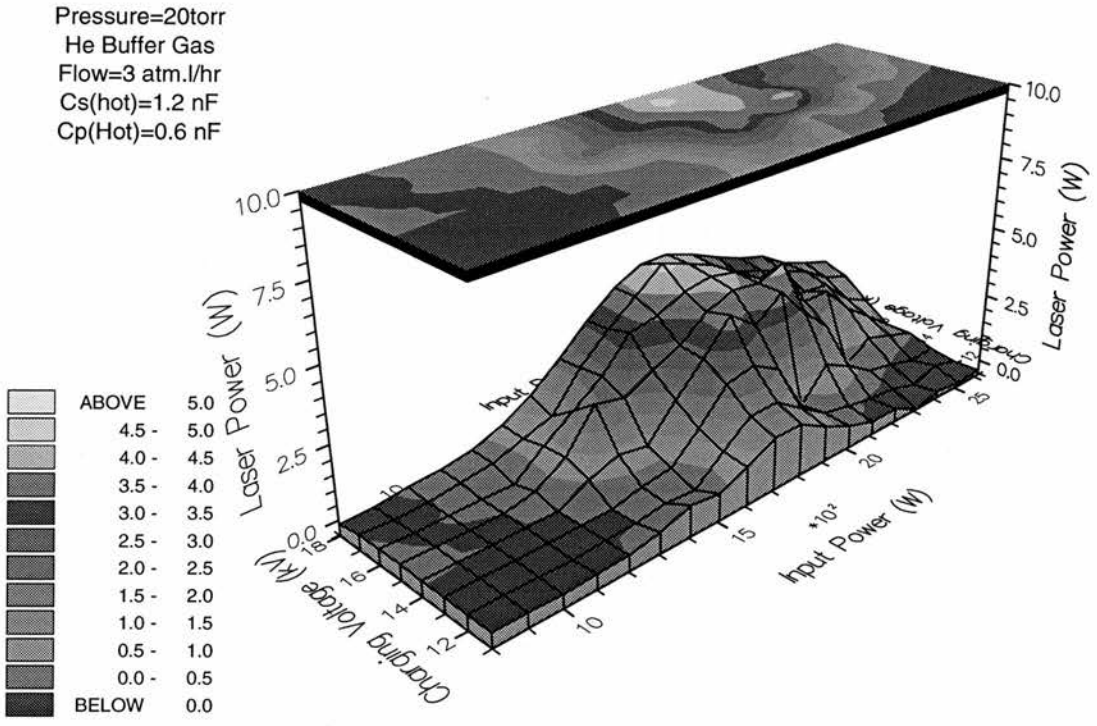

Figure 6.3b: Laser power at 1.13 μm as a function of charging voltage and input power at a pressure of 38 torr.

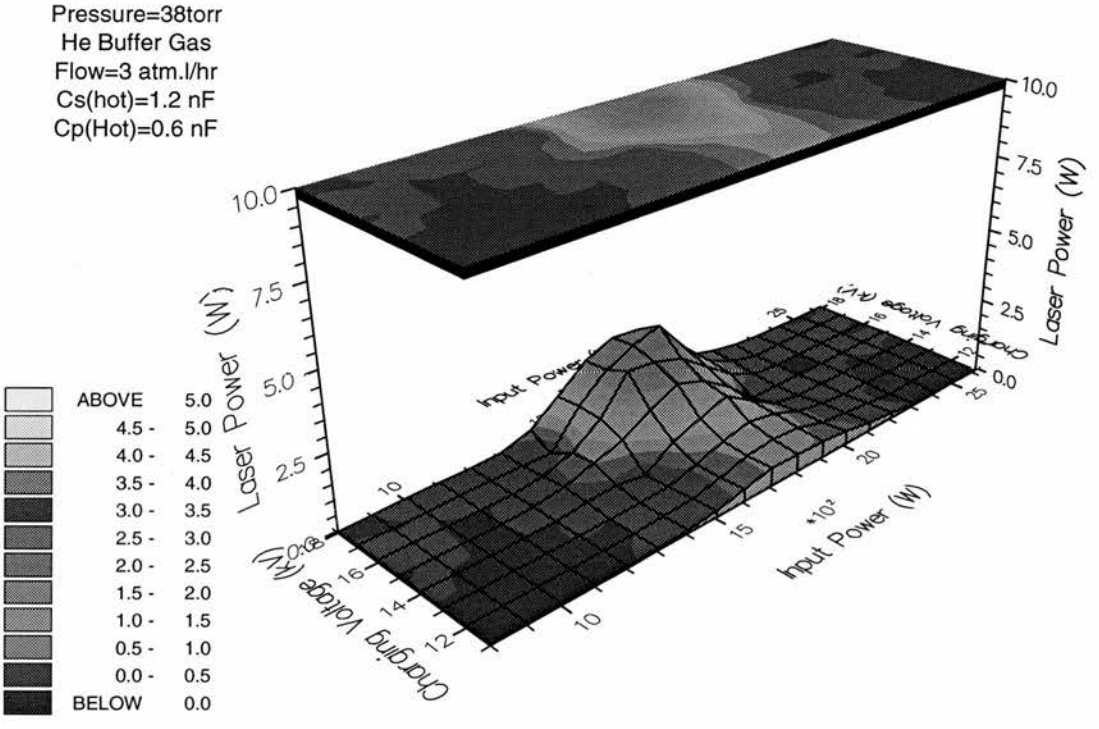

Figure 6.3c: Laser power at 1.13 μm as a function of charging voltage and input power at a pressure of 52 torr.

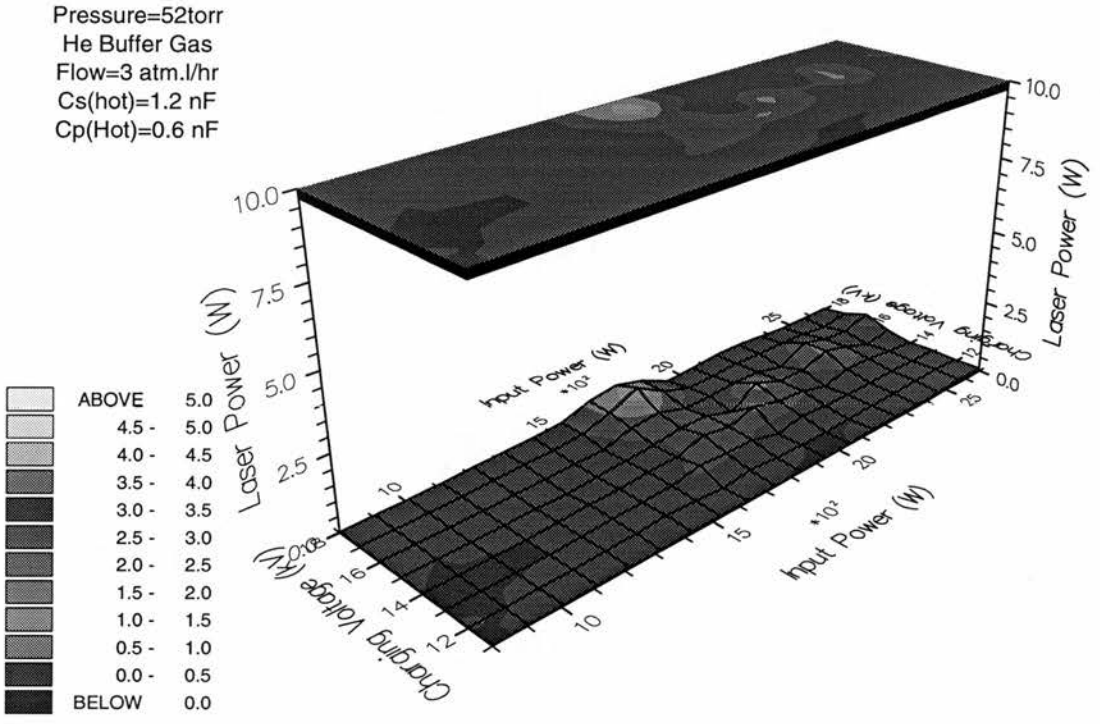

52 torr), but then decreased as the pressure was increased further (above 52 torr). Problems were encountered at low helium pressures with both discharge stability and the lifetime of each barium load. The latter was the chief reason why measurements for the laser power were not taken for helium pressures below 20 torr.

When a low pressure of neon buffer gas was used (see Section 5.2.1), the laser power was believed to be inhibited by either poor lower laser level depopulation, or inefficient electron-ion recombination, caused by the low collision frequency for momentum transfer. The effect of the addition of H_2 on the laser power was found to be most pronounced at these low neon pressures, primarily because of the increased electron collision frequency for momentum transfer. This was believed to result in both a reduction in the metastable population and also in the prepulse free electron density. The latter enhanced the E/N (electric field to number density) ratio, leading to enhanced upper level excitation. The electron collision cross section for momentum transfer is much higher for helium than for neon [2], hence the optimum pressure is likely to be lower using helium rather than neon as the buffer gas. The output power will be higher with a helium buffer gas because of the higher E/N that can be attained in the presence of good (adequate) electron cooling.

The observed decrease in the laser power at 1.13 μm with increasing buffer gas pressure could not be explained solely in terms of a reduction in the upper level excitation caused by a decrease in the E/N ratio. This is because the laser power at 1.50 μm initially increased with increasing pressure. As discussed previously, because of the shared upper level, any decrease to the upper level excitation should reduce the laser power at both 1.13 μm and 1.50 μm equally. For this reason, the observed decrease in the laser power at 1.13 μm and the increase at 1.50 μm could be only be caused by a lower laser level effect, and a direct result of the competition which exists between the two transitions. Increasing the helium pressure from 20 torr to 38 torr increased the electron collision frequency and consequently increased the ability of the helium to cool the electrons effectively and hence reduced the metastable lower laser level population of the 1.50 μm transition. The decrease in the metastable population for the 1.50 μm transition lead to an

increase in laser oscillation at 1.50 μm which prevented a threshold inversion being established for the 1.13 μm transition becasuse of depletion of the upper laser level population. This appeared to have the effect of enhancing laser oscillation at 1.50 μm at the expense of laser oscillation at 1.13 μm which was also reflected in the laser pulse waveforms (discussed more fully in Section 6.2.2). At higher (~70 torr) buffer gas pressures, the laser power at both 1.13 μm and 1.50 μm decreased with increasing helium pressure. This is likely to be due to the reduction in the E/N ratio. A similar conclusion was drawn for the pressure dependence of laser power using a neon buffer gas, discussed in Section 5.2.1. For both the 1.13 and 1.50 μm transitions, the optimum pressure for maximum laser power was lower for helium than for neon (<20 torr and <52 torr for the 1.13 μm and 1.50 μm transitions respectively using helium and ~50 torr for both transitions using neon).

6.2.2 Temporal Evolution of Laser Pulse Waveforms

Figures 6.4a,b show how (a) the temporal evolution of the 1.13 μm and (b) the temporal evolution of the 1.50 μm laser pulse varied as functions of charging voltage for a constant input power of 1800 W (based on stored energy). The helium buffer gas was maintained at a constant pressure of 20 torr. The laser pulses were measured using the HgCdTe detector as described in Section 3.6, with specific laser transitions being measured using narrow bandpass filters (described in Section 3.6.1). All the laser pulse intensities shown and discussed in this section were measured on axis (ie at the beam centre).

The effect of increasing the charging voltage whilst maintaining a constant input power, was to cause the onset of both the 1.13 μm and 1.50 μm laser pulses to occur at earlier times with respect to the onset of the tube current, a trend also observed when only a neon buffer gas was used (discussed in Section 5.2.3). This could be due to a number of reasons which are outlined as follows. First, the axial field strength during the excitation pulse was greater for higher charging voltages (discussed in Section 6.2.3). This would result in an increase in the E/N (electric field to number density) ratio, thereby raising the

electron energy in the excitation pulse and hence the overall excitation to the upper laser level. In addition, the increase in pulse input energy with increasing charging voltage would also favour excitation to the upper laser level. This was indicated by a increased pulse width of both the 1.13 μm and 1.50 μm laser pulses with increasing charging voltage. Both would result in the threshold population inversion being established earlier in the excitation pulse. Second, a lower metastable population at the beginning of the excitation pulse would also explain the observed decrease in delay between the onset of the tube current and laser oscillation. As the charging voltage was increased, the corresponding PRF was decreased (in order to maintain a constant input power), which allowed a longer time for electron cooling in the interpulse period, and consequently enhanced deactivation of the metastable levels. A reduction in the population of the lower metastable laser level would also allow a threshold inversion to be established earlier in the excitation pulse.

As the charging voltage was increased, the mid-pulse minimum which occurred in the 1.50 μm transition pulse intensity became more pronounced. This minimum also corresponded to the onset of laser oscillation at 1.13 μm. Increasing the charging voltage increased the electric field and hence should increase the overall excitation to the upper laser level, and hence increase the laser power at both wavelengths. Figures 6.2 and 6.3 clearly show that this did not happen, despite the increase in the 1.50 μm pulse energy with increasing charging voltage (indicated by an increase in the area of the 1.50 μm laser pulse waveform). Instead, the laser power increased at 1.13 μm whilst the laser power at 1.50 μm remained approximately constant, ie, the 1.13 μm transition was enhanced instead of the 1.50 μm transition. Figure 6.4 shows how the delay between the onset of laser oscillation at 1.13 μm and 1.50 μm decreased with increasing charging voltage. This suggested that the threshold inversion was being established earlier at 1.13 μm relative to that at 1.50 μm. There are several possible explanations for this. One is that the input pulse energy increases with charging voltage. Another is that the decrease in the metastable population caused by the increase in the interpulse period may be more pronounced for the 1.13 μm metastable level than for that of the 1.50 μm transition, because of the relative energies of each with respect to the ground state.

Figure 6.4a: Temporal evolution of the 1.13 μm laser pulse as a function of charging voltage.

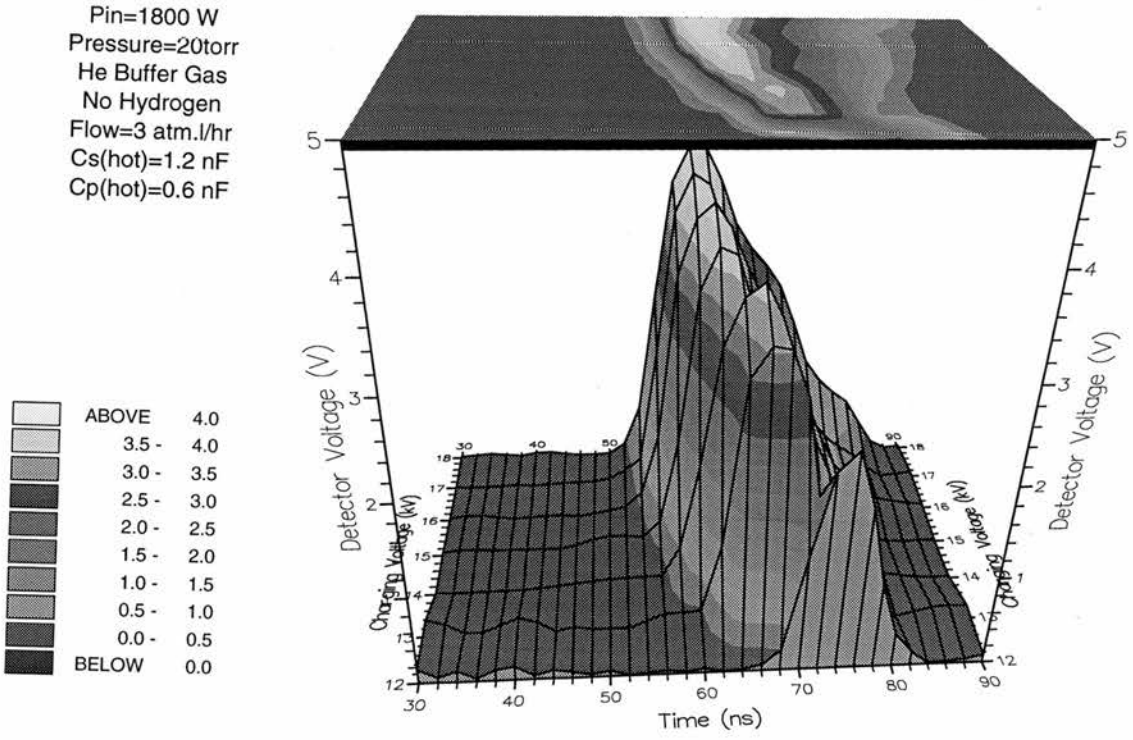

Figure 6.4b: Temporal evolution of the 1.50 μm laser pulse as a function of charging voltage.

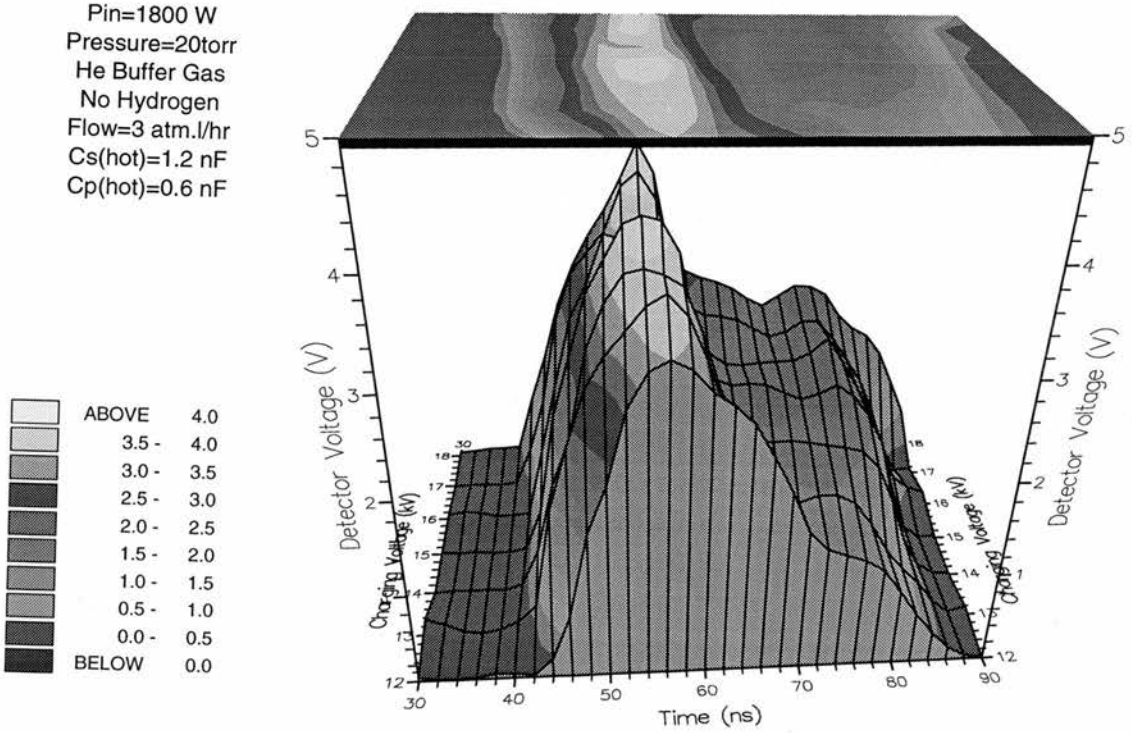

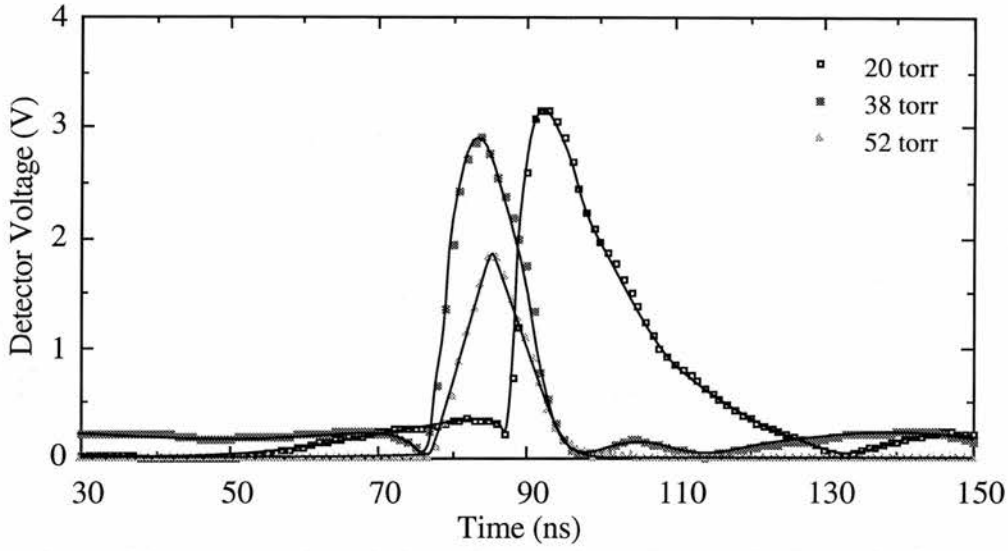

Figure 6.5a: Temporal evolution of the 1.13 μm laser pulse intensity for various helium buffer gas pressures for a constant input power of 1800 W.

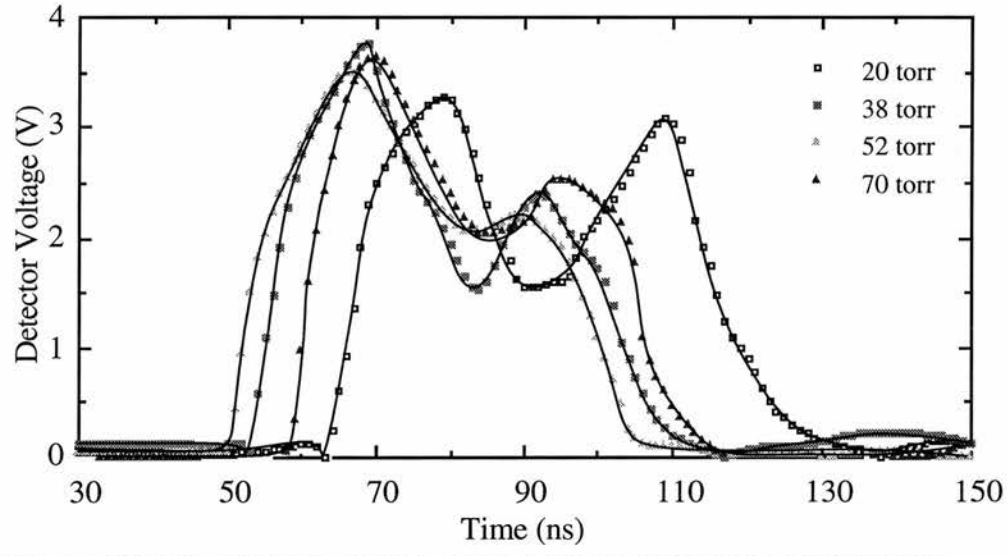

Figure 6.5b: Temporal evolution of the 1.50 μm laser pulse intensity for various helium buffer gas pressures for a constant input power of 1800 W.

Figures 6.5a,b show (a) the 1.13 μm and (b) the 1.50 μm laser pulse waveforms for helium buffer gas pressures of 20, 38, 52 and 70 torr. The charging voltage, PRF and storage capacitance were 17 kV, 10.2 kHz and 1.2 nF respectively, corresponding to an input power of 1.8 kW. As discussed above and shown in Figures 6.2 and 6.3, the laser power at 1.13 μm decreased with increasing pressure whilst the laser power at 1.50 μm increased for small pressure increments, peaked, then

decreased at higher pressures. Figures 6.4a and 6.4b show that the minimum in the 1.50 μm laser pulse intensity, which corresponded to the onset of laser oscillation at 1.13 μm, became less pronounced as the pressure was increased. In Section 4.4.2, this minimum was attributed to a build-up of the 1.50 μm metastable level. If this were the case then increasing the pressure would decrease the metastable population because of the increased electron/buffer-gas collision frequency. This would tend to make the mid-pulse minimum in the 1.50 μm pulse intensity less pronounced, which was indeed found to be the case.

6.2.3 Tube Current and Tube Voltage Waveforms

Figure 6.6 shows the tube current waveform for various charging voltages ranging from 12 kV to 18 kV, for a constant input power of 1800 W. The buffer gas used was helium at a pressure of 20 torr and the storage capacitance was 1.2 nF (hot value). A characteristic step was observed in the tube current waveform, which occurred in approximately the same place for all the charging voltages selected, even though the interpulse period was increased. In Chapters 4 and 5, the tube current, from the onset of the excitation pulse up to this characteristic step, was believed to be carried by free electrons which had remained from the previous pulse. The step was believed to correspond to the point at which secondary collisional ionisation processes accelerated within the tube, and hence how far up the current pulse the step was indicated the degree of preionisation within the laser tube [3]. Figure 6.6 suggests that, within the margin of error, the preionisation density did not decrease with increasing charging voltage (whilst maintaining a constant input power by reducing the PRF), as it appeared to when only neon was used as the buffer gas. However, in general the step did occur much earlier when helium was used than when neon was used as the buffer gas. For comparison, Figure 5.15a shows the tube current waveform using only a neon buffer gas, for a charging voltage, PRF, input power and pressure of 16 kV, 11.5 kHz, 1800 W and 52 torr respectively. Furthermore, the tube current waveforms obtained using helium were more comparable to a neon buffer gas with several percent of hydrogen or deuterium

additives present (discussed in Section 4.4.3). This suggested that helium was more effective at electron cooling than neon, resulting in more efficient electron-ion recombination and a lower electron density.

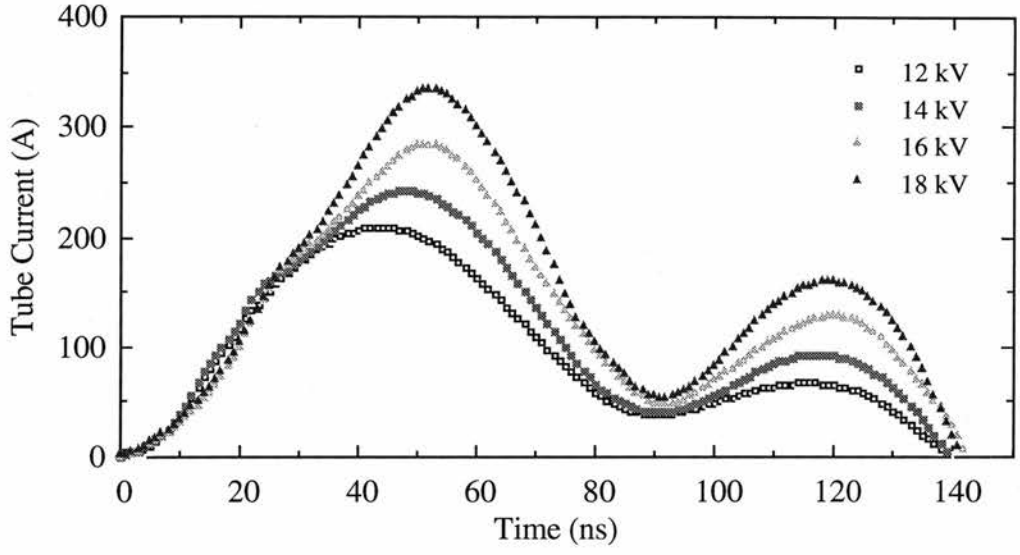

Figure 6.6: Tube current waveform for various charging voltages with a constant input power of 1.8 kW using a helium buffer gas.

According to Equation 3.15, a lower pressure would reduce the electron collision frequency and hence reduce the degree of electron-ion recombination. This would result in an increase in the preionisation density. However, the position of the step in the waveform occurred significantly earlier when helium was used instead of neon, despite the fact that the helium pressure was substantially lower. Figure 6.7 shows a graph of the 'tube breakdown potential' (defined as the tube voltage corresponding to the step in the tube current waveform) as a function of charging voltage for a constant input power of 1.8 kW using 52 torr neon and 20 torr helium. Larger 'tube breakdown potentials' were obtained when helium was used instead of neon. This reflected the greater ability of helium atoms to undergo elastic collisions with electrons, resulting in faster electron cooling, and thus enhanced electron-ion recombination, and increased laser tube impedance. The larger axial electric field strengths, and the reduced number densities obtained using helium instead of neon, are both likely reasons for the much larger average laser output powers obtained.

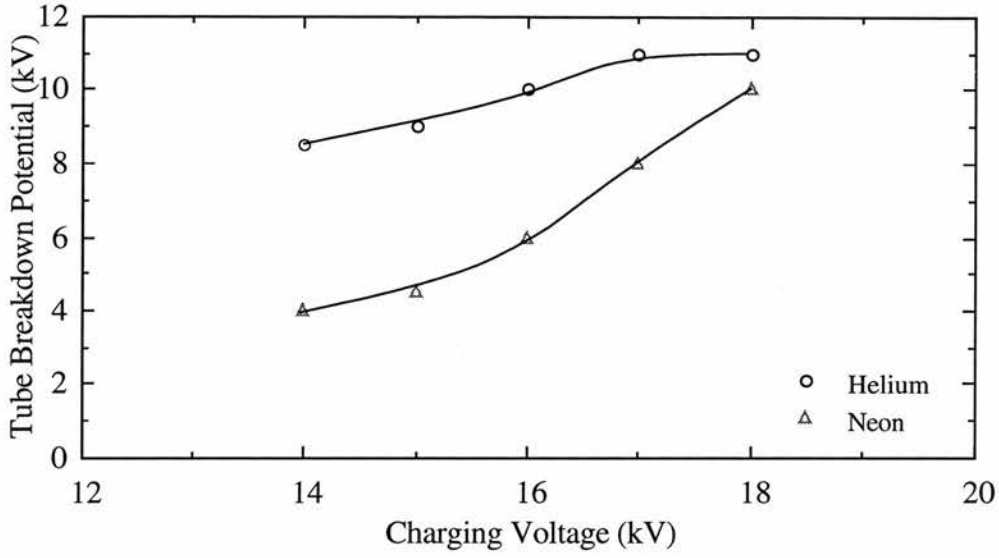

Figure 6.7: 'Tube breakdown potential' as a function of charging voltage using helium and neon buffer gases for a constant input power of 1.8 kW.

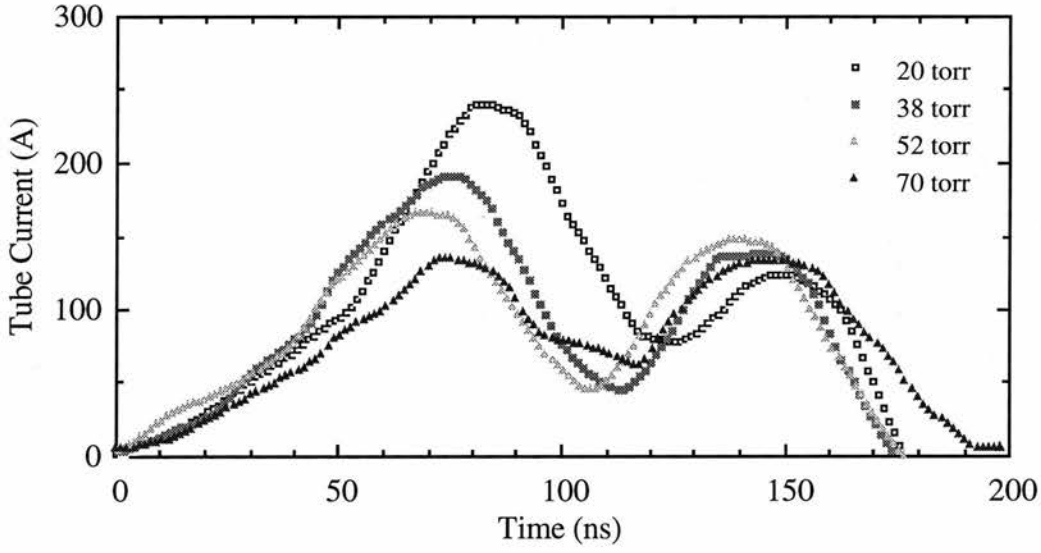

Figure 6.8a: Tube current waveform for a constant input power of 1.8 kW for various helium buffer gas pressures.

Figures 6.8a and 6.8b show the tube current and the tube voltage waveforms respectively for helium pressures of 20, 38 and 52 torr. In each case, the charging voltage, PRF and input power were 17 kV, 10.2 kHz and 1800 W respectively. The effect of increasing the pressure was to increase the 'tube breakdown potential' (as defined above) and to decrease the step in the tube current waveform. These trends were as expected, since

an increase in the pressure would increase the electron collision frequency, resulting in increased electron-ion recombination because of the increased electron cooling.

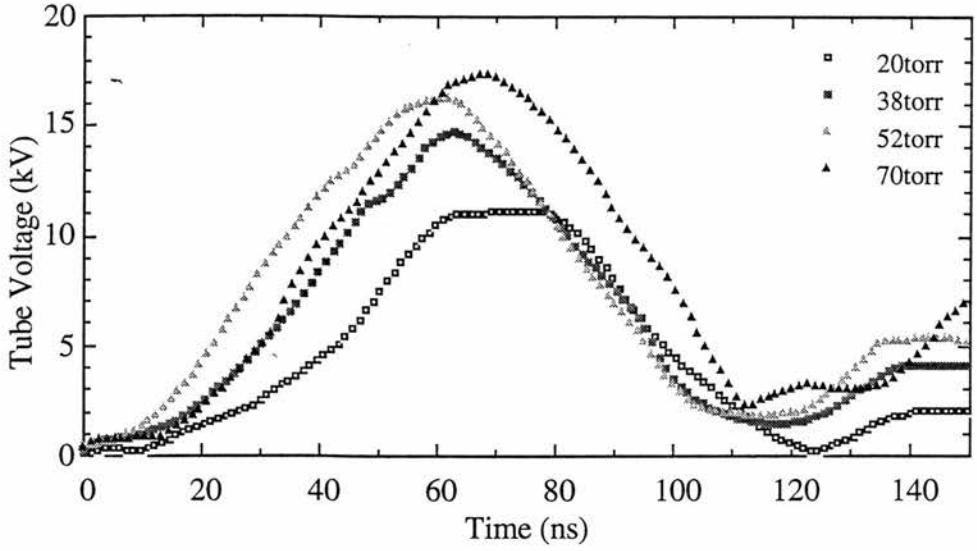

Figure 6.8b: Tube voltage waveform at a constant input power of 1.8 kW for various helium buffer gas pressures.

6.2.4 Power Delivery to Tube

Figure 6.9 shows how (i) the total power delivered to the tube, (ii) the power delivered to the tube up to the onset of laser oscillation at 1.50 μm and (iii) the power delivered to the tube over the duration of the 1.50 μm laser pulse varied with charging voltage. The input power was maintained at 1.8 kW (based on stored energy), by correspondingly decreasing the PRF when the charging voltage was increased. A similar analysis was carried out in Section 5.6 using both neon and a premix of neon and hydrogen as the buffer gases.

The effect of increasing the storage capacitance was to decrease the power delivered before the onset of laser oscillation at 1.50 μm, and to increase the power delivered over the duration of the 1.50 μm laser pulse. The total power delivered using a helium buffer gas was significantly higher than when only neon was used, and was comparable with the input power using a premix of neon and 3% H_2. In Section 5.6, the increase in power delivered with the addition of H_2 to the neon buffer gas was explained in terms of the increase in the tube impedance caused by the decrease in the preionisation density. The

increase in the power delivered obtained using helium instead of neon could also be explained in terms of the larger tube impedance, as a result of improved electron-ion recombination.

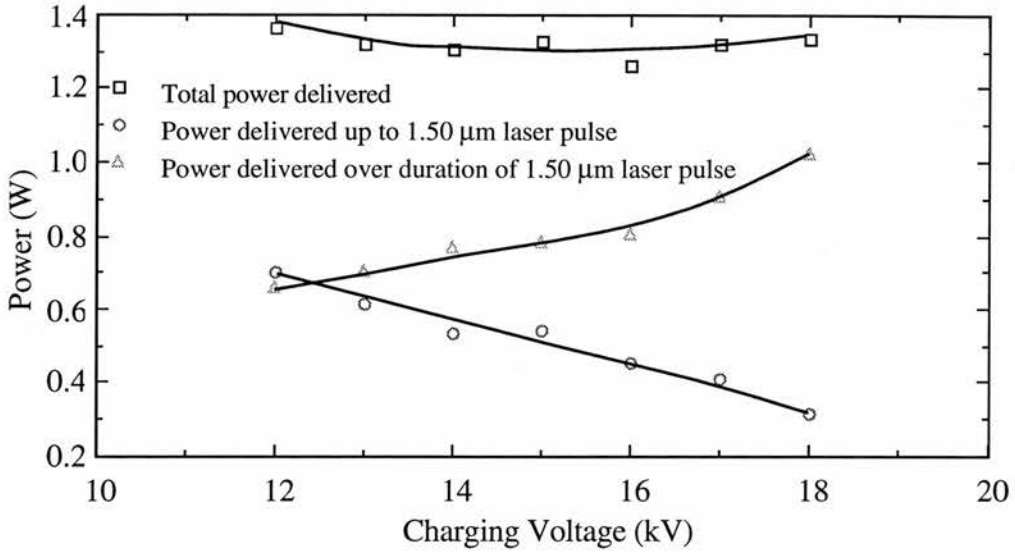

Figure 6.9: (i) Total power delivered to the laser tube (ii) power delivered before the onset of laser oscillation at 1.50 μm and (iii) power delivered over the duration of the 1.50 μm laser pulse as a function of charging voltage for a constant input power of 1800 W.

6.3 Storage Capacitance Dependence

6.3.1 Laser Power

Figures 6.10, 6.11 and 6.12 show contour plots of how the total laser power, the laser power at 1.50 μm and the laser power at 1.13 μm respectively varied, as functions of charging voltage and input power (based on stored energy), for storage capacitances of (a) 1.2 nF, (b) 1.7 nF, (c) 2.2 nF and (d) 2.4 nF. The capacitance values quoted were all based on 'hot' values (see Section 3.7). In all cases, a peaking capacitor was used to increase the tube current risetime. This was chosen to have half the capacitance of the storage capacitor.

In Section 5.2.3, when only a neon buffer gas was used, the largest total laser output powers were obtained at relatively high charging voltages (16 kV to 18 kV) and moderate input powers (~1.8 kW to 2.0 kW). These were found to be independent of the value of the storage capacitance selected. When only a helium buffer gas was used, the largest total laser power obtained also occurred for relatively large charging voltages and

Figure 6.10a: Total laser power as a function of charging voltage and input power at Cs=1.2 nF.

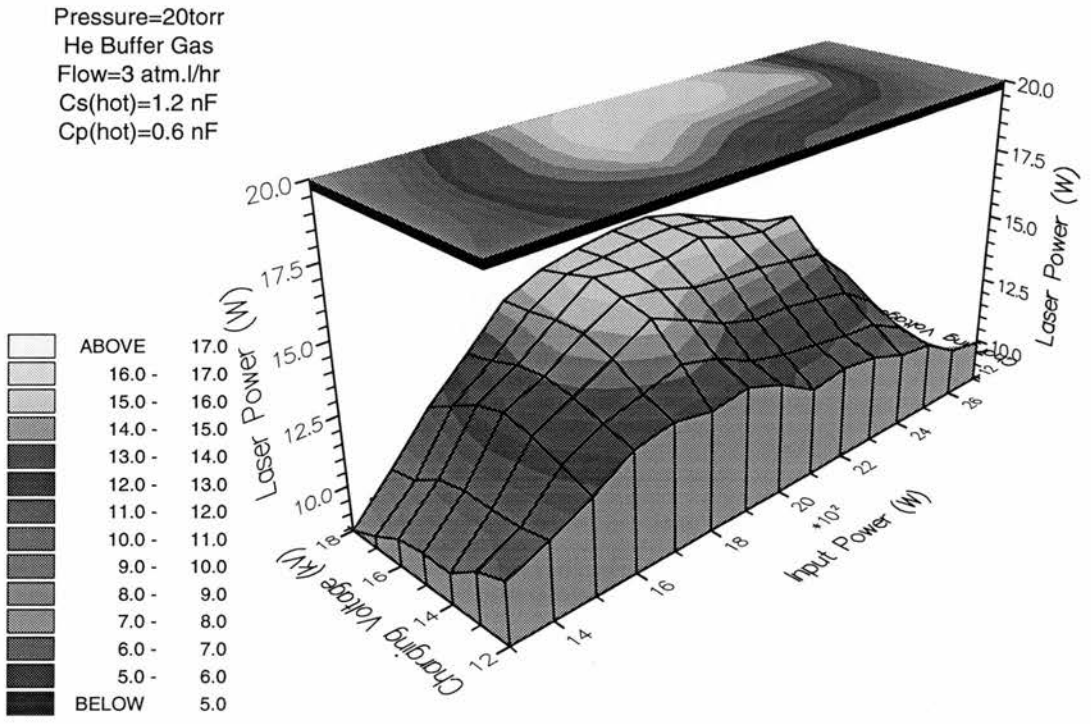

Figure 6.10b: Total laser power as a function of charging voltage and input power at Cs=1.7 nF.

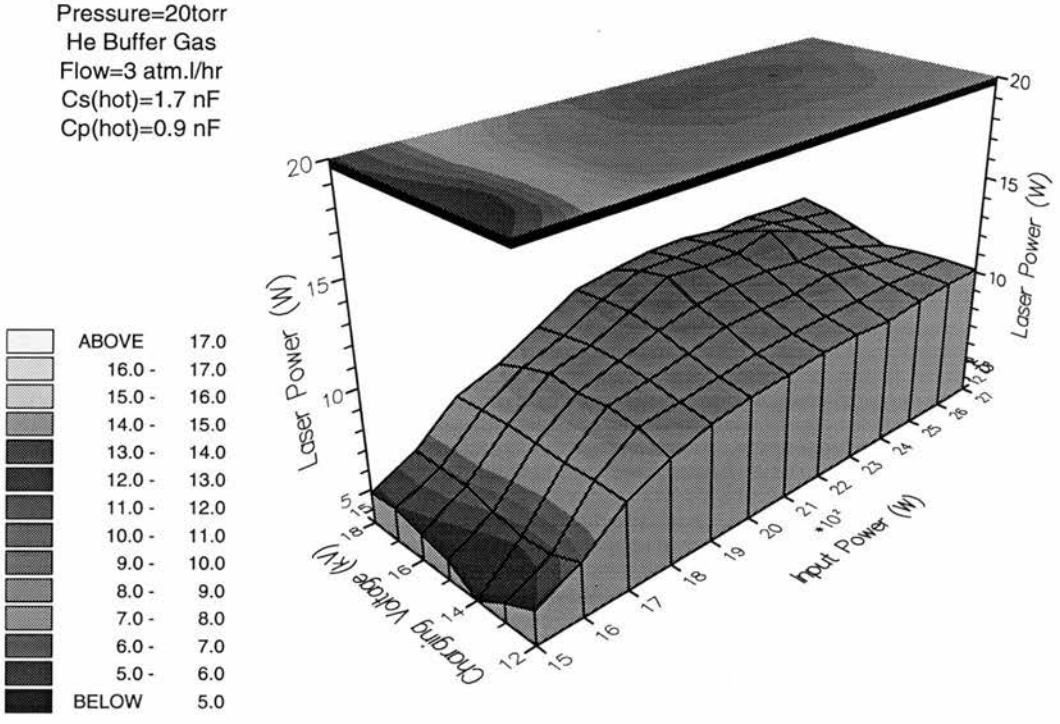

Figure 6.10c: Total laser power as a function of charging voltage and input power at Cs=2.2 nF.

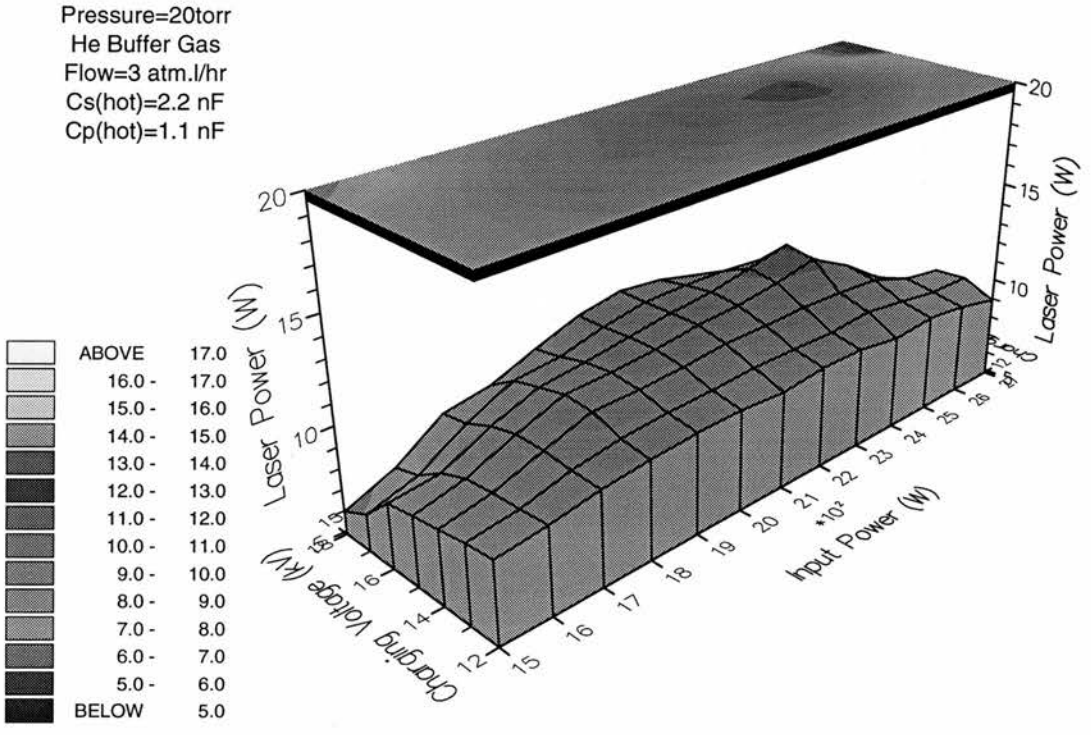

Figure 6.10d: Total laser power as a function of charging voltage and input power at Cs=2.4 nF.

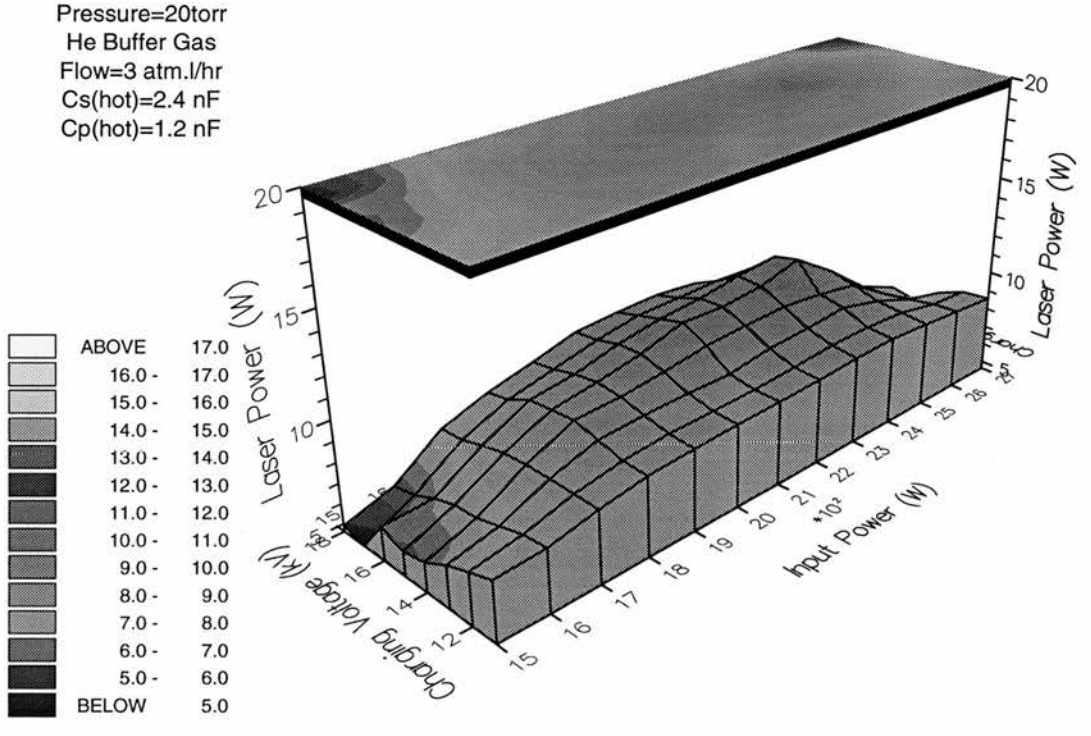

Figure 6.11a: Laser power at 1.50 μm as a function of charging voltage and input power at Cs=1.2 nF.

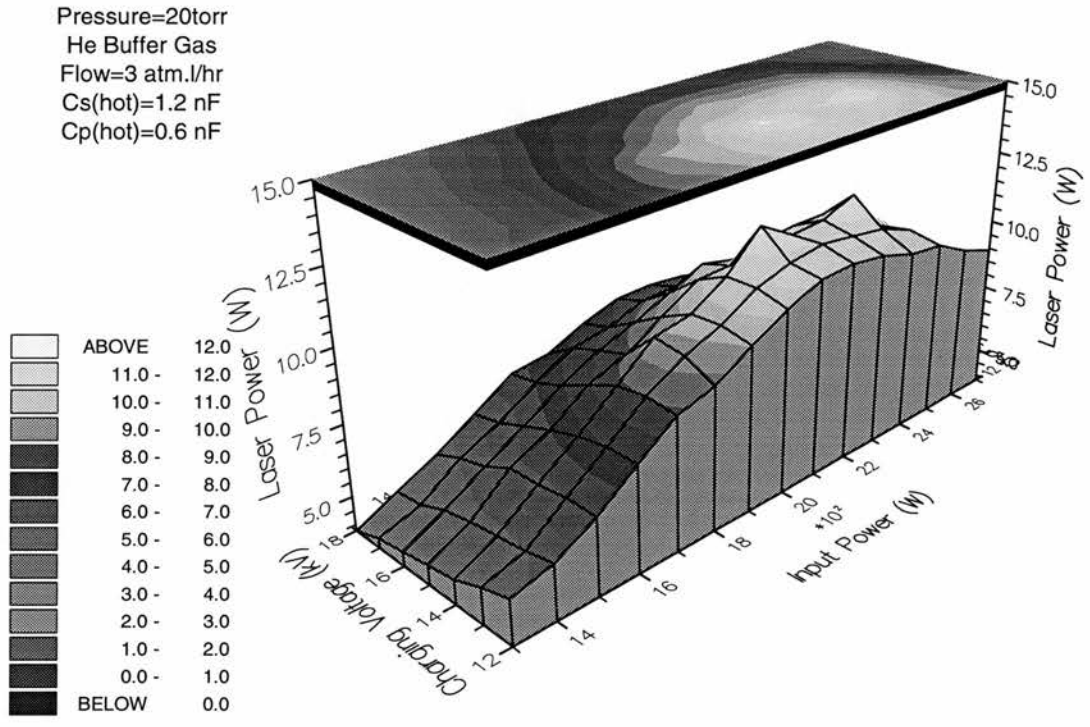

Figure 6.11b: Laser power at 1.50 μm as a function of charging voltage and input power at Cs=1.7 nF.

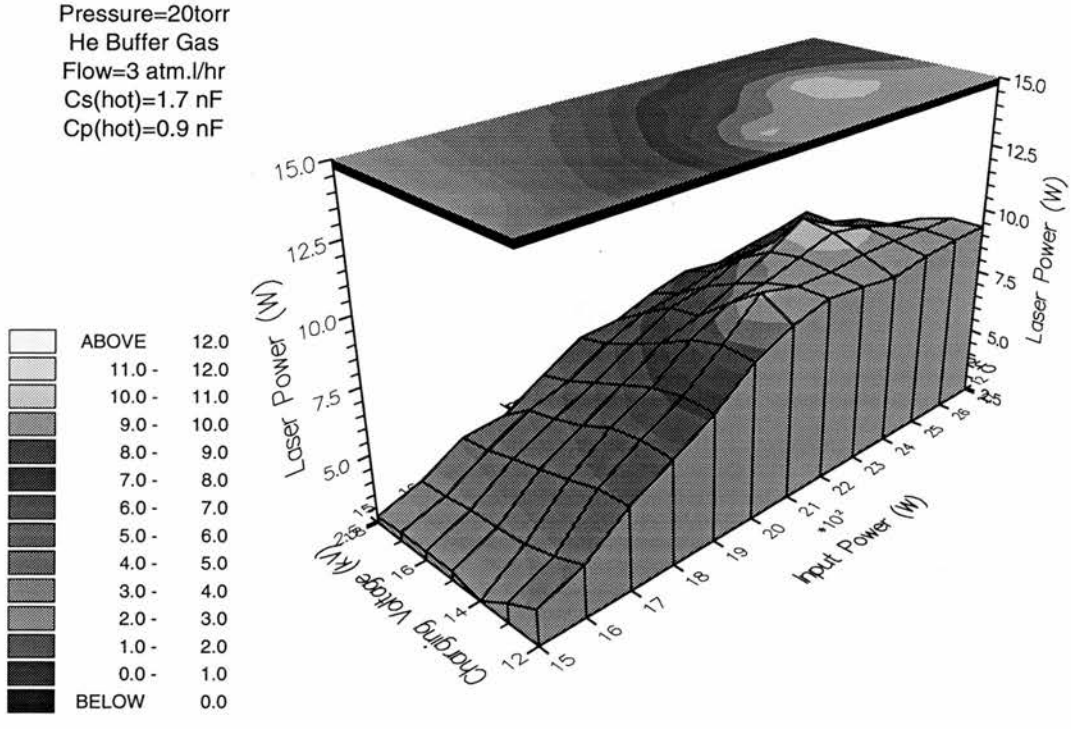

Figure 6.11c: Laser power at 1.50 μm as a function of charging voltage and input power at Cs=2.2 nF.

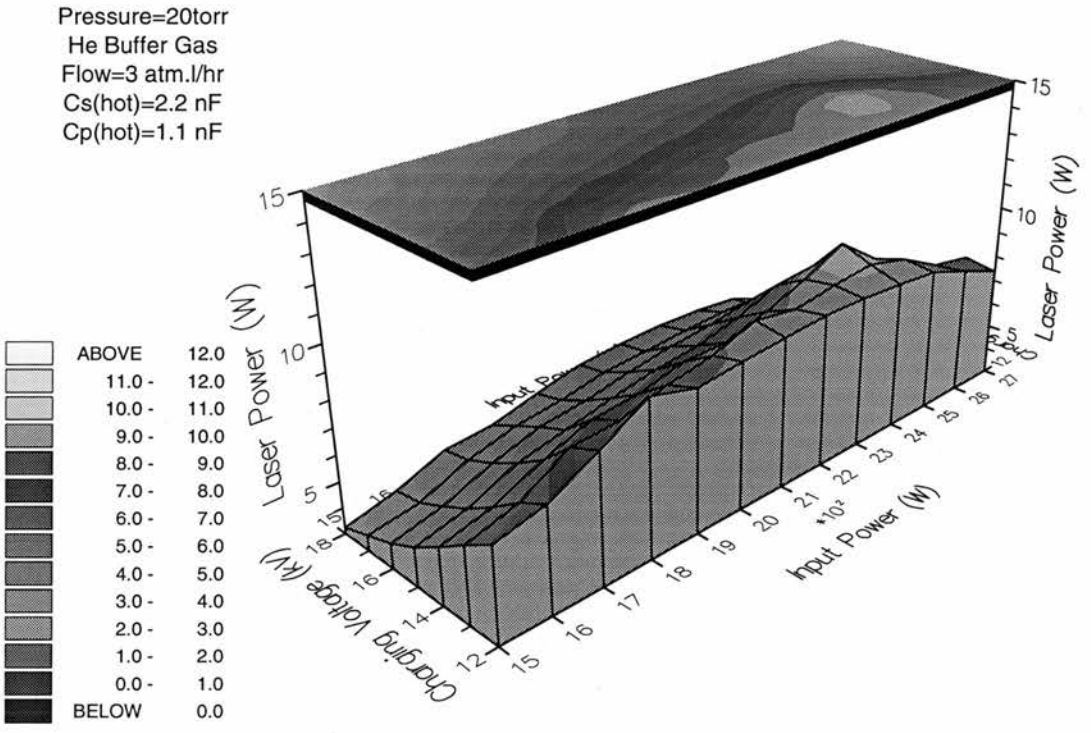

Figure 6.11d: Laser power at 1.50 μm as a function of charging voltage and input power at Cs=2.4 nF.

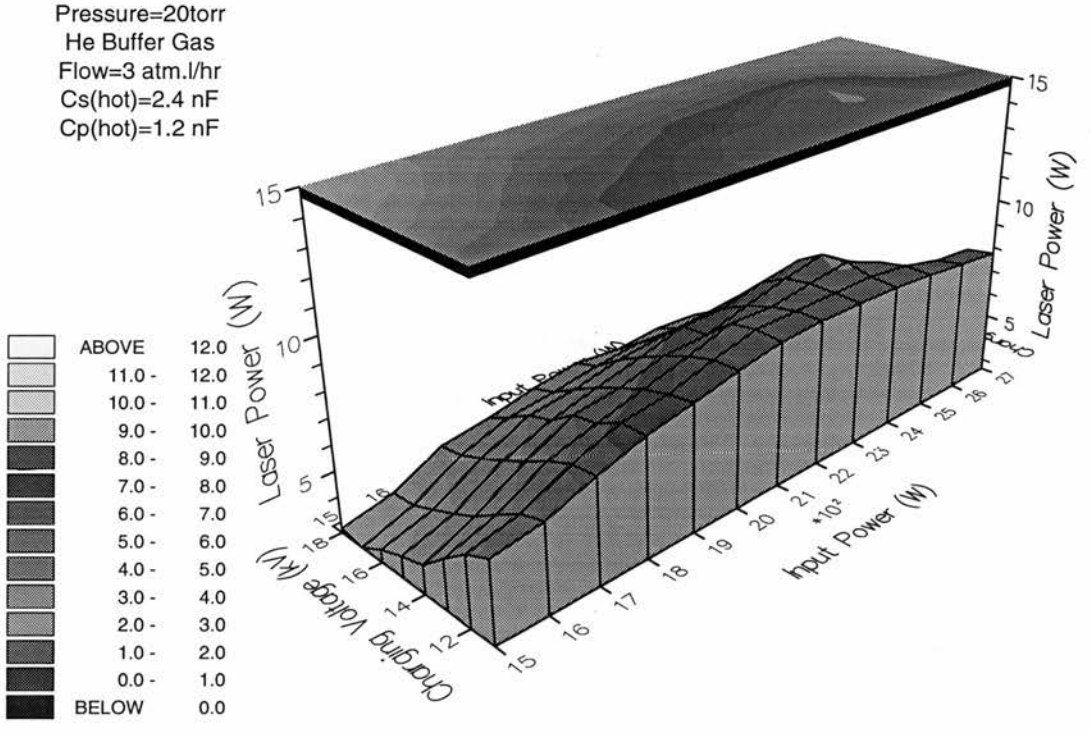

Figure 6.12a: Laser power at 1.13 μm as a function of charging voltage and input power at Cs=1.2 nF.

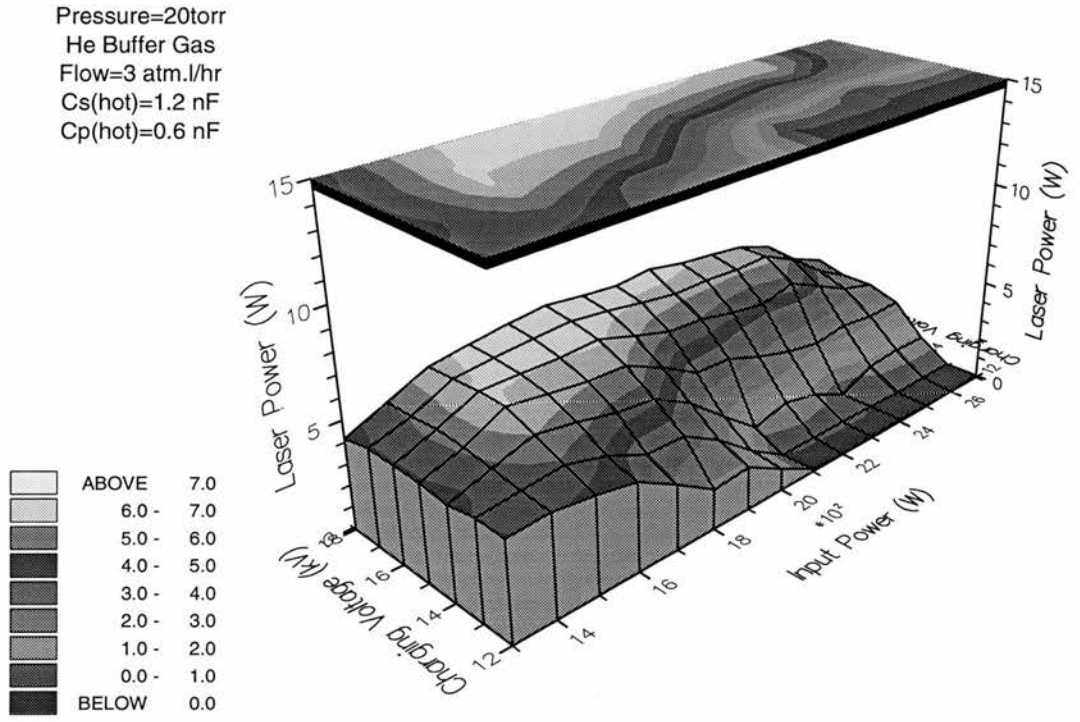

Figure 6.12b: Laser power at 1.13 μm as a function of charging voltage and input power at Cs=1.7 nF.

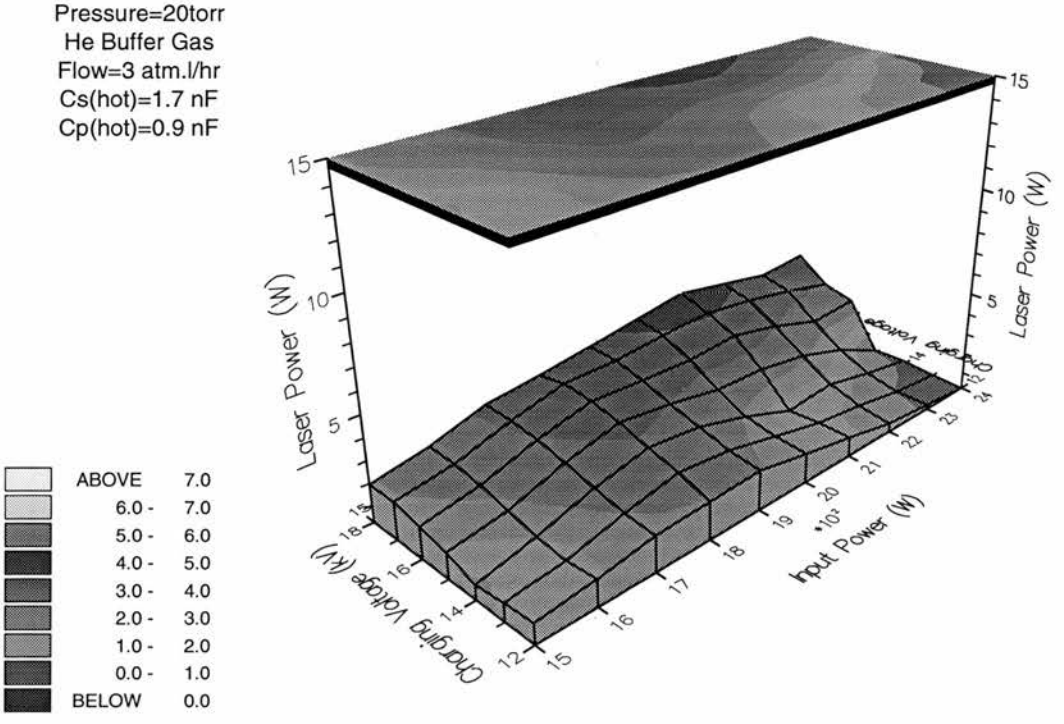

Figure 6.12c: Laser power at 1.13 μm as a function of charging voltage and input power at Cs=2.2 nF.

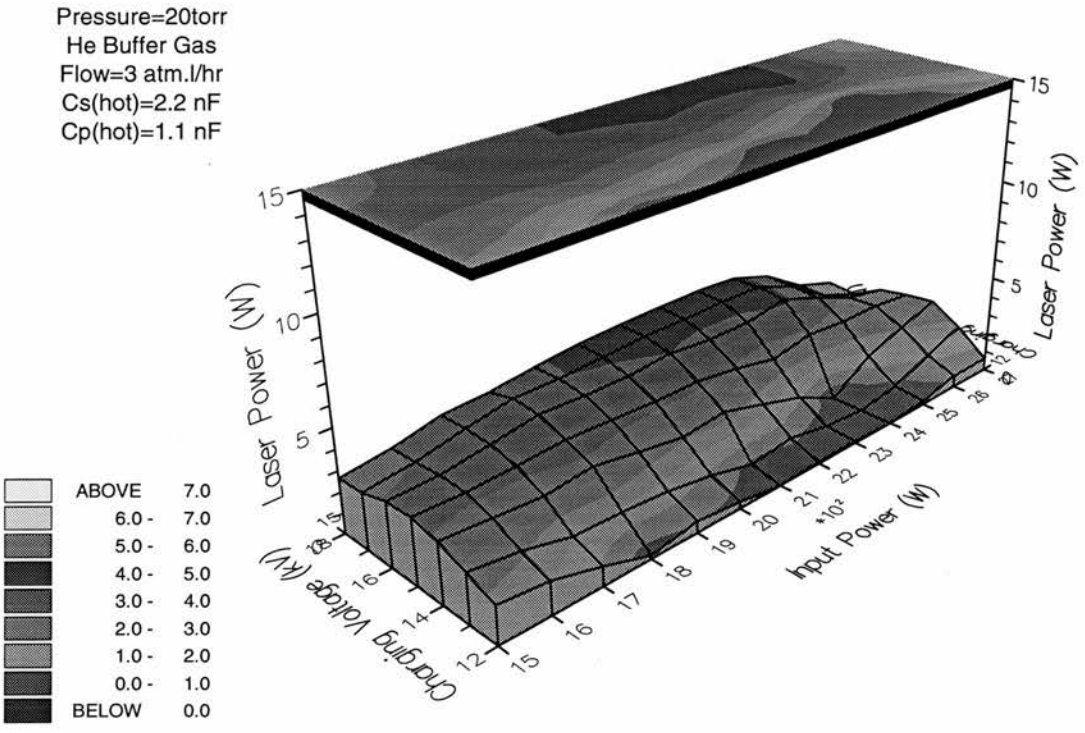

Figure 6.12d: Laser power at 1.13 μm as a function of charging voltage and input power at Cs=2.4 nF.

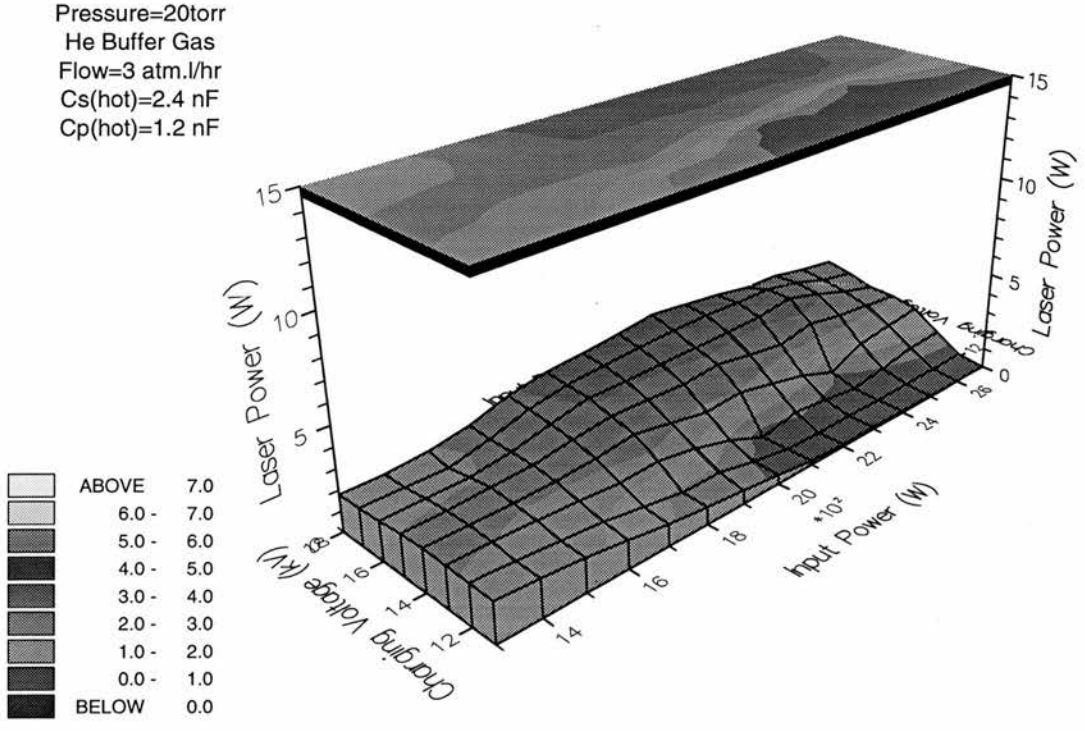

moderate input powers, as discussed in Section 6.2. Figures 6.10a-d clearly show that the maximum total laser power was obtained when the storage capacitor took smaller values (~1.2 nF). Furthermore, the optimum charging voltage and input power for maximum total laser power appeared to remain independent of the storage capacitance. Although the total laser power was still increasing with decreasing storage capacitance, measurements for values smaller than 1.2 nF were not taken, since the thyratron tended to latch because there was insufficient time available for it to recover.

When only neon was used as the buffer gas, the storage capacitance which gave maximum laser power was 2.4 nF, with a similar optimum charging voltage and input power as when only helium was used as the buffer gas (see Section 5.2.3). However, when H_2 was added to the neon buffer gas, the storage capacitance which gave the maximum laser power decreased to 1.2 nF, whilst the charging voltage and input power remained approximately constant. In order to maintain the optimum input power and charging voltage, the PRF was increased as the storage capacitance was decreased. Hence, although the optimum input powers using helium, neon, or a premix of neon and 3% H_2 as the buffer gas were all comparable, the larger PRFs, using either helium or a premix of neon and hydrogen, favoured high average total laser output powers. There have been a number of studies concerning the the upper limit to the PRF of metal vapour lasers; some suggest that it is caused by a high prepulse metastable population [4], others suggest that it is caused by an excessively high prepulse free electron density [5]. Whichever is the case, the fact that the optimum PRF appeared to be higher using either helium, or a premix of neon and hydrogen as the buffer gas, compared to the case when only neon was used, would suggest that the upper limit to the PRF was caused by inefficient electron cooling in the interpulse period (see Section 1.3.5).

6.3.2 Tube Current and Tube Voltage Waveforms

Figure 6.13 shows how (i) the peak tube current and (ii) the tube current corresponding to the characteristic step in the tube current waveform, varied with storage capacitance for a constant input power, charging voltage and helium buffer gas pressure of

1.8 kW (based on stored energy), 17 kV and 20 torr respectively. The characteristic step in the tube current waveform decreased (the PRF was reduced) with increasing storage capacitance whilst the peak current increased (corresponding to an increase in the energy input).

As discussed previously, the step in the tube current waveform is believed to give an indication of the preionisation density within the laser tube. It was therefore not unexpected that an increase in the capacitance and a corresponding decrease in the PRF (to maintain a constant input power), decreased the step in the waveform, indicating a decrease in the preionisation density. The phenomenon was more pronounced when neon was used (see Section 5.4) instead of helium because of the reduced ability of neon to cool electrons effectively in the interpulse period.

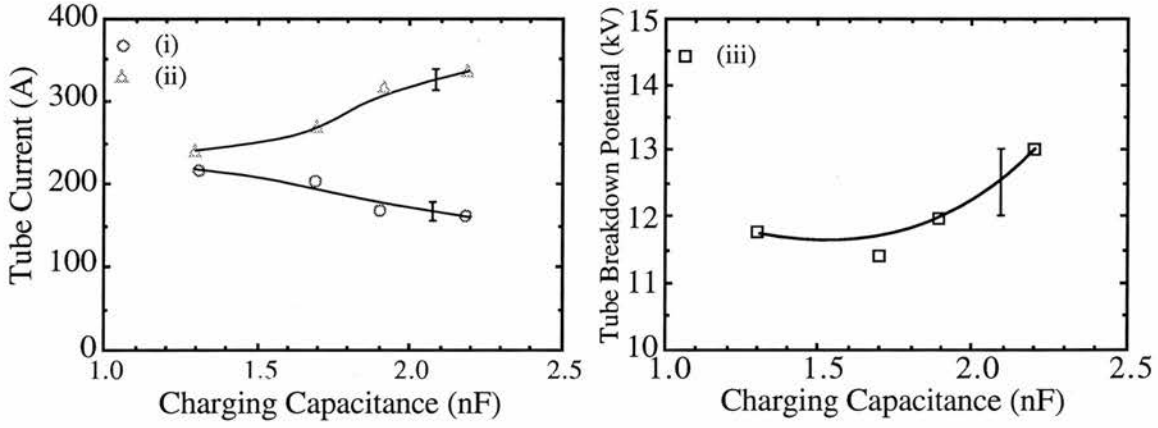

Figure 6.13: (i) Peak tube current, (ii) tube current corresponding to step in tube current waveform and (iii) 'tube breakdown potential' as a function of storage capacitance.

The decrease in preionisation density with increasing storage capacitance was also reflected in the 'tube breakdown potential' (defined here as the tube voltage which corresponded to the step in the tube current waveform). This tended to increase with increasing storage capacitance and hence with decreasing PRF, as is also shown in Figure 6.13.

6.4 H_2 and D_2 Addition to a Helium Buffer Gas

6.4.1 Laser Power

An analysis was carried out using helium buffer gas, similar to the procedure described in Chapter 4 for a neon buffer gas. The laser power, tube current, tube voltage

and the laser pulse waveforms were monitored as functions of various percentages of H_2 and D_2 added to a helium buffer gas. The input power, charging voltage, PRF, buffer gas pressure and storage capacitance were maintained at 1.8 kW, 16 kV, 11.5 kHz, 20 torr and 1.2 nF (hot value) respectively. These represented the optimum discharge conditions for maximum total laser power using only a helium buffer gas (see Sections 6.2 and 6.3). The H_2 and D_2 were purged from the laser prior to turning off each time.

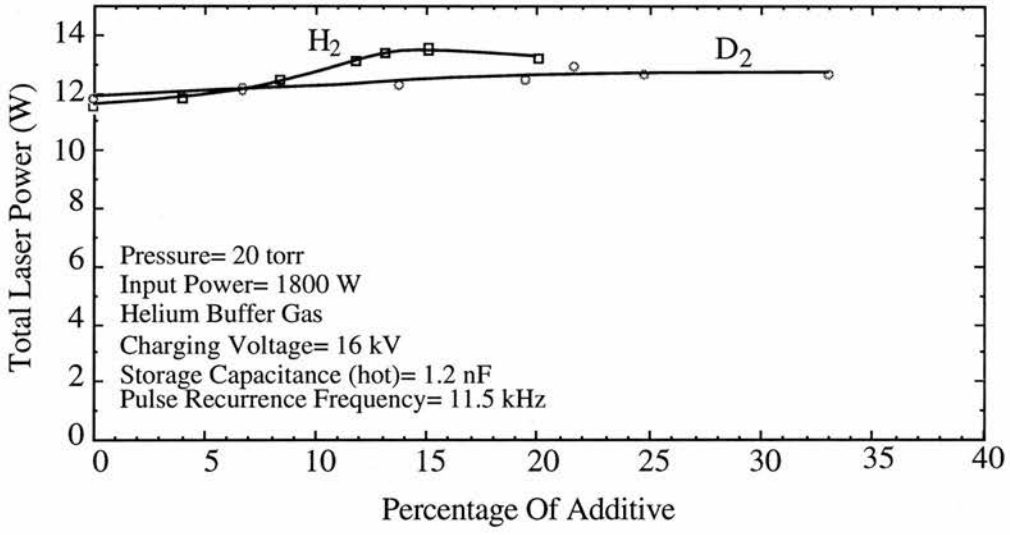

Figure 6.14a: Total laser power as a function of percentage of hydrogen and deuterium additive.

Figures 6.14a,b,c shows how (a) the total laser power, (b) the laser power at 1.50 μm and (c) 1.13 μm varied as functions of percentage of added H_2 and D_2.

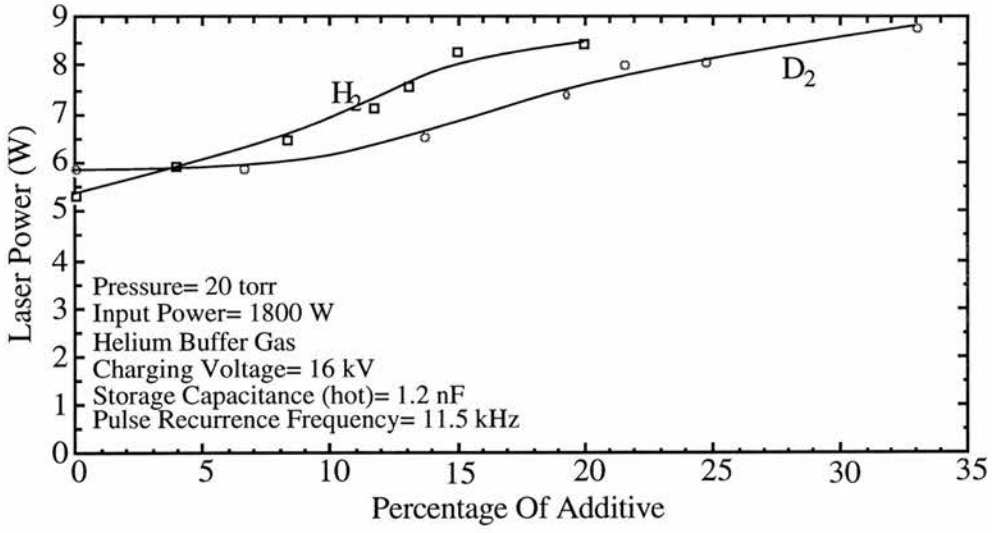

Figure 6.14b: Laser power at 1.50 μm as a function of percentage added hydrogen and deuterium.

Although the addition of either H_2 and D_2 to the helium buffer gas did not appear to

increase the total laser power, one effect was to change the relative contributions to the total laser power from the 1.13 μm and 1.50 μm transitions. The laser power at 1.50 μm increased with increasing percentage of H_2 and D_2, whilst the laser power at 1.13 μm decreased with increasing percentage of either H_2 or D_2. This observed increase at 1.50 μm was greater with H_2 additives than with D_2. Indeed, larger percentages of D_2 were required for a comparable increase in laser power. In addition, the decrease in laser power at 1.13 μm was more pronounced with H_2 additives than with D_2. It is interesting to note that when neon was used as the buffer gas, the percentages of either H_2 or D_2 required to change significantly the contributions at 1.13 μm and 1.50 μm to the total laser power, were considerably lower than when helium was used as the buffer gas. This behaviour reflected the relative closeness of the mass of helium to either H_2 or D_2, and indeed reflected the relative closeness of the collision cross sections for momentum transfer. This explains why larger quantities of additive were required before there was any appreciable difference in the laser power observed when a helium buffer gas was used.

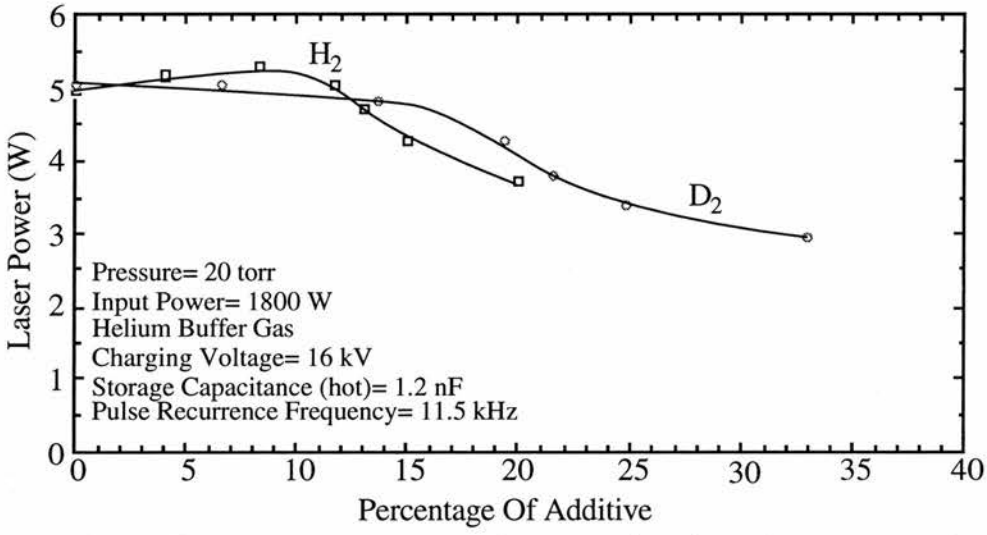

Figure 6.14c: Laser power at 1.13 μm as a function of percentage of added hydrogen and deuterium.

6.4.2 Tube Current and Tube Voltage Waveforms

Figures 6.15a,b show the tube current waveform obtained for various percentages of (a) H_2 and (b) D_2 additives to a helium buffer gas. As in the case when a neon buffer gas was used, a step was observed in the leading edge of the tube current, which decreased with increasing percentage of additive. Larger percentages of D_2 were required than H_2 in

order to obtain similar decreases in the tube current waveform step. When these results were compared to those obtained using neon as the buffer gas, it was found that much larger percentages of H_2 and D_2 were required when helium was used as the buffer gas before any appreciable decrease in the step was observed.

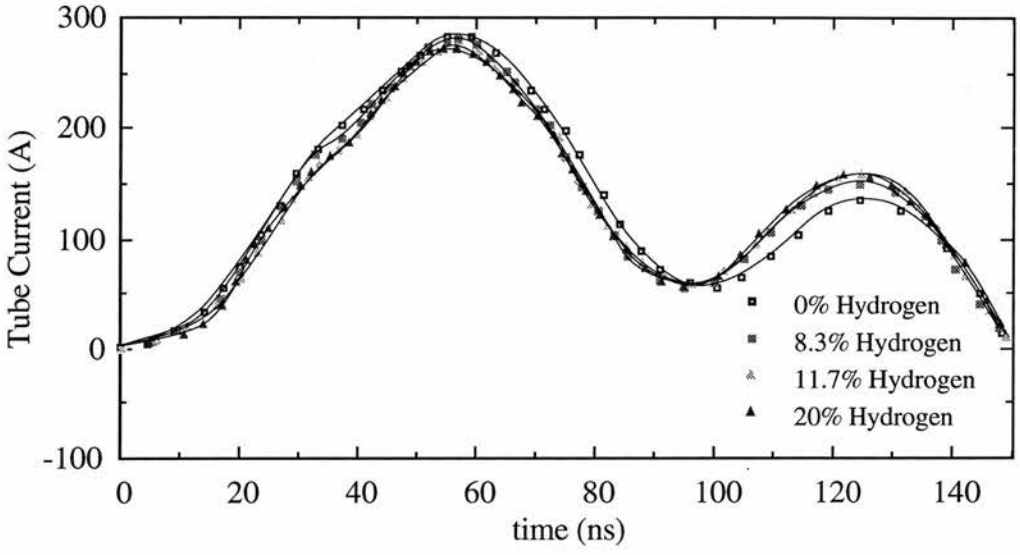

Figure 6.15a: Tube current as a function of time for various percentages of hydrogen.

The fact that the step on the leading edge of the tube current waveform was much lower using only helium compared to using only neon as the buffer gas suggested that the

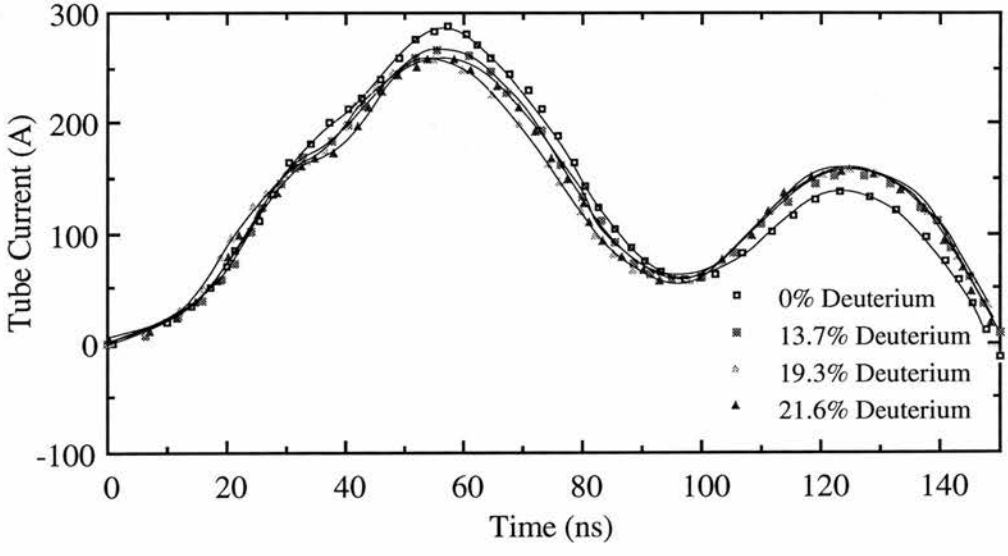

Figure 6.15b: Tube current as a function of time for various percentages of deuterium.

preionisation density was much lower with a helium buffer gas. This is consistent with the fact that the efficiency of energy transfer (and hence electron cooling) is inversely

proportional to the mass of the buffer gas [6]. Using helium is therefore likely to result in enhanced electron-ion recombination and hence in a reduced preionisation density.

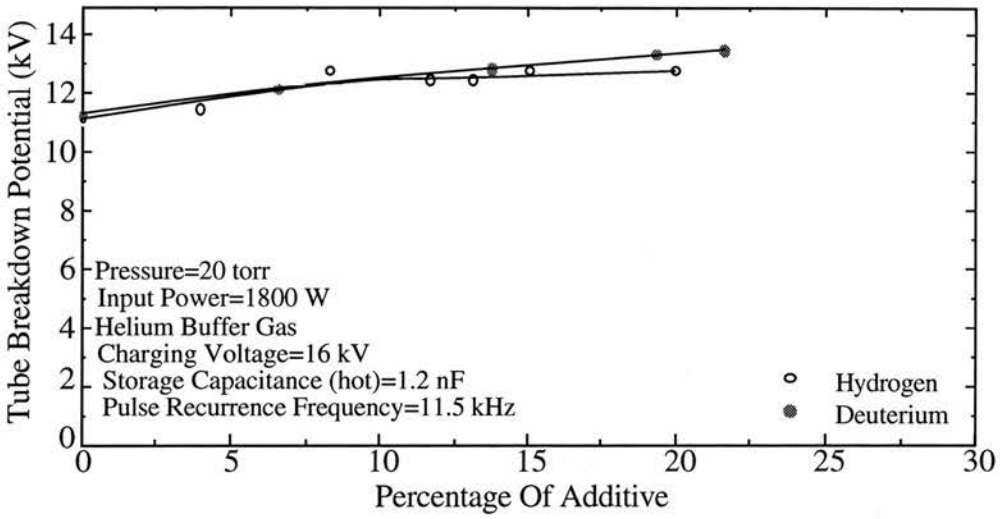

Figure 6.16: 'Tube breakdown potential' as a function of percentage of additive for constant input power based on stored energy.

The same method was used to evaluate the 'tube breakdown potential' as in Sections 6.2.3 and 4.4.3. Figure 6.16 also shows how the tube breakdown potential increased when either H_2 or D_2 was added to a helium buffer gas. The observed increase was significantly less when helium was used compared to when neon was used as the buffer gas, increasing from 11 to 13 kV with 15% H_2 or D_2 added to helium, and from 5.5 to 11.5 and 12.0 kV with 8% H_2 and 8% D_2 respectively added to neon. This marginal increase obtained using helium as the buffer gas was attributed to the greater ability of helium than neon to cool electrons in the discharge afterglow efficiently. The larger electric field obtained using helium rather than neon is one important factor which explains the larger total laser output powers obtained.

6.4.3 Laser Pulse Waveforms

In Section 4.4.2, the effect of H_2 and D_2 addition to a neon buffer gas was to increase laser oscillation at 1.50 μm at the expense of laser oscillation at 1.13 μm. This was attributed to increased metastable deactivation caused by an increased electron collision frequency.

Figure 6.17a: 1.13 μm laser pulse as a function of time and percentage of hydrogen added.

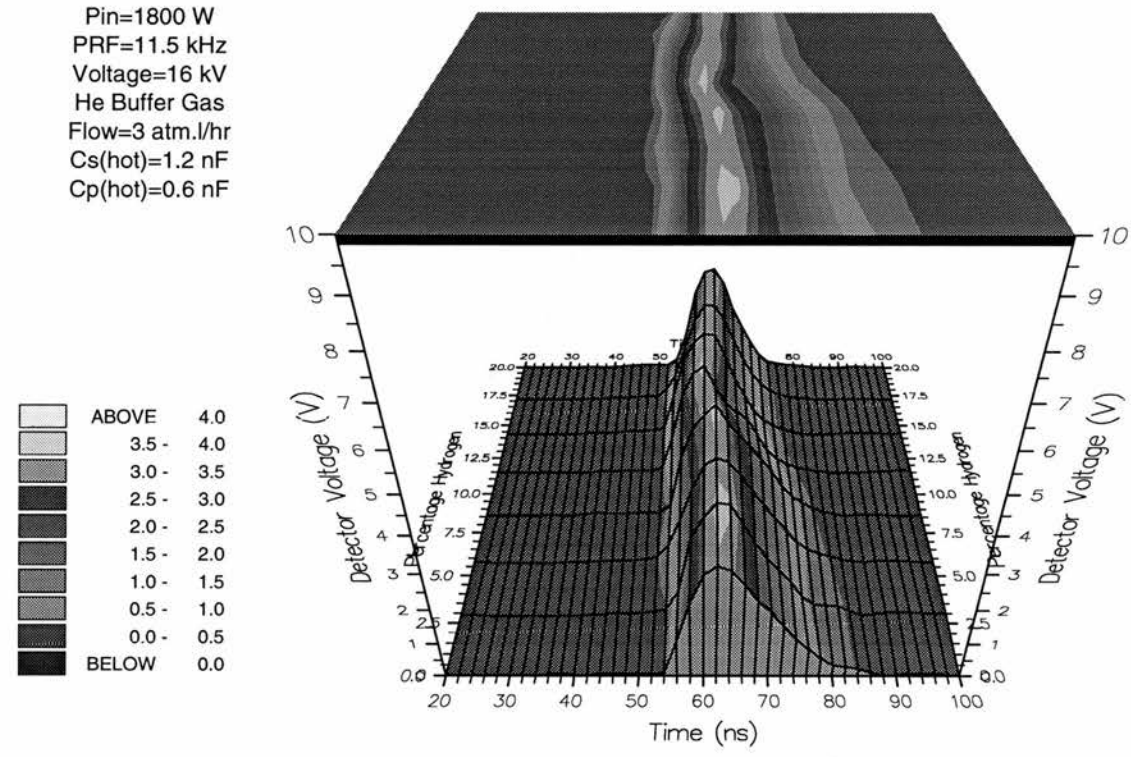

Figure 6.17b: 1.50 μm laser pulse as a function of time and percentage of hydrogen added.

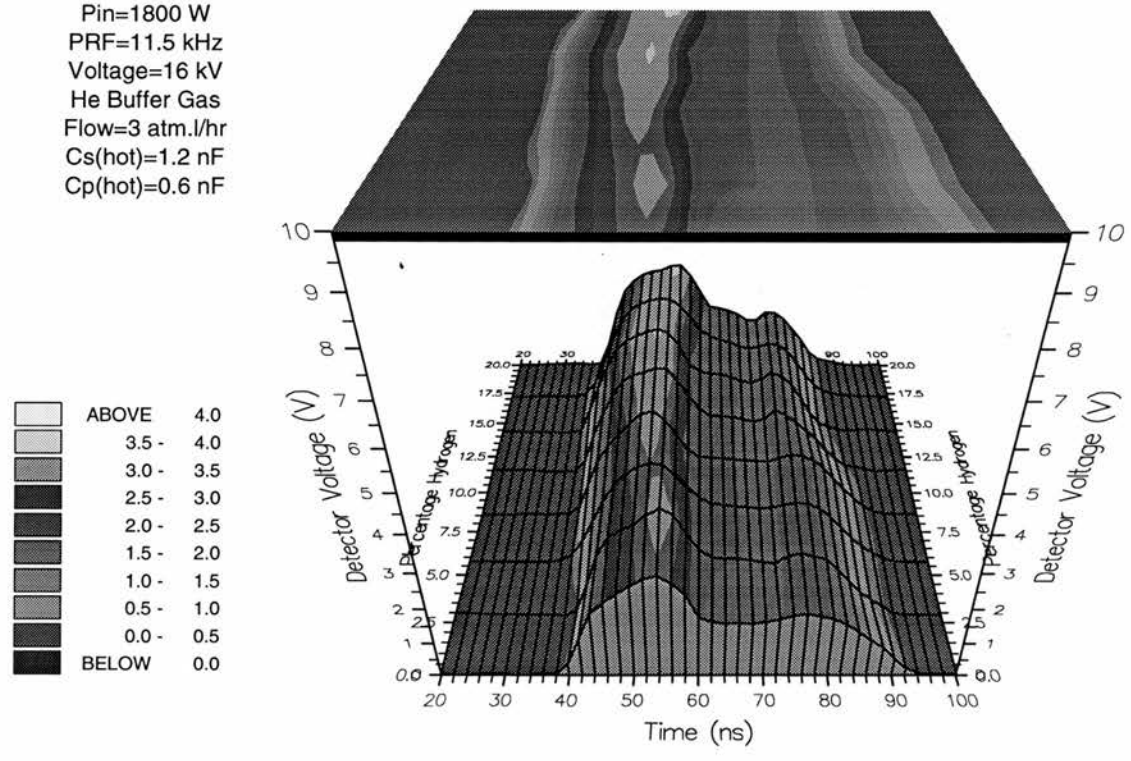

Figure 6.17a,b shows a contour plots of (a) the 1.13 μm and (b) the 1.50 μm laser pulse intensity as functions of percentage of H_2 additives. The discharge conditions were identical to those discussed in Section 6.4.1, i.e. the input power, charging voltage and PRF were maintained at 1.8 kW, 16 kV and 11.5 kHz respectively. The percentage of H_2 ranged from 0% to 10%. In both cases, the laser pulse occurred earlier with respect to the onset of the tube current when H_2 was added to the laser. However, the decrease in delay was much less pronounced than when H_2 were added to a neon buffer gas. There was also an increase in laser oscillation at 1.50 μm at the point of onset of laser oscillation at 1.13 μm. Once again, the effect was much less marked than when neon was used. Indeed, much larger percentages of H_2 were required before any appreciable change in the waveform could be observed when helium was used instead of neon.

These observations and comparisons with neon suggested that the effect of H_2 additive was less pronounced using a helium buffer gas than a neon buffer gas. When neon was used, laser oscillation at 1.50 μm was believed to be inhibited by a high prepulse metastable population. One of the effects of H_2 additives was to increase the degree of metastable depopulation in the interpulse period. The fact that much larger quantities of either H_2 was required before there was any noticeable change when helium was used reflected the increased ability of helium to cool electrons and therefore to hasten depopulation the metastable levels.

6.5 Summary

In this chapter, the dependence of total laser power, laser power at 1.13 μm and 1.50 μm on the charging voltage, PRF, input power (based on stored energy), buffer-gas pressure and storage capacitance using a helium buffer-gas has been presented. In general larger output powers at 1.13 μm and 1.50 μm were obtained when helium was used than when neon was used. The input powers for maximum laser power at 1.13 μm and 1.50 μm using a helium buffer gas were comparable to the input powers for maximum laser power using neon which suggested that the upper limit to the input power was likely

to be the thermal population of the metastable lower laser levels and not caused by inefficient electron cooling in the interpulse period.

The optimum pressure was found to be considerably lower when helium was used as the buffer gas to when neon was used. This is primarily because helium has a much higher electron collision cross-section for momentum transfer than neon which results in more efficient electron cooling. This results in enhanced electron-ion recombination and higher tube impedances leading to greater E/N ratio which favours excitation to the upper laser level (see Section 1.3.5).

The maximum total laser power was obtained for a lower storage capacitance using helium instead of neon as the buffer-gas (corresponding to a higher PRF since the input power and charging voltage for maximum laser power were comparable to when neon was used). The capacitance value for maximum total laser power when using helium was similar to when 3% H_2 was added to a neon buffer gas. In Chapter 5 the decrease in the optimum capacitance value with the addition of H_2 was attributed to enhanced electron cooling. The same explanation is likely to apply here, i.e. helium has a higher electron collision cross-section than neon and because of its lighter mass will more readily undergo elastic collisions with electrons. This results in enhanced electron-ion recombination and increased metastable depopulation in the interpulse period.

The effects of H_2 and D_2 addition on the laser output power using a helium buffer-gas was investigated. Although there was only a marginal increase in the total laser power when either H_2 or D_2 was added to the laser, the contributions to the total power from the 1.13 μm and 1.50 μm was found to change as the percentage of additive was increased. As when a neon buffer gas was used, the laser power at 1.13 μm decreased with increasing percentage of additive whereas the laser power at 1.50 μm increased. Larger percentages of D_2 than H_2 were required to obtain a similar decrease in laser power at 1.13 μm which again reflected the trends observed for H_2 and D_2 addition to a neon buffer gas. However, when a helium buffer gas was used, the percentages of H_2 and D_2 required to cause the laser power at 1.13 μm to significantly decrease were much higher than when

a neon buffer gas were used. This was because helium and H_2 or D_2 are more comparable than neon and H_2 or D_2 in their abilities to cool the electrons in the interpulse period.

The greater ability of helium than neon to cool the electrons in the interpulse period is also reflected in the step in the tube current waveform. This was found to occur considerably earlier when He was used as the buffer-gas compared to when neon was used. The effect of H_2 and D_2 additives on the step in the tube current waveform was to cause the step in the tube current waveform to occur at earlier times although the effect was much less pronounced using helium as the buffer gas compared to when neon was used.

6.6 References

[1] M. Madigan, L. O. Hocker, J. H. Flint, C. F. Dewey JR, IEEE J. Quantum Electron. **QE-16** (12) pp 1294-1296 (1980).

[2] J. L. Delcroix, 'Plasma Physics', **2** Wiley, New York pp 163 -167 (1968).

[3] D. R. Jones, S. N. Halliwell, C. E. Little, Opt. Comm. **111** pp 394-402 (1994).

[4] V. V. Kazakov, S. V. Markova, G. G. Petrash, Sov. J. Quantum Electron. **14** (5) pp 642-647 (1984).

[5] P. A. Bokan, Sov. J. Quantum Electron. **15** (5) pp 622-626 (1980).

[6] M. J. Withford, D. J. W. Brown, J. A. Piper, Opt. Comm. **110** pp 699-707 (1994).

Chapter 7

Conclusion and Discussion for Future Work

7.1 Summary

In the present study, a BVL has been constructed to operate reliably with tube lifetimes extending to several hundred hours. For the first time large (>40%) increases in the total laser power and laser efficiency have been observed with the addition of small percentages of hydrogen to a neon buffer gas of a BVL. This has resulted in the highest total laser power (14.3 W) and efficiency (1.0%) being obtained to date. It has been the purpose of this study to determine the underlying mechanisms which limit the laser power of the BVL, and to explain the observed increases with the addition of small percentages of hydrogen and deuterium additives to the buffer gas in terms of the kinetic mechanisms which occur within the discharge tube. The main effects of the addition of hydrogen and deuterium to the buffer gas of a BVL are summarised in the following subsections:

7.1.1 Influence of Hydrogen and Deuterium on the Optimum Discharge Conditions

The discharge conditions which gave the maximum total laser power using neon or helium were found to be very different. When helium was used, the optimum buffer

gas pressure was approximately 20 torr, whereas when neon was used the pressure was approximately 50 torr. In addition, although the optimum charging voltage and input power (based on stored energy) were approximately the same (at 16 kV and 1800 W respectively), the optimum PRF was found to be significantly higher (and hence the optimum storage capacitance was considerably lower) when helium was used instead of neon. The lower optimum pressures and higher optimum PRFs when using helium instead of neon could be explained in terms of the increased ability of helium to cool the electrons in the interpulse period, thereby reducing the metastable lower laser level population and also the preionisation density.

The addition of 3% H_2 to a neon buffer gas increased the total laser power and the overall laser efficiency for all discharge conditions (i.e. PRFs, charging voltages, pressures etc.). This increase was most pronounced when the laser was operated at higher PRFs and lower buffer gas pressures. Indeed, when a neon buffer gas with 3% added H_2 was used, the optimum discharge conditions for maximum laser power occurred at PRFs which were comparable to when a helium buffer gas was used. The maximum total laser power and laser efficiency which could be obtained using neon with 3% added H_2 were 14.3 W and 1.0% respectively. These output powers and efficiencies are the highest reported to date for a BVL. H_2 was also added to a helium buffer gas, and although no increase in the total laser power was observed, the contribution to the total laser power from the 1.13 μm transition decreased whilst the contribution from the 1.50 μm transition increased.

The dependence of laser power on the percentage of H_2, D_2 or He additive to a neon buffer gas was investigated. It was found that the laser power at 1.50 μm increased with increasing percentage of additive whereas the laser power at 1.13 μm increased for small additive percentages, peaked, then decreased as the percentage was increased further. Approximately twice as much D_2, and four times as much He as H_2 was required to cause the laser power at 1.13 μm to reach this peak in laser power. This trend reflected the energy transfer efficiency for a three-body electron/buffer gas collision, i.e. doubling

the mass of the additive caused the efficiency of energy transfer to decrease by a factor of two.

Because the 1.13 μm and 1.50 μm laser transitions share a common upper laser level, the observed increase in laser power at 1.50 μm and the corresponding decrease at 1.13 μm with increasing percentage of additive above the optimum values could only be explained in terms of a metastable lower laser level phenomenon. This is because any increase in upper level excitation should enhance laser oscillation at both transitions equally. This suggested that one effect of the additives was to decrease the metastable population of the 1.50 μm transition, although it was not clear whether the 1.50 μm metastable level was being depopulated to the ground-state or transferring to the 1.13 μm metastable level thereby hindering laser oscillation at 1.13 μm. H_2 proved most effective at reducing the 1.50 μm metastable population followed by D_2 and finally He.

7.1.2 Influence of Hydrogen and Deuterium on the Tube Current and Tube Voltage Waveforms

Another effect of increasing the percentage of additive to either a helium or neon buffer gas was an increase in the tube voltage and a decrease in the tube current, indicating that the tube impedance increased with increasing additive percentage. The increase in the tube impedance was most pronounced when a neon buffer gas was used, with H_2 additives resulting in the greatest increase, and He the least. The increase in the tube impedance was also characterised by a step which occurred in the tube current waveform. This tended to decrease and occur earlier in the excitation pulse with increasing percentage of additive. For comparable percentages of additives, the step occurred earliest with H_2, then D_2 and latest with He additives. When helium was used instead of neon, the step occurred much earlier, with much larger percentages of additives being required before any appreciable change in the step could be observed.

The tube current up to the step in the tube current waveform was believed to be carried by remnant electrons with the step corresponding to the point at which collisional ionisation processes began to greatly accelerate, resulting in tube 'breakdown'. Thus the

effect of the addition of additives to the buffer gas was to cause the preionisation density within the tube to decrease.

7.1.3 Influence of Hydrogen and Deuterium on the Power Delivery to the Laser Tube

The laser head inductance was determined experimentally and estimated to be 200 nH. This was used to evaluate the power delivery to the laser tube from the resistive component of the measured tube voltage. For discharge conditions corresponding to maximum total laser power, only approximately 55% of the electrical power stored on the storage capacitor was deposited into the laser tube. The rest was delivered to other circuit components, such as the thyratron. Adding H_2, D_2 or He to the buffer gas increased the total power delivered to the laser tube by around 10%. For comparable percentages of each, the increase in power delivery was greatest with H_2, followed by D_2, then He. Another effect of H_2, D_2 and He additives was to change the temporal power delivered to the laser tube. Increasing the percentage of additive decreased the power delivered up to the onset of laser oscillation at 1.50 μm, and increased the power delivered over the duration of the 1.50 μm laser pulse. This was presumably because of improved matching from the charging to discharging circuit caused by the decrease in the preionisation density.

7.1.4 Influence of Hydrogen and Deuterium on the Temporal and Spatial Evolution of the 1.13 μm and 1.50 μm Laser Pulse Intensity Waveforms

The influence of H_2, D_2 and He additives on the temporal and spatial evolution of the 1.13 μm and 1.50 μm laser pulse intensity waveforms was investigated. The effect of the addition of H_2, D_2 and He to a neon buffer gas and H_2 and D_2 additives to a helium buffer gas was to cause the onset of laser oscillation at 1.50 μm to occur at earlier times with respect to the beginning of the excitation pulse. A similar phenomenon was observed when the buffer gas pressure was increased. The decrease in the pulse delay was

attributed to either a reduction in the metastable population, or an increase in upper level excitation because of the increased tube impedance (E/N) The addition of hydrogen to a neon buffer gas increased the on-axis laser pulse intensity at both 1.13 μm and 1.50 μm, changing the spatial intensity profile at both wavelengths from a flat-top intensity profile to a more Gaussian-like profile.

7.2 Conclusions

The addition of hydrogen and deuterium to either a neon or helium buffer gas has been found to strongly influence the discharge tube kinetics and consequently the laser power at the two principle laser transitions at 1.13 μm and 1.50 μm. Enhanced electron cooling in the interpulse period with the addition of hydrogen or deuterium to the buffer gas is believed to be key factor which accounts for the observations summarised in Section 7.1. Enhanced eleceton cooling may enhance laser performance due to:

a) Increased metastable depopulation of the lower laser levels.

b) Enhanced E/N due to more efficient electron/ion recombination which can lead to:

(i) Improved xcitation to the upper laser level because of higher average electron energies in the excitation pulse.

(ii) More efficient energy transfer and better match of energy delivered from the storage capacitor to the gain medium.

7.3 Future Work

In previous chapters a number of inferences have been drawn from the observed results and trends concerning the influence of H_2 and D_2 additives to either neon or helium buffer gases. In particular, there has been a great deal of discussion about the effect these additives have on the preionisation density, laser tube impedance and the

metastable population. An important step in establishing the principal mechanism by which H_2 and D_2 increase the total laser power is to measure the effects of these additives on the metastable lower laser level population and the prepulse free-electron density in the interpulse period. There are a number of experiments which may be carried out to measure these parameters.

Interferometric methods are perhaps the most frequently used methods for measuring the free electron density. Such methods use a probe beam (usually at 10.6 μm) which is split 50:50 with one half being directed down the axis of the laser tube. The two beams are recombined and the resulting fringe pattern analysed. This method makes use of the minute refractive index changes which occur within a plasma where the free electron density changes [2]. Another interferometric method which may be used to evaluate the electron density is to measure the Doppler and Stark broadening of hydrogen lines [1] within the discharge plasma. This method also enables the temporal and radial dependence of the electron density to be determined.

The hook method [2] is the most common one used to measure the ground state, upper resonance and lower metastable level densities. This takes advantage of the spectral dependence of refractive index, and particularly anomalous dispersion, which occurs near spectral lines. The hook method enables both radial and temporal population densities to be determined experimentally.

7.4 References

[1] P. Blau, I. Smilanski, J. Appl. Phys **72** (3) pp 849-854 (1992).

[2] 'Modern Optical Methods for Gas Dynamic Research', ed. D. S. Dosanjh, Plenum Press, New York (1971).

CX1535

LIQUID COOLED HYDROGEN-FILLED TRIPLE GRID CERAMIC THYRATRON

The data to be read in conjunction with the Hydrogen Thyratron Preamble.

ABRIDGED DATA

Hydrogen-filled triple grid (pentode) thyratron with ceramic/metal envelope, designed for liquid immersion cooling and featuring low jitter, firing time and drift. The third grid makes the tube suitable for high power switching at very high repetition rates and permits a very short anode circuit recharge time. A hydrogen reservoir is incorporated together with an automatic current control, giving precise gas control inside the thyratron over wide variations of reservoir voltage.

Peak forward anode voltage	25	kV max
Peak anode current	1000	A max
Average anode current	1.25	A max
Anode heating factor (see note 1)	500×10^9	V.A.p.p.s. max ☆
Peak output power	12.5	MW max
Pulse repetition frequency	100	kHz max

GENERAL

Electrical

Cathode (connected internally to one end of heater)	barium aluminate	
Cathode and reservoir heater voltage (see note 2)	$6.3 \pm 5.0\%$	V ☆
Cathode and reservoir heater current	21	A ☆
Tube heating time (minimum)	5.0	min
Anode to grid 2 capacitance (see note 3)	<1.0	pF
Grid input capacitance (see note 4)	40	pF

Mechanical

Seated height	134.0 mm (5.275 inches) max ☆
Clearance required below mounting flange	40.0 mm (1.575 inches) min
Overall diameter (mounting flange)	88.9 mm (3.500 inches) nom
Net weight	1.5 kg (3.3 pounds) approx
Mounting position (see note 5)	any
Tube connections	see outline

☆ Indicates a change.

October 1978

Supersedes January 1976 Issue

Cooling

The tube is designed to be operated totally immersed in a liquid coolant.

Maximum temperature of envelope	150	°C

Further information is contained in the relevant section of the Preamble.

PULSE MODULATOR SERVICE

MAXIMUM AND MINIMUM RATINGS (Absolute values)

	Min	Max	
Anode			
Peak forward anode voltage (see note 6)	–	25	kV
Peak inverse anode voltage (see note 7)	–	25	kV
Peak anode current	–	1000	A
Average anode current	–	1.25	A
Rate of rise of anode current (see note 8)	–	5000	A/μs
Anode heating factor (see note 1)	–	500×10^9	V.A.p.p.s. ☆
Grid 3			
Grid 3 to cathode resistor	0	20	Ω ☆
Grid 2			
Unloaded grid 2 drive pulse voltage (see note 9)	300	1000	V
Grid 2 pulse duration	0.5	–	μs
Rate of rise of grid 2 pulse (see note 8)	3.0	–	kV/μs
Grid 2 pulse delay (see note 9)	0.5	–	μs
Peak inverse grid 2 voltage	–	450	V
Loaded grid 2 bias voltage	–50	–500	V ☆
Forward impedance of grid 2 drive circuit	50	250	Ω
Grid 1 – D.C. Primed			
D.C. grid 1 unloaded priming voltage	75	150	V
D.C. grid 1 priming current	50	150	mA

☆ Indicates a change.

Appendix I

MAXIMUM AND MINIMUM RATINGS – continued

	Min	Max	
Grid 1 – Pulsed			
Unloaded grid 1 drive pulse voltage (see note 9)	300	1000	V
Grid 1 pulse duration	2.0	–	μs
Rate of rise of grid 1 pulse (see note 8)	1.0	–	kV/μs
Peak inverse grid 1 voltage	–	450	V
Loaded grid 1 bias voltage			see note 10
Peak grid 1 drive current	1.0	2.0	A
Cathode and Reservoir			
Heater voltage		6.3 ± 5.0%	V
Heating time	5.0	–	min
Environmental (See note 11)			
Ambient temperature	−46	+110	°C

CHARACTERISTICS

	Min	Typical	Max	
Critical d.c. anode voltage for conduction (see note 12)	–	0.5	2.0	kV
Anode delay time (see notes 12 and 13)	–	0.2	0.3	μs
Anode delay time drift (see notes 12 and 14)	–	20	45	ns
Time jitter (see note 12)	–	3.0	5.0	ns
Cathode and reservoir heater current (at 6.3 V)	17.5	21.0	22.5	A
Pulse repetition frequency (see note 15)	–	–	100	kHz
Recovery time (see note 16 and curves on page 8)	–	6.0	8.0	μs

NOTES

1. For anode heating factors above 100 x 10^9 a flow of oil must be directed into the anode cup. At the highest anode heating factor the tube must be run in an adiabatic mode, with a maximum on period of 1 second and a maximum on-off ratio of 40%.

☆ Indicates a change.

2. The reservoir heater can be supplied from the same transformer as the cathode heater or from a separate transformer. In either case it must be decoupled with a 0.5 μF paper capacitor in parallel with a 1000 pF silvered mica capacitor, or capacitors with comparable performance.
3. The anode to grid 2 capacitance is measured with grid 3 connected to cathode.
4. The input capacitance is the capacitance between grid 1 and grid 2 connected together and grid 3 and cathode connected together. It must be taken into account in trigger circuit design since it loads the trigger drive pulse.
5. The tube must be mounted by means of its mounting flange.
6. The maximum permissible peak forward voltage for instantaneous starting is 20 kV and there must be no overshoot.
7. The peak inverse voltage including spike must not exceed 10 kV for the first 25 microseconds after the anode pulse.
8. This rate of rise refers to that part of the leading edge of the pulse between 25% and 75% of the pulse amplitude.
9. Measured with respect to cathode. When grid 1 is pulse driven, the last 0.25 μs of the top of the grid 1 pulse must overlap the corresponding first 0.25 μs of the top of the delayed grid 2 pulse.
10. D.C. negative bias voltages must not be applied to grid 1. When grid 1 is pulse driven, the potential of grid 1 may vary between −10 and +5 V with respect to cathode potential during the period between the completion of recovery and the commencement of the succeeding grid pulse.
11. The tubes are subjected to the following tests on a sampling basis.
    (a) **Recovery Time.** The recovery time is checked under the conditions specified in note 16.
    (b) **Survival under Vibration and Heater Cycling.** The tubes are vibrated at 2 g at a sweep rate of one octave per minute from 9 to 1000 Hz for 70 hours in each of 3 planes, together with heater cycling at a 10 minute on–off cycle. See note 5.
    (c) **Long Duration Shock.** The tubes are tested at 50 g for 11 ms with two blows in each plane. See note 5.
    (d) **High Temperature Test.** The tubes are tested at an ambient liquid temperature of 110 °C under normal operating conditions for 5 hours.

    (e) **Low Temperature Instant Start.** The tubes are cooled to −46 °C and subjected to a 5 minute warm-up period with 6.0 V on the heater and reservoir. The tubes must withstand a snap start at 16 kV and operate satisfactorily.
    (f) **Standby Life.** The tubes are run with a 6.3 V heater voltage applied for 1000 hours.
12. Typical figures are obtained on test using conditions of minimum pulse drive to both grids. Improved performance can be expected by increasing grid drive or by the use of a smoothed d.c. cathode heater supply voltage.
13. The time interval between the instant at which the rising unloaded grid 2 pulse reaches 25% of its pulse amplitude and the instant when anode conduction takes place.
14. The drift in delay time over a period from 2 minutes to 10 minutes after reaching full voltage.
15. Advice on operation at high pulse repetition frequencies is available from English Electric Valve Company Limited.
16. Measured after a current pulse of 1000 A, with a grid 2 bias of −100 V, a recovery impedance of 500 Ω and a 1 kV anode probe pulse.

HEALTH AND SAFETY HAZARDS

EEV hydrogen thyratrons are safe to handle and operate, provided that the relevant precautions stated herein are observed. English Electric Valve Company does not accept responsibility for damage or injury resulting from the use of electronic devices it produces. Equipment manufacturers and users must ensure that adequate precautions are taken. Appropriate warning labels and notices must be provided on equipments incorporating EEV devices and in operating manuals.

High Voltage

Equipment must be designed so that personnel cannot come into contact with high voltage circuits. All high voltage circuits and terminals must be enclosed and fail-safe interlock switches must be fitted to disconnect the primary power supply and discharge all high voltage capacitors and stored charges in the electronic devices before allowing access. Interlock switches must not be bypassed to allow operation with access doors open.

X-Ray Radiation

X-rays may be emitted by the CX1535 but the radiation is usually reduced to a safe level by the steel panels of the equipment in which the tube operates.

☆ Indicates a change.

☆ OUTLINE

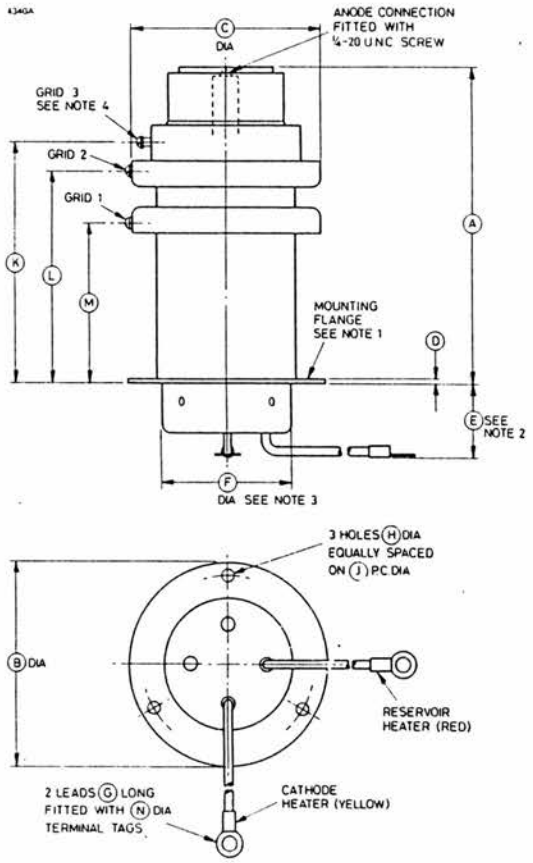

☆ Indicates a change.

☆ Outline Dimensions (All dimensions without limits are nominal)

Ref	Millimetres	Inches
A	131.0 ± 3.0	5.157 ± 0.118
B	88.90 ± 0.25	3.500 ± 0.010
C	83.0 ± 1.5	3.268 ± 0.059
D	2.5 ± 0.25	0.098 ± 0.010
E	40.0 max	1.575 max
F	56.0 max	2.205 max
G	160.0 ± 10.0	6.299 ± 0.394
H	5.0 ± 0.1	0.197 ± 0.004
J	76.2 ± 0.1	3.000 ± 0.004
K	99.0 ± 2.5	3.898 ± 0.098
L	87.0 ± 2.5	3.425 ± 0.098
M	65.0 ± 2.5	2.559 ± 0.098
N	6.35	0.250

Inch dimensions have been derived from millimetres.

Outline Notes

1. The mounting flange is the connection for the cathode, cathode heater return and reservoir heater return.
2. A minimum clearance of 40.0 mm (1.575 inches) must be allowed below the mounting flange.
3. The recommended mounting hole is 58.0 mm (2.283 inches) diameter.
4. Grid connections fitted with 8–32 UNC screws, round head, ¼-inch (6.35 mm) long.

☆ Indicates a change.

MAXIMUM RECOVERY CHARACTERISTICS

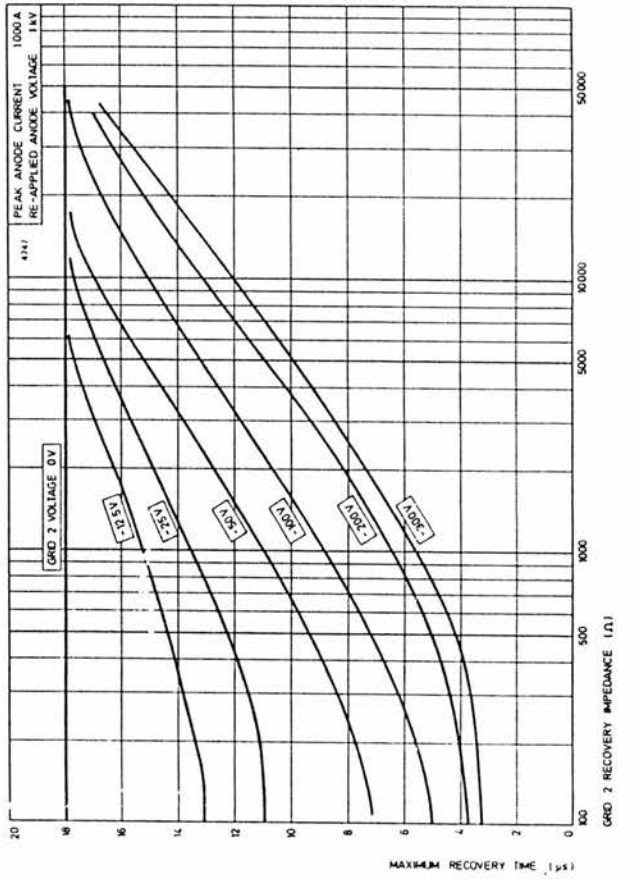

English Electric Valve Company Limited
Chelmsford, Essex, England

Appendix II

The following is a Fortran 77 program listing for the routine used to subtract the background from the laser pulse waveforms. The abcissa axis must me in units of ns, and extend over the range from 0 ns to 150 ns inclusive. In addition, the program uses NAG routines to interpolate each of the waveforms which must be installed on the computer prior to compiling the program.

```
      program curve_fit

c     **********************
c     Program curve fits laser pulse and background waveforms,
c     subtracts one from the other then writes to file.
c     Note: data points must range from 0-150 (in ns).
c     **********************

c     ***setup variables***

      implicit none
      integer M,IFAIL,maxpt,npts,Bpts,NptsB
      integer i
      parameter(maxpt=300)
      real*8 X1(maxpt),Y1(maxpt),D1(maxpt)
      real*8 PX1(maxpt),PY1(maxpt),xstart,xstep,xBstart,xBstep
      real*8 PXB(maxpt),PYB(maxpt),DB(maxpt)
      real*8 XB(maxpt),YB(maxpt),CLP(maxpt)
      character*32 input_dat,output_dat,Background_file

      print*,'name of input data file...'
      read*,input_dat

      print*,'number of data points...'
      read*,M

      print*,'enter background data file...'
      read*,BackGround_file

      print*,'enter number of data points...'
      read*,Bpts
```

```
      print*,'name of output data file...'
      read*,output_dat

      open(unit=8,file=input_dat,status='unknown')
      open(unit=9,file=background_file,status='unknown')
      open(unit=10,file=output_dat,status='unknown')


      if (M.gt.maxpt) then
         print*,'HELP, M=',M
         print*,'maxpt=',maxpt
        stop
      end if

      if (Bpts.gt.maxpt) then
         print*,'HELP, Bpts=',Bpts
         print*,'maxpt=',maxpt
        stop
      end if

      if (npts.gt.maxpt) then
         print*,'HELP, npts=',npts
         print*,'maxpt=',maxpt
        stop
      end if


c     ***routine to curve-fit the laser pulse data***

      do i=1,M
        read(8,*) X1(i),Y1(i)
      end do

      close(8)

      IFAIL=0

      call E01BEF(M,X1,Y1,D1,IFAIL)

      xstart=0.0
      xstep=1.0
      npts=151

      do i=1,npts
       PX1(i)=(i-1)*xstep
      end do

      IFAIL = 0

      call E01BFF(M,X1,Y1,D1,npts,PX1,PY1,IFAIL)

c     ***routine to curve-fit the background data***

      do i=1,Bpts
        read(9,*)XB(i),YB(i)
      end do
```

```
      close(9)

      IFAIL=0

      call E01BEF(Bpts,XB,YB,DB,IFAIL)

      xBstart=0.0
      xBstep=1.0
      nptsB=151

      do i=1,nptsB
        PXB(i)=(i-1)*xBstep
      end do

      IFAIL = 0

      call E01BFF(Bpts,XB,YB,DB,nptsB,PXB,PYB,IFAIL)

c     ***writing corrected laser pulse data to file***

      do i=1,nptsB
         CLP(i)=PY1(i)-PYB(i)
         write(10,*)PXB(i),CLP(i)
      end do

      close(10)

      print*,'Corrected laser pulse data written to file:',output_dat

      end
```

Appendix III

The following is a Fortran 77 program listing for the routine used to evaluate L_{head}, using Equation (3.5), ie, when the tube current is zero. The abcissa axis must me in units of ns, and extend over the range from 0 ns to 150 ns inclusive. In addition, the program uses NAG routines to interpolate each of the waveforms which must be installed on the computer prior to compiling the program.

```
      program curve_fit

c     **********************
c     Program evaluates the laser head inductance at the point
c     where I=0 Note: data points must range from 0-150 (in ns).
c     **********************

c     ***setup variables***

      implicit none
      integer IFAIL,maxpt,npts,num
      integer i,Impts,Vmpts,J,ipt
      integer npts
      parameter(maxpt=300)
      real*8 t(maxpt),Imeas(maxpt),DI(maxpt)
      real*8 Pt(maxpt),PImeas(maxpt),tstart,tstep
      real*8 tmin(50),tmax(50),ttmin,GIind
      real*8 s(maxpt),Vmeas(maxpt),DV(maxpt)
      real*8 Tv(maxpt),PVmeas(maxpt),Vind,tvmin
      real*8 L,GImeas(maxpt)
      character*32 Im_dat,Vm_dat
      EXTERNAL E01BGF

      print*,'name of Imeasured data file...'
      read*,Im_dat

      print*,'number of data points...'
      read*,Impts

      print*,'name of Vmeasured data file...'
      read*,Vm_dat

      print*,'number of Vmeasured data points...'
```

```
      read*,Vmpts

c     **********************
      open(unit=7,file=Im_dat,status='unknown')
      open(unit=8,file=Vm_dat,status='unknown')
c     **********************

      if (Impts.gt.maxpt) then
         print*,'HELP, Impts=',Impts
         print*,'maxpt=',maxpt
        stop
      end if

      if (Vmpts.gt.maxpt) then
         print*,'HELP, Vmpts=',Vmpts
         print*,'maxpt=',maxpt
        stop
      end if

c     ***routine to interpolate tube current waveform***

      do i=1,Impts
            read(7,*) t(i),Imeas(i)
      end do

      close(7)

      IFAIL=0

      call E01BEF(Impts,t,Imeas,DI,IFAIL)

      tstart=0.0
      tstep=1.0
      npts = 151

      do i=1,npts
        Pt(i)=(i-1)*tstep
      end do

      IFAIL = 0

      call E01BFF(Impts,t,Imeas,DI,npts+1,Pt,PImeas,IFAIL)

c     ***routine to evaluate points when tube current is zero***

      J = 0

      do i=1,npts
         if (PImeas(i).le.0.0) then
           if (PImeas(i-1).ge.0.0) then
             J=J+1
             tmin(j) = Pt(i-1)
             tmax(j) = Pt(i)
           end if
         end if
      end do

      do i=1,J
```

```
        print*,'J=',i,tmin(i),tmax(i)
      end do

      print*,'Which value of J should be used?'
      read*,ipt

c     ***iteration process to establish more accurately,***
c     ***the time when the tube current is zero***

      npts=101

      do i=1,npts
        Pt(i)=tmin(ipt)+(i-1)*0.01
      end do

      IFAIL = 0

      call E01BGF(Impts,t,Imeas,DI,npts,Pt,PImeas,GImeas,IFAIL)

      do i=1,npts
c     print*, Pt(i),PImeas(i),GImeas(i)
        if (PImeas(i).lt.0.0) then
          if (PImeas(i-1).ge.0.0) then
            num = i-1
            ttmin = Pt(i-1)
              GIind = GImeas(i-1)
          end if
        end if
      end do

c     ***routine to interpolate the tube voltage waveform***

      do i=1,Vmpts
           read(8,*) s(i),Vmeas(i)
      end do

      close(8)

      IFAIL=0

      call E01BEF(Vmpts,s,Vmeas,DV,IFAIL)

      npts = 151

      do i=1,npts
        Tv(i)=Pt(i)
      end do

      IFAIL = 0

      call E01BFF(Vmpts,s,Vmeas,DV,npts,Tv,PVmeas,IFAIL)

c     ***calculation of the laser head inductance***

      tvmin = Tv(num)
      Vind = PVmeas(num)

      print*,'When time=',ttmin,' ns'
```

```
print*,'Inductive voltage= ',Vind,' V'
L = Vind/GIind
print*,'and laser head inductance= ',L,' nH'
stop
end
```

Appendix IV

The following is a Fortran 77 program listing for the routine used to evaluate L_{head}, using Equation (3.8), ie, at the peak of the tube current. The abcissa axis must me in units of ns, and extend over the range from 0 ns to 150 ns inclusive. In addition, the program uses NAG routines to interpolate each of the waveforms which must be installed on the computer prior to compiling the program.

```
      program curve_fit

c     **********************
c     This program evaluates Lhead from the apparent power,
c     for variable ammounts of smoothed tube current and tube
c     voltage data. Note: data points must range from 0-150 (in ns).
c     **********************

c     ***setup variables***

      implicit none
      integer IFAIL,maxpt,npts,nest,nk,lwrk
      parameter (maxpt=300)
      integer i,Impts,Vmpts,Gnpts,J,ipt,nestv,nkv
      integer npts1,npts2,left,lwrkv,iwrkv(maxpt),iwrk(maxpt)
      real*8 k(maxpt),c(maxpt),fp,smv,wv(maxpt),cv(maxpt)
      real*8 t(maxpt),Imeas(maxpt),w(maxpt)
      real*8 Pt(maxpt),tstart,tstep
      real*8 GImeas(maxpt),wrk(5000),sdif(4),sm
      real*8 tmin(50),tmax(50),ttmin,ttmax,amp1(maxpt)
      real*8 s(maxpt),Vmeas(maxpt),amp(maxpt)
      real*8 Ps(maxpt),sdifv(4),amp2(maxpt)
      real*8 vol(maxpt),vol1(maxpt),tres
      real*8 Power(maxpt),DP(maxpt),PPower(maxpt)
      real*8 Gt(maxpt),GPower(maxpt),kv(maxpt),fpv
      real*8 Pt1(maxpt),PImeas1(maxpt),GImeas1(maxpt),DI1(maxpt)
      real*8 Pt2(maxpt),PImeas2(maxpt),GImeas2(maxpt)
      real*8 Imeas_tres,GImeas_tres,GI2meas_tres,GPower_tres
      real*8 L
      real*8 wrkv(5000)
      character*32 Im_dat,Vm_dat
      character*1 start
```

```
c       ***read in waveform data***

        print*,'name of Imeasured data file...'
        read*,Im_dat

        print*,'number of data points...'
        read*,Impts

        print*,'name of Vmeasured data file...'
        read*,Vm_dat

        print*,'number of Vmeasured data points...'
        read*,Vmpts

c       **********************
        open(unit=7,file=Im_dat,status='unknown')
        open(unit=8,file=Vm_dat,status='unknown')
c       **********************

        if (Impts.gt.maxpt) then
           print*,'HELP, Impts=',Impts
           print*,'maxpt=',maxpt
          stop
        end if

        if (Vmpts.gt.maxpt) then
           print*,'HELP, Vmpts=',Vmpts
           print*,'maxpt=',maxpt
          stop
        end if

c       ***routine to smooth the tube current waveform***

        do i=1,Impts
                read(7,*) t(i),Imeas(i)
                if (Imeas(i).eq.0.0) then
                w(1) = 1.0
                else
                  w(i) = abs(200.0/Imeas(i))
                end if
        end do

        close(7)

        print*,'enter smoothing factor (current)'
        read*,sm

        nest = Impts+4
        lwrk = 4.0*Impts+16.0*nest+41
        start = 'c'
        IFAIL=0

        call E02BEF(start,Impts,t,Imeas,w,sm,nest,nk,k,c,fp
     1     ,wrk,lwrk,iwrk,IFAIL)

        print*,fp
```

```
      tstart=0.0
      tstep=1.0
      npts = 151

      do i=1,npts
        Pt(i)=(i-1)*tstep
        IFAIL = 0
        left = 1
        call E02BCF(nk,k,c,Pt(i),left,sdif,IFAIL)
        amp(i) = sdif(1)
        amp1(i) = sdif(2)
        amp2(i) = sdif(3)
      end do

c     ***routine to smooth the tube voltage waveform***

      do i=1,Vmpts
            read(8,*) s(i),Vmeas(i)
            if (Vmeas(i).eq.0.0) then
            wv(1) = 1.0
            else
              wv(i) = abs(200.0/Vmeas(i))
            end if

      end do

      close(8)

      print*,'enter smoothing factor (voltage)'
      read*,smv

      nestv = Vmpts+4
      lwrkv = 4.0*Vmpts+16.0*nestv+41
      start = 'c'
      IFAIL=0

      call E02BEF(start,Vmpts,s,Vmeas,wv,smv,nestv,nkv,kv,cv,fpv
     1    ,wrkv,lwrkv,iwrkv,IFAIL)

      print*,fpv

      npts = 151

      do i=1,npts
        Ps(i)=Pt(i)
        IFAIL = 0
        left = 1
        call E02BCF(nkv,kv,cv,Ps(i),left,sdifv,IFAIL)
        vol(i) = sdifv(1)
        vol1(i) = sdifv(2)
      end do

c     ***selection of peak tube current***

      J = 0

      do i=1,npts
        GImeas(i)=amp1(i)
```

```
      if (GImeas(i).le.0.0) then
        if (GImeas(i-1).ge.0.0) then
          J=J+1
          tmin(j) = Pt(i-1)
          tmax(j) = Pt(i)
        end if
      end if
    end do

    do i=1,J
      print*,'Peak current between: J=',i,tmin(i),tmax(i)
    end do

    print*,'Which value of J should be used?'
    read*,ipt

c   ***Iterration process for accurately finding the time***
c   ***corresponding to when dI/dt=0***

    npts1=101

    do i=1,npts1
      Pt1(i)=tmin(ipt)+(i-1)*0.01
    end do

    IFAIL = 0

    call E01BGF(npts,Pt,amp,amp1,npts1,Pt1,PImeas1,GImeas1,IFAIL)


    do i=1,npts1
      if (GImeas1(i).lt.0.0) then
        if (GImeas1(i-1).ge.0.0) then
          ttmin = Pt1(i-1)
            ttmax = Pt1(i)
        end if
      end if
    end do

    npts1 = 101

    do i=1,npts1
      Pt1(i)=ttmin+(i-1)*0.0001
    end do

    IFAIL = 0

    call E01BGF(npts,Pt,amp,amp1,npts1,Pt1,PImeas1,GImeas1,IFAIL)

    do i=1,npts1
      if (GImeas1(i).lt.0.0) then
        if (GImeas1(i-1).ge.0.0) then
          ttmin = Pt1(i-1)
            ttmax = Pt1(i)
        end if
      end if
    end do
```

```
      npts1 = 101

      do i=1,npts1
        Pt1(i)=ttmin+(i-1)*0.000001
      end do

      IFAIL = 0

      call E01BGF(npts,Pt,amp,amp1,npts1,Pt1,PImeas1,GImeas1,IFAIL)


      do i=1,npts1
          if (GImeas1(i).lt.0.0) then
            if (GImeas1(i-1).ge.0.0) then
              tres = Pt1(i-1)
            end if
          end if
      end do

      print*,'Time corresponding to peak tube current is ',tres

      IFAIL = 0

      call E01BEF(npts1,Pt1,GImeas1,DI1,IFAIL)

      npts2 = npts1

      do i=1,npts2
        Pt2(i)=Pt1(i)
      end do

      IFAIL = 0

      call E01BGF(npts1,Pt1,GImeas1,DI1,npts2,Pt2,PImeas2,GImeas2,IFAIL)

      Imeas_tres = PImeas1(tres)
      GImeas_tres = GImeas1(tres)
      GI2meas_tres = GImeas2(tres)

      print*,'When dImeas/dt=0.0'
      print*,'I=',Imeas_tres
      print*,'dImeas/dt=',GImeas_tres
      print*,'d2Imeas/dt2=',GI2meas_tres

c     ***Evaluation of aaparrent Power***
c     ***and gradient of apparrent Power***

      npts1 = 151

      do i=1,npts
        Power(i) = Vol(i)*amp(i)
      end do

      IFAIL=0

      call E01BEF(npts,Pt,Power,DP,IFAIL)

      Gnpts = npts
```

```
      do i=1,npts
        Gt(i) = Pt(i)
      end do

      IFAIL = 0

      call E01BGF(npts,Pt,Power,DP,Gnpts,Gt,PPower,GPower,IFAIL)

c     ***evaluation of laser head inductance***

      print*,'DVI/dt=',GPower(tres)

      GPower_tres = GPower(tres)

      L = GPower_tres/(Imeas_tres*GI2meas_tres)

      print*,'Laser head inductance,L=',L,' nH'

      end
```

Appendix V

The following is a Fortran 77 program listing for the routine used to evaluate the temporal energy and total power deposition in to the laser tube. The abcissa axis must me in units of ns, and extend over the range from 0 ns to 150 ns inclusive. In addition, the program uses NAG routines to interpolate each of the waveforms which must be installed on the computer prior to compiling the program.

```
      program curve_fit

c     **********************
c     Program curve fits tube current and tube voltage waveforms
c     and, for a given laser head inductance, will evaluate the
c     temporal evolution of the energy deposition in to the tube
c     (per pulse). In addition, the program will also evaluate
c     the average power deposited over any given time interval.
c     Note: data points must range from 0-150 (in ns).
c     **********************

c     ***setup variables***

      implicit none
      integer IFAIL,maxpt,npts,maxpt,nest,nestv
      parameter(maxpt=300)
      integer i,Impts,Vmpts,left,cont
      integer nk,lwrk,iwrk(maxpt)
      integer nkv,lwrkv,iwrkv(maxpt)
      real*8 t(maxpt),Imeas(maxpt),w(maxpt)
      real*8 sm,k(maxpt),c(maxpt),fp,wrk(5000)
      real*8 sdif(4),amp(maxpt),amp1(maxpt),amp2(maxpt)
      real*8 Pt(maxpt),tstart,tstep
      real*8 s(maxpt),Vmeas(maxpt)
      real*8 Ps(maxpt),LBOUND,UBOUND,INT,PRF,Pfin
      real*8 Power(maxpt),L,DP(maxpt)
      real*8 wv(maxpt),smv,kv(maxpt),cv(maxpt),fpv,wrkv(5000)
      real*8 sdifv(4),vol(maxpt)
      character*32 Im_dat,Vm_dat,Out_dat
      character*1 start
      EXTERNAL E02BEF,E02BCF
```

```
      print*,'name of Imeasured data file...'
      read*,Im_dat

      print*,'number of data points...'
      read*,Impts

      print*,'name of Vmeasured data file...'
      read*,Vm_dat

      print*,'number of Vmeasured data points...'
      read*,Vmpts

      print*,'name of output data file...'
      read*,Out_dat

c     **********************
      open(unit=7,file=Im_dat,status='unknown')
      open(unit=8,file=Vm_dat,status='unknown')
      open(unit=10,file=Out_dat,status='unknown')
c     **********************

      if (Impts.gt.maxpt) then
         print*,'HELP, Impts=',Impts
         print*,'maxpt=',maxpt
        stop
      end if

      if (Vmpts.gt.maxpt) then
         print*,'HELP, Vmpts=',Vmpts
         print*,'maxpt=',maxpt
        stop
      end if

c     ***routine to smooth tube current waveform***

      do i=1,Impts
            read(7,*) t(i),Imeas(i)
            if (Imeas(i).eq.0.0) then
            w(1) = 1.0
            else
              w(i) = abs(200.0/Imeas(i))
            end if
      end do

      close(7)

      print*,'enter smoothing factor (current)'
      read*,sm

      nest = Impts+4
      lwrk = 4.0*Impts+16.0*nest+41
      start = 'c'
      IFAIL=0

      call E02BEF(start,Impts,t,Imeas,w,sm,nest,nk,k,c,fp
     1    ,wrk,lwrk,iwrk,IFAIL)

      print*,fp
```

```
      tstart=0.0
      tstep=1.0
      npts = 151

      do i=1,npts
        Pt(i)=(i-1)*tstep
        IFAIL = 0
        left = 1
        call E02BCF(nk,k,c,Pt(i),left,sdif,IFAIL)
        amp(i) = sdif(1)
        amp1(i) = sdif(2)
        amp2(i) = sdif(3)
      end do

c     ***routine to smooth the tube voltage waveform****

      do i=1,Vmpts
            read(8,*) s(i),Vmeas(i)
            if (Vmeas(i).eq.0.0) then
            wv(1) = 1.0
            else
              wv(i) = abs(200.0/Vmeas(i))
            end if

      end do

      close(8)

      print*,'enter smoothing factor (voltage)'
      read*,smv

      nestv = Vmpts+4
      lwrkv = 4.0*Vmpts+16.0*nestv+41
      start = 'c'
      IFAIL=0

      call E02BEF(start,Vmpts,s,Vmeas,wv,smv,nestv,nkv,kv,cv,fpv
     1     ,wrkv,lwrkv,iwrkv,IFAIL)

      print*,fpv

      npts = 151

      do i=1,npts
        Ps(i)=Pt(i)
        IFAIL = 0
        left = 1
        call E02BCF(nkv,kv,cv,Ps(i),left,sdifv,IFAIL)
        vol(i) = sdifv(1)
c       write(10,*) Ps(i),vol(i)
      end do

c     ***routine to evaluate temporal energy deposition***

      print*,'input value of inductance'
      read*,L
```

```
      do i=1,npts
      Power(i) = (amp(i)*(vol(i)-L*amp1(i)))*1.0E-9
      write(10,*)Pt(i),amp(i),vol(i),Power(i)
      end do

      close(10)

c     ***routine to evaluate power deposition****

      IFAIL=0

      call E01BEF(npts,Pt,Power,DP,IFAIL)

100   print*,'enter lower bound (ns)...'
      read*,LBOUND
      print*,'enter upper bound (ns)...'
      read*,UBOUND

      IFAIL = 0

      call E01BHF(npts,Pt,Power,DP,LBOUND,UBOUND,INT,IFAIL)

      print*,'enter PRF (Hz)...'
      read*,PRF

      Pfin = INT*PRF

      print*,'integral between',LBOUND,' ns and',UBOUND,' ns'
      print*,'gives a power deposition of',Pfin,' W'


      print*,'enter 1 to integrate over different limits'
      read*,cont

      if (cont.eq.1) then
        goto 100
      else
        goto 200
      end if


200   end
```

Appendix VI

The following is a Fortran 77 program listing for the routine used to evaluate the temporal evolution of the electron density during the course of the excitation pulse, using a neon buffer gas with any percentage of hydrogen added. The program compensates for the increased collision frequency with hydrogen addition. The abcissa axis must me in units of ns, and extend over the range from 0 ns to 150 ns inclusive. In addition, the program uses NAG routines to interpolate each of the waveforms which must be installed on the computer prior to compiling the program.

```
      program curve_fit

c     **********************
c     Program evaluates the resistive voltage, then calculates
c     the electron density using a Neon buffer gas for any
c     percentage of added hydrogen to a neon buffer gas. Data
c     for Time, current, voltage, electron density is saved as a file.
c     The value for Lhead is assumed to be known.
c     Note: data points must range from 0-150 (in ns).
c     **********************

c     ***setup variables***

      implicit none
      integer IFAIL,maxpt,npts,maxpt,nest,nestv
      parameter(maxpt=300)
      integer i,Impts,Vmpts,left
      integer nk,lwrk,iwrk(maxpt)
      integer nkv,lwrkv,iwrkv(maxpt)
      real*8 t(maxpt),Imeas(maxpt),w(maxpt)
      real*8 sm,k(maxpt),c(maxpt),fp,wrk(5000)
      real*8 sdif(4),amp(maxpt),amp1(maxpt),amp2(maxpt)
      real*8 Pt(maxpt),tstart,tstep
      real*8 s(maxpt),Vmeas(maxpt)
      real*8 Ps(maxpt)
      real*8 Power(maxpt),L,ne1(maxpt),ne2(maxpt),ne(maxpt),d1,H
      real*8 wv(maxpt),smv,kv(maxpt),cv(maxpt),fpv,wrkv(5000)
```

```
      real*8 sdifv(4),vol(maxpt)
      character*32 Im_dat,Vm_dat,Out_dat
      character*1 start
      EXTERNAL E02BEF,E02BCF

      print*,'name of Imeasured data file...'
      read*,Im_dat

      print*,'number of data points...'
      read*,Impts

      print*,'name of Vmeasured data file...'
      read*,Vm_dat

      print*,'number of Vmeasured data points...'
      read*,Vmpts

      print*,'name of output data file...'
      read*,Out_dat

c     **********************
      open(unit=7,file=Im_dat,status='unknown')
      open(unit=8,file=Vm_dat,status='unknown')
      open(unit=10,file=Out_dat,status='unknown')
c     **********************

      if (Impts.gt.maxpt) then
         print*,'HELP, Impts=',Impts
         print*,'maxpt=',maxpt
        stop
      end if

      if (Vmpts.gt.maxpt) then
         print*,'HELP, Vmpts=',Vmpts
         print*,'maxpt=',maxpt
        stop
      cnd if

c     ***routine to smooth the current waveform***

      do i=1,Impts
            read(7,*) t(i),Imeas(i)
            if (Imeas(i).eq.0.0) then
            w(1) = 1.0
            else
              w(i) = abs(200.0/Imeas(i))
            end if
      end do

      close(7)

      print*,'enter smoothing factor (current)'
      read*,sm

      nest = Impts+4
      lwrk = 4.0*Impts+16.0*nest+41
      start = 'c'
      IFAIL=0
```

```
      call E02BEF(start,Impts,t,Imeas,w,sm,nest,nk,k,c,fp
     1    ,wrk,lwrk,iwrk,IFAIL)

      print*,fp

      tstart=0.0
      tstep=1.0
      npts = 151

      do i=1,npts
        Pt(i)=(i-1)*tstep
        IFAIL = 0
        left = 1
        call E02BCF(nk,k,c,Pt(i),left,sdif,IFAIL)
        amp(i) = sdif(1)
        amp1(i) = sdif(2)
        amp2(i) = sdif(3)
      end do

c     ***routine to smooth the tube voltage vaveform***

      do i=1,Vmpts
            read(8,*) s(i),Vmeas(i)
            if (Vmeas(i).eq.0.0) then
            wv(1) = 1.0
            else
              wv(i) = abs(200.0/Vmeas(i))
            end if

      end do

      close(8)

      print*,'enter smoothing factor (voltage)'
      read*,smv

      nestv = Vmpts+4
      lwrkv = 4.0*Vmpts+16.0*nestv+41
      start = 'c'
      IFAIL=0

      call E02BEF(start,Vmpts,s,Vmeas,wv,smv,nestv,nkv,kv,cv,fpv
     1    ,wrkv,lwrkv,iwrkv,IFAIL)

      print*,fpv

      npts = 151

      do i=1,npts
        Ps(i)=Pt(i)
        IFAIL = 0
        left = 1
        call E02BCF(nkv,kv,cv,Ps(i),left,sdifv,IFAIL)
        vol(i) = sdifv(1)
      end do

c     ***evaluation of electron density (per cubic metre)***
```

```
print*,'input value of inductance'
read*,L

print*,'input percentage of hydrogen'
read*,H

do i=1,npts
Power(i) = amp(i)*(vol(i)-L*amp1(i))
d1 = -(2.0*i)/420
ne1(i) = 3.3E21*abs(amp(i))*dexp(d1)/abs(vol(i)-L*amp1(i))
ne2(i) = 2.0E22*abs(amp(i))/abs(vol(i)-L*amp1(i))
ne(i) = (H/100)*ne2(i) + ((100-H)/100)*ne1(i)
write(10,*)Pt(i),amp(i),vol(i),ne(i)
end do

close(10)

end
```